PART I. SILYL KETENES AS BUILDING BLOCKS FOR SMALL MOLECULES AND

POLYMERS; PART II. THE INCORPORATION OF REDOX SMALL MOLECULES INTO

DEEP EUTECTIC SOLVENTS FOR THE DEVELOPMENT OF NEW ELECTROLYTES

By

SARAH MITCHELL

Submitted in partial fulfillment of the requirements

For the degree of Doctor of Philosophy

Dissertation Advisor: **Prof. Emily Pentzer**

Department of Chemistry

CASE WESTERN RESERVE UNIVERSITY

JANUARY 2022

CASE WESTERN RESERVE UNIVERSITY

SCHOOL OF GRADUATE STUDIES

We hereby approve the dissertation of

Sarah Mitchell

Candidate for the degree of Doctor of Philosophy*

Committee Chair:

Prof. Michael Zagorski

Committee Member:

Prof. Irene Lee

Committee Member:

Prof. Gregory Tochtrop

Committee Member:

Prof. Michael Hore

Date of Defense

August 3rd, 2021

***We also certify that written approval has been obtained for any propriety material**

contained therein.

Table of Contents

List of Tables

List of Abbreviations

Radical polymerization	RP
Ring opening polymerization	ROP
Ring opening methathesis polymerization	ROMP
Grignard metathesis polymerization	GRIM
Group transfer polymerization	GTP
Lewis acid	LA
Trimethylsilyl ketene	TMS ketene
Nuclear magnetic resonance	NMR
Fourier-transform infrared spectroscopy	FTIR
Gas chromatography-mass spectrometry	GC-MS
Methyldiphenyl silyl ketene	MDPS ketene
Dichloromethane	DCM
Triisopropylsilyl ketene	TIPS ketene
Triethylsilyl ketene	TES ketene
Dimethylphenyl silyl ketene	DMPS ketene
Triphenylsilyl ketene	TPhS ketene
Tetrahydrofuran	THF
Methyl trimethylsilyl dimethylketene acetal	MTS
N-heterocyclic carbenes	NHC
Methyl methacrylate	MMA
Sodium hydride	NaH
Poly(methyl methacrylate)	PMMA
Boron trifluoride diethyl etherate	$BF_3 \cdot OEt_2$
Aluminum isopropoxide	$Al(O^iPr)_3$
Tris(pentafluorophenyl) borane	$B(C_6F_5)_3$
Tetrabutylammonium bromide	TBAB
Tert-butyldiphenylsilyl ketene	TBDPS ketene
1,3-Diisopropylimidazolium chloride	NHC
Triphenylborane	BPh_3
Trimethylsilyl cyanide	TMS cyanide

Room temperature	RT
Case Western Reserve University	CWRU
Texas A&M University	TAMU
Electron spray ionization	ESI
Deprotonation	DePro
Nucleophilic addition	NuAdd
Redox flow battery	RFB
Deep eutectic solvent	DES
Hydrogen bond acceptor	HBA
Hydrogen bond donor	HBD
Ionic liquid	IL
2,2,6,6-tetramethylpiperidin-1-yl)oxyl	TEMPO
4-hydroxy TEMPO	4HT
Phenothiazine	PHZ
Cyclic voltammetry	CV
Choline chloride	ChCl
Ethylene glycol	EG
Dicyclohexylcarbodiimide	DCC
Melting point	T_m
Decomposition temperature	$T_{0.005}$ loss
Thermogravimetric analysis	TGA
Vogel-Fulcher-Tamann	VFT
Diffusion coefficients	D
Ethyl-phenothiazine	EPT
Methoxyethyl-phenothiazine	MEPT
Dimethylformamide	DMF
N-bromosuccinimde	NBS
Dimethoxy-methoxyethyl phenothiazine	DMeMEPT
Dimethoxy-ethyl phenothiazine	DMeEPT
Lithium aluminum hydride	$LiAlH_4$
9-Fluorenylmethoxycarbonyl	Fmoc

Dimethyl sulfoxide   DMSO

Electron paramagnetic resonance   EPR

1,4-dimethoxybenzenes   DBB

Energy Frontier Research Center   EFRC

Acknowledgements

I would like to thank my advisor, Dr. Emily Pentzer for her great mentorship, guidance, and support through my graduate school career. She has provided me many experiences that has shaped the scientist and person I am today. My journey the past 5 years was not expected, but I wouldn't change any of the experiences I had for a second.

To my committee members, Professor Zagorski, Professor Lee, Professor Tochtrop, and Professor Hore. Thank you for time, advice, and agreeing to be on my committee. I truly appreciate the flexibility.

To Professor Gray, thank you for being such a help in this unique situation. Your help and guidance has made the process smoother.

To the Pentzer lab members both past and present, thank you for your continued support and words of encouragement, also for the fun and spontaneous moments in lab. A special thanks to Yuanhui Xiang for our many conversions on silyl ketenes, your ideas, and support.

Lastly, to my family and friends, especially my parents, sisters, David, Emily, and Kyra, your support has meant the world to me outside of the grad school bubble. And to Zak, Jay, and Maria, this group made grad school so much better and enjoyable, I wish you all the best.

Abstract

Part I: Silyl Ketenes as Building Blocks for Small Molecules and Polymers; Part II: The

Incorporation of Redox Small Molecules into Deep Eutectic Solvents for the Development of

New Electrolytes

By

SARAH MITCHELL

The composition of a polymer backbone dictates the properties and applications of the material, and the chemical composition is inherited from its monomer. It is of interest to access new properties for materials, and in turn the need for new polymeric backbones. Cumulated double bonds are an interesting class of monomers that can produce three distinct polymeric backbones, the most common being isocyanates, allenes, and ketenes. The controlled polymerization of isocyanates and allenes has been thoroughly studied, however ketenes tend to self-dimerize and controlled polymerization is difficult to achieve. A solution to this issue is to use silyl ketenes, which are stabilized by the β-silicon effect. The Pentzer lab has explored radical and anionic pathways, with no success of controlled polymerization, a better understanding of silyl ketene reactivity is necessary. Group transfer polymerization is a technique commonly used to polymerize methacrylates and acrylates using a silyl ketene acetal as an intiator and a catalyst. Herein, part I one of this thesis will examine the reactivity of silyl ketenes with Lewis acid catalysts, nucleophile, and silyl substituent and how these variables affect the formation of an α-silyl carbonyl, leading to better selection of polymerization conditions. Group transfer polymerization of silyl ketenes will also be explored, evaluating potential initiators, catalysts, and reaction conditions.

Deep eutectic solvents (DES) are mixtures composed of a hydrogen bond donor and a hydrogen bond acceptor, in which the hydrogen bond network formed lowers the melting point creating a eutectic mixture. DES are considered "greener" than ionic liquids, due to the individual components being non-toxic and biodegradable. DES are also easy to synthesize and have a multitude of applications; for example, DES could be used as an electrolyte by incorporating a redox active species into the H-bond network. These solutions have great potential as an electrolyte system to overcome issues with current electrolytes, such as low solubility of redox active species, Coulombic efficiency, and conductivity. Redox active derivatives of interest are selected for their potential to be modified to tune the solubility and electrochemical behavior. Herein, part II of this thesis examines two different redox active species. A library of TEMPO derivatives was synthesized to vary linker size, cation identity, and anion identity. Three TEMPO salts including imidazolium, pyrrolidinium and quarternary ammonium functionality were chosen to be incorporated into ethaline and the physical properties and electrochemical behavior of the solutions were evaluated. A library of phenothiazine derivatives was synthesized and the electrochemical behavior was examined in ethaline.

Part I: Silyl Ketenes as Building Blocks for Small Molecules and Polymers

Chapter 1

Introduction to Cumulated Double Bonds as Monomers

Portions of this chapter appear in the following manuscript:

1.1 General overview of polymers/polymerizations

Polymers are used in nearly every facet of life, from food storage to medical technologies, greatly impacting the world and making modern life possible. The field of polymer science continues to grow and evolve as new needs arise, leading to advances in synthetic methods,[1–5] polymer architectures,[6–11] polymer compositions, and polymer processing techniques.[12–18] The chemical composition of polymers determines the intra- and interchain interactions which in turn affect the properties of the polymer, including toughness, thermal stability, degradability, and the applications of the polymer.[19–23] The chemical composition of a polymer also determines potential post-polymerization modification reactions and compatibility with various additives. Ongoing research encompasses production of extreme molecular weight polymers and new polymer architectures. One of the most recent focuses in polymer research is the recyclability of polymers; including upcycling current polymers, producing polymers from sustainable starting materials, and controlled degradation of polymers.[24–35]

Polymers are prepared by either step growth or chain growth polymerization techniques (Figure 1.1).[36,37] Step growth polymerization utilizes di-functional small molecules as monomers; the monomers then react to form dimers, the dimers then react to form trimers or higher order oligomers, and so on to form linear high molecular weight polymers. In contrast, chain growth polymerizations give more control than step growth polymerization; the end group identity and
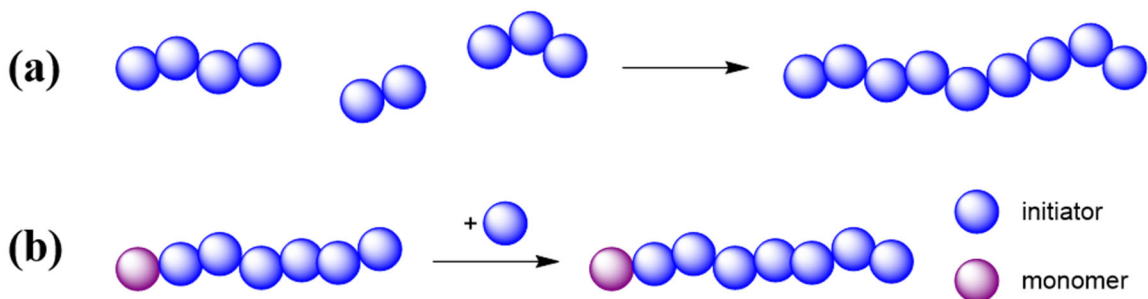
Figure 1.1. Schematic representation of (a) step growth, (b) chain growth polymerizations.

the molecular weight of the polymer can be controlled while maintaining low dispersities. Chain growth polymerization techniques include radical polymerization (RP),[38] ring opening polymerization,[39] ring opening metathesis polymerization (ROMP),[40] group transfer polymerization (GTP), and Grignard metathesis polymerization (GRIM).[41–43] Chain growth polymerizations utilize monomers that have a unit of unsaturation (i.e, double bond or ring), in which the unit of unsaturation is lost upon polymerization.

1.2 Cumulated double bonds as monomers

An interesting class of monomers that are suitable for chain growth polymerization are cumulated double bonds of the general form X=Y=Z, in which the central atom is carbon. The pi bonds are orthogonal due to them sharing a central sp-hybridized carbon atom and therefore they are not conjugated (Figure 1.2a). The most common cumulated double bonds are isocyanates (O=C=N),
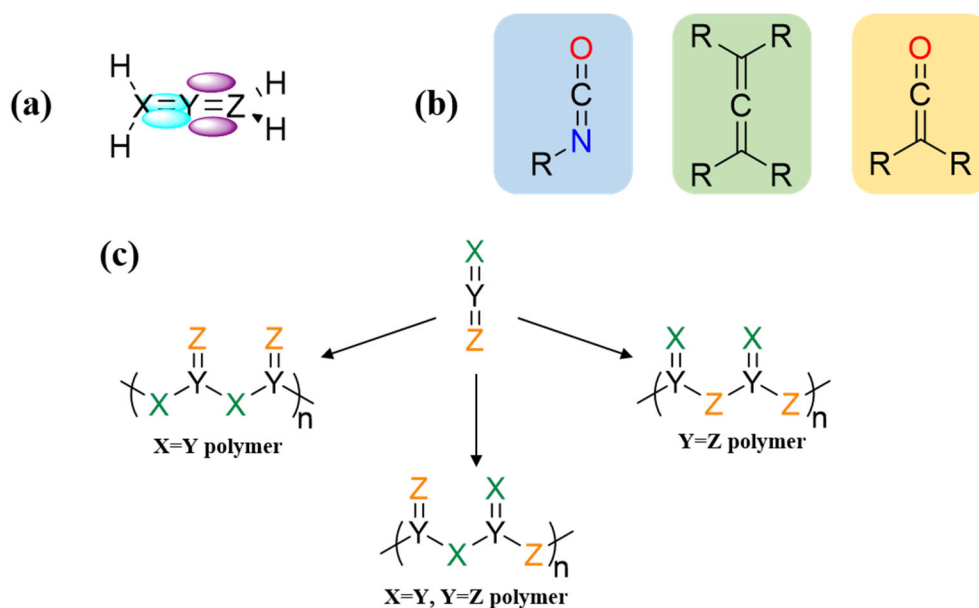
Figure 1.2. (a) Orthogonality of the pi bonding orbitals of cumulated double bonds; (b) common cumulated double bonds of isocyanate (blue), allene (green), ketene (yellow); (c) different polymerization routes of cumulated double bonds.

allenes (C=C=C), and ketenes (O=C=C), all isoelectronic with each other (Figure 1.2b). The orthogonality of these compounds allow for unique reactivity including the opportunity to access three different polymer backbones from a single monomer upon polymerization (Figure 1.2c). Polymerization can occur through the X=Y bond, Y=Z bond, or the alternate between X=Y and Y=Z.

1.3   Isocyanates as Monomers

1.3.1   Isocyanate Reactivity

Isocyanates are a highly reactive class of compounds of the form R-N=C=O, where the reactivity is influenced by the electron deficient nature of the central carbon atom. The carbon atom is susceptible to nucleophilic attack and reacts with alcohols, amines, water, thiols, and carboxylic acids resulting in carbonyl-containing functional groups. Alternatively, the oxygen and nitrogen atoms of isocyanates react with electrophiles, where the nitrogen atom reacts less commonly. This unique reactivity allows for isocyanates to be used in a variety of chemical transformations including being utilized as intermediates in complex synthetic schemes. For example, the Hofmann rearrangement and the Curtius rearrangement both form isocyanate intermediates.[44] Isocyanates are also known to form dimers at low temperatures and trimers at high temperatures in the presence of acidic or basic catalysts (Figure 1.3).[45,46]
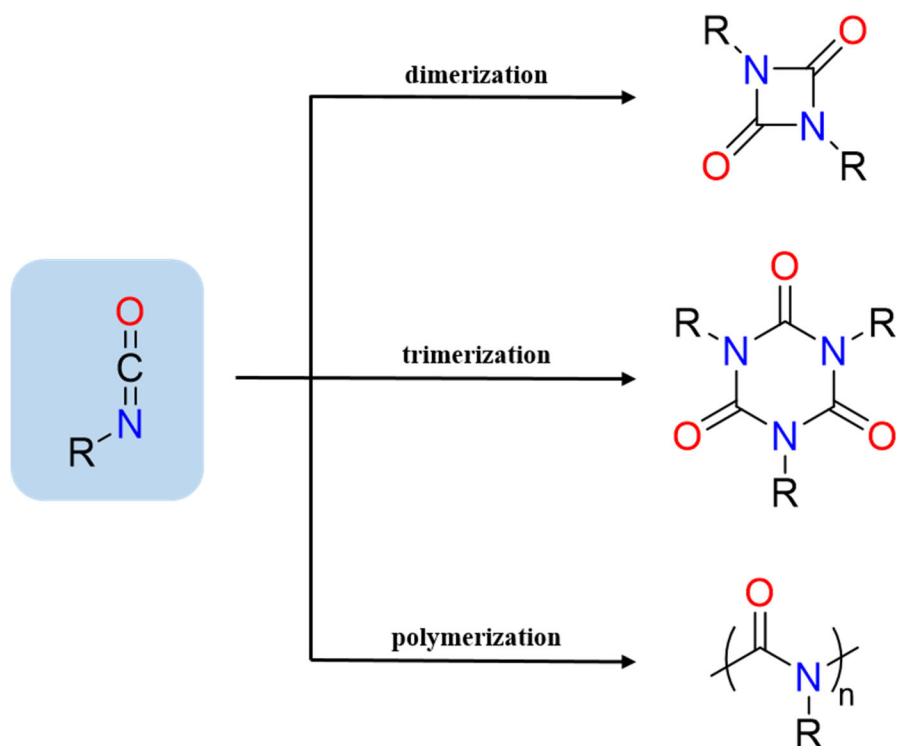
Figure 1.3. Resulting products from the dimerization, trimerization, and polymerization of isocyanates.

1.3.2 Anionic Polymerization of Isocyanates

Isocyanates are the most developed cumulated double bonds used as monomers and have been used to produce polyisocyanates, but more commonly polyureas and polyurethanes. Many of these isocyanate derived polymers can be produced on an industrial scale, for example polyurethanes.[45,47] The polymerization of isocyanates was first discovered in 1937 when an aliphatic diisocyanate and diamine was reacted to form polyurea and an aliphatic diisocyanate and glycol was reacted to form polyurethane.[48] Alternatively, the isocyanate functional group can be used as monomer in chain growth polymerizations to produce polyisocyanates with a –N(R)C(O)- backbone where the nitrogen atom bears a R pendant group (*N*-substituted 1-nylons).
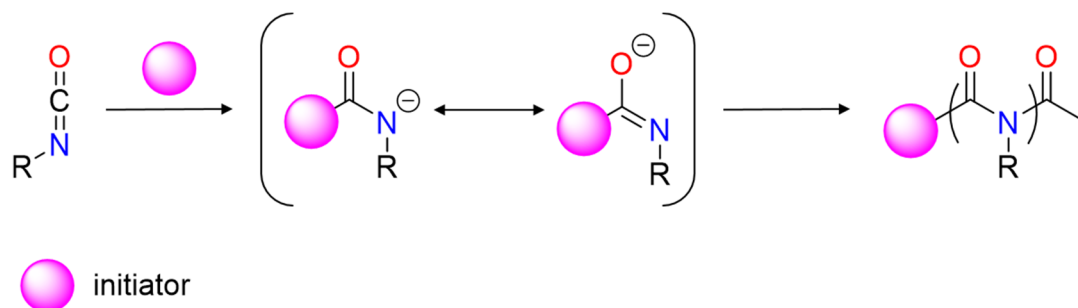
Scheme 1.1. Anionic polymerization of isocyanate monomers.

Unfortunately, early development of these polymers were limited due to backbiting during polymerization which led to cyclic trimers.[46,49,50]

A variety of polymerization techniques have been used in attempts to form polyisocyantates, most commonly anionic polymerization (Scheme 1.1). The first report of the anionic polymerization of a monofunctional isocyanate was first reported by Shashoua *et al.* in 1959, where both aliphatic and aromatic isocyanates were polymerized with sodium cyanide as an initiator in polar solvents.[46,49] It was proposed that the mechanism for initiation was the attack of the anion at the electrophilic carbon of the isocyanate. This resulted in the formation of an amidate anion with negative charge delocalized across the nitrogen and oxygen atoms; propagation was mainly observed through the nitrogen atom. Unfortunately, intrachain backbiting was observed and cyclic trimers were obtained along with a linear polymer chain that exhibited high dispersity. It was later found that by adding bulky additives, controlled anionic polymerization could be achieved leading to polymers with low dispersites and controlled molar mass.[51] The bulky additives sterically protected the propagating anion which prevented backbiting and the formation of cyclic trimers.[51–58] For example, Lee *et al.* reported the polymerization of 3-(triethoxysilyl)propyl isocyanate using sodium naphthalenide as initiator in the presence of a crown ether. The sodium ion was trapped in the crown ether, which led to fast propagation and suppression of backbiting.[51]

1.3.3 Coordination Polymerization of Isocyanates

Transition metal catalyzed coordination polymerization techniques have also been utilized, in which metal complexes were used to produce controlled polymerizations of isocyanates. Patten *el al*. first demonstrated this technique in 1991 with Titanium (IV) complexes and alkyl isocyanates, with no cyclic trimers observed.[59] After this initial work, more CpTiCl$_2$X complexes were developed (Cp = η^5-cyclopentadiene, X = OCH$_2$CF$_3$, N(CH$_3$)$_2$, and CH$_3$). Many isocyanates can be polymerized with these catalysts, excluding isocyanates bearing sterically bulky substituents or aromatic isocyanates.[60,61] The proposed mechanism for initiation is the migratory insertion of the alkoxide from the Ti to the carbon of the isocyanate to form a titanium-amidate species that then propagates.[61,62] Termination occurs through protonation, so the alkoxide group becomes the chain end functionality. Further studies have been done on bimetallic and trimetallic titanium complexes that produce flexible polymer segments between the rigid polyisocyanates.[62]

1.3.4 Properties of Polyisocyanates

Polyisocyanates are rod-like polymers that exhibit a helical conformation both in solution and solid state due to the rigidity of the amide in the polymeric backbone.[63,64] Due to the helical conformation, these polymers and their rigidity are the properties of polyisocyanates that have been thoroughly studied. These polymers have been used to mimic the secondary structure of proteins, as optical switches, chiral recognitions structures, and liquid crystal materials.[65–69] The mesogenic polymers were either polyisocyanates with short alkyl chains that are soluble enough to make concentrated polymer solutions (no strong interchain interactions) or aryl polyisocyanates where the aromatic group is directly attached to the nitrogen atom.[70] Polyisocyanates have also been found to be depolymerizable under various conditions, including with the use of catalytic amounts of sodium cyanide and di-*n*-butylamine. The proposed mechanism of depolymerization

involves abstracting the proton from the polymer chain then followed by depolymerization or backbiting to produce either monomer or dimers/trimers, respectively. The mechanism is dependent on the polyisocyanate.[49]

1.4 Allenes as Monomers

1.4.1 Allene Reactivity

Allenes are a class of compounds of the form $R_2C=C=CR_2$, where the R groups can be hydrogen, alkyl, aryl, or alkoxy groups. The high degree of unsaturation, polarizability of π-bond, and geometry contribute to the wide range of reactivity of allenes, including electrophilic additions, cyclization reactions, and rearrangements.[71] Additionally, allenes have been used in the synthesis of various macromolecules -ranging from cyclic oligomers (4-9 membered rings) to polymers.[72–75] Polymerization can occur through both carbon-carbon double bonds: the less substituted C=C (1,2), the more substituted C=C (2,3), or a combination of both C=C (1,2 and 2,3). All three of the polymer backbones contain alternating sp^2 and sp^3 hybridized carbon atoms, allowing for further post-polymerization functionalization (Figure 1.4).

1.4.2 Coordination of Polymerization of Allenes

Similarly, to isocyanates, the polymerization of allenes has been studied since the 1950s. Various techniques have been used to polymerize allenes, including radical and cationic techniques, both of which producing oligomer and polymers with uncontrolled molar mass.[76–78] Alternatively, coordination polymerization with transition metal complexes has been utilized to achieve controlled polymerization of allenes. The mechanism is typically the allene coordinates to the transition metal complex followed by migratory insertion to initiate the polymerization, followed my propagation. A large variety of mono-, di-, and tri-substituted allenes have been examined
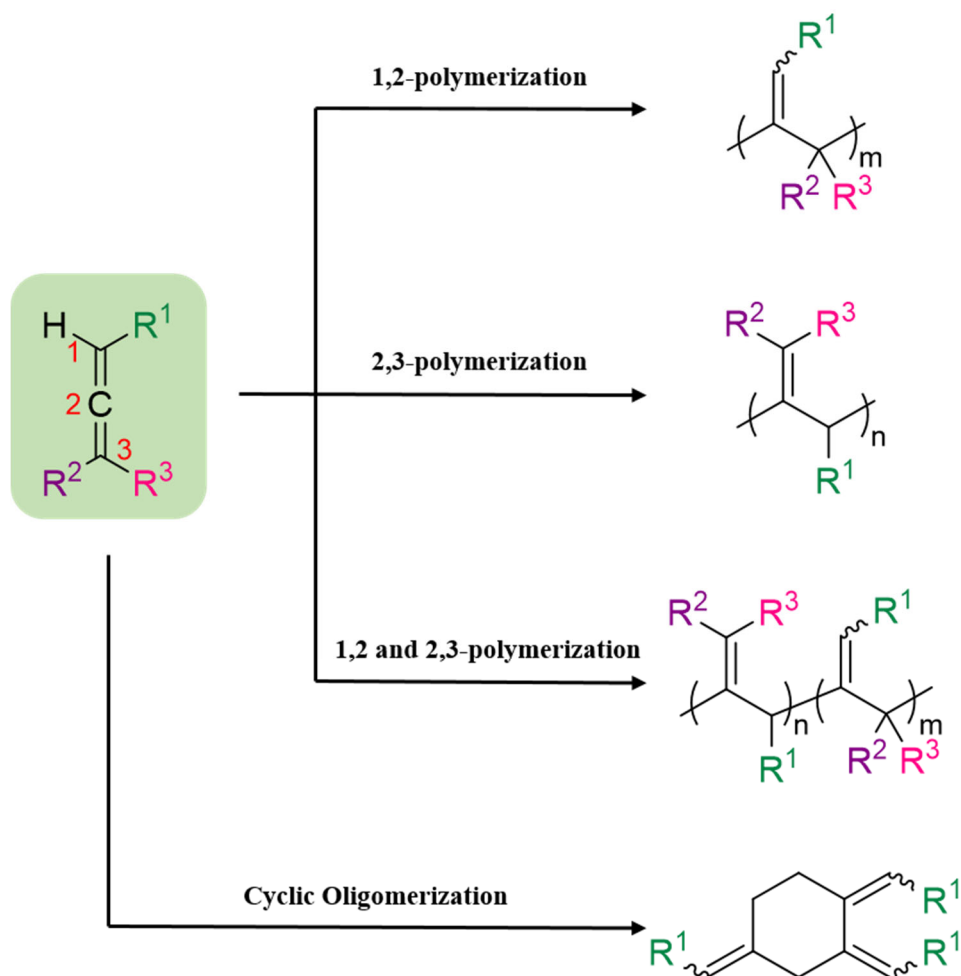
Figure 1.4. Three possible backbones from allene polymerization and a common cyclic oligomer as a side product.

9

with varying alkoxy, phenyl, alkyl, and alkoxycarbonyl substituents.[79] By differing the electronic properties and steric nature of the substituents on the allenes, both the rate of polymerization and regioreactivity are affected.

The most common substituents for allene monomers are aryl- and alkyl-substituted allenes. Endo *et al.* examined allenes that varied the R^1, R^2, and R^3 substituents with various alkyl chain lengths and aryl rings, with [(π-allyl)-NiOCOCF₃]₂ as the initiator (Scheme 1.2).[80] The substituents on monosubstituted allenes had little effect on polymerization and all gave good control of molecular weight; however, bulkier substituents had a slightly smaller ratio of 1,2:2,3 propagation. For example, *t*-butylallene exhibited a 0:100 1,2:2,3 propagation ratio whereas cyclohexyl allene exhibited an 8:92 1,2:2,3 propagation ratio. A similar trend was observed for disubstituted allenes where bulkier substituents had a smaller ratio of 1,2:2,3 propagation, however the rate of polymerization was slower than monosubstituted allenes and the trisubstitued allenes did not polymerize.[80] Additional studies have been done with phenyl-substituted allenes looking at groups with different electronic and steric considerations using various transition metal complexes (e.g., rhodium, cobalt, nickel, and rare-earth metal complexes (Sc, Lu, Tm, Y, and Gd)).[81–83] There has also been a handful of studies looking at alkoxy allene derivatives, in which one of the substituents bears the electron-donating –OR group.

R^1=H, R^2=*n*-C₆H₁₃, R^3=CH₃
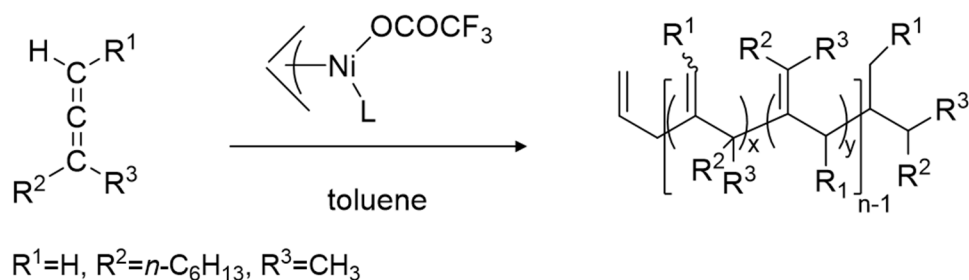
Scheme 1.2. Coordination polymerization of alkylallene derivatives.

1.4.3 Properties of Polyallenes

Though the polymerization of allenes has been well studied, the applications of these polymers has been understudied, with very limited examples. Yamauchi *et al*. used phenoxy-substituted allene as a monomer and a diallene cross-linker in coordination dispersion copolymerization to produce polymer microspheres.[84] These authors also incorporated a hydroxyl containing allene that was used for further post polymerization modification. Sakai *et al.* prepared thin films from block copolymers containing a polyethylene glycol and a polyallene block.[85] The thin film consisted of perpendicular nanocylindrical structures. A spattering of reports has demonstrated the high crystallinity of polyallenes, in which polymers that exhibit high regularity are strictly 2,3-polymeric backbones.[83,86]

1.5 Ketenes as Monomers

1.5.1 Ketene Reactivity

Ketenes are a highly reactive class of compounds of the form $O=C=CR_2$ where the R groups can be hydrogen, alkyl, or aryl groups as well as these groups can be different in identity. Similar to isocyanates and allenes, ketenes self-dimerize to form cyclic dimers, unfortunately, ketenes have a higher tendency to self-react, limiting their use as monomers in chain growth polymerizatoins. The dimerization of ketenes occurs through a [2+2] cycloaddition, in which dimerization can take plase through both the C=C double bond and the C=O double bond.[87–89] There are 2 main class of ketenes: ketoketenes ($O=C=CR_2$) and aldoketenes ($O=C=CHR$), in which aldoketenes have a lower tendency to self-dimerize. Similarly, to allene monomers, ketenes can produce 3 different polymeric backbones depending on how polymerization takes place: polyketene acetal, polyketone, and polyester (Figure 1.5).

1.5.2 Various Polymerization Techniques of Ketenes

The polymerization of ketenes was first discovered in 1925 by Henry Staudinger, where dimethylketene was polymerized with triethylamine as the initiator; however, the definitive structure wasn't initially obtained.[90] Natta *et al*. were the first to demonstrate that different polymeric backbones could be obtained when using ionic catalysts in toluene at -60°C, specifically
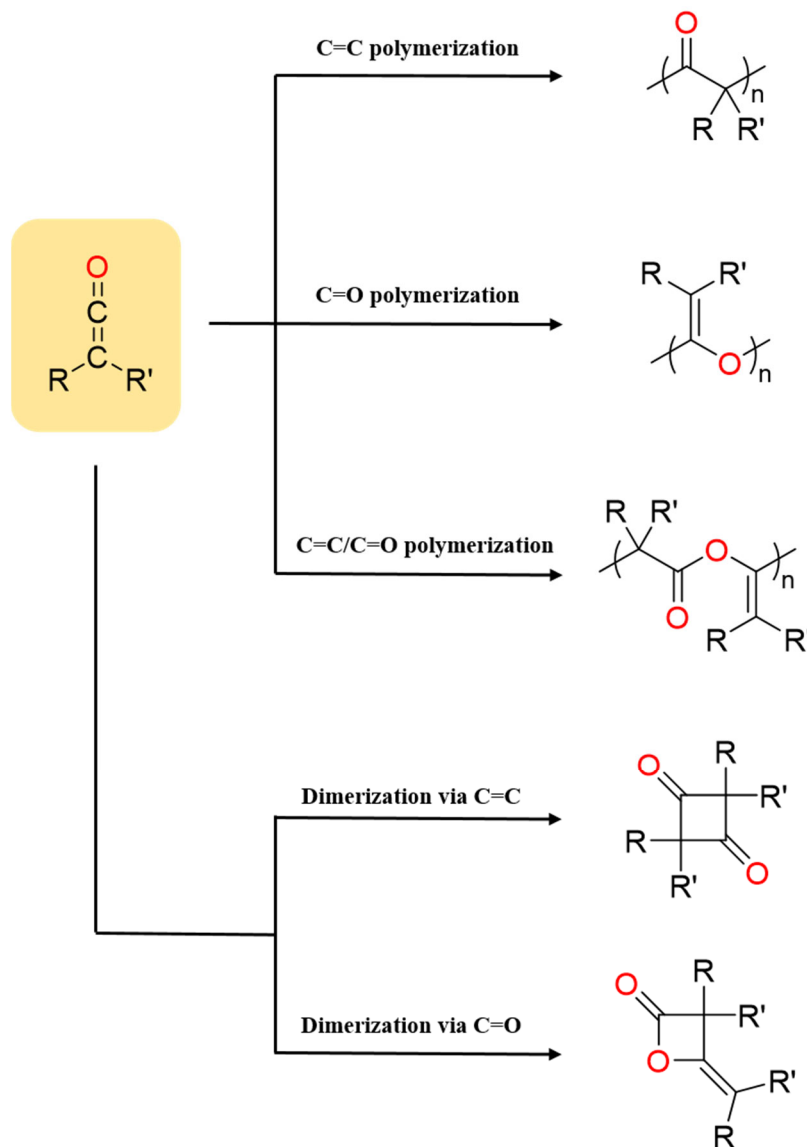
Figure 1.5. Three possible backbones from ketene polymerization and dimerization via the C=C and C=O bonds.

polyketone and polyester backbone.[91] A few years later, Pregaglia *et al.* obtained polyketene acetal

from polymerizing dimethylketene with Lewis bases (tertiary amines) in polar solvents, utilizing

Lewis bases as initiators.[92]

Over the past few decades, both anionic and cationic polymerization techniques have been used to

polymerize ketenes. For anionic polymerization, the proposed mechanism is an anion attacks the

central carbon of the ketene, forming and enolate anion, followed by propagation. The formation

of the enolate allows for either C-acylation and O-acylation yielding the polyketone and

polyketene acetal backbones, respectively.[93] In contrast, alternating C- and O- acylation leads to

the formation of the polyester backbone. Of the literature reported for the polymerization of

ketenes, anionic polymerization primarily gives polyester backbones.[91,94–97] For example, Sudo *et

al.* polymerized ethylphenylketene to produce the polyester homopolymer using *n*-butyl lithium as

an initiator.[98] In comparison to anionic polymerization of ketenes, the cationic polymerization of

ketenes is sparsely reported. Here, the proposed mechanism uses an electrophilic initiator that

coordinates to the oxygen atom of the ketene rendering the central carbon atom more susceptible

for nucleophilic attack by another ketene unit. The resulting polymeric backbone is dependent on

the initiator and solvent polarity. For example, Natta *et al.* polymerized dimethylketene with

aluminum tribromide as the initiator in toluene to produce the polyketone backbone; however,

when triethyl aluminum was used, the polyester backbone was obtained.[99] The system was further

explored by Egret *et al.*, looking at various solvent systems with both individual solvents and

mixture of solvents; for example, toluene, CCl_4, diethyl ether, nitrobenzene/CCl_4, and

nitrobenzene/acetonitrile among others.[100] Depending on the solvent system, the reaction time and

temperature varied, as well as formation of cyclic byproducts.

1.5.3 Copolymerization of Ketenes

Due to the high reactivity of ketenes, many early reports of ketene polymerization focused on the copolymerization of ketenes with ketones, aldehydes, and isocyanates. Natta *et al.* used *n*-butyl lithium as an initiator to copolymerize acetone and dimethyl ketene, in which highly crystalline polyesters were produced. When dimethyl ketene was copolymerized with benzaldehyde and aldehyde derivatives using alkyl lithium reagents, the obtained copolymers varied in crystallinity.[91,94] Block copolymers have been obtained with ethylphenylketene and *tert*-butyl methacrylate using *n*-butyl lithium as an initiator, and this protocol was extended to additional ketene monomers. Nagai *et al.* was able to demonstrate enantioselective control of the copolymerization of ketene and aldehyde monomers.[101,102] These studies led to the synthesis of optically active polyesters, resulting from the copolymerization of ketenes and aldehyde monomers.

1.6 Silyl Ketenes

1.6.1 Silyl Ketene Reactivity

Silyl ketenes, of the form $O=C=CHSiR_3$, are a sub-class of ketenes in which a silyl substituent is attached to the terminal carbon of the cumulated double bond (Figure 1.6). The silyl substituent can consist of various R groups ranging across alkyl and aryl groups, which can alter the solubility of the compound (and of the resulting polymer). In contrast to alkyl and aryl ketenes, silyl ketenes
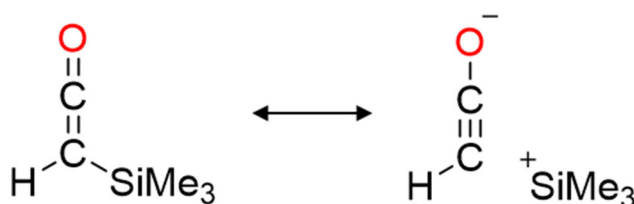
Figure 1.6. Beta-silicon effect of silyl ketene.

are inherently more stable and easier to use, as well as less reactive under ambient conditions.[103] This is attributed to the β-silicon effect or hyperconjugation, where the electrons from the σ-orbital of the C-Si bond delocalize into the coplanar π*-orbital of the C=O bond (Figure 1.6).[103] As with aldo and ketoketenes, silyl ketenes can produce 3 different polymeric backbones: including a polyketene acetal, polyketone, and a polyester.

1.6.2 Synthesis of Silyl Ketenes

Silyl ketenes have been synthesized with a variety of methods. A commonly reported synthesis includes pyrolysis of an alkynyl ether to form the desired silyl ketene (Scheme 1.3a).[104,105]
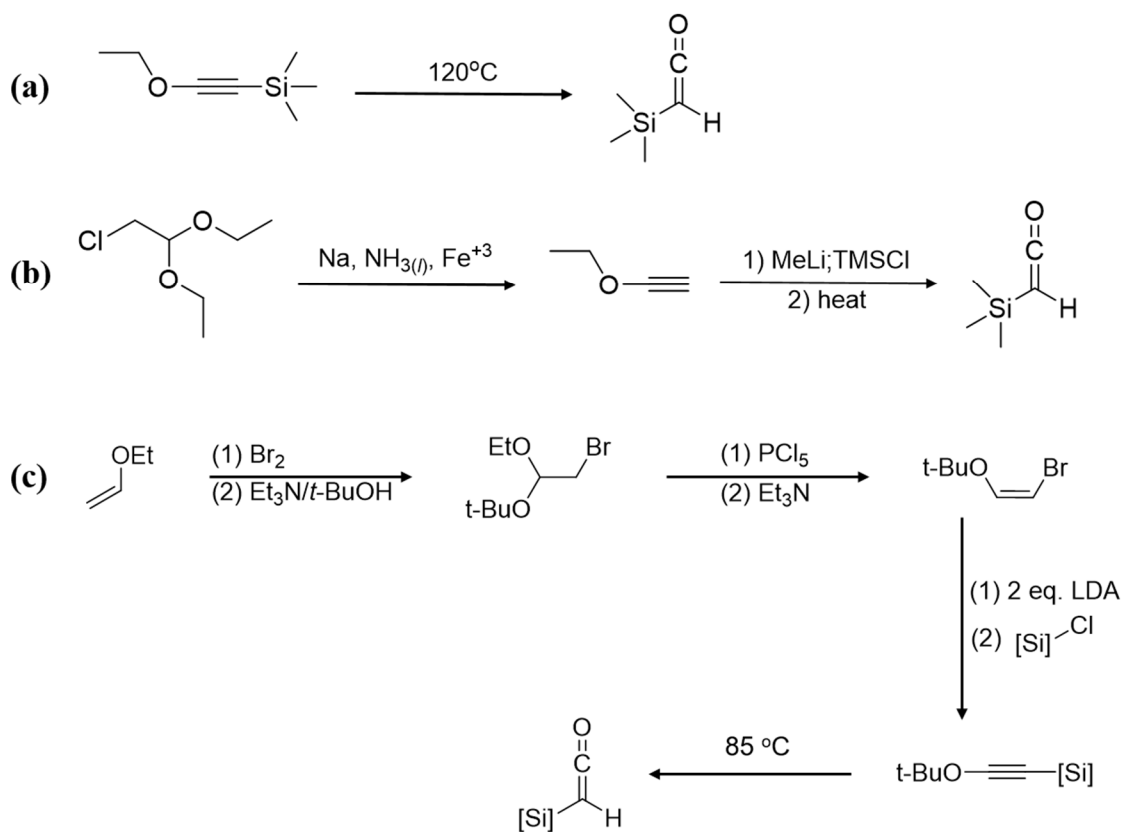
Scheme 1.3. Syntheses of silyl ketenes; (a) pyrolysis of alkylnyl ether, (b) elimination of an acetal to form ethoxyacetylene, followed by reaction with a silane and heat, (c) procedure used in Pentzer lab.

Alternatively, Black *et al*. reported the double elimination of chloroacetaldehyde diethyl acetal to form ethoxyacetylene, which was then reacted with methyllithium and chlorotrimethylsilane to obtain silylated alkyne (Scheme 1.3b).[106] Once purified, the silylated alkyne was heated to temperatures > 100 °C, forming the desired cumulated double bond structure. A similar process is used in the Pentzer lab to synthesize silyl ketenes, in which the desired ketenes are obtained in a multi-step reaction followed by a thermal rearrangement of an alkyne (Scheme 1.3c).[107,108]

Additionally, silyl ketenes have been synthesized without the use of pyrolysis or a thermal rearrangement. Lutsenko *et al*. and Baigrie *et al*. reported reacting an acid chloride with triethylamine to undergo a dehydrochlorination to afford the desired ketene.[109,110] Olah and coworkers reported the formation of trimethylsilyl ketene from the dehydration of trimethylsilylacetic acid.[111] Similarly, acetic acid derivatives can undergo zinc dehalogenation to form silyl ketenes, however multiple ketenes could be obtained depending on the acetic acid derivative. Additional methods to generate silyl ketenes include silyation of an alkynyl ether with an iodosilanes,[112,113] photochemical Wolff rearrangements,[114,115] and others.

1.6.3   Polymerization of Silyl Ketenes

Some work has been done previously in the Pentzer lab on silyl ketene reactivity and the polymerization of silyl ketenes. Initially, radical polymerization techniques were used with typical radical initiators, however no reactions were observed. Focus then shifted to anionic polymerization techniques, utilizing alkoxide initiators. It was found that modest MW polymers could be obtained with sodium and potassium *tert*-butoxide in THF.[108] The backbone of the obtained polymer contained a complex mixture of functionalities; including the polyester, polyketene acetal, polyketone, silyl enol ethers (Brook rearrangement), and α-silyl esters (Scheme 1.4a). When the counterion of the initiator was changed to lithium no polymer was obtained, but

rather a 2-pyranone compound was obtained (Scheme 1.4b).[116] It was determined that the 2-pyranone structure was a trimer of the silyl ketene monomer. The terminal carbon is deprotonated to form an alkynoate anion which undergoes nucleophilic addition of a silyl ketene, which is then followed by thermal rearrangement.

Further evaluation of reagents showed there maybe selectivity between whether nucleophilic addition or deprotonation occurs. Lithium thiolates were found to selectively undergo nucleophilic addition when *tert*-butyl diphenyl silyl ketene were used with neat conditions and well-defined oligomers were obtained (Scheme 1.4c).[117] The composition of these oligomers were thoroughly
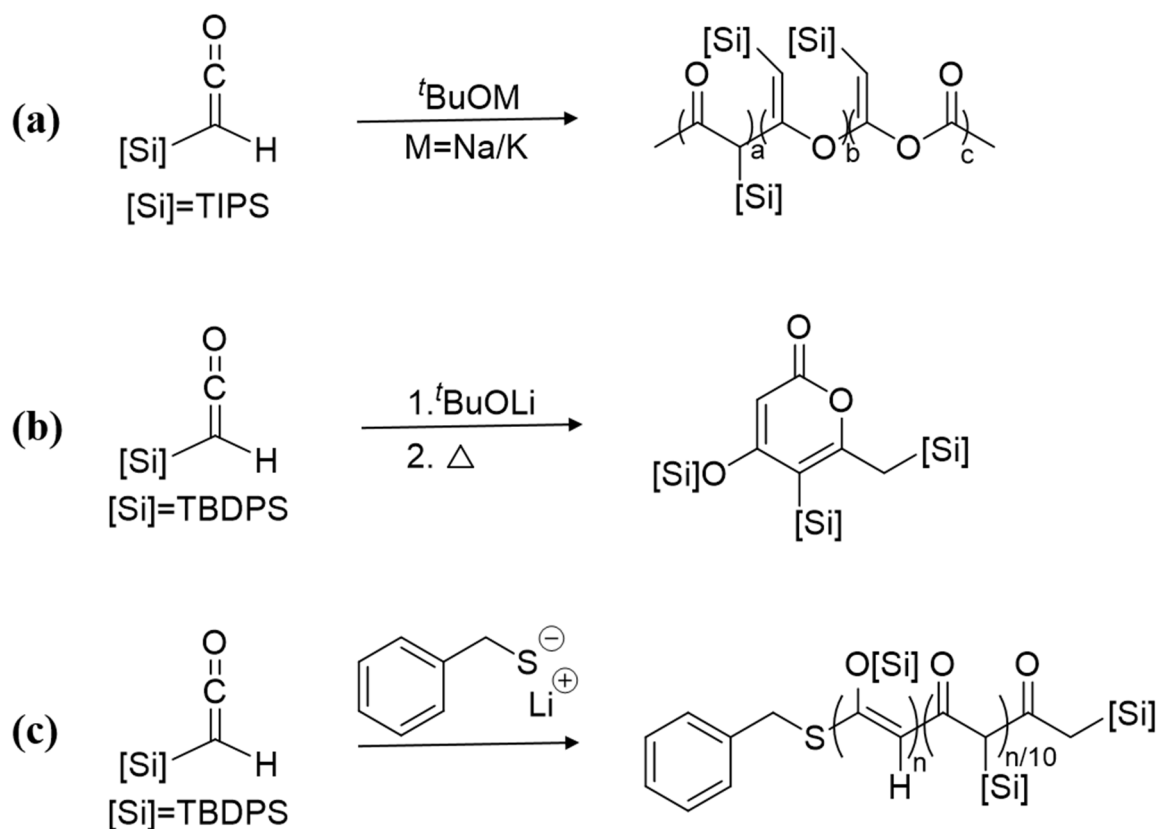
Scheme 1.4. Previous work from the Pentzer lab utilizing silyl ketenes as monomers; (a) anionic polymerization with alkoxide initiators; (b) formation of 2-pyranone from trimer; (c) lithium thiolates as initiators favoring nucleophilic addition.

characterized via IR and NMR spectroscopies. Polymerization of the C=C was prominent, which polymerization of the C=O and Brook rearrangement also being observed. When THF or cyclohexane was used, different six-membered ring products were obtained. These experimental findings were complimented with computational studies that indicate the functional groups found in the backbone dictate the rigidity of the oligomer.

1.7   Summary

Cumulated double bonds are an interesting class of compounds, the possibility of obtaining three possible backbones from one monomer is intriguing. The polymerization of isocyanates and allenes have been thoroughly studied; as well as the properties of polyisocyanates. The polymerization of ketenes, however, is understudied due to the high reactivity of ketenes and their tendency to self-dimerize. Silyl ketenes, pose the solution to this problem, with the β-silicon effect stabilizing the compound. This allows for silyl ketenes to be readily used on the benchtop and to be stored without the fear of dimerization occurring. The silicon substituent can also be used to influence the solubility of the resulting polymer. From the previous work in the Pentzer lab, silyl ketenes have great potential as monomers, however the reactivity of silyl ketenes under polymerization conditions needs further exploration. The following chapters will examine silyl ketene reactivity and their potential as monomers. Focus will remain on using Lewis acid catalysts and group transfer polymerization techniques.

1.8   References

(1)   Buss, B. L.; Miyake, G. M. Photoinduced Controlled Radical Polymerizations Performed in Flow: Methods, Products, and Opportunities. Chem. Mater. 2018, 30 (12), 3931–3942. https://doi.org/10.1021/acs.chemmater.8b01359.

(2)   Reis, M. H.; Leibfarth, F. A.; Pitet, L. M. Polymerizations in Continuous Flow: Recent Advances in the Synthesis of Diverse Polymeric Materials. ACS Macro Lett. 2020, 9 (1), 123–133. https://doi.org/10.1021/acsmacrolett.9b00933.

(3)   Holloway, J. O.; Wetzel, K. S.; Martens, S.; Du Prez, F. E.; Meier, M. A. R. Direct Comparison of Solution and Solid Phase Synthesis of Sequence-Defined Macromolecules. Polym. Chem. 2019, 10 (28), 3859–3867. https://doi.org/10.1039/c9py00558g.

(4)   Vrijsen, J. H.; Osiro Medeiros, C.; Gruber, J.; Junkers, T. Continuous Flow Synthesis of Core Cross-Linked Star Polymers: Via Photo-Induced Copper Mediated Polymerization. Polym. Chem. 2019, 10 (13), 1591–1598. https://doi.org/10.1039/c9py00134d.

(5)   Reis, M. H.; Davidson, C. L. G.; Leibfarth, F. A. Continuous-Flow Chemistry for the Determination of Comonomer Reactivity Ratios. Polym. Chem. 2018, 9 (13), 1728–1734. https://doi.org/10.1039/c7py01938f.

(6)   Radzinski, S. C.; Foster, J. C.; Scannelli, S. J.; Weaver, J. R.; Arrington, K. J.; Matson, J. B. Tapered Bottlebrush Polymers: Cone-Shaped Nanostructures by Sequential Addition of Macromonomers. ACS Macro Lett. 2017, 6 (10), 1175–1179. https://doi.org/10.1021/acsmacrolett.7b00724.

(7)   Lee, J.; Kalin, A. J.; Yuan, T.; Al-Hashimi, M.; Fang, L. Fully Conjugated Ladder Polymers. Chem. Sci. 2017, 8 (4), 2503–2521. https://doi.org/10.1039/C7SC00154A.

(8)   Kensy, V. K.; Tritt, R. L.; Haque, F. M.; Murphy, L. M.; Knorr, D. B.; Grayson, S. M.; Boydston, A. J. Molecular Weight Control via Cross Metathesis in Photo-Redox Mediated Ring-Opening Metathesis Polymerization. Angew. Chemie - Int. Ed. 2020, 59, 2–8. https://doi.org/10.1002/anie.202000434.

(9)   Carmean, R. N.; Becker, T. E.; Sims, M. B.; Sumerlin, B. S. Ultra-High Molecular Weights via Aqueous Reversible-Deactivation Radical Polymerization. Chem 2017, 2 (1), 93–101. https://doi.org/10.1016/j.chempr.2016.12.007.

(10)   Beyer, V. P.; Kim, J.; Remzi Becer, C. Synthetic Approaches for Multiblock Copolymers. Polym. Chem. 2020, 11 (7), 1271–1291. https://doi.org/10.1039/c9py01571j.

(11)   Teo, Y. C.; Lai, H. W. H.; Xia, Y. Synthesis of Ladder Polymers: Developments, Challenges, and Opportunities. Chem. - A Eur. J. 2017, 23 (57), 14101–14112. https://doi.org/10.1002/chem.201702219.

(12)   Shafranek, R. T.; Millik, S. C.; Smith, P. T.; Lee, C. U.; Boydston, A. J.; Nelson, A. Stimuli-Responsive Materials in Additive Manufacturing. Prog. Polym. Sci. 2019, 93, 36–67. https://doi.org/10.1016/j.progpolymsci.2019.03.002.

(13)   Wei, P.; Leng, H.; Chen, Q.; Advincula, R. C.; Pentzer, E. B. Reprocessable 3D-Printed Conductive Elastomeric Composite Foams for Strain and Gas Sensing. ACS Appl. Polym. Mater. 2019, 1 (4), 885–892. https://doi.org/10.1021/acsapm.9b00118.

(14)   Ligon, S. C.; Liska, R.; Stampfl, J.; Gurr, M.; Mülhaupt, R. Polymers for 3D Printing and Customized Additive Manufacturing. Chem. Rev. 2017, 117 (15), 10212–10290. https://doi.org/10.1021/acs.chemrev.7b00074.

(15)   Zaquen, N.; Yeow, J.; Junkers, T.; Boyer, C.; Zetterlund, P. B. Visible Light-Mediated Polymerization-Induced Self-Assembly Using Continuous Flow Reactors. Macromolecules 2018, 51 (14), 5165–5172. https://doi.org/10.1021/acs.macromol.8b00887.

(16)   Scott, P. J.; Kasprzak, C. R.; Feller, K. D.; Meenakshisundaram, V.; Williams, C. B.; Long, T. E. Light and Latex: Advances in the Photochemistry of Polymer Colloids. Polym. Chem. 2020. https://doi.org/10.1039/d0py00349b.

(17)   Varlas, S.; Keogh, R.; Xie, Y.; Horswell, S. L.; Foster, J. C.; O'Reilly, R. K. Polymerization-Induced Polymersome Fusion. J. Am. Chem. Soc. 2019, 141 (51), 20234–20248. https://doi.org/10.1021/jacs.9b10152.

(18)   Canning, S. L.; Smith, G. N.; Armes, S. P. A Critical Appraisal of RAFT-Mediated Polymerization-Induced Self-Assembly. Macromolecules 2016, 49 (6), 1985–2001. https://doi.org/10.1021/acs.macromol.5b02602.

(19)   Arrington, K. J.; Haag, J. V.; French, E. V.; Murayama, M.; Edgar, K. J.; Matson, J. B. Toughening Cellulose: Compatibilizing Polybutadiene and Cellulose Triacetate Blends. ACS Macro Lett. 2019, 8 (4), 447–453. https://doi.org/10.1021/acsmacrolett.9b00136.

(20)   Blasco, E.; Sims, M. B.; Goldmann, A. S.; Sumerlin, B. S.; Barner-Kowollik, C. 50th Anniversary Perspective: Polymer Functionalization. Macromolecules 2017, 50 (14), 5215–5252. https://doi.org/10.1021/acs.macromol.7b00465.

(21)   Xu, J.; Eagan, J. M.; Kim, S. S.; Pan, S.; Lee, B.; Klimovica, K.; Jin, K.; Lin, T. W.; Howard, M. J.; Ellison, C. J.; Lapointe, A. M.; Coates, G. W.; Bates, F. S. Compatibilization of Isotactic Polypropylene (IPP) and High-Density Polyethylene (HDPE) with IPP-PE Multiblock Copolymers. Macromolecules 2018, 51 (21), 8585–8596. https://doi.org/10.1021/acs.macromol.8b01907.

(22)   Xiang, T.; Wang, L. R.; Ma, L.; Han, Z. Y.; Wang, R.; Cheng, C.; Xia, Y.; Qin, H.; Zhao, C. S. From Commodity Polymers to Functional Polymers. Sci. Rep. 2015, 4, 4604. https://doi.org/10.1038/srep04604.

(23)   Barkley, D. A.; Jiang, N.; Sen, M.; Endoh, M. K.; Rudick, J. G.; Koga, T.; Zhang, Y.; Gang, O.; Yuan, G.; Satija, S. K.; Kawaguchi, D.; Tanaka, K.; Karim, A. Chain Conformation near

the Buried Interface in Nanoparticle-Stabilized Polymer Thin Films. Macromolecules 2017, 50 (19), 7657–7665. https://doi.org/10.1021/acs.macromol.7b01187.

(24)   Chakma, P.; Konkolewicz, D. Dynamic Covalent Bonds in Polymeric Materials. Angew. Chemie - Int. Ed. 2019, 58 (29), 9682–9695. https://doi.org/10.1002/anie.201813525.

(25)   He, C.; Shi, S.; Wang, D.; Helms, B. A.; Russell, T. P. Poly(Oxime-Ester) Vitrimers with Catalyst-Free Bond Exchange. J. Am. Chem. Soc. 2019, 141 (35), 13753–13757. https://doi.org/10.1021/jacs.9b06668.

(26)   De Hoe, G. X.; Zumstein, M. T.; Tiegs, B. J.; Brutman, J. P.; McNeill, K.; Sander, M.; Coates, G. W.; Hillmyer, M. A. Sustainable Polyester Elastomers from Lactones: Synthesis, Properties, and Enzymatic Hydrolyzability. J. Am. Chem. Soc. 2018, 140 (3), 963–973. https://doi.org/10.1021/jacs.7b10173.

(27)   Lundberg, D. J.; Lundberg, D. J.; Hillmyer, M. A.; Dauenhauer, P. J. Techno-Economic Analysis of a Chemical Process to Manufacture Methyl-ε-Caprolactone from Cresols. ACS Sustain.   Chem.   Eng.   2018,   6   (11),   15316–15324. https://doi.org/10.1021/acssuschemeng.8b03774.

(28)   Li, L.; Chen, X.; Jin, K.; Torkelson, J. M. Vitrimers Designed Both to Strongly Suppress Creep and to Recover Original Cross-Link Density after Reprocessing: Quantitative Theory and Experiments.   Macromolecules   2018,   51   (15),   5537–5546. https://doi.org/10.1021/acs.macromol.8b00922.

(29)   El-Zaatari, B. M.; Ishibashi, J. S. A.; Kalow, J. A. Cross-Linker Control of Vitrimer Flow. Polym. Chem. 2020. https://doi.org/10.1039/d0py00233j.

(30)   Lewis, S. E.; Wilhelmy, B. E.; Leibfarth, F. A. Upcycling Aromatic Polymers through C-H Fluoroalkylation. Chem. Sci. 2019, 10 (25), 6270–6277. https://doi.org/10.1039/c9sc01425j.

(31)   Lewis, S. E.; Wilhelmy, B. E.; Leibfarth, F. A. Organocatalytic C–H Fluoroalkylation of Commodity Polymers. Polym. Chem. 2020. https://doi.org/10.1039/c9py01884k.

(32)   Arslan, M.; Acik, G.; Tasdelen, M. A. The Emerging Applications of Click Chemistry Reactions in the Modification of Industrial Polymers. Polym. Chem. 2019, 10 (28), 3806–3821. https://doi.org/10.1039/c9py00510b.

(33)   Short, G. N.; Nguyen, H. T. H.; Scheurle, P. I.; Miller, S. A. Aromatic Polyesters from Biosuccinic Acid. Polym. Chem. 2018, 9 (30), 4113–4119. https://doi.org/10.1039/c8py00862k.

(34)   Gandini, A.; Lacerda, T. M.; Carvalho, A. J. F.; Trovatti, E. Progress of Polymers from Renewable Resources: Furans, Vegetable Oils, and Polysaccharides. Chem. Rev. 2016, 116 (3), 1637–1669. https://doi.org/10.1021/acs.chemrev.5b00264.

(35)   Hatton, F. L. Recent Advances in RAFT Polymerization of Monomers Derived from Renewable Resources. Polym. Chem. 2020, 11 (2), 220–229. https://doi.org/10.1039/c9py01128e.

(36)   Odian, G. Principles of Polymerization, 4th ed.; John Wiley & Sons, Inc.: Hoboken, New Jersey, 2004.

(37)   Rudin, A.; Choi, P. The Elements of Polymer Science & Engineering, 3rd ed.; Academic Press, 2012. https://doi.org/10.1016/B978-0-12-382178-2.00007-9.

(38)   Handbook of Radical Polymerization; Matyjaszewski, K., Davis, T. P., Eds.; John Wiley & Sons, Inc., 2002.

(39)   Handbook of Ring-Opening Polymerization; Dubois, P., Coulembier, O., Raquez, J., Eds.; Wiley-VCH Verlag GmbH & Co. KGaA, 2009.

(40)   Buchmeiser, M. R. Ring-Opening Metathesis Polymerization. In Ring-Opening Polymerization; Dubois, P., Coulembier, O., Raquez, J., Eds.; Wiley-VCH Verlag GmbH & Co. KGaA, 2009; pp 197–225.

(41)   Chen, Y.; Kakuchi, T. Organocatalyzed Group Transfer Polymerization. Chem. Rec. 2016, 16 (4), 2161–2183. https://doi.org/10.1002/tcr.201600034.

(42)   Stefan, M. C.; Javier, A. E.; Osaka, I.; McCullough, R. D. Grignard Metathesis Method (GRIM): Toward a Universal Method for the Synthesis of Conjugated Polymers. Macromolecules 2009, 42 (1), 30–32. https://doi.org/10.1021/ma8020823.

(43)   Stefan, M. C.; Bhatt, M. P.; Sista, P.; Magurudeniya, H. D. Grignard Metathesis (GRIM) Polymerization for the Synthesis of Conjugated Block Copolymers Containing Regioregular Poly(3-Hexylthiophene). Polym. Chem. 2012, 3 (7), 1693–1701. https://doi.org/10.1039/c1py00453k.

(44)   Ozaki, S. Recent Advances in Isocyanate Chemistry. Chem. Rev. 1972, 72 (5), 457–496. https://doi.org/10.1021/cr60279a002.

(45)   Lyman, D. J. Polyurethanes. I. The Solution Polymerization of Diisocyanates with Ethylene Glycol. J. Polym. Sci. 1960, 45 (145), 49–59. https://doi.org/10.1002/pol.1960.1204514505.

(46)   Shashoua, V. E. The Homopolymerization of Monoisocyanates. J. Am. Chem. Soc. 1959, 81 (12), 3156–3156.

(47)   Sardon, H.; Pascual, A.; Mecerreyes, D.; Taton, D.; Cramail, H.; Hedrick, J. L. Synthesis of Polyurethanes Using Organocatalysis: A Perspective. Macromolecules 2015, 48 (10), 3153–3165. https://doi.org/10.1021/acs.macromol.5b00384.

(48)   Sharmin, E.; Zafar, F. Polyurethane: An Introduction; IntechOpen, 2012. https://doi.org/10.5772/51663.

(49)   Shashoua, V. E.; Sweeny, W.; Tietz, R. F. The Homopolymerization of Monoisocyanates. J. Am. Chem. Soc. 1960, 82 (4), 866–873.

(50)   Okamoto, Y.; Nagamura, Y.; Hatada, K.; Khatri, C.; Green, M. M. An Unexpected Chiral Spiro Tetramer Offers Mechanistic Insight into an Improved Sodium Cyanide Initiated Polymerization of N-Hexyl Isocyanate in Toluene. Macromolecules 1992, 25 (20), 5536–5538. https://doi.org/10.1021/ma00046a066.

(51)   Lee, J. S.; Ryu, S. W. Anionic Living Polymerization of 3-(Triethoxysilyl)Propyl Isocyanate. Macromolecules 1999, 32 (6), 2085–2087. https://doi.org/10.1021/ma9817065.

(52)   Shin, Y. D.; Ahn, J. H.; Lee, J. S. Anionic Polymerization of Isocyanates with Optical Functionalities. Polymer (Guildf). 2001, 42 (19), 7979–7985. https://doi.org/10.1016/S0032-3861(01)00324-X.

(53)   Shin, Y. D.; Kim, S. Y.; Ahn, J. H.; Lee, J. S. Synthesis of Poly(n-Hexyl Isocyanate) by Controlled Anionic Polymerization in the Presence of NaBPh4. Macromolecules 2001, 34 (8), 2408–2410. https://doi.org/10.1021/ma0019813.

(54)   Chae, C.-G.; Seo, H.-B.; Bak, I.-G.; Lee, J.-S. Synthesis of Amphiphilic Helix−Coil−Helix Poly(3- (Glycerylthio)Propyl Isocyanate)-Block-Polystyrene-Block-Poly(3- (Glycerylthio)Propyl Isocyanate). Macromolecules 2018, 51 (3), 697–704.

(55)   Zorba, G.; Vazaios, A.; Pitsikalis, M.; Hadjichristidis, N. Anionic Polymerization of N-Hexyl Isocyanate with Monofuctional Initiators. Synthesis of Well-Defined Diblock Copolymers with Styrene and Isoprene. J. Polym. Sci. Part A Polym. Chem. 2005, 43 (16), 3533–3542. https://doi.org/10.1002/pola.20831.

(56)   Ahn, J. H.; Shin, Y. D.; Nath, G. Y.; Park, S. Y.; Rahman, M. S.; Samal, S.; Lee, J. S. Unprecedented Control over Polymerization of N-Hexyl Isocyanate Using an Anionic Initiator Having Synchronized Function of Chain-End Protection. J. Am. Chem. Soc. 2005, 127 (12), 4132–4133. https://doi.org/10.1021/ja0427000.

(57)   Min, J.; Shah, P. N.; Ahn, J. H.; Lee, J. S. Effects of Different Reactive Oxyanionic Initiators on the Anionic Polymerizaition of N-Hexyl Isocyanate. Macromolecules 2011, 44 (9), 3211–3216. https://doi.org/10.1021/ma200414f.

(58)   Min, J.; Yoo, H. S.; Shah, P. N.; Chae, C. G.; Lee, J. S. Enolate Anionic Initiator, Sodium Deoxybenzoin, for Leading Living Natures by Formation of Aggregators at the Growth Chain Ends. J. Polym. Sci. Part A Polym. Chem. 2013, 51 (8), 1742–1748. https://doi.org/10.1002/pola.26550.

(59)   Patten, T. E.; Novak, B. M. "Living" Titanium(IV) Catalyzed Coordination Polymerizations of Isocyanates. J. Am. Chem. Soc. 1991, 113 (13), 5065–5066. https://doi.org/10.1021/ja00013a055.

(60)   Patten, T. E.; Novak, B. M. Organotitanium(IV) Compounds as Catalysts for the Polymerization of Isocyanates: The Polymerization of Isocyanates with Functionalized Side Chains. Macromolecules 1993, 26 (3), 436–439. https://doi.org/10.1021/ma00055a005.

(61)   Patten, T. E.; Novak, B. M. Living Organotitanium(IV)-Catalyzed Polymerizations of Isocyanates. J. Am. Chem. Soc. 1996, 118 (8), 1906–1916. https://doi.org/10.1021/ja9534516.

(62)   Hoff, S. M.; Novak, B. M. Complex Architectures through Living Polymerizations. The Synthesis of "Once-Broken Worms" and Triblock Copolymers Using Bimetallic Initiators. Macromolecules 1993, 26 (15), 4067–4069. https://doi.org/10.1021/ma00067a056.

(63)   Natta, G.; DiPietro, J.; Cambini, M. Crystalline Polymers of Phenyl- and n-Butylisocyanates. Macromol. Chem. Phys. 1962, 56 (1), 200–207.

(64)   Goodman, M.; Chen, S. Optically Active Polyisocyanates. Macromolecules 1970, 3 (4), 398–402. https://doi.org/10.1007/978-3-540-72816-0_15718.

(65)   Green, M. M.; Peterson, N. C.; Sato, T.; Teramoto, A.; Cook, R.; Lifson, S. A Helical Polymer with a Cooperative Response to Chiral Information. Science (80-.). 1995, 268 (5219), 1860–1866. https://doi.org/10.1126/science.268.5219.1860.

(66)   Maeda, K.; Okamoto, Y. Synthesis and Conformation of Optically Active Poly(Phenyl Isocyanate)s Bearing an ((S)-(R-Methylbenzyl)Carbamoyl) Group. Macromolecules 1998, 31 (4), 1046–1052. https://doi.org/10.1021/ma970948m.

(67)   Green, M. M.; Khatri, C. A.; Reidy, M. P.; Levon, K. Dilute-Solution Chiral Optical Changes Signal the Thermally Reversible Gelation of Poly(n-Hexyl Isocyanate) in Hydrocarbon Solvents. Macromolecules 1993, 26 (17), 4723–4725. https://doi.org/10.1021/ma00069a050.

(68)   Maxein, G.; Mayer, S.; Zentel, R. Structure-Property Relations in Cholesteric Networks from Chiral Polyisocyanates. Macromolecules 1999, 32 (18), 5747–5754. https://doi.org/10.1021/ma990326w.

(69)   Itou, T.; Teramoto, A. Isotropic-Liquid Crystal Phase Equilibrium in Solutions of Semiflexible Polymers: Poly(Hexyl Isocyanate). Macromolecules 1988, 21 (7), 2225–2230. https://doi.org/10.1021/ma00185a058.

(70)   Aharoni, S. M. Rigid Backbone Polymers. 2. Polyisocyanates and Their Liquid-Crystal Behavior. Macromolecules 1979, 12 (1), 94–103. https://doi.org/10.1021/ma60067a021.

(71)   Taylor, D. R. The Chemistry of Allenes. Chem. Rev. 1967, 67 (3), 317–359. https://doi.org/10.1021/cr60247a004.

(72)   Rivera-Fuentes, P.; Diederich, F. Allenes in Molecular Materials. Angew. Chemie - Int. Ed. 2012, 51 (12), 2818–2828. https://doi.org/10.1002/anie.201108001.

(73)   Weinstein, B.; Fenselau, A. . Oligomers of Allene. Part II. Dimers and Trimers Formed in the Thermal Polymerisation of Liquid Allene. J. Chem. Soc. C 1967, 368–372.

(74)   Weinstein, B.; Fenselau, A. H. Oligomers of Allene. III. Tetramers Formed in the Thermal Polymerization of Liquid Allene. J. Org. Chem. 1967, 32 (7), 2278–2283. https://doi.org/10.1021/jo01282a041.

(75)   Dai, S. H.; Dolbier, W. R. Oligomerization and Co-Oligomerizations of Allene. J. Org. Chem. 1972, 37 (7), 950–955. https://doi.org/10.1021/jo00972a007.

(76)   Takahashi, T.; Yokozawa, T.; Endo, T. Cationic Polymerization of Methoxyallene with Lewis   Acids.   Die   Makromol.   Chemie   1991,   192   (5),   1207–1212. https://doi.org/10.1002/macp.1991.021920519.

(77)   Takahashi, T.; Yokozawa, T.; Endo, T. Cationic Polymerization of Gamma-Methyl- and Alpha-Methylphenylallene. J. Polym. Sci. Part A Polym. Chem. 1992, 30, 583–587.

(78)   Yokozawa, T.; Tanaka, M.; Endo, T. Radical Polymerization of Alkoxyallenes. Chem. Lett. 1987, 16 (9), 1831–1834. https://doi.org/10.1246/cl.1987.1831.

(79)   Suzuki, M.; Takao, T.; Sakamoto, N.; Tomita, I.; Endo, T. Ni-Catalyzed Living Coordination Polymerization of Allenes Having Si-Based Functional Groups. Polymer Journal. 1999, pp 1021–1024. https://doi.org/10.1295/polymj.31.1021.

(80)   Endo, T.; Takagi, K.; Tomita, I. Design and Synthesis of Polymerizable Cumulated Double Bond System. - Living Coordination Polymerization of Alkylallenes by Π-Allylnickel Catalyst-. Tetrahedron 1997, 53 (45), 15187–15196. https://doi.org/10.1016/S0040-4020(97)00956-3.

(81)   Choi, J. C.; Osakada, K.; Yamaguchi, I.; Yamamoto, T. Polymerization of Arylallenes Catalyzed by Organo-Rhodium(I) and -Cobalt (I) Complexes to Give Structurally Regulated High-Mass   Polymers.   Appl.   Organomet.   Chem.   1997,   11   (12),   957–961. https://doi.org/10.1002/(SICI)1099-0739(199712)11:12<957::AID-AOC654>3.0.CO;2-1.

(82)   Takagi, K.; Tomita, I.; Endo, T. A Novel Living Coordination Polymerization of Phenylallene Derivatives by π-Allylnickel Catalyst. Macromolecules 1997, 30 (24), 7386–7390. https://doi.org/10.1021/ma9708959.

(83)   Lin, F.; Liu, Z.; Wang, T.; Cui, D. Highly 2,3-Selective Polymerization of Phenylallene and Its Derivatives with Rare-Earth Metal Catalysts: From Amorphous to Crystalline Products. Angew. Chemie - Int. Ed. 2017, 56 (46), 14653–14657. https://doi.org/10.1002/anie.201707601.

(84)   Yamauchi, A.; Shirai, A.; Kawabe, K.; Iwamoto, T.; Wakiya, T.; Nishiyama, H.; Inagi, S.; Tomita, I. Well-Defined Polymer Microspheres Formed by Living Dispersion Polymerization: Precisely Functionalized Crosslinked Polymer Microspheres from Monomers Possessing Cumulated Double Bonds. Asia Mater. 2016, 8, 1–12. https://doi.org/10.1038/am.2016.123.

(85)   Sakai, K.; Nishiyama, H.; Inagi, S.; Tomita, I.; Hibi, Y.; Komura, M.; Nose, K.; Iyoda, T. Synthesis of Well-defined Block Copolymer Composed of Flexible Amphiphilic Poly(Ethylene Glycol) and Hydrophobic Liquid Crystalline Segments by Living Coordination Polymerization of Allene Derivatives and Its Application to Thin Film with Perpendicularly. J. Polym. Sci. 2020, No. January, 1–8. https://doi.org/10.1002/pol.20190165.

(86)   Havinga, R.; Schors, A.; Visser, J. W. Preparation and Properties of Polyallenes . II . Phase Transitions of Polyallene. J. Macromol. Sci. 1968, 2 (1), 21–30. https://doi.org/10.1080/00222336808053344.

(87)   Huisgen, R.; Otto, P. The Mechanism of Dimerization of Dimethylketene. J. Am. Chem. Soc. 1968, 90 (19), 5342–5343. https://doi.org/10.1021/ja01021a090.

(88)   Elam, E. U. Ketenes. XI. Preparation of β-Lactone Dimer by Dimerization of Dimethylketene in the Presence of Derivatives of Trivalent Phosphorus. J. Org. Chem. 1967, 32 (1), 215–216. https://doi.org/10.1021/jo01277a053.

(89) Hasek, R. H.; Clark, R. D.; Elam, E. U.; Martin, J. C. The Chemistry of Dimethylketene Dimer. IV. The Polyester and β-Lactone Dimer of Dimethylketene. J. Org. Chem. 1962, 27 (1), 60–64. https://doi.org/10.1021/jo01048a015.

(90) Staudinger, H. Ketene: Uber Additions Und Polymerisationreaktionen Des Dimethylketens. Helvetica 1925, 8 (1), 306–332.

(91) Natta, G.; Mazzanti, G.; Pregaglia, G.; Binaghi, M. Alternating Copolymers of Dimethylketene with Ketones. J. Am. Chem. Soc. 1960, 82 (20), 5511–5512. https://doi.org/10.1021/ja01505a057.

(92) Pregaglia, G. F.; Binaghi, M.; Cambini, M. Polydimethylketene with Carbon- Oxygen Backbone Stnicture. Macromol. Chem. Phys. 1963, 67 (1), 10–30.

(93) Yamashita, Y.; Miura, S.; Nakamura, M. Ambident Nature of the Polydimethylketene Anion. Die Makromol. Chemie 1963, 68 (1), 31–47. https://doi.org/10.1002/macp.1963.020680104.

(94) Natta, G.; Mazzanti, G.; Pregaglia, G. F.; Pozzi, G. Alternating Copolymers Having a Stereoregular Polyester Structure. J. Polym. Sci. 1962, 58 (166), 1201–1210. https://doi.org/10.1002/pol.1962.1205816676.

(95) Tsunetsugu, T.; Arimoto, K.; Fueno, T.; Furukawa, J. Polymerization of Methylphenylketene and Its Copolymerization with Benzaldehyde. Macromol. Chem. Phys. 1968, 112 (1), 210–219.

(96) Yamashita, S.; Nunomoto, Y. Polymerizability of Diphenylketene. Kogyo Kagaku Zasshi 1968, 71 (12), 2067–2072.

(97) Dyer, E.; Sincich, E. Anionic Copolymerization of Isocyanates With Ketenes. J. Polym. Sci. Polym. Chem. Ed. 1973, 11 (6), 1249–1260. https://doi.org/10.1002/pol.1973.170110612.

(98) Sudo, A.; Uchino, S.; Endo, T. Development of a Living Anionic Polymerization of Ethylphenylketene: A Novel Approach to Well-Defined Polyester Synthesis. Macromolecules 1999, 32 (5), 1711–1713. https://doi.org/10.1021/ma981567r.

(99) Natta, G.; Mazzanti, G.; Pregaglia, G.; Binaghi, M.; Peraldo, M. Crystalline Polymers of Dimethylketene. J. Am. Chem. Soc. 1960, 82 (17), 4742–4743. https://doi.org/10.1021/ja01502a073.

(100) Egret, H.; Couvercelle, J. P.; Belleney, J.; Bunel, C. Cationic Polymerization of Dimethyl Ketene. Eur. Polym. J. 2002, 38 (10), 1953–1961. https://doi.org/10.1016/S0014-3057(02)00102-7.

(101) Nagai, D.; Sudo, A.; Endo, T. Stereocontrolled Anionic Alternating Copolymerization of Ethylphenylketene with Benzaldehyde by a Bisoxazoline Ligand. J. Polym. Sci. Part A Polym. Chem. 2004, 42 (21), 5384–5388. https://doi.org/10.1002/pola.20310.

(102) Nagai, D.; Sudo, A.; Endo, T. Anionic Alternating Copolymerization of Ketene and Aldehyde: Control of Enantioselectivity by Bisoxazoline-Type Ligand for Synthesis of Optically Active Polyesters. Macromolecules 2006, 39 (26), 8898–8900. https://doi.org/10.1021/ma0620971.

(103) Tidwell, T. T. Ketenes II, 2nd ed.; John Wiley & Sons, Inc.: Hoboken, New Jersey, 2006.

(104) Ruden, R. A. Trimethylsilylketene. Acylation and Olefination Reactions. J. Org. Chem. 1974, 39 (24), 3607–3608. https://doi.org/10.1021/jo00938a041.

(105) Valentí, E.; Pericàs, M. A.; Serratosa, F. Convenient Synthesis of Silylketenes from 1-Tert-Butoxy-2-Silylethynes. J. Org. Chem. 1990, 55 (1), 395–397. https://doi.org/10.1021/jo00288a081.

(106) Black, T. H.; Farrell, J. R.; Probst, D. A.; Zotz, M. C. A High Yielding, Reproducible Synthesis of Trimethylsilylketene. Synth. Commun. 2002, 32 (13), 2083–2088. https://doi.org/10.1081/SCC-120004861.

(107) Pericàs, M. A.; Serratosa, F.; Valentí, E. An Efficient Synthesis of Tert-Alkoxyethynes. Tetrahedron 1987, 43 (10), 2311–2316. https://doi.org/10.1016/S0040-4020(01)86815-0.

(108) Xiang, Y.; Burrill, D. J.; Bullard, K. K.; Albrecht, B. J.; Tragesser, L. E.; McCaffrey, J.; Lambrecht, D. S.; Pentzer, E. Polymerization of Silyl Ketenes Using Alkoxide Initiators: A Combined Computational and Experimental Study. Polym. Chem. 2017, 8 (35), 5381–5387. https://doi.org/10.1039/C7PY00858A.

(109) Lutsenko, I. F.; Baukov, Y. I.; Kostyuk, A. S.; Savelyeva, N. I.; Krysina, V. K. Interaction of Ketene with Silylated Amines or Amides. J. Organomet. Chem. 1969, 17 (2), 241–262. https://doi.org/10.1016/S0022-328X(00)88613-1.

(110) Baigrie, L. M.; Seiklay, H. R.; Tidwell, T. T. Stereospecific Formation of Enolates from Reaction of Unsymmetrical Ketenes and Organolithium Reagents. J. Am. Chem. Soc. 1985, 107 (19), 5391–5396. https://doi.org/10.1021/ja00305a012.

(111) Olah, G. A.; Wu, A.; Farooq, O. Intramolecular Dehydration of Dialkylacetic Acids and Trimethylsilylacetic Acid with Dicyclohexylcarbodiimide to the Corresponding Stable Ketenes. Synthesis (Stuttg). 1989, 568.

(112) Sakurai, H.; Shirahata, A.; Sasaki, K.; Hosomi, A. A Convenient Synthesis of Iodotrimethylsilane and Its Use in the Preparation of Silylketenes. Synthesis (Stuttg). 1979, 740.

(113) Pons, J.; Kocienski, P. A Synthesis of (-)-Tetrahydrolipstatin. Tetrahedron Lett. 1989, 30 (14), 1833–1836.

(114) Brückmann, R.; Schneider, K.; Maas, G. Wolff Rearrangement of (1-Diazo-2-Oxoalkyl) Silanes. Tetrahedron 1989, 45 (17), 5517–5530. https://doi.org/10.1016/S0040-4020(01)89498-9.

(115) Gerhard Maas; Brückmann, R. Preparation of 1-Aryl-2-Siloxyalkynes from Silylated Alpha-Diazo Carbonyl Compounds. J. Org. Chem 1985, 50, 2801–2802.

(116) Xiang, Y.; Rheingold, A. L.; Pentzer, E. B. Synthesis of Highly Functionalized 2-Pyranone from Silyl Ketene. ACS Omega 2018, 3 (8), 9419–9423. https://doi.org/10.1021/acsomega.8b01531.

(117) Xiang, Y.; Mitchell, S.; Rheingold, A. L.; Lambrecht, D. S.; Pentzer, E. Oligomerization of Silyl Ketene: Favoring Chain Extension over Backbiting. Macromolecules 2019, 52 (16), 6126–6134. https://doi.org/10.1021/acs.macromol.9b00752.

Part I: Silyl Ketenes as Building Blocks for Small Molecules and Polymers

Chapter 2

Lewis Acid-Activated Reactions of Silyl Ketenes for the Preparation of α-Silyl Carbonyl Compounds

Portions of this chapter appear in the following manuscript:

2.1   Introduction

Silyl ketenes have been used in a variety of transformations to produce small molecules ranging from silyl ketene acetals which are initiators for group transfer polymerization to various cyclic molecules from cycloadditions. Similarly, to other cumulated doubles bonds, cycloadditions are very accessible with silyl ketenes through self-dimerization and other techniques. For example, silyl ketenes have been reacted with saturated aldehydes undergoing a [2+2] cycloaddition to form 2-oxetanones in the presence of a Lewis acid.[118]   There have been multiple additional reports also utilizing the [2+2] cycloaddition of silyl ketenes and aldehydes to form various oxetanones.[119–121] Rossé *et al*. further expanded the scope of this reaction by performing a ring-opening reaction with the 2-oxetanones and thiols to form sulfanyl-carboxylic acid derivatives.[122] [2+2] cycloadditions have also been utilized with silyl ketenes to produce a variety of other compounds; including cyclobutanones,[123,124] β-lactams,[20] and β-lactones.[125,126] Silyl ketenes have also been used in [4+2] cycloadditions with diazadienes to produce pyrimidine and with isocyanates to produce a silyloxyoxazinone.[127–129]   Silyl ketenes have been used in a number of reactions that are not cycloadditions. For example, silyl ketenes were reacted with Wittig reagents to produce allenes and underwent a Peterson elimination to produce silylated alkynes.[129,130] Prior work from the Pentzer lab reported that we silyl ketenes can react with anionic initiators to form oligomers, and with alkoxide initiators to form a polymer with a mixture of backbone functional groups (esters, ketene acetal, ketone).[108,117] The limitation in these systems was the occurrence of backbiting and secondary reactions.

In literature Lewis acids (LAs) have been used to activate carbonyl-containing compounds for a variety of reactions, including polymerizations.[131,132] Particularly, a LA can coordinate to the oxygen atom of a carbonyl, making the carbon atom more electrophilic and susceptible to the addition of a nucleophile.[133,134] For example, LAs have been used to catalyze the ring opening

polymerization of lactones, where the LA coordinates to the carbonyl and a nucleophile can ring open the lactone promoting polymerization. This approach can be applied to silyl ketenes, were the oxygen atom of the ketene coordinates to a LA and the central atom of the ketene becomes more electrophilic. For example, Ruden *et al.* used a catalytic amount of the $BF_3 \cdot OEt_2$ to activate trimethylsilyl (TMS) ketene and illustrated the addition of t-butyl alcohol to the central carbon for the preparation of an α-silyl ester.[135] The use of a LA decreased the reaction time from 48 h for the non-catalyzed reaction to only 2 min. In a similar vein, zinc halide salts and organocerium reagents have been used to catalyze the formation of α-silyl esters from silyl ketenes.[136–140]

α-Silyl carbonyls provide an interesting scaffold for further modification, but are difficult to prepare by more traditional approaches. For example, if the carbon atom alpha to the carbonyl of an ester is deprotonated, the resulting enolate undergoes O-silylation upon reaction with, e.g., a trialkyl silyl chloride. For modification, α-silyl esters can undergo Peterson olefination to produce alkenes or reaction with Grignard reagents gives access to β-keto silanes.[141,142] These compounds can also be used to synthesize silyl ketene acetals, which can be used as initiators for GTP.[143–146] As such, preparation of α-silyl carbonyls are attractive and a method that can be applicable to a broad range of nucleophiles and silyl groups would be beneficial. This would also lead to a better understanding of silyl ketene reactivity and how LAs could be used to polymerize silyl ketene.

2.2   Approach

Herein, I report the preparation of α-silyl esters, α-silyl amides, and α-silyl thioesters from silyl ketenes with catalytic amounts of LA using a variety of nucleophiles (Figure 2.1). These reactions were performed at room temperature and under 5 minutes. First the LA identity was optimized by investigating boranes, metal triflates, and an aluminum alkoxide, determining which LA was best at facilitating nucleophilic addition at the central carbon. The nucleophiles examined include alcohols, amines, and thiols that are primary, secondary, and tertiary nucleophiles, as well as phenol derivatives bearing electron-donating or –withdrawing groups at various positions. This approach was then expanded to a variety of silyl ketenes, examining the impact of steric bulk and electronics of the silyl substituent on the reaction. This work gives a better understanding of how silyl ketenes can be used as building blocks for α-silyl carbonyl functionalities as well as provides a foundation for developing silyl ketenes as monomers.
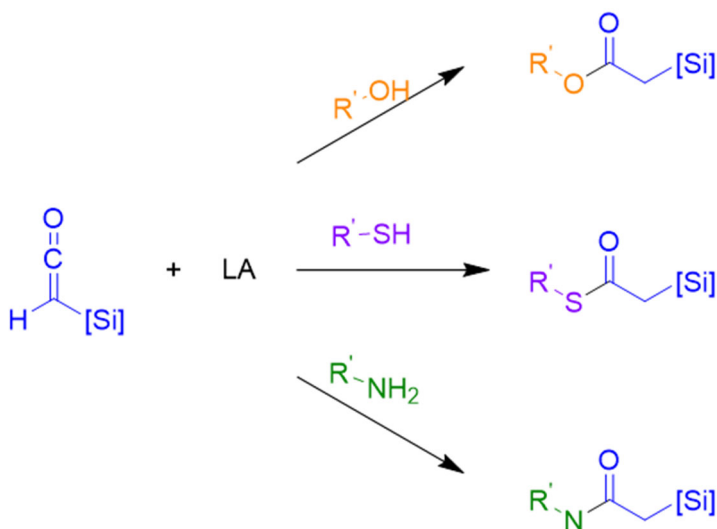
Figure 2.1. Formation of α-silyl carbonyls via the activation of silyl ketenes with LAs.

2.3 Lewis Acid Selection

2.3.1 Synthesis of silyl ketene

All silyl ketenes reported in this thesis were synthesized through a previously reported method,[108,147,148] as shown in Scheme 2.1. Ethyl vinyl ether was reacted with bromine and *tert*-butanol to form a mixed acetal **(1)**. Once purified via work-up and distillation, the mixed acetal is reacted with phosphorous pentachloride and triethylamine to and form a cis alkene **(2)**, also purified via work-up and distillation. The isolated cis alkene is then reacted with lithium diisopropylamide to eliminate bromine, followed by reaction of desired silyl chloride to form an alkyne **(3)** purified via column chromatography. The alkyne is then heated to 85°C to undergo a thermal rearrangement to afford the final silyl ketene **(4)** and purified through distillation. The multi-step reaction is the same for all silyl substituents, however the final purification process may differ. Each silyl substituent can be readily prepared on a large scale and stored for several months under inert gas and at low temperatures. The product identity and purity was characterized by ^{1}H nuclear magnetic resonance (NMR) and ^{13}C NMR spectroscopy, Fourier-transform infrared spectroscopy (FTIR), and gas chromatography-mass spectrometry (GC-MS).
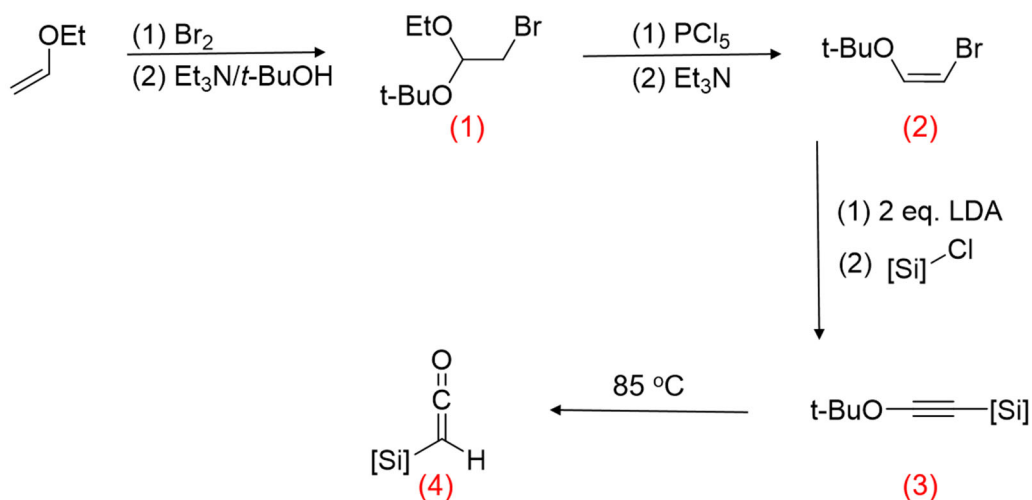
Scheme 2.1. Synthesis of silyl ketenes.

2.3.2 Preliminary Non-Catalyzed Reaction

To understand the non-catalyzed reaction, benzyl alcohol and d (MDPS) ketene were stirred in dichloromethane (DCM) at room temperature. The reaction was monitored using FTIR spectroscopy until full ketene consumption was observed. Ketenes exhibit a characteristic stretching frequency due to the cumulated double bond at ~2100 cm^{-1}. The disappearance of the ketene stretch was accompanied by the appearance of the carbonyl stretch at ~1700 cm^{-1} (Figure A2.1). Full consumption of ketene was observed after 4 days and the reaction yielded the corresponding α-silyl ester in 50% isolated yield (column chromatography).

2.3.3 Lewis Acid Scope

To overcome the sluggish nature of this reaction, various LAs were evaluated for the ability to activate the silyl ketene, much like has been done for ketones and esters. The LA is expected to coordinate to the oxygen atom of the silyl ketene which would make the central carbon more electrophilic and therefore more susceptible to nucleophilic attack. The LAs investigated were BF$_3$·OEt$_2$, Al(O^{i}Pr)$_3$, B(C$_6$F$_5$)$_3$, La(OTf)$_3$, and Mg(OTf)$_2$. Each LA was evaluated at 0.2 and 1.2 molar equivalent to triisopropylsilyl (TIPS) and triethylsilyl (TES) ketene, using benzyl alcohol and benzyl mercaptan as nucleophiles. (Table A2.1) Each LA produced the corresponding α-silyl ester in significantly less reaction time (<1 hr), with BF$_3$·OEt$_2$ producing the highest isolated yield (95%) and shortest reaction times, even with the use of substoichiometric amounts. BF$_3$·OEt$_2$ was chosen to explore the nucleophilic and silyl substituent scope of this reaction (Scheme 2.2).
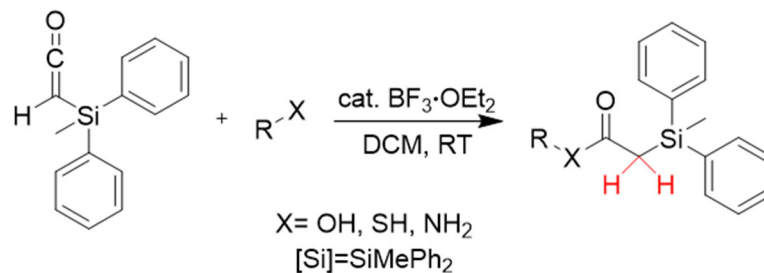
Scheme 2.2. Formation of α-silyl carbonyls exploring the nucleophilic scope with MDPS ketene.

2.4 Nucleophilic Scope

2.4.1 Alcohol Nucleophiles

Initially, the reaction of 11 different alcohols with MDPS ketene were examined, including primary, secondary, and tertiary aliphatic alcohols, as well as phenols was electro-withdrawing and –donating groups at different positions. Each of alcohols examined produced the
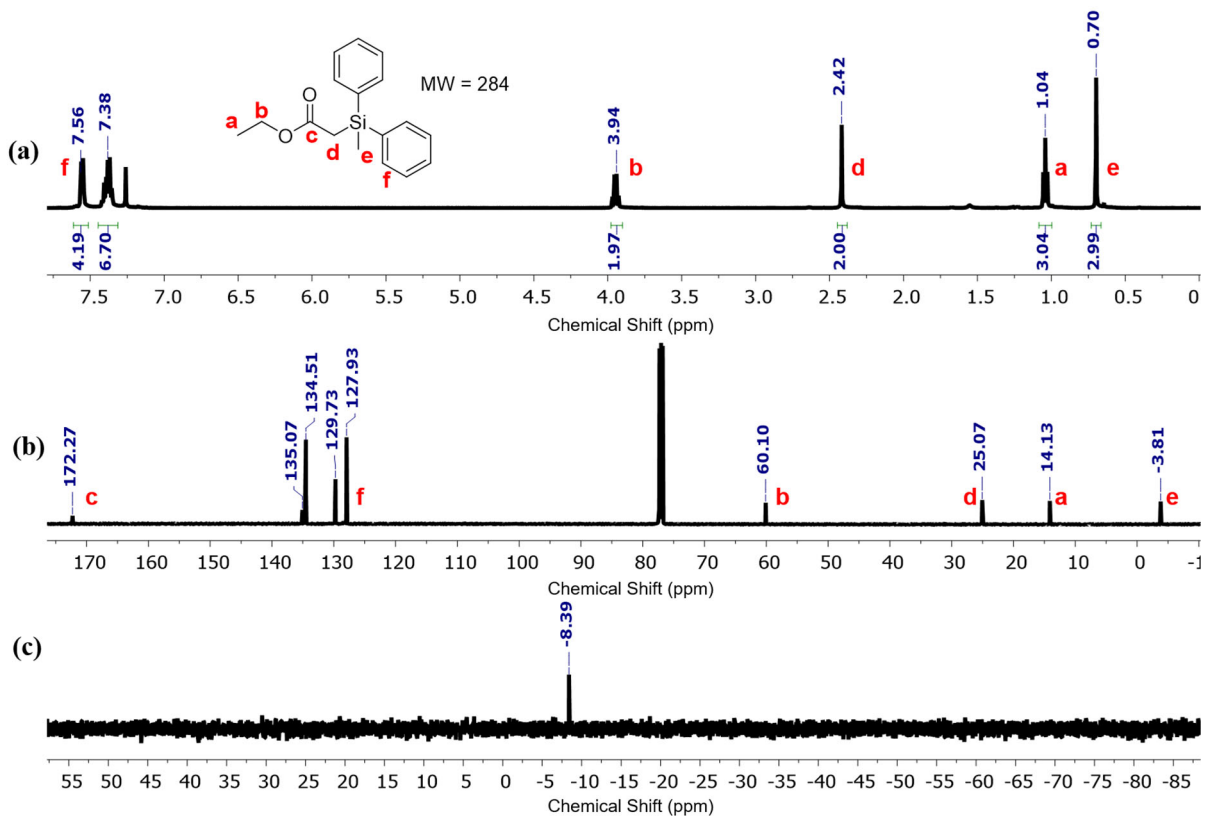
Figure 2.2. Characterization of compound **1** (a) ^{1}H NMR, (b) ^{13}C NMR, (c) ^{29}Si NMR.

corresponding α-silyl ester in good isolated yields (>60%) in less than five minutes. (Table 2.1) Each product was characterized with ^{1}H, ^{13}C, and ^{29}Si NMR, FTIR spectroscopy, and MS; Figure 2.2 shows the NMR spectrum for α-methyldiphenylsilyl acetate (compound **1**) (Figure A2.2, compound **1** FTIR and mass spectra). Comparing the reactions of the primary, secondary, and tertiary aliphatic alcohols and phenol, no significant difference in time to completion or yield was

Table 2.1. Evaluation of alcohol and phenol nucleophile scope with MDPS ketene ([Si] = CH$_3$Ph$_2$) catalyzed by BF$_3$.
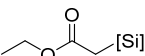
Compound	Nucleophile	Product	% yield	C=O (cm^{-1})	Δ_{CH2} (ppm)
1			61	1717	2.42
2			78	1709	2.40
3			79	1704	2.34
4			61	1734	2.66
5			80	1732	2.64
6			75	1735	2.65
7			69	1735	2.69
8			61	1743	2.68
9			78	1737	2.67
10			70	1749	2.71
11			75	1713	2.48
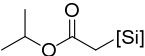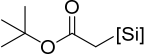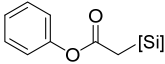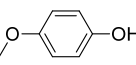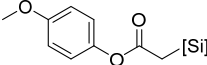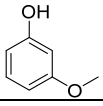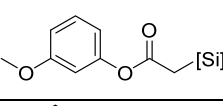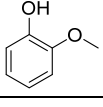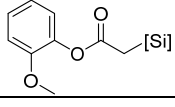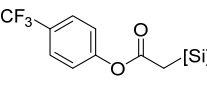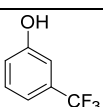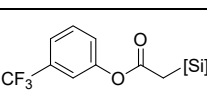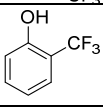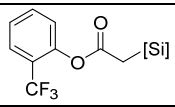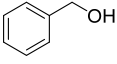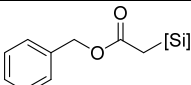
observed. In contrast, for substitution phenols electron-donating substituents produced slightly higher isolated yields that those with electron-withdrawing groups for example 4-methoxyphenol produced a 80% yield whereas 4-(trifluoromethyl)phenol produced a 61% yield. This could be due to the electron density on the oxygen atom making it a better nucleophile. No significant trend was observed by varying the position of the substituents on the phenol ring, suggesting similar inductive and resonance effects. Each of the α-silyl esters exhibited similar spectra, with little difference in the chemical shift of the C**H**$_2$SiR$_3$ in ^{1}H NMR or the C=O stretch in FTIR.

2.4.2   Amine and Thiol

The scope of nucleophiles was then expanded to amines and thiols to produce α-silyl amides and α-silyl thioesters, respectively (Table 2.2). Primary and secondary amines, as well as aniline produced the corresponding α-silyl amides in higher isolated yields compared to the α-silyl esters. Aniline, for example, produced the corresponding amide in 92% isolated yield (compound **14**), whereas phenol produced the corresponding ester in 61% isolated yield. The α-silyl amides were all characterized with the same methods as the α-silyl esters and had high purity within limits of NMR analysis. Alkyl and aryl thiols did indeed produce the corresponding α-silyl thioesters, however the isolated yields were significantly lower than the esters and amides. No significant trend was observed for the thiol nucleophiles (Table 2.2).

Table 2.2. Evaluation of amine and thiol nucleophile scope with MDPS ketene catalyzed by BF_3.

Compound	Nucleophile	Product	% yield	C=O (cm⁻¹)	Δ_{CH2} (ppm)
12			64	1626	2.28
13			77	1622	2.44
14			92	1635	2.47
15			50	1670	2.80
16			37	1668	2.76
17			5	1667	2.70
18			40	1693	2.89
19			39	1687	2.86
20			45	1696	2.91
21			72	1674	2.82
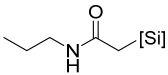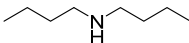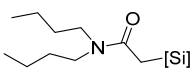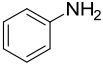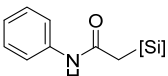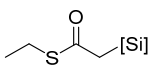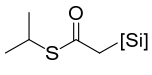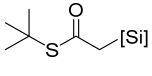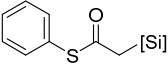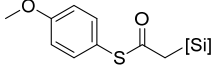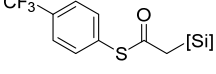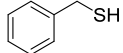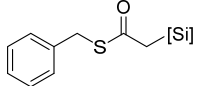
2.5   Silyl Substrate Scope

To further evaluate the scope of the LA-activated reaction the silyl substrate scope was examined. The ketenes investigated were TES, TIPS, dimethyl phenyl silyl (DMPS), and triphenylsilyl (TPhS) (Table 2.3). These silyl substrates were selected to assess how the steric bulk and electronic properties of the silyl substitution impact the reactivity and product formation. The use of TES and TIPS ketene allowed the impact of only steric bulk, and not the electronics of the compound, to be considered; TIPS is much bulkier and sterically hindered than TES.

Table 2.3. Evaluation of silyl substituent scope with 4-methoxyphenol, 4-methoxythiophenol, or aniline catalyzed by BF$_3$.
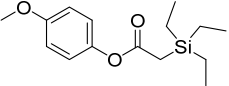
Compound	Nucleophile	Product	% yield	C=O (cm^{-1})	Δ_{CH2} (ppm)
TES 1			70	1735	2.10
TES 2			45	1691	2.37
TES 3			82	1642	1.94
TIPS 1			66	1735	2.16
TIPS 2			81	1694	2.42
TIPS 3			77	1642	1.96
DMPS 1			53	1734	2.33
DMPS 2			47	1687	2.57
DMPS 3			71	1639	2.15
TPhS 1			74	1732	2.96
TPhS 2			24	1687	3.19
TPhS 3			58	1635	2.78
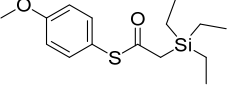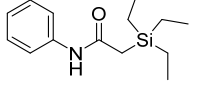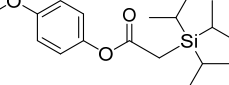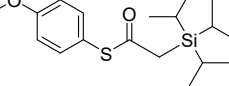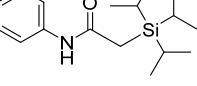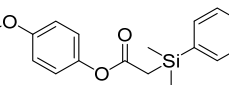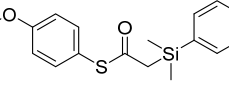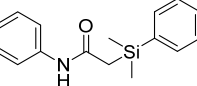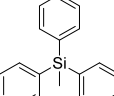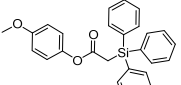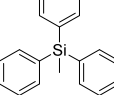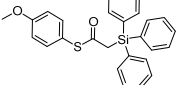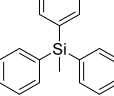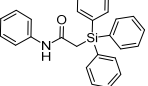
Alternatively, the use of DMPhs and TPhS ketene allow the impact of the electronic demand, and not steric bulk, to be evaluated.

Again, $BF_3 \cdot OEt_2$ was the LA of choice and used in a catalytic amount to activate the different silyl ketenes. Each silyl ketene was reacted with 4-methoxyphenol, 4-methoxythiophenol, and aniline as the nucleophiles. For all of the silyl groups, the corresponding α-silyl esters and α-silyl amines were readily prepared and easily purified in reasonable isolated yields (>50%) and full consumption of ketene was observed in > 5 mins. Similarly, to the nucleophilic scope, the α-silyl thioesters were obtained in lower yield (~25%) with the exception of **TIPS 2** which was obtained in a surprisingly high 81% yield. The peaks corresponding to the C**H**$_2$SiR$_3$ in the ^{1}H NMR spectra shifted downfield with an increasing number of phenyl rings on the silyl group, similarly to the terminal proton in the corresponding silyl ketene. The chemical shift in the ^{1}H NMR spectra for the terminal proton for TES and TIPS ketene are 1.64 and 1.69, respectively; and for DMPhS and TPhS ketene the chemical shifts are 2.23 and 2.48 respectively. The silyl group had no impact on the C=O stretching frequency in the FTIR spectra.

2.6   Summary

In summary, silyl ketenes were activated with LAs to produce α-silyl esters, α-silyl amides, and α-silyl thioesters, in a method that is applicable to a wide scope of nucleophiles and silyl ketene substituents. These products are formed under mild reaction conditions by activating the silyl ketene with a catalytic amount of LA and adding a desired nucleophile. Of the LAs examined, $BF_3 \cdot OEt_2$ performed the best and resulted in full consumption of ketene in <5 min. The nucleophiles used covered a broad range, including primary, secondary, and tertiary alcohols; phenols; primary and secondary amines; aniline; and primary, secondary, and tertiary thiols. Alcohol and amine-based nucleophiles led to better-isolated yields than the sulfur-based

nucleophiles and all of the product obtained were readily purified through column chromatography. The LA-activated reaction of silyl ketenes is applicable to all silyl substituents evaluated, with similar reaction time and yield regardless of steric demands or electronic considerations of the silyl group. Moreover, this work gives an understanding on how a variety of silyl ketenes react with a broad range of nucleophiles and readily available LAs. This knowledge can help ongoing studies identify how LAs can be used to activate silyl ketenes and enable their polymerization.

2.7 Appendix

General Considerations. All purchased chemicals were used directly as received, unless otherwise stated. All reactions were performed under an inert atmosphere. DCM and THF were obtained by passing the commercial grade solvent through a column of activated neutral alumina in a Dow-Grubbs solvent system from Pure Process Technology (Nashua, NH). All ^{1}H, ^{13}C, ^{29}Si NMR were collected on a Bruker Ascend III HD 500 MHz NMR instrument equipped with prodigy probe and shifts are reported relative to the residual solvent peak, as noted. All NMR spectra were collected using CDCl$_3$ as the solvent unless otherwise noted. FTIR spectra were acquired using an Agilent Cary 630 FTIR in the ATR mode. ESI spectra were obtained on a THERMO Finniagn LCQ DECA ion trap mass spectrometer equipped with an external AP ESI ion source (only triphenylsilyl TPhS ketenes). THERMO DSQ II Series Single Quadrupole GC/MS.

General Procedure for Silyl Ketene Synthesis. (Z)-1-Bromo-2-tert-butoxylethene (A) was prepared using a previously reported method.[10,11,28,29] In an oven-dried round-bottom flask, 2 equiv of LDA (48 mL, 0.096 mol LDA, 2 mol/L in THF/ethylbenzene/ hexane) and dry THF (48 mL) were cooled to −78 °C with a dry ice/ acetone bath under N2 (g). A mixture of A (7.08, 0.04 mol) and dry THF (16 mL) was prepared in an addition funnel and added dropwise to the

LDA/THF solution. After addition, the reaction was warmed to room temperature and stirred for 3 h. After 3 h, the reaction mixture was cooled to 0 °C using an ice water bath. The corresponding silyl chloride was added (0.048 mol). The reaction was warmed to room temperature and stirred for 4 h. The mixture wastransferred to a separation funnel and quenched with an aqueous solution of sat. NaHCO3 (80 mL). The aqueous layer was washed with hexanes (2 × 20 mL). The organic layers were combined and washed with 0.5 N HCl (2 × 80 mL), H2O (120 mL), and an aqueous solution of saturated NaCl (120 mL). The organic layer was dried with Na2SO4, filtered, and solvent-removed under reduced pressure. The crude alkyne product was purified through column chromatography of the silica gel. The silica gel was basified with a 2.5 vol % Et3N in hexanes prior to loading product to the column. The product was= eluted with 100% hexanes. A pale yellow oil was obtained; it was heated to 85 °C under N2(g) for 2 h. The final ketene product was purified through vacuum distillation.

Procedure for Control Experiment (no LA). An oven-dried round bottom flask was purged with vacuum and put under an inert atmosphere (N2(g)). Dry DCM (1 mL) was added to the round bottom flask (RBF). Methyl diphenyl silyl ketene (1 eq, 1.3 mmol) and benzyl alcohol (1.2 eq, 1.6 mmol) were then added simultaneously to the RBF. The reaction was stirred for 96 hours under N2(g) at room temperature. The reaction was monitored with FTIR, till full ketene consumption was observed. Solvent was removed and the product was purified with column chromatography. The column was built with 100% hexanes and silica gel. The product was eluted with 9:1 hexanes:ethyl acetate. The product was dried under vacuum.

General Procedure for α-Silyl Carbonyl Compounds. An oven-dried RBF was purged with vacuum and put under an inert atmosphere (N2(g)). Dry DCM (1 mL) and a catalytic amount of BF3•OEt2 (1 drop) was added to the RBF. The desired ketene (1 eq.) and nucleophile (1.2 eq.)

were then added simultaneously to the RBF. The reaction was stirred for ~5 minutes under $N_2(g)$ at room temperature. The reaction was monitored with FTIR, till full ketene consumption was observed. Solvent was removed and the product was purified with column chromatography. The column was built with 100% hexanes and silica gel. The product was eluted with 9:1 hexanes:ethyl acetate. The product was dried under vacuum.

Figure A2.1. Control experiment performed with no Lewis acid. The reaction was monitored with FTIR to see the consumption of the ketene peak at ~2100 cm^{-1}.
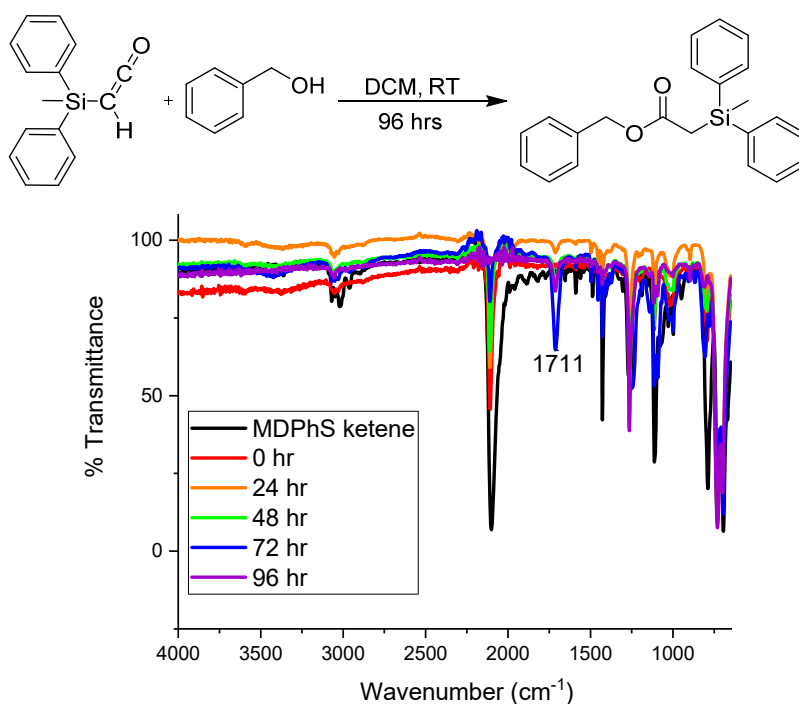
Table A2.1. Lewis acid scope.
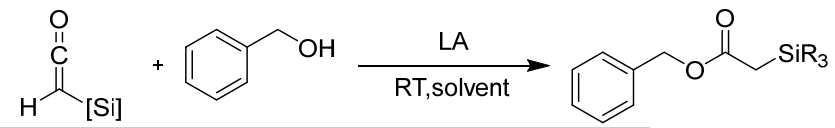
	LA	Solvent	Reaction time (min)	Yields	
				[Si]=TIPS	[Si]=TES
1.2 eq.	[1]LA= BF$_3$ •OEt$_2$	Diethylether	<2	95	80
	[2]LA= Al(O^{i}Pr$_2$)$_3$	THF	~15	90	87
	[3]LA= B(C$_6$F$_5$)$_3$	DCM	~10	94	39
	[4]LA=La(OTf)$_3$	DCM	<2	66	74
	[5]LA=Mg(OTf)$_2$	DCM	~60	63	80
	[6]LA=EtMgBr	Diethylether	<2	23	32
0.2 eq.	[1]LA= BF$_3$ •OEt$_2$	Diethylether	<2	86	77
	[2]LA= Al(O^{i}Pr$_2$)$_3$	THF	~15	27	58
	[3]LA= B(C$_6$F$_5$)$_3$	DCM	<2	70	67
	[4]LA=La(OTf)$_3$	DCM	<2	68	69
	[5]LA=Mg(OTf)$_2$	DCM	~15	86	79
	[6]LA=EtMgBr	Diethylether	<2	9	23

*each LA was added in both 1.2 or 0.2 equivalents to the reaction mixture. It was found that

BF$_3$•OEt$_2$ can also be added in a catalytic amount.
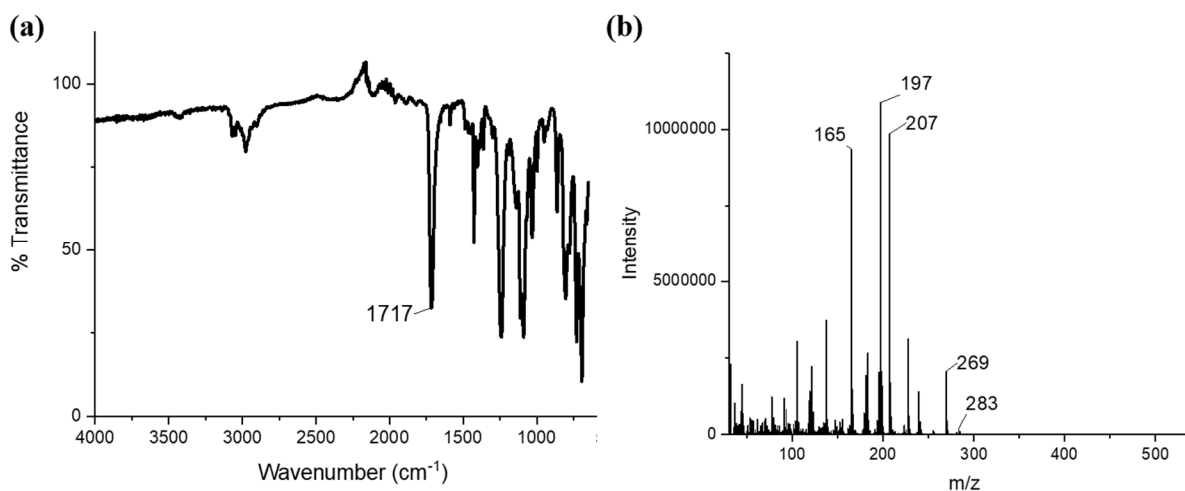
Figure A2.2. Table 2.1, entry 1. (a) FTIR, (b) mass spectroscopy.

Figure A2.3. Table 2.1, entry 2. (a) ^{1}H NMR, (b) ^{13}C NMR, (c) ^{29}Si NMR, (d) FTIR, (e) mass spectroscopy.
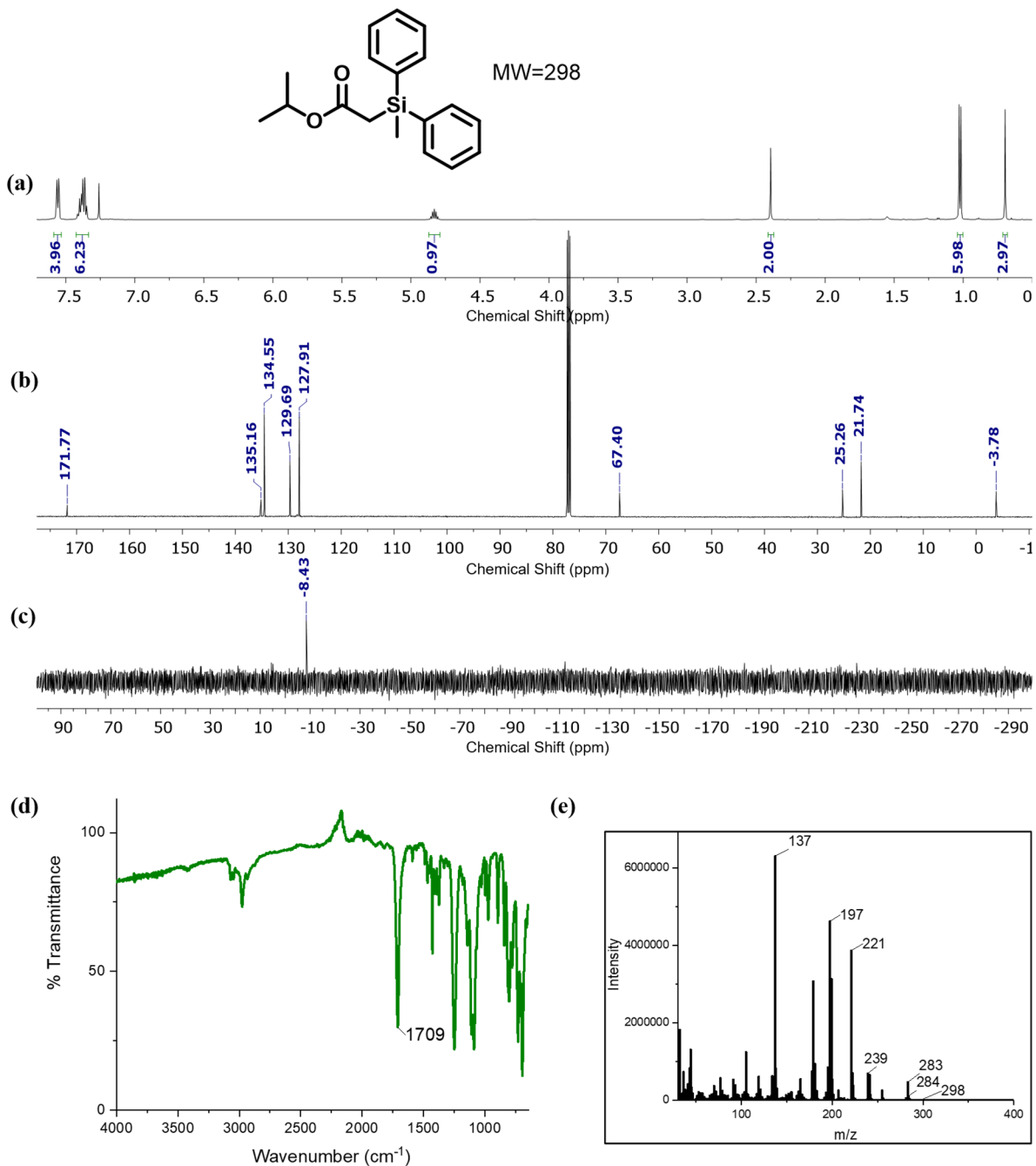
Figure A2.4. Table 2.1, entry 3. (a) ^{1}H NMR, (b) ^{13}C NMR, (c) ^{29}Si NMR, (d) FTIR, (e) mass spectroscopy.
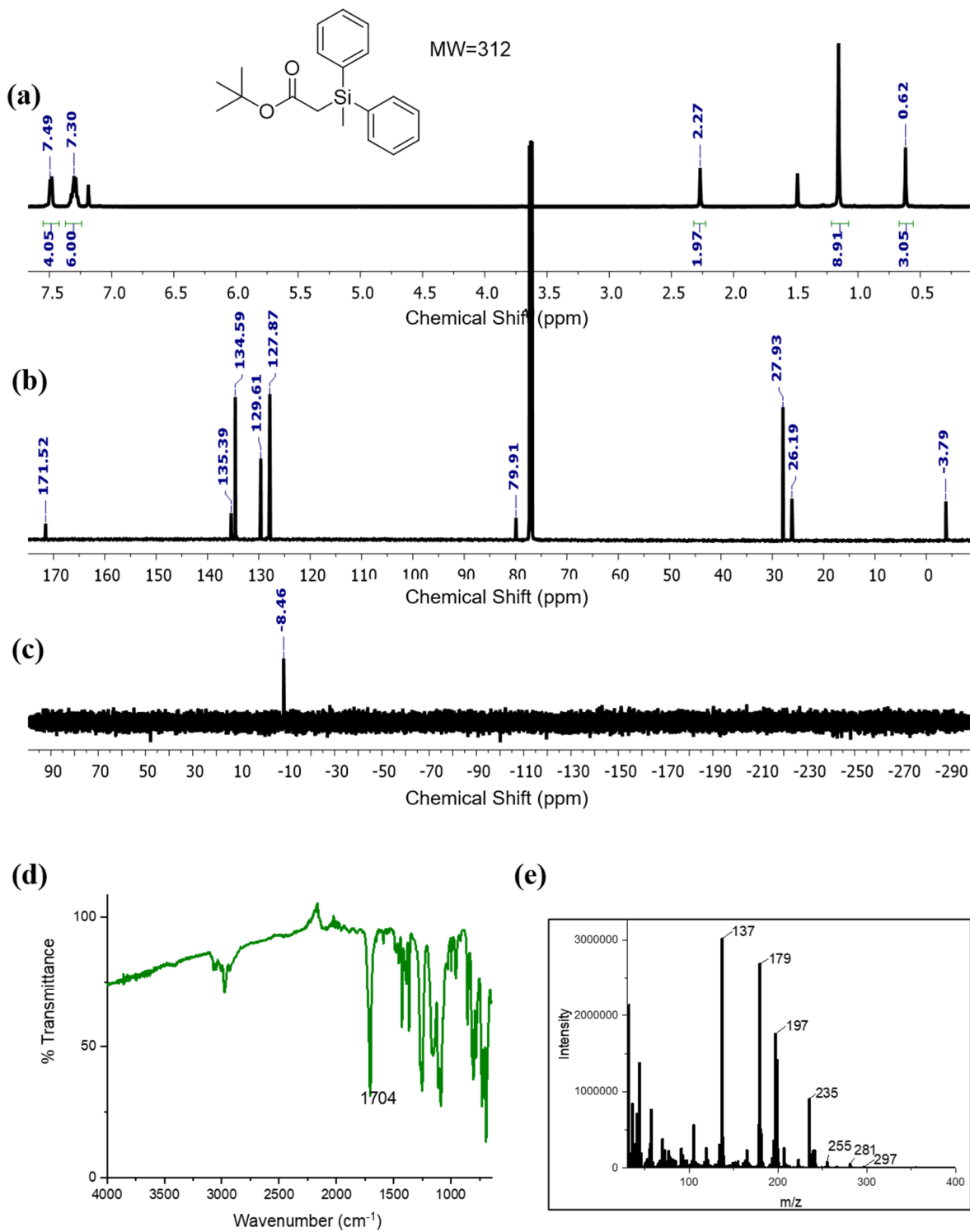
Figure A2.5. Table 2.1, entry 4. (a) ^{1}H NMR, (b) ^{13}C NMR, (c) ^{29}Si NMR, (d) FTIR, (e) mass spectroscopy.
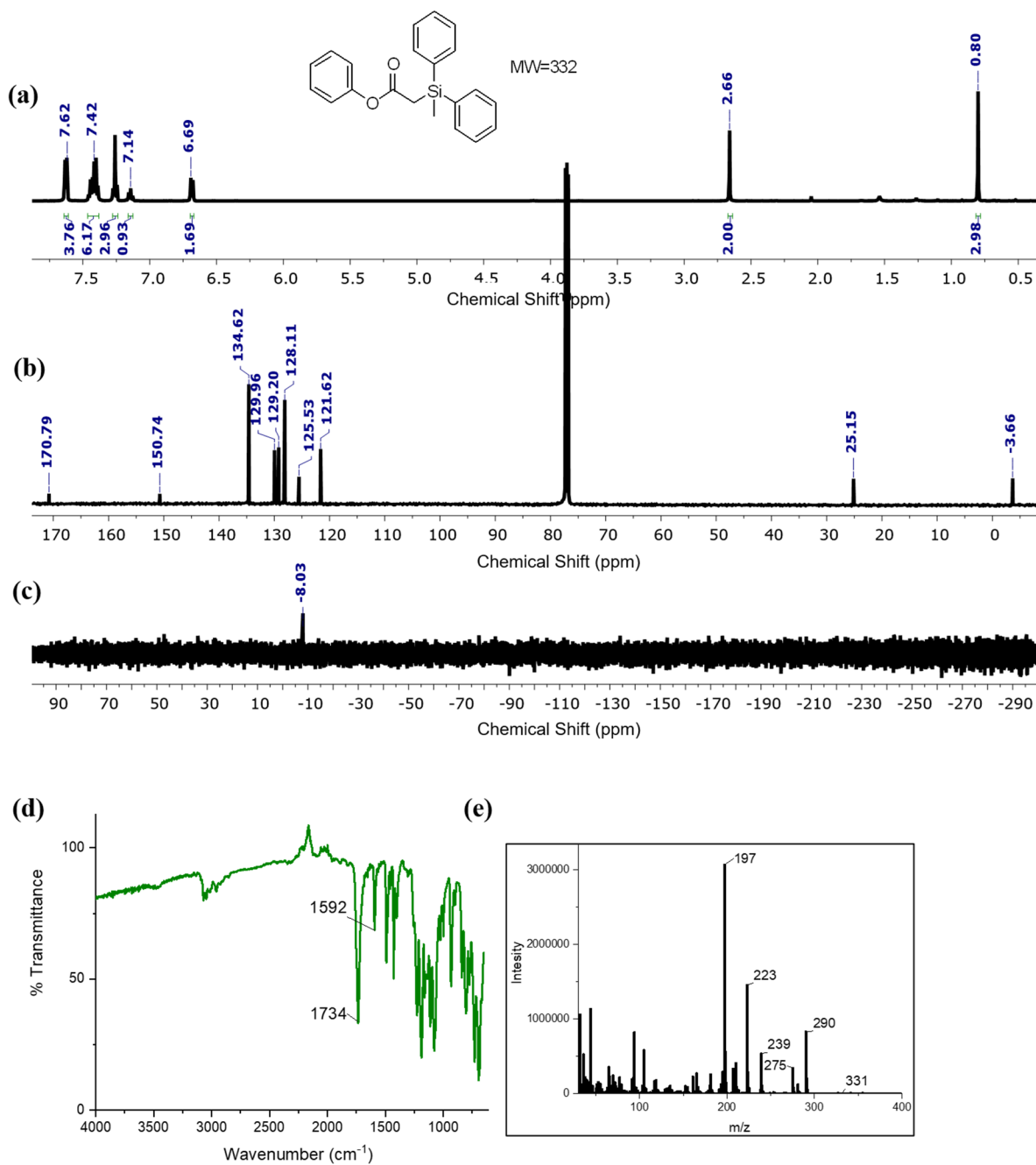
Figure A2.6. Table 2.1, entry 5. (a) ^{1}H NMR, (b) ^{13}C NMR, (c) ^{29}Si NMR, (d) FTIR, (e) mass spectroscopy.
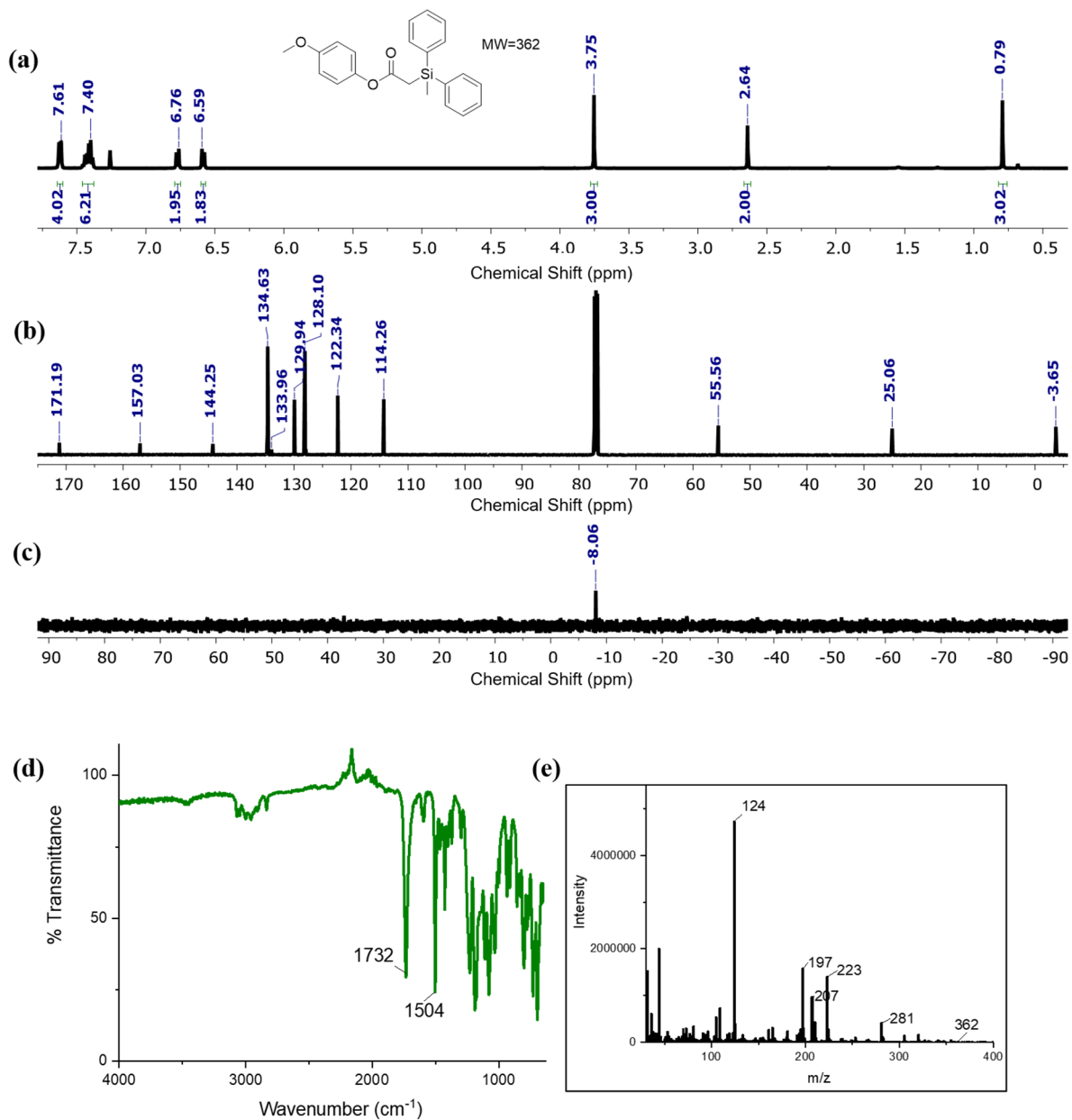
Figure A2.7. Table 2.1, entry 6. (a) ^{1}H NMR, (b) ^{13}C NMR, (c) ^{29}Si NMR, (d) FTIR, (e) mass spectroscopy.
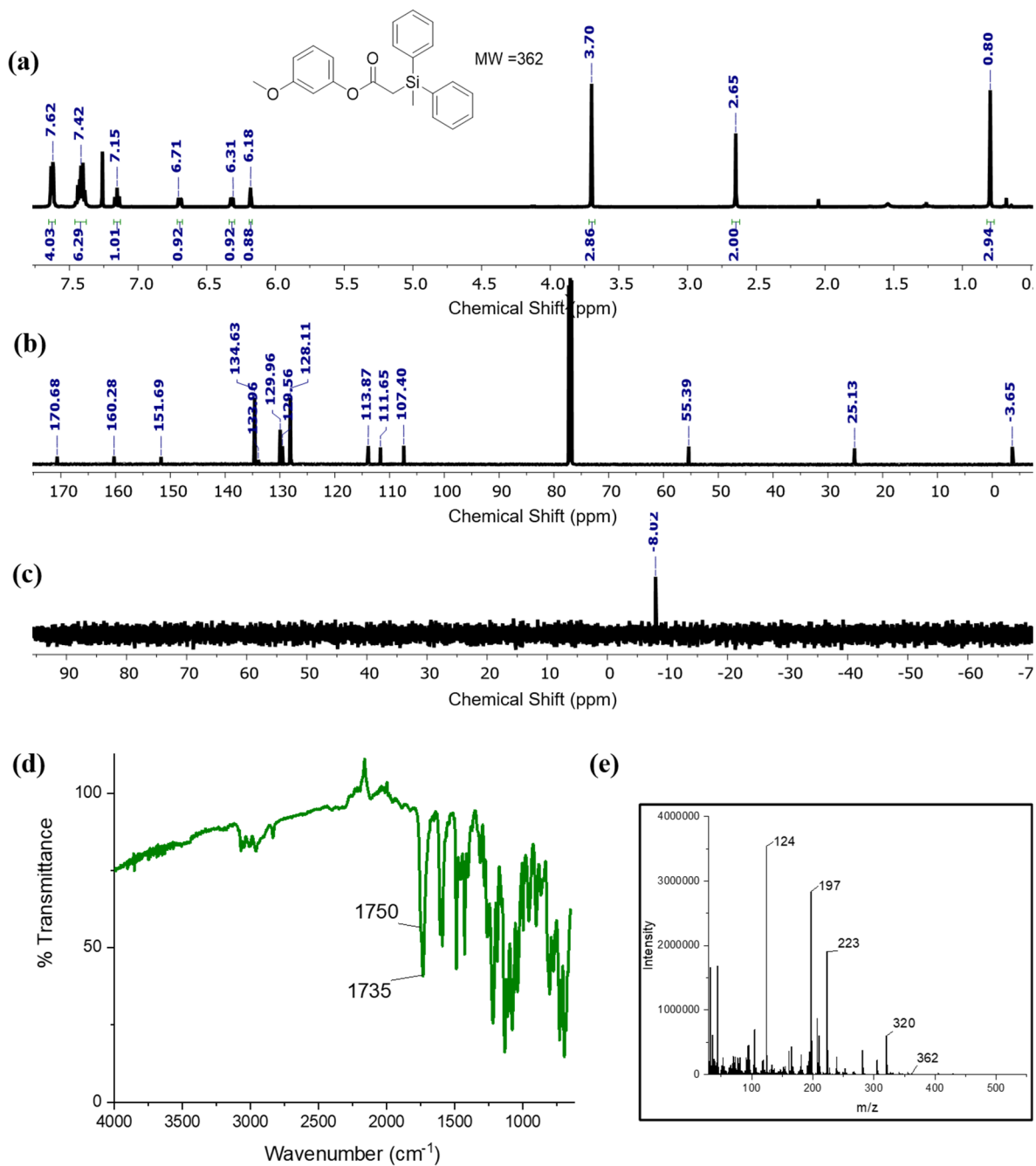
Figure A2.8. Table 2.11, entry 7. (a) ^{1}H NMR, (b) ^{13}C NMR, (c) ^{29}Si NMR, (d) FTIR, (e) mass spectroscopy.
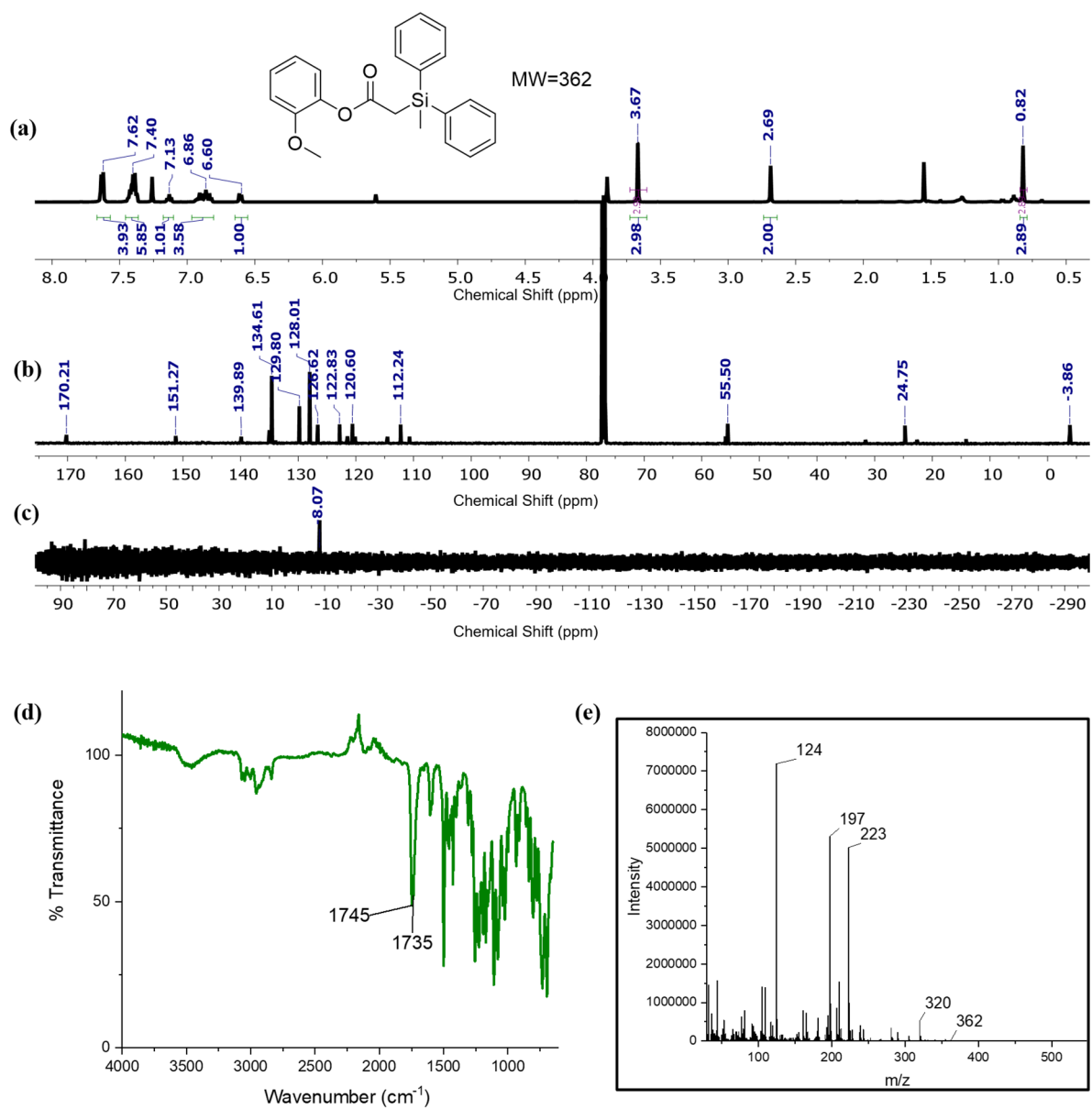
Figure A2.9. Table 2.1, entry 8. (a) ^{1}H NMR, (b) ^{13}C NMR, (c) ^{29}Si NMR, (d) FTIR, (e) mass spectroscopy.
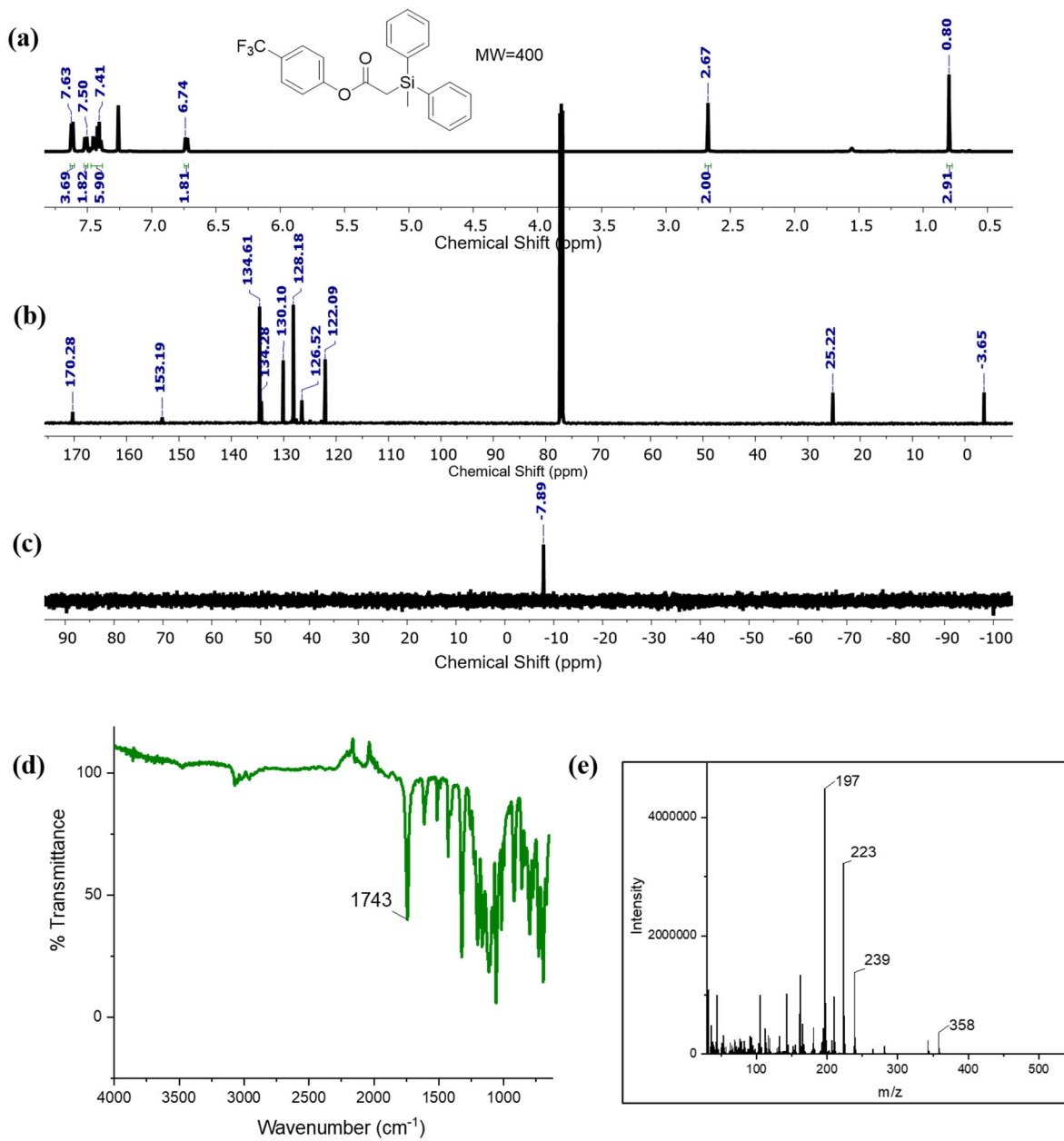
Figure A2.10. Table 2.1, entry 9. (a) ^{1}H NMR, (b) ^{13}C NMR, (c) ^{29}Si NMR, (d) FTIR, (e) mass spectroscopy.
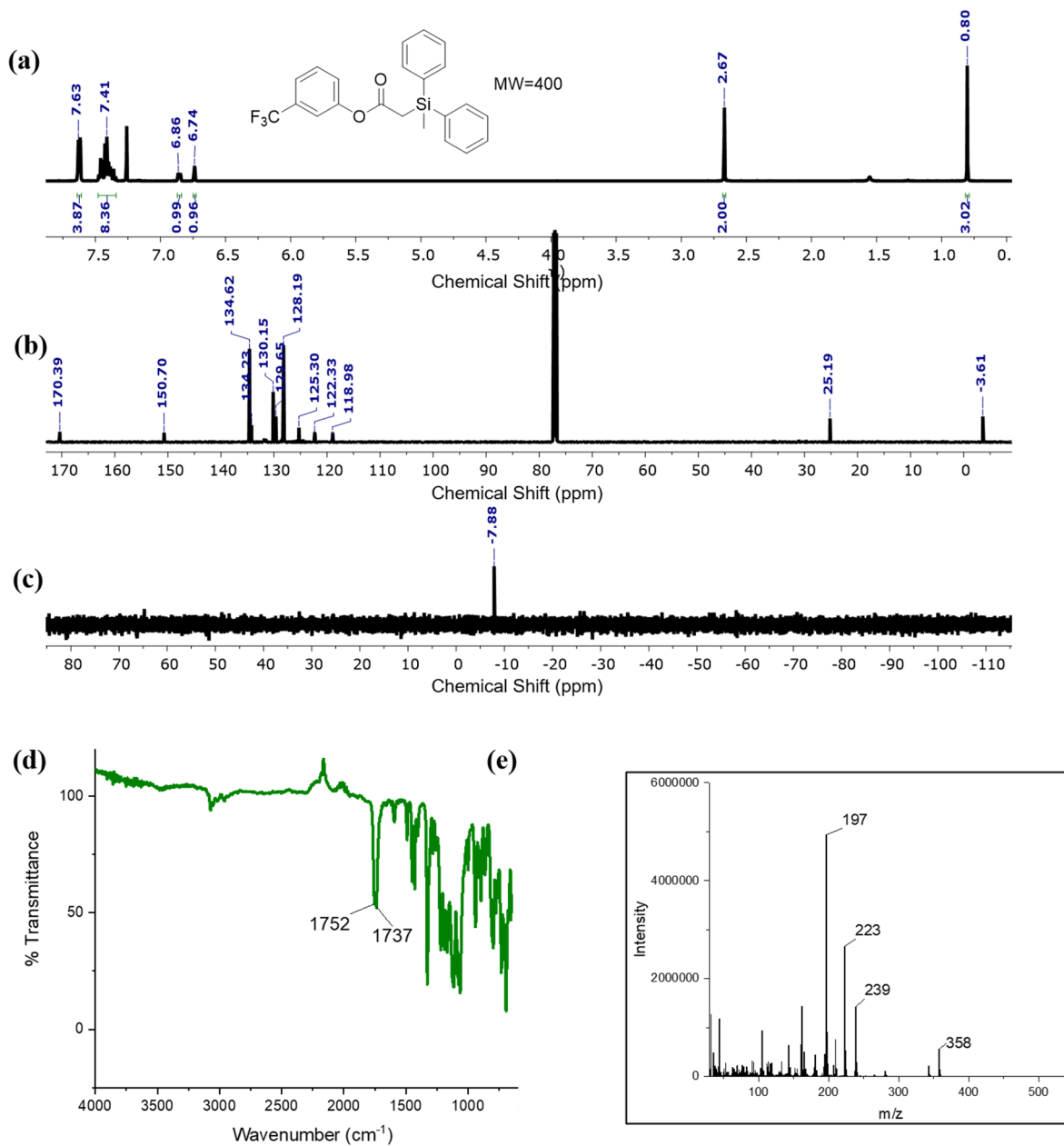
Figure A2.11. Table 2.1, entry 10. (a) ^{1}H NMR, (b) ^{13}C NMR, (c) ^{29}Si NMR, (d) FTIR, (e) mass spectroscopy.
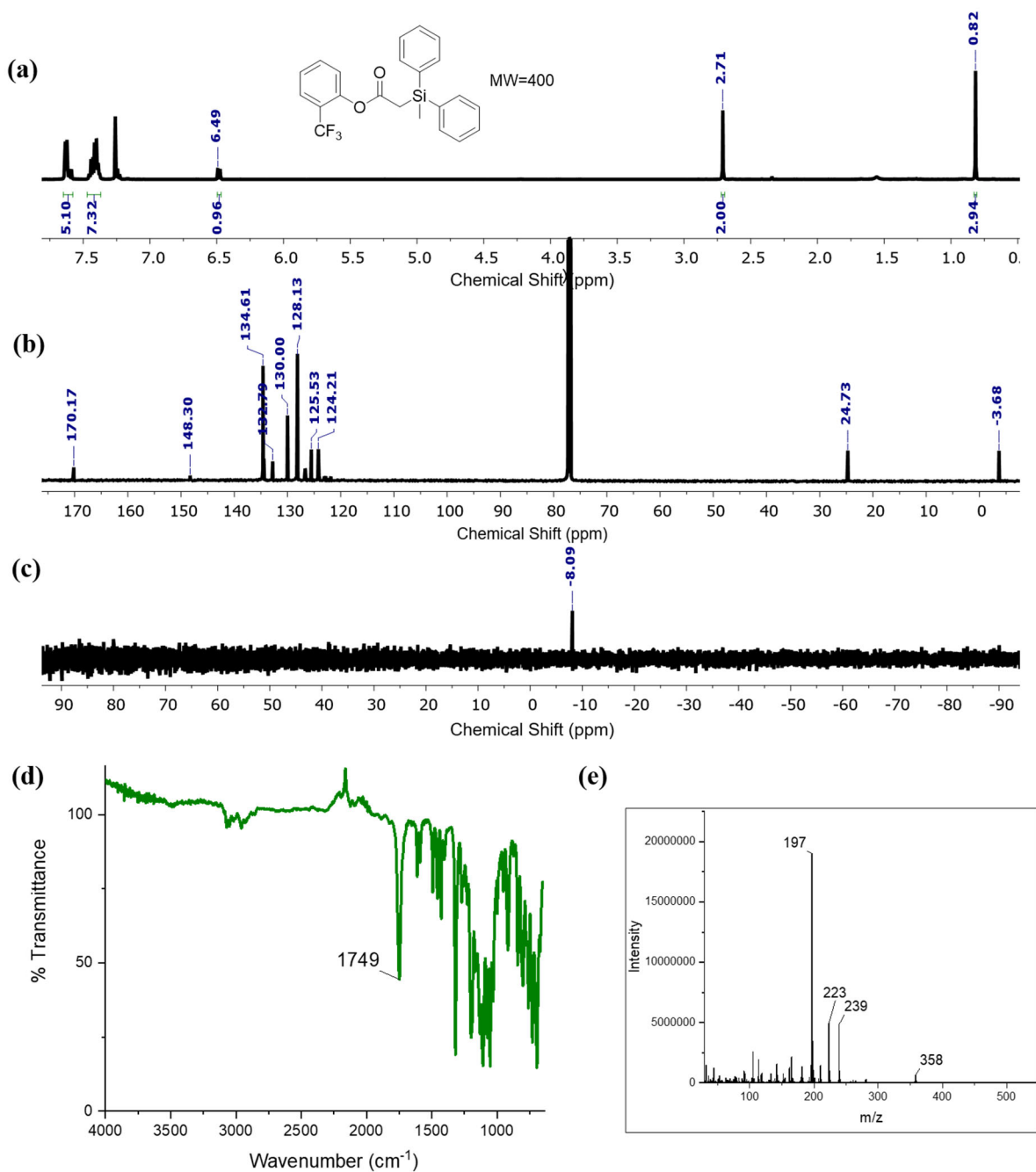
Figure A2.12. Table 2.1, entry 11. (a) ^{1}H NMR, (b) ^{13}C NMR, (c) ^{29}Si NMR, (d) FTIR, (e) mass spectroscopy.
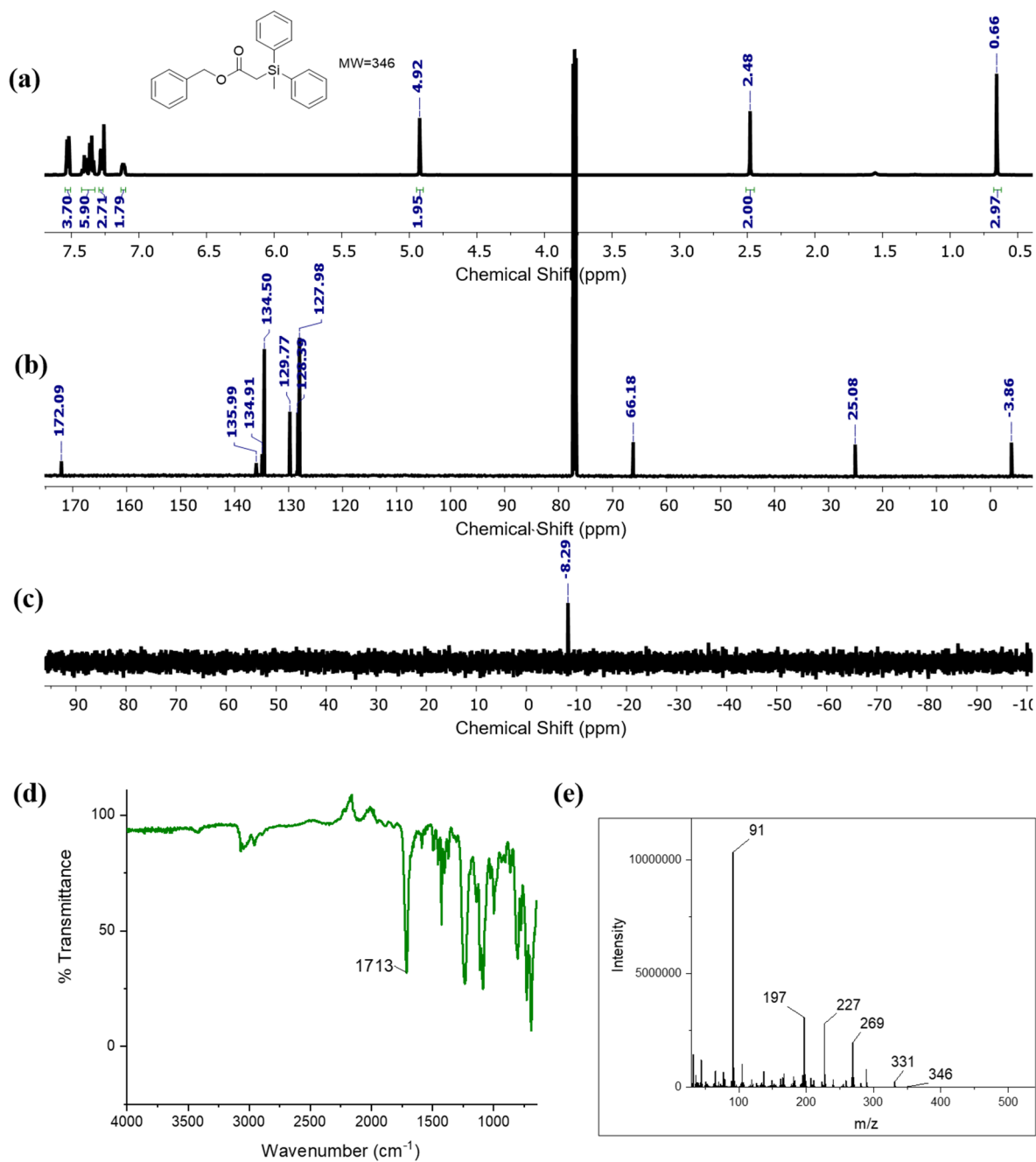
Figure A2.13. Table 2.2, entry 12. (a) ^{1}H NMR, (b) ^{13}C NMR, (c) ^{29}Si NMR, (d) FTIR, (e) mass spectroscopy.
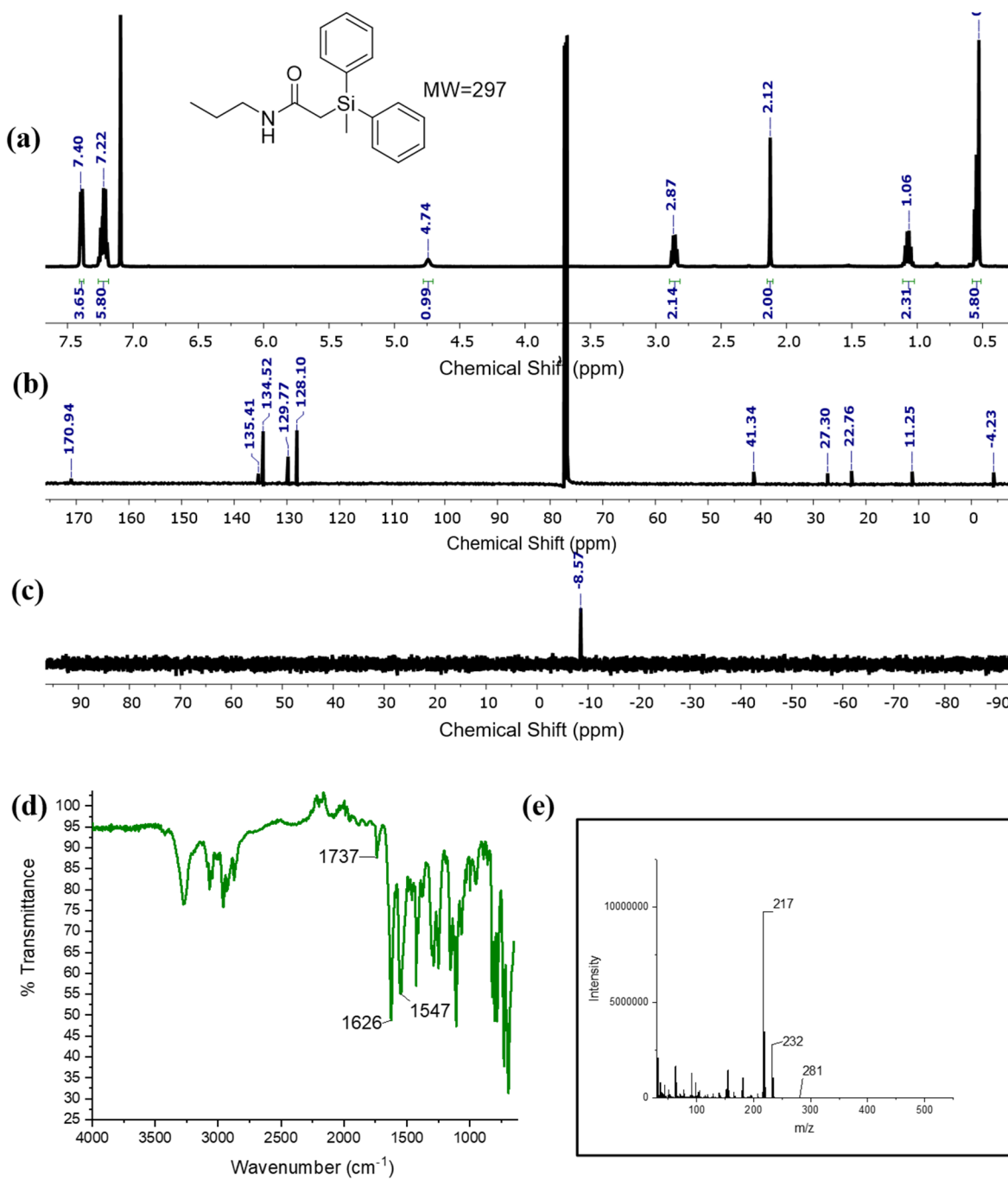
Figure A2.14. Table 2.2, entry 13. (a) ^{1}H NMR, (b) ^{13}C NMR, (c) ^{29}Si NMR, (d) FTIR, (e) mass spectroscopy.
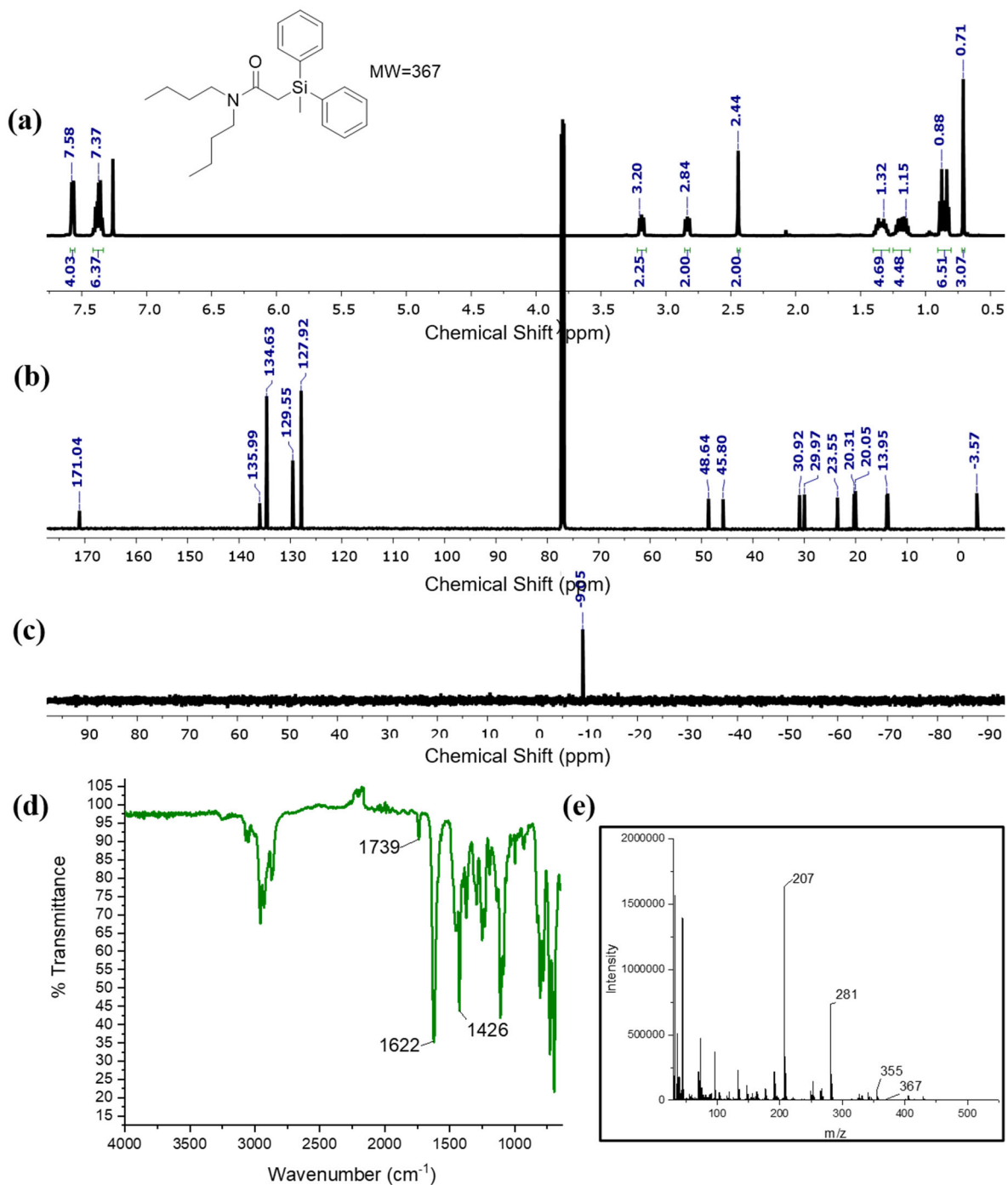
Figure A2.15. Table 2.2, entry 14. (a) ^{1}H NMR, (b) ^{13}C NMR, (c) ^{29}Si NMR, (d) FTIR, (e) mass spectroscopy.
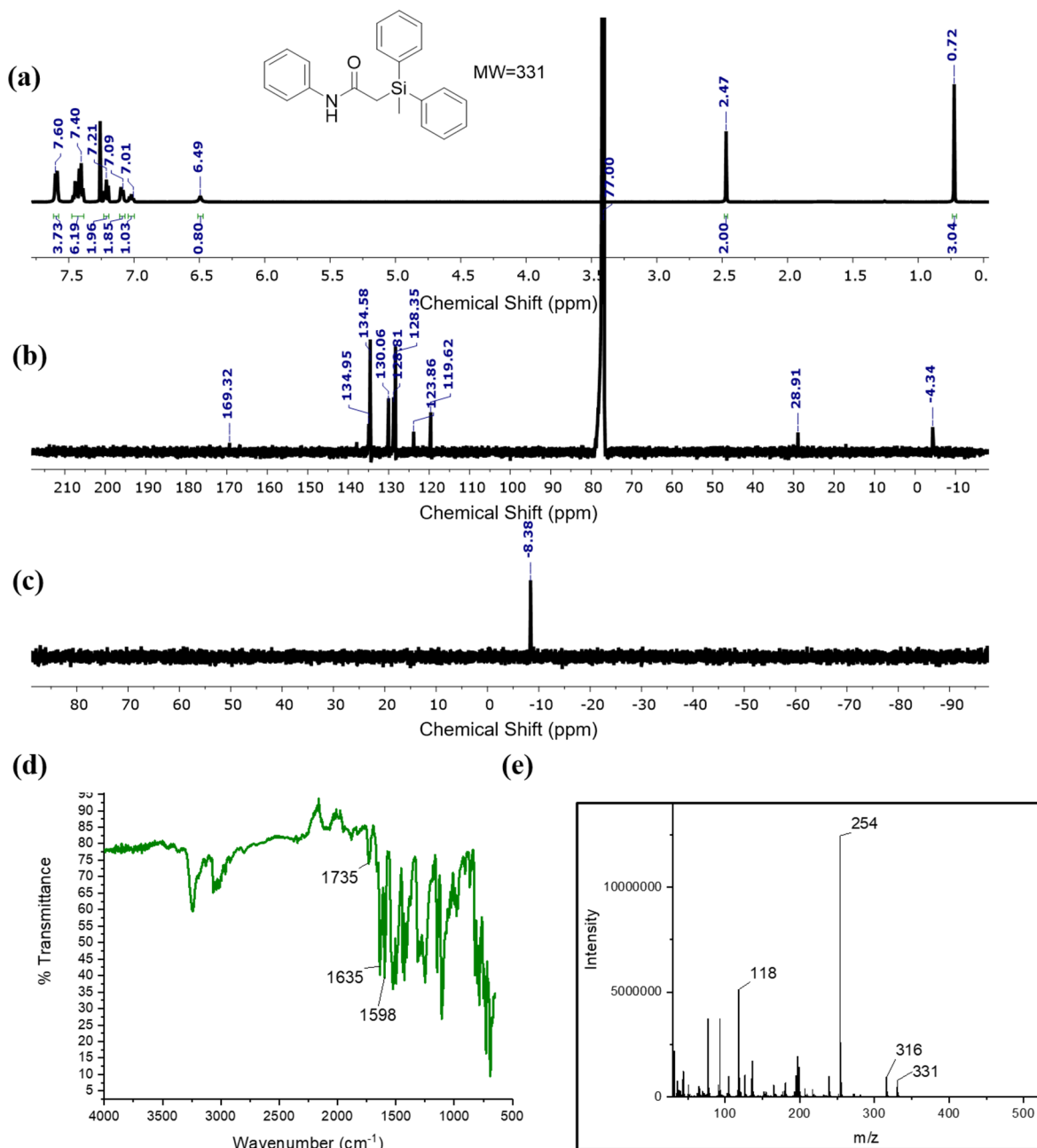
Figure A2.16. Table 2.2, entry 15. (a) ^{1}H NMR, (b) ^{13}C NMR, (c) ^{29}Si NMR, (d) FTIR, (e) mass spectroscopy.
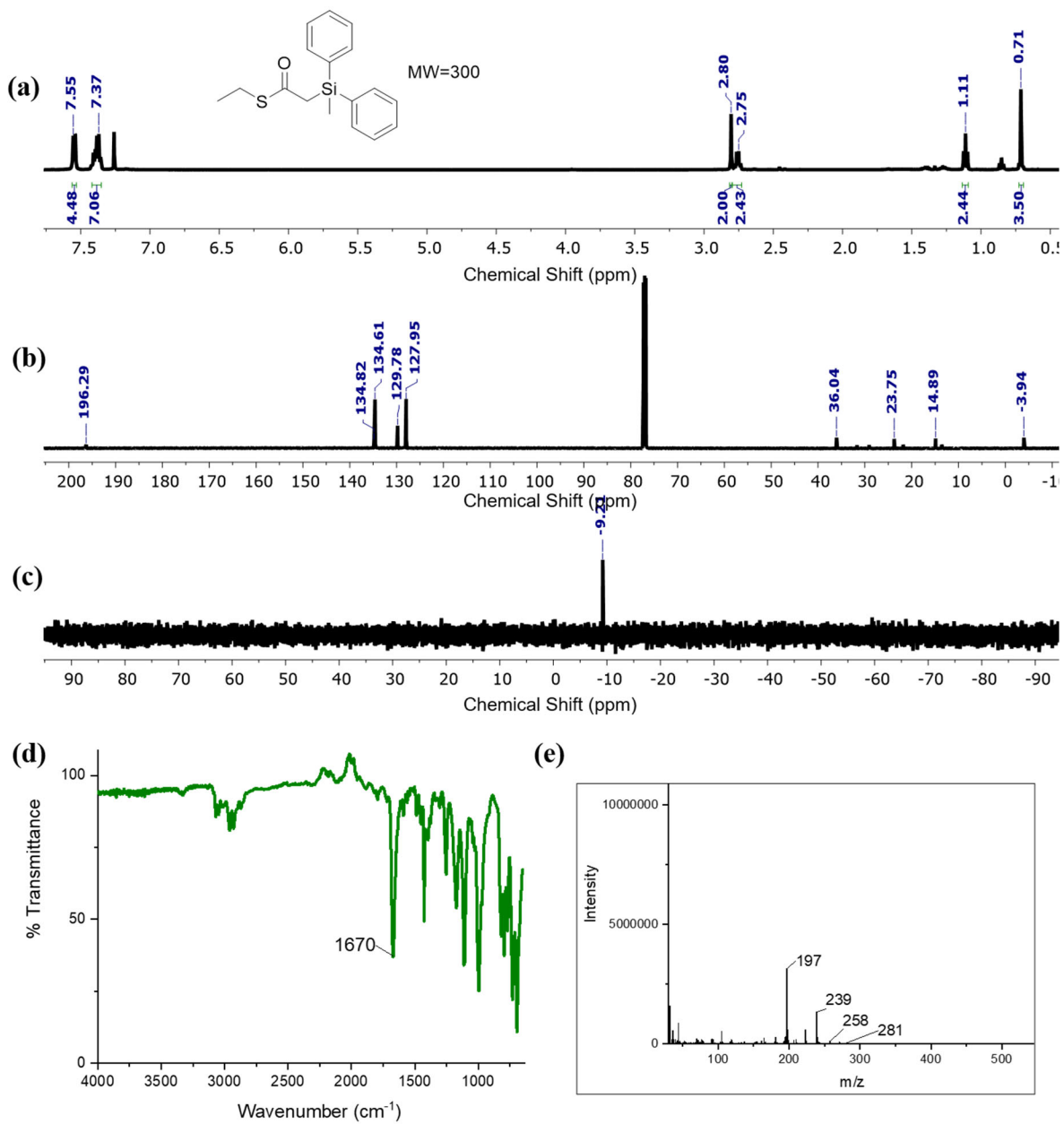
Figure A2.17. Table 2.2, entry 16. (a) ^{1}H NMR, (b) ^{13}C NMR, (c) ^{29}Si NMR, (d) FTIR, (e) mass spectroscopy.
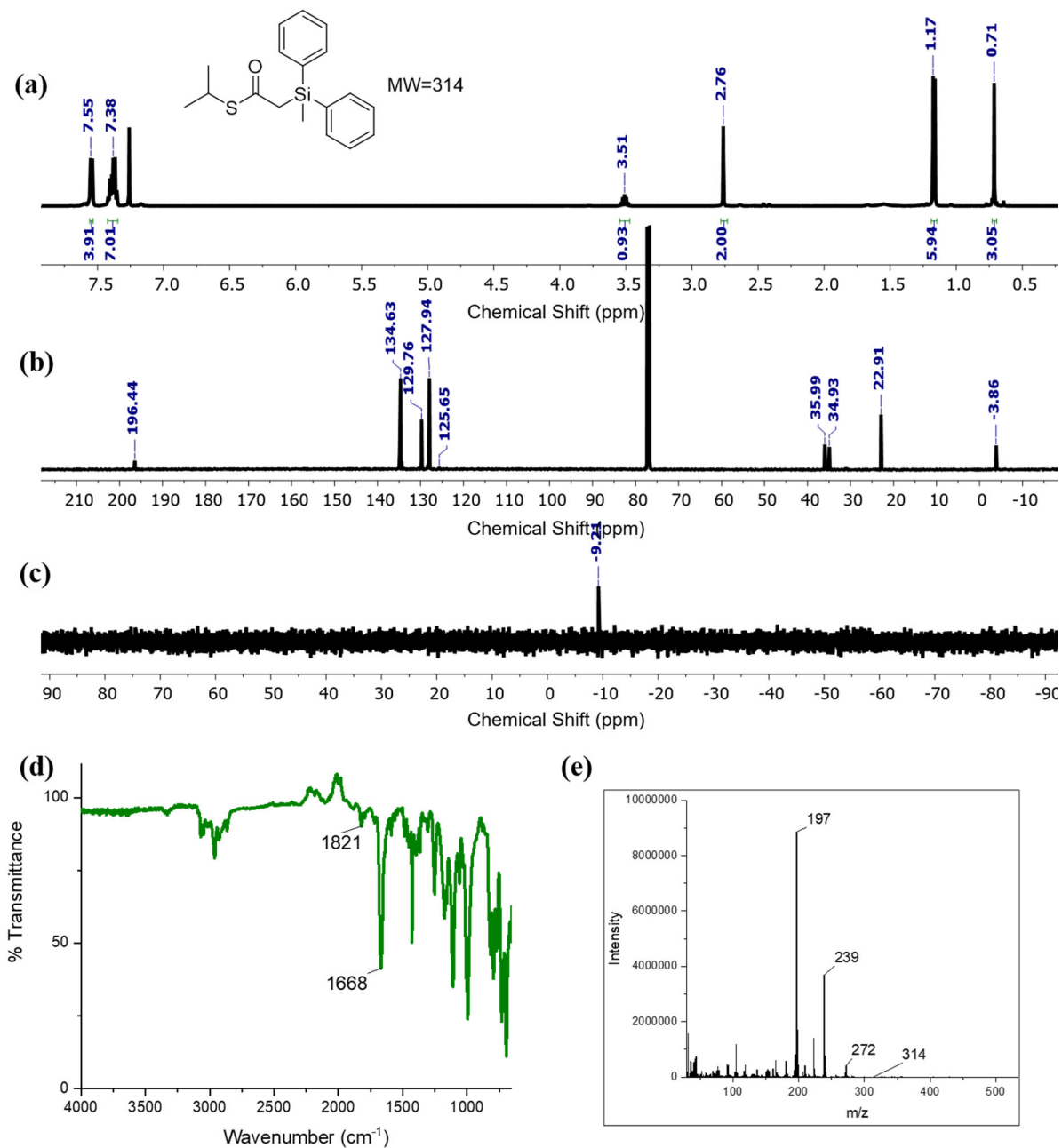
Figure A2.18. Table 2.2, entry 17. (a) ^{1}H NMR, (b) ^{13}C NMR, (c) ^{29}Si NMR, (d) FTIR, (e) mass spectroscopy.
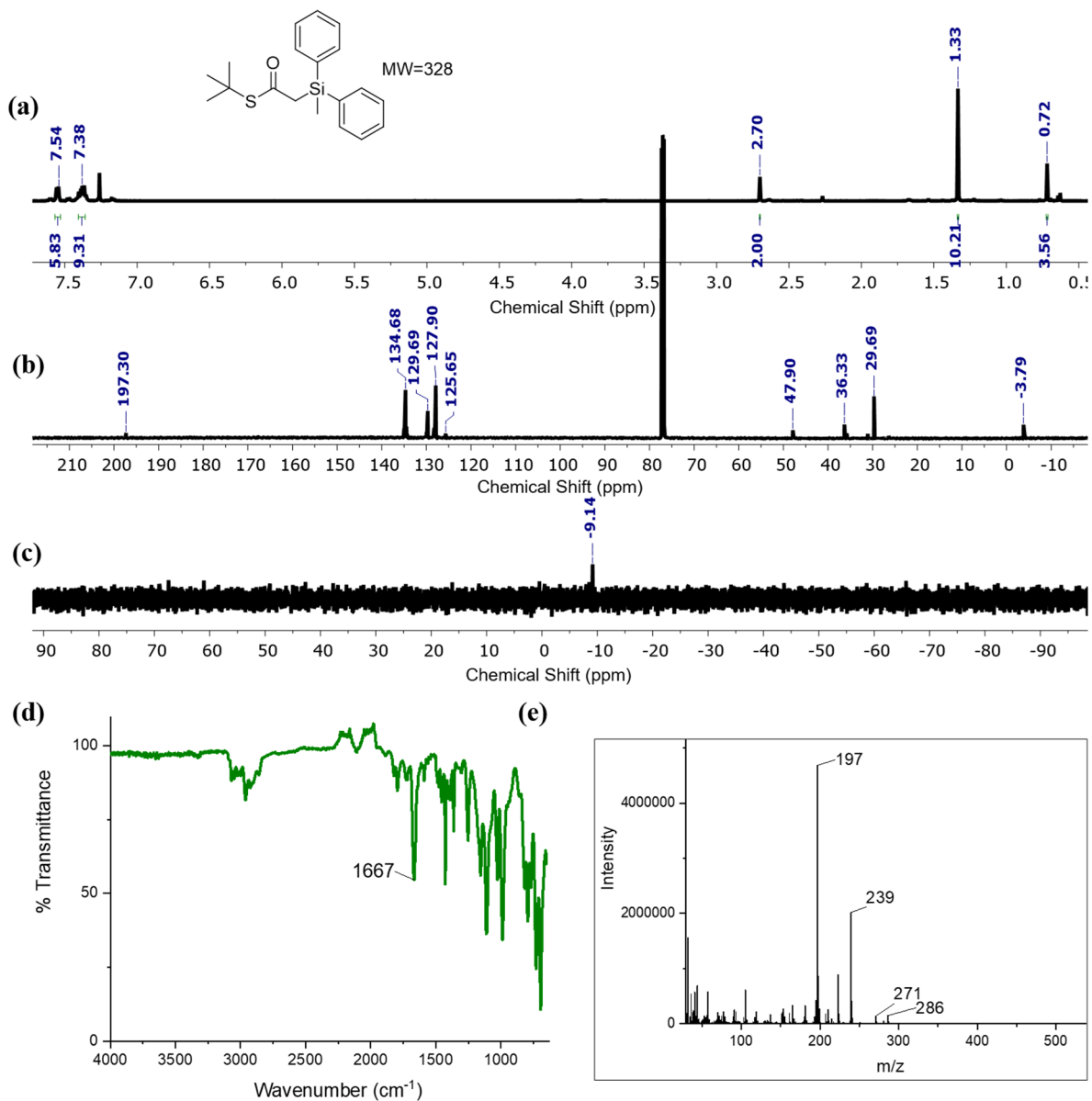
Figure A2.19. Table 2.2, entry 18. (a) ^{1}H NMR, (b) ^{13}C NMR, (c) ^{29}Si NMR, (d) FTIR, (e) mass spectroscopy.
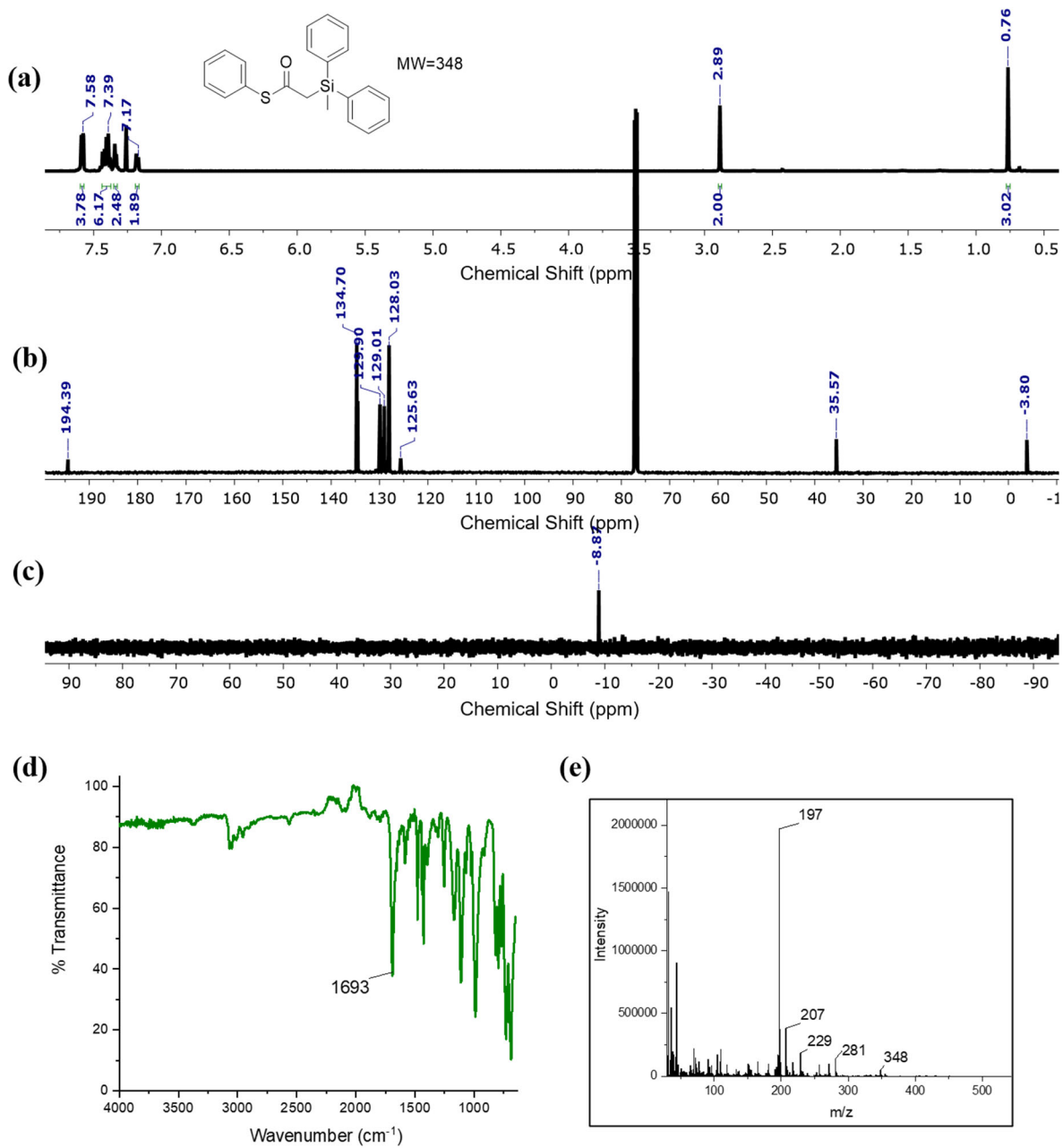
Figure A2.20. Table 2.2, entry 19. (a) ^{1}H NMR, (b) ^{13}C NMR, (c) ^{29}Si NMR, (d) FTIR, (e) mass spectroscopy.
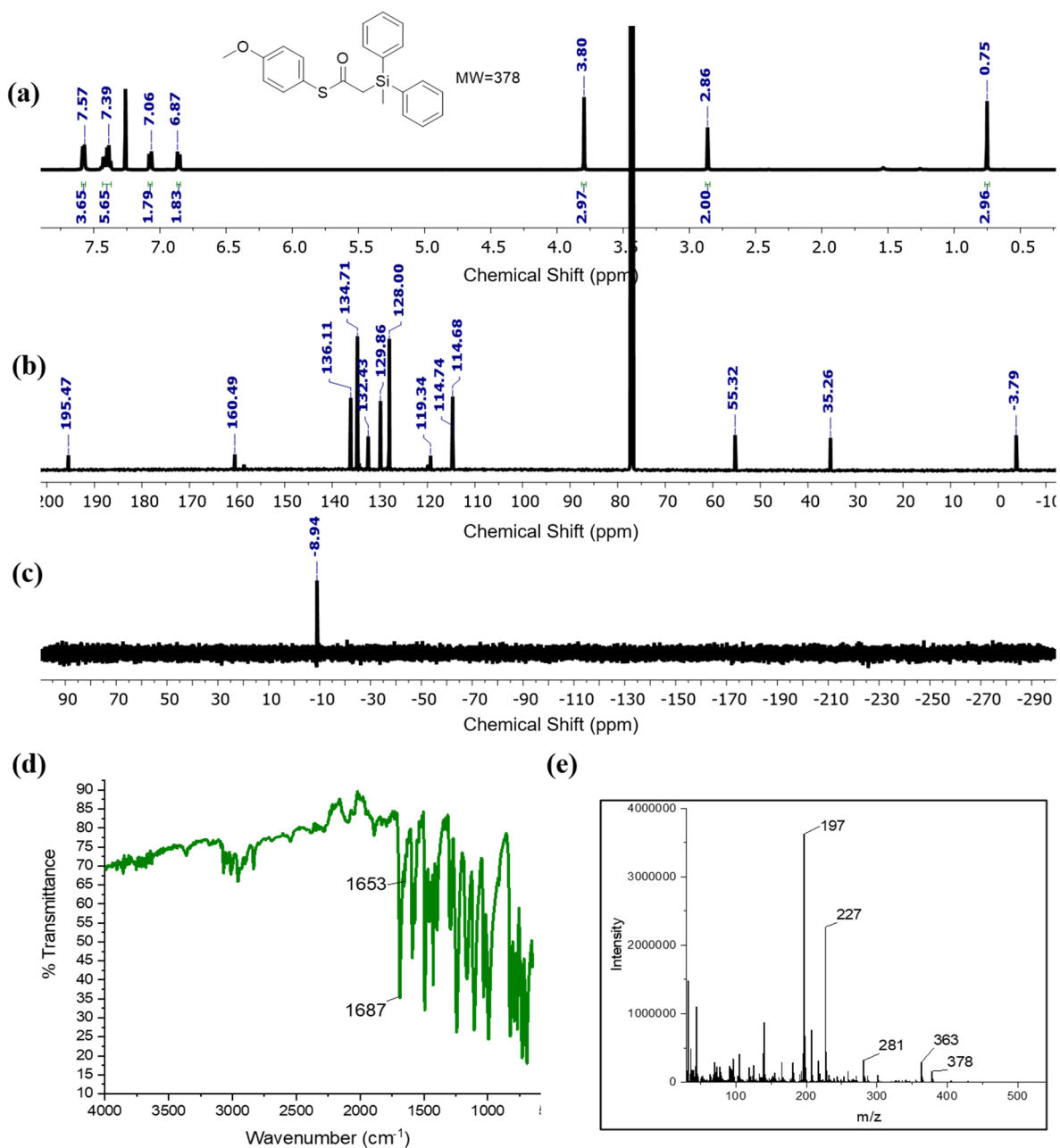
Figure A2.21. Table 2.2, entry 20. (a) ¹H NMR, (b) ¹³C NMR, (c) ²⁹Si NMR, (d) FTIR, (e) mass spectroscopy.
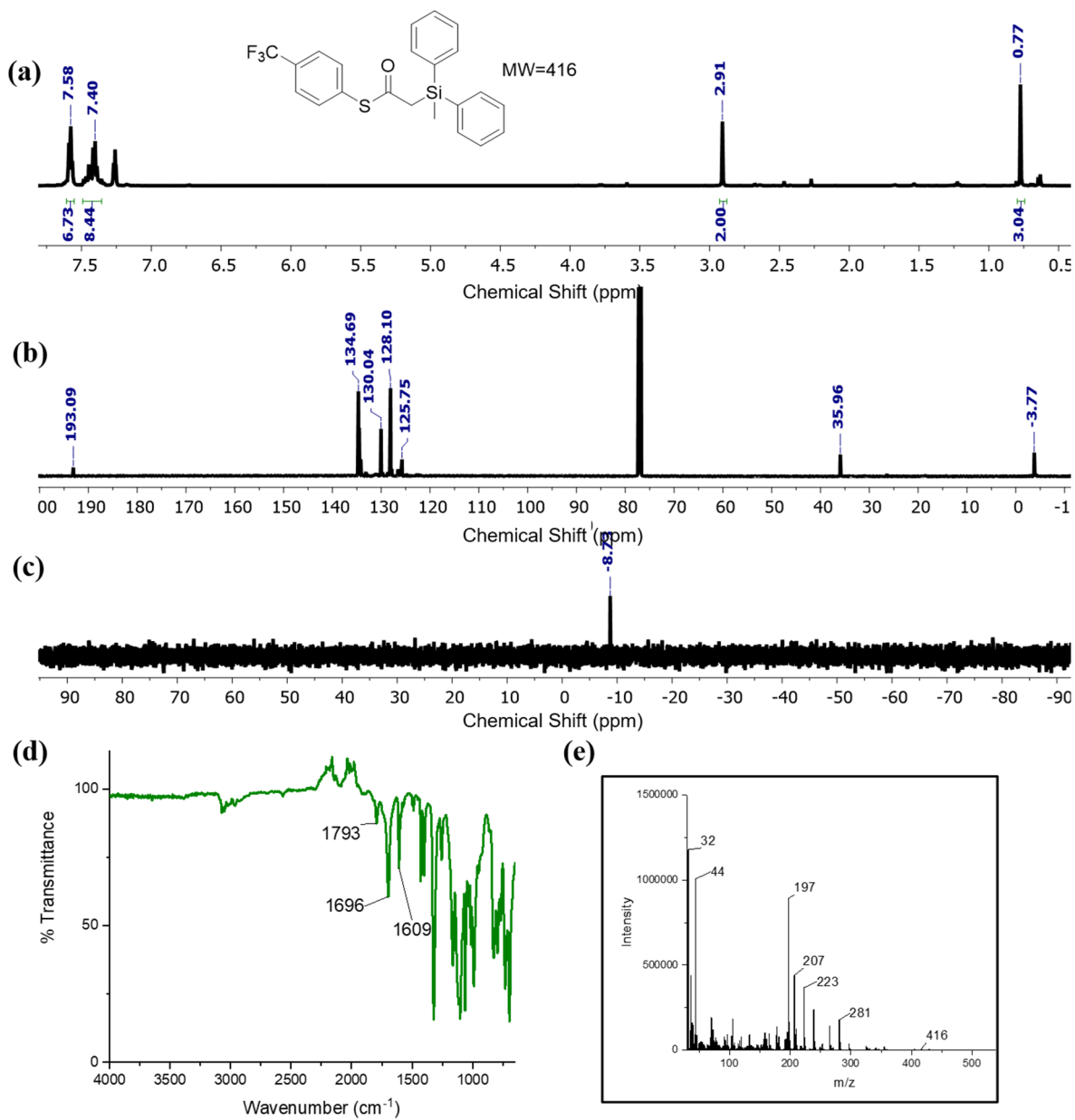
Figure A2.22. Table 2.2, entry 21. (a) ^{1}H NMR, (b) ^{13}C NMR, (c) ^{29}Si NMR, (d) FTIR, (e) mass spectroscopy.
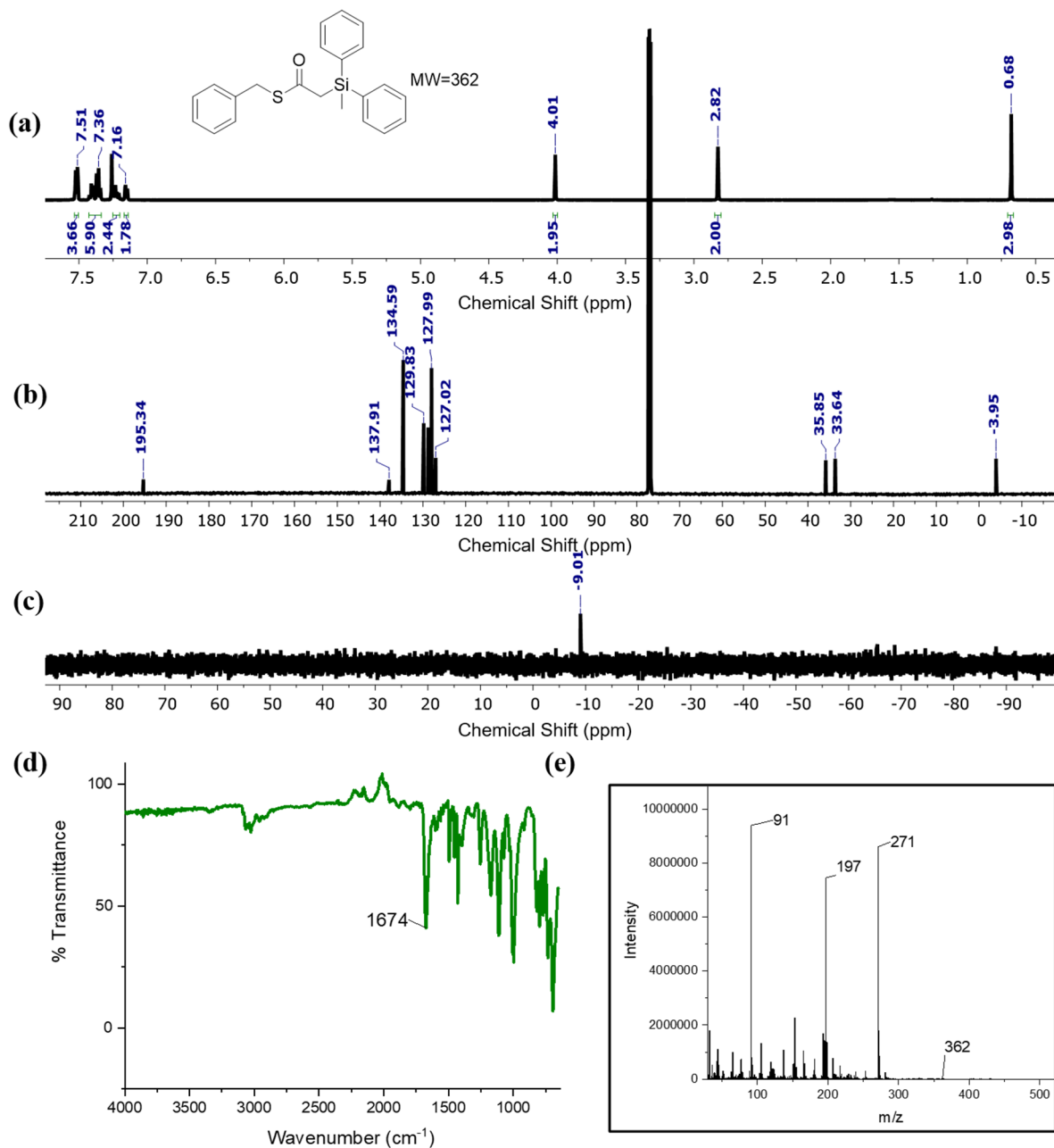
Figure A2.23. Table 2.3, entry TES 1. (a) ^{1}H NMR, (b) ^{13}C NMR, (c) ^{29}Si NMR, (d) FTIR, (e) mass spectroscopy.
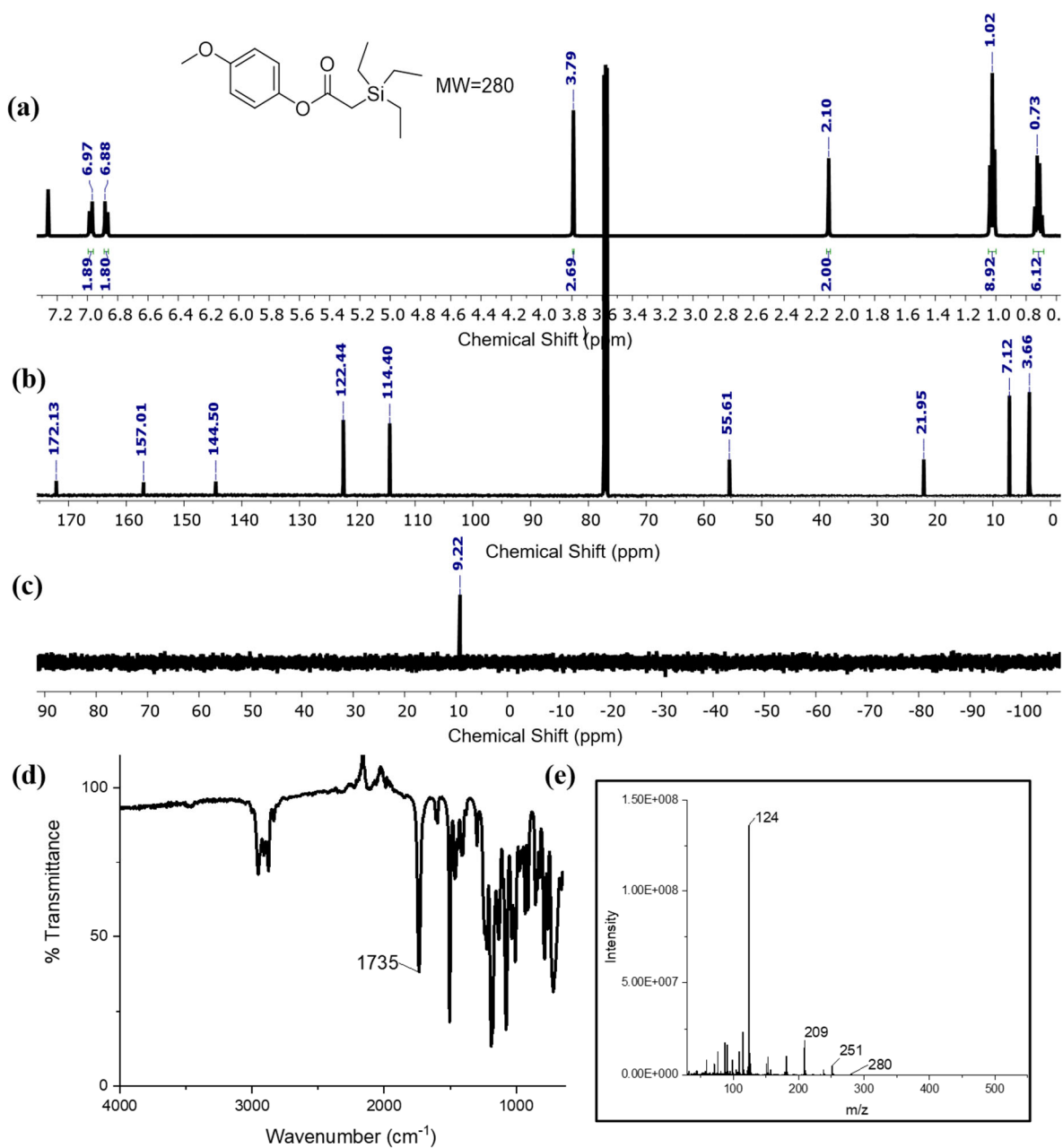
Figure A2.24. Table 2.3, entry TES 2. (a) ^{1}H NMR, (b) ^{13}C NMR, (c) ^{29}Si NMR, (d) FTIR, (e) mass spectroscopy.
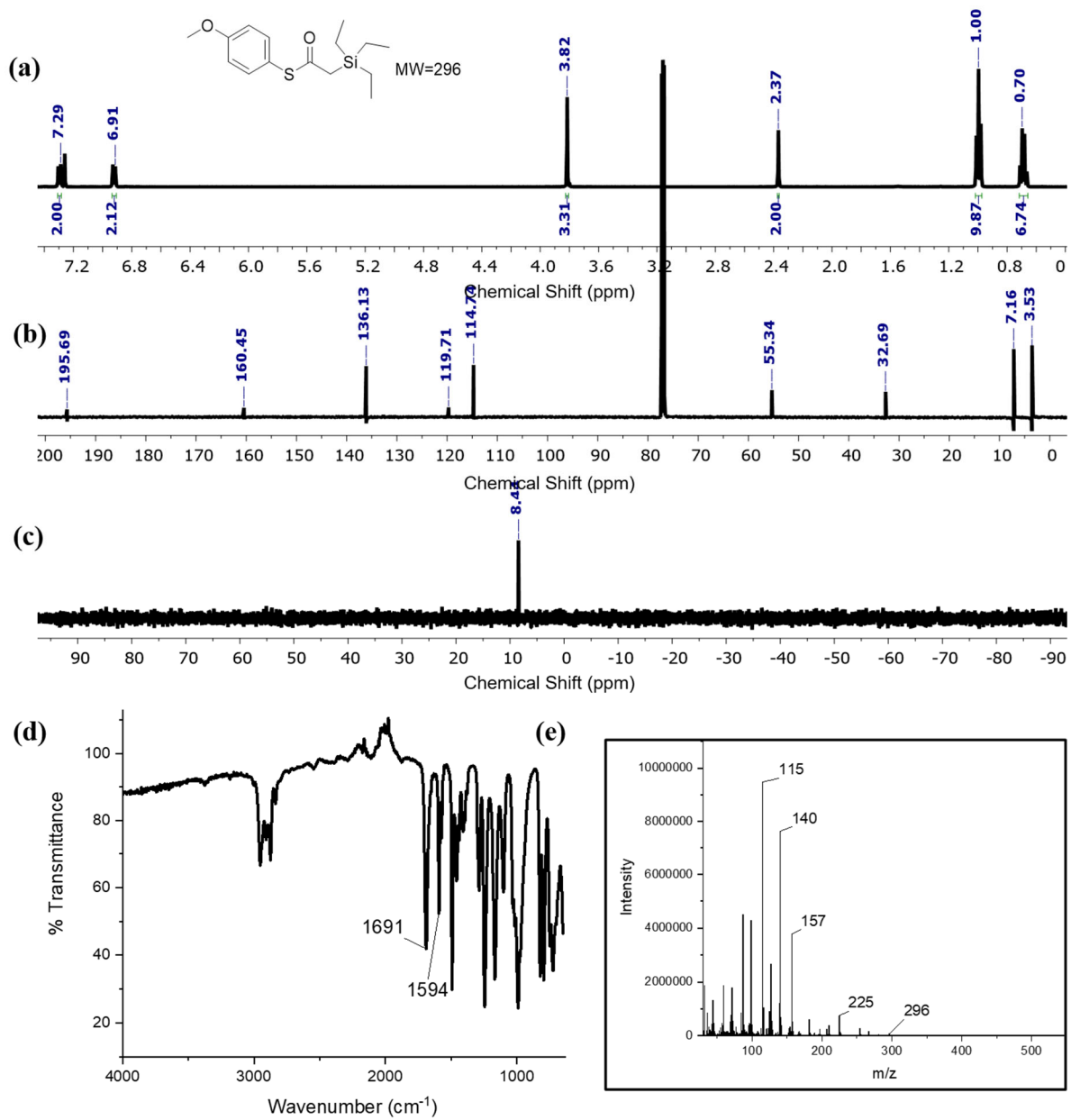
Figure A2.25. Table 2.3, entry TES 3. (a) ^{1}H NMR, (b) ^{13}C NMR, (c) ^{29}Si NMR, (d) FTIR, (e) mass spectroscopy.
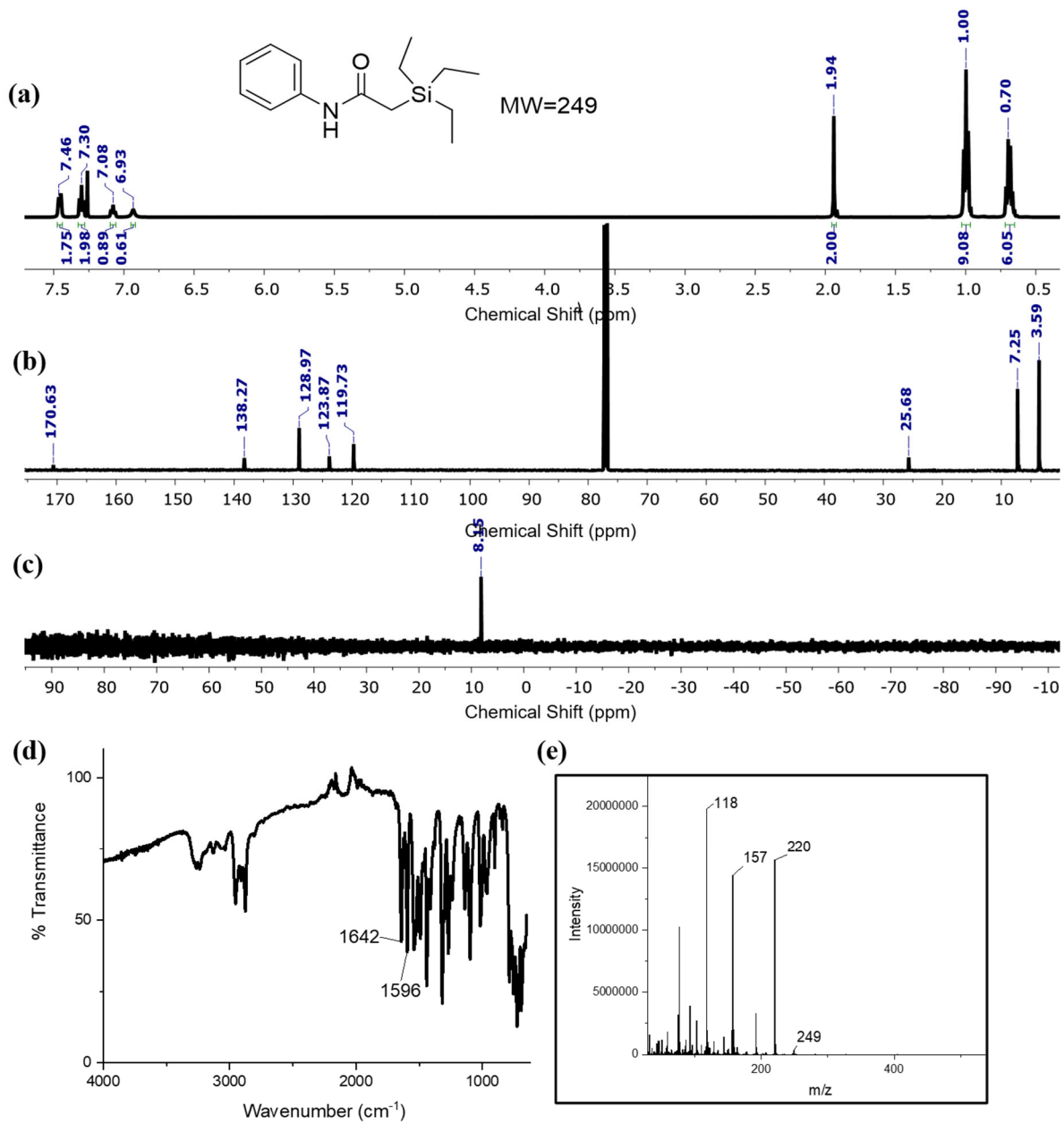
Figure A2.26. Table 2.3, entry TIPS 1. (a) ^{1}H NMR, (b) ^{13}C NMR, (c) ^{29}Si NMR, (d) FTIR, (e) mass spectroscopy.
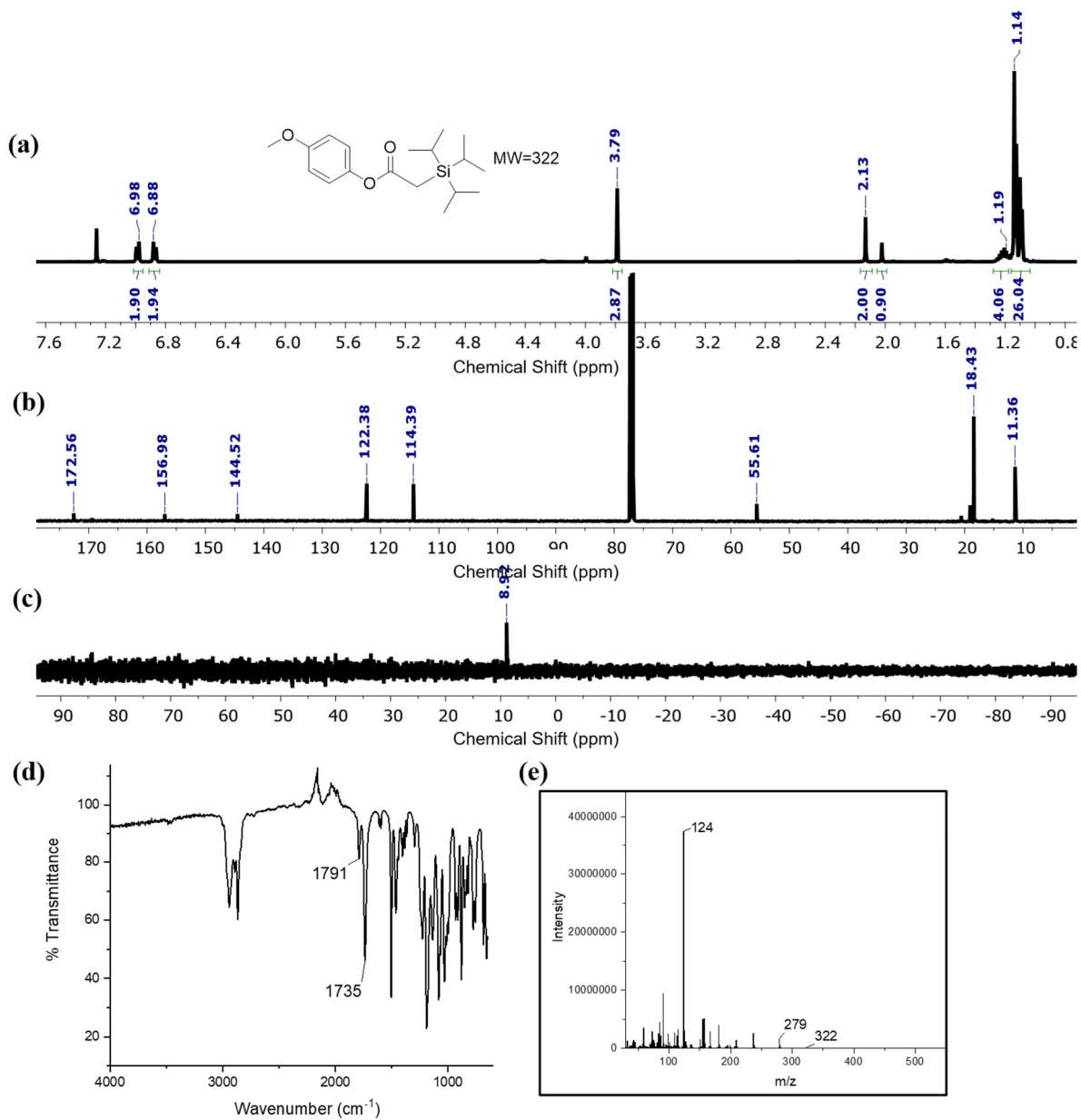
Figure A2.27. Table 2.3, entry TIPS 2. (a) ^{1}H NMR, (b) ^{13}C NMR, (c) ^{29}Si NMR, (d) FTIR, (e) mass spectroscopy.
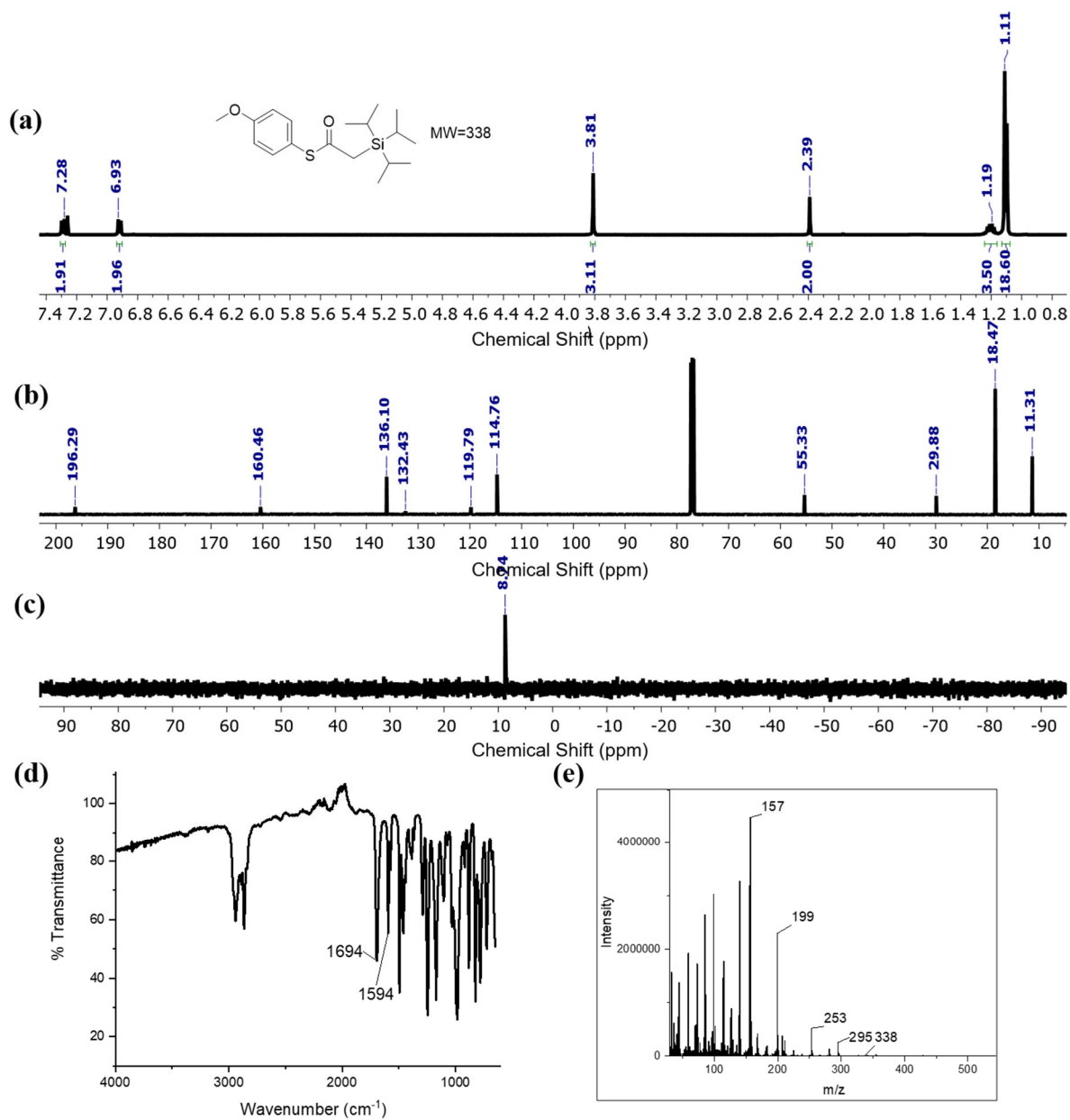
Figure A2.28. Table 2.3, entry TIPS 3. (a) ^{1}H NMR, (b) ^{13}C NMR, (c) ^{29}Si NMR, (d) FTIR, (e) mass spectroscopy.
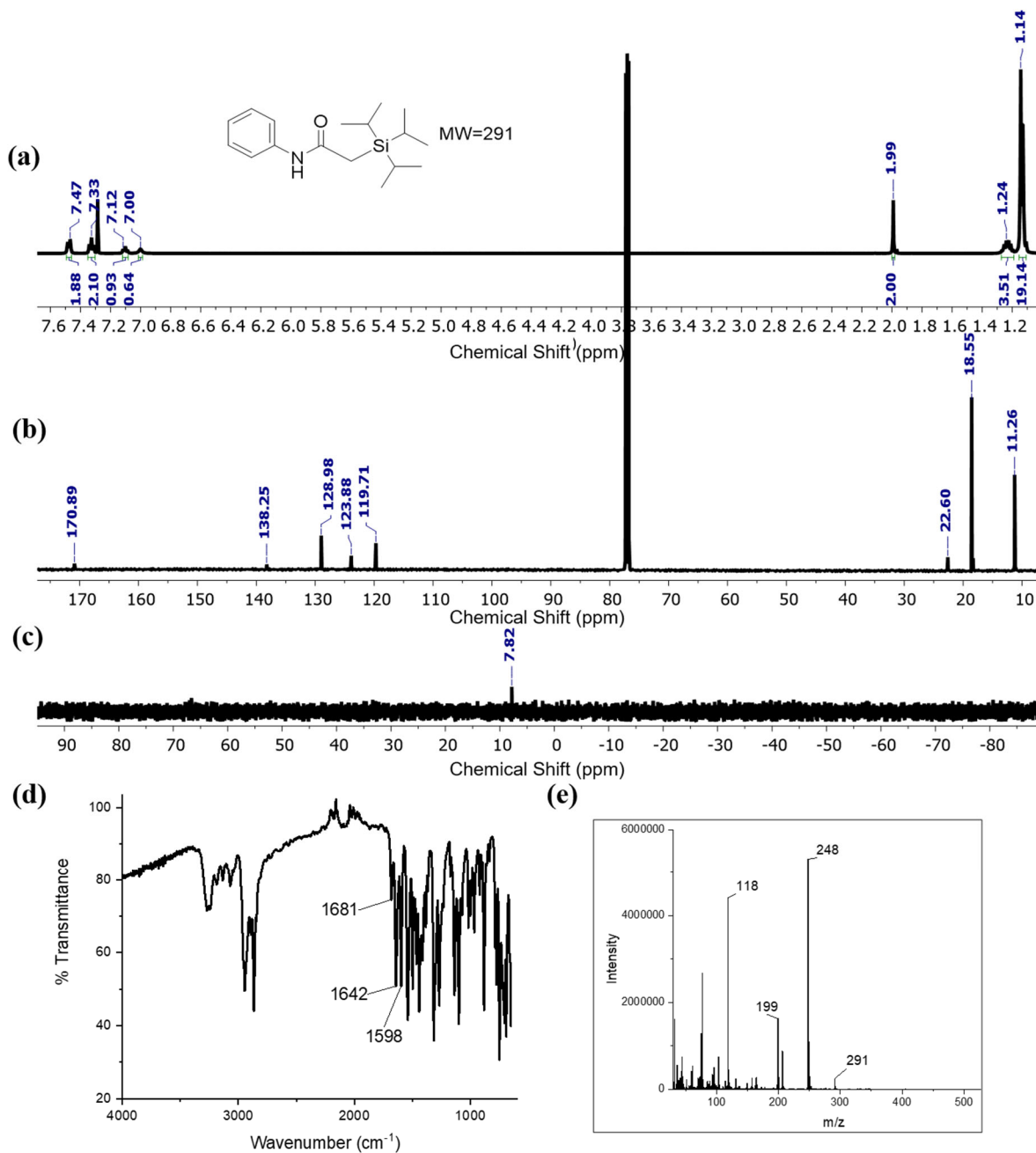
Figure A2.29. Table 2.3, entry DMPS 1. (a) ^{1}H NMR, (b) ^{13}C NMR, (c) ^{29}Si NMR, (d) FTIR, (e) mass spectroscopy.
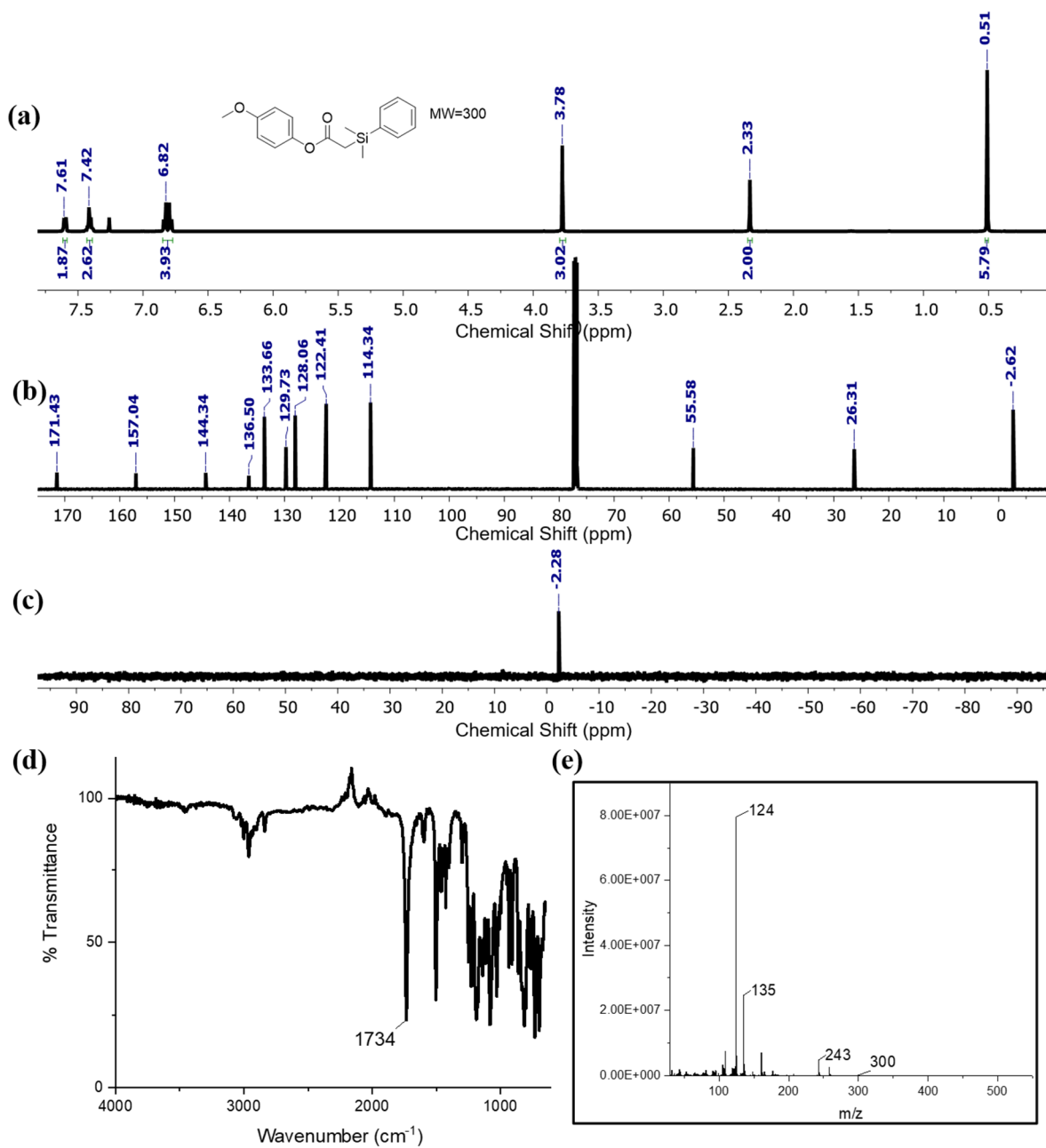
Figure A2.30. Table 2.3, entry DMPS 2. (a) ^{1}H NMR, (b) ^{13}C NMR, (c) ^{29}Si NMR, (d) FTIR, (e) mass spectroscopy.
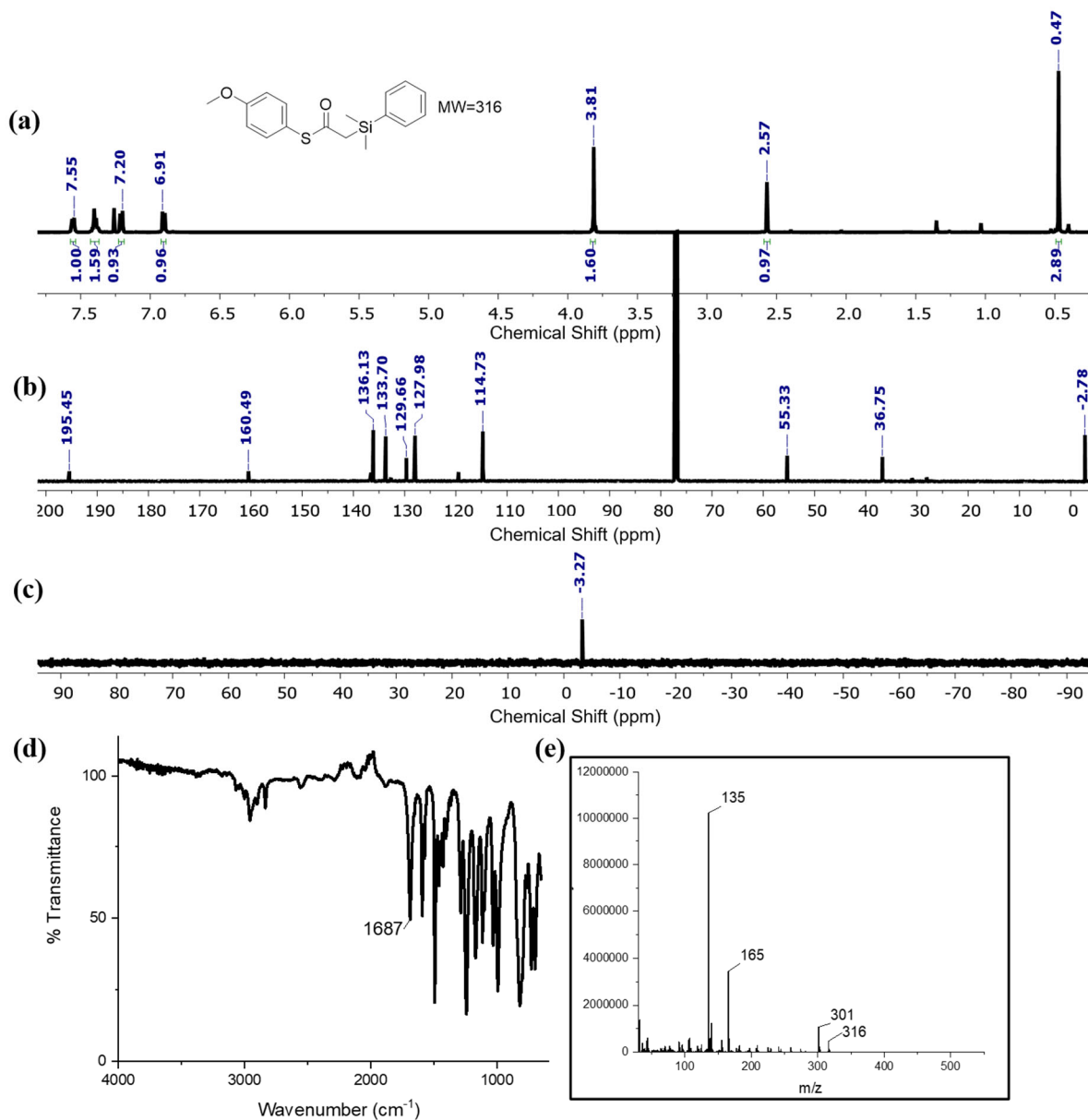
Figure A2.31. Table 2.3, entry DMPS 3. (a) ^{1}H NMR, (b) ^{13}C NMR, (c) ^{29}Si NMR, (d) FTIR, (e) mass spectroscopy.
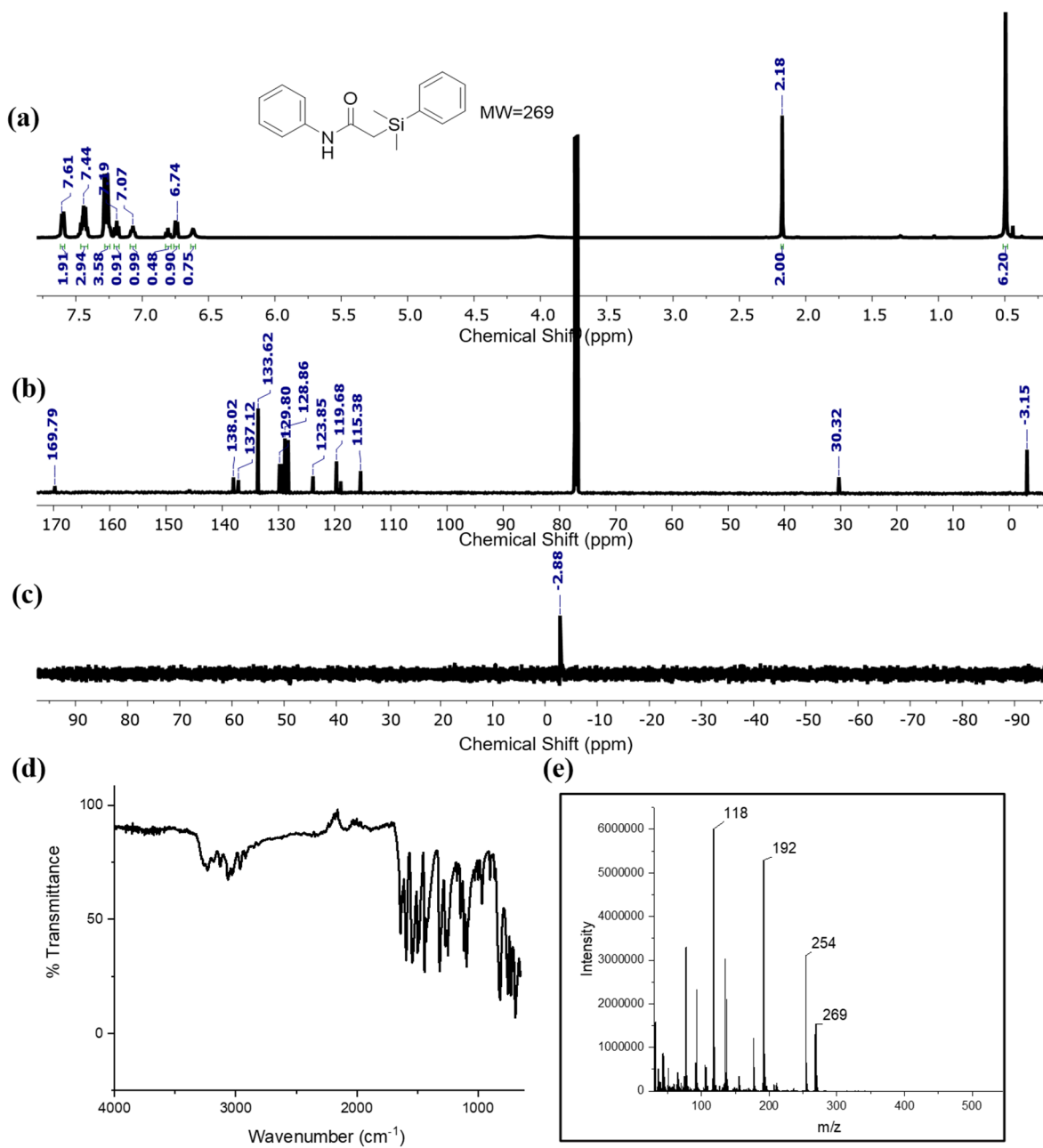
Figure A2.32. Table 2.3, entry TPhS 1. (a) ^{1}H NMR, (b) ^{13}C NMR, (c) ^{29}Si NMR, (d) FTIR, (e) mass spectroscopy.
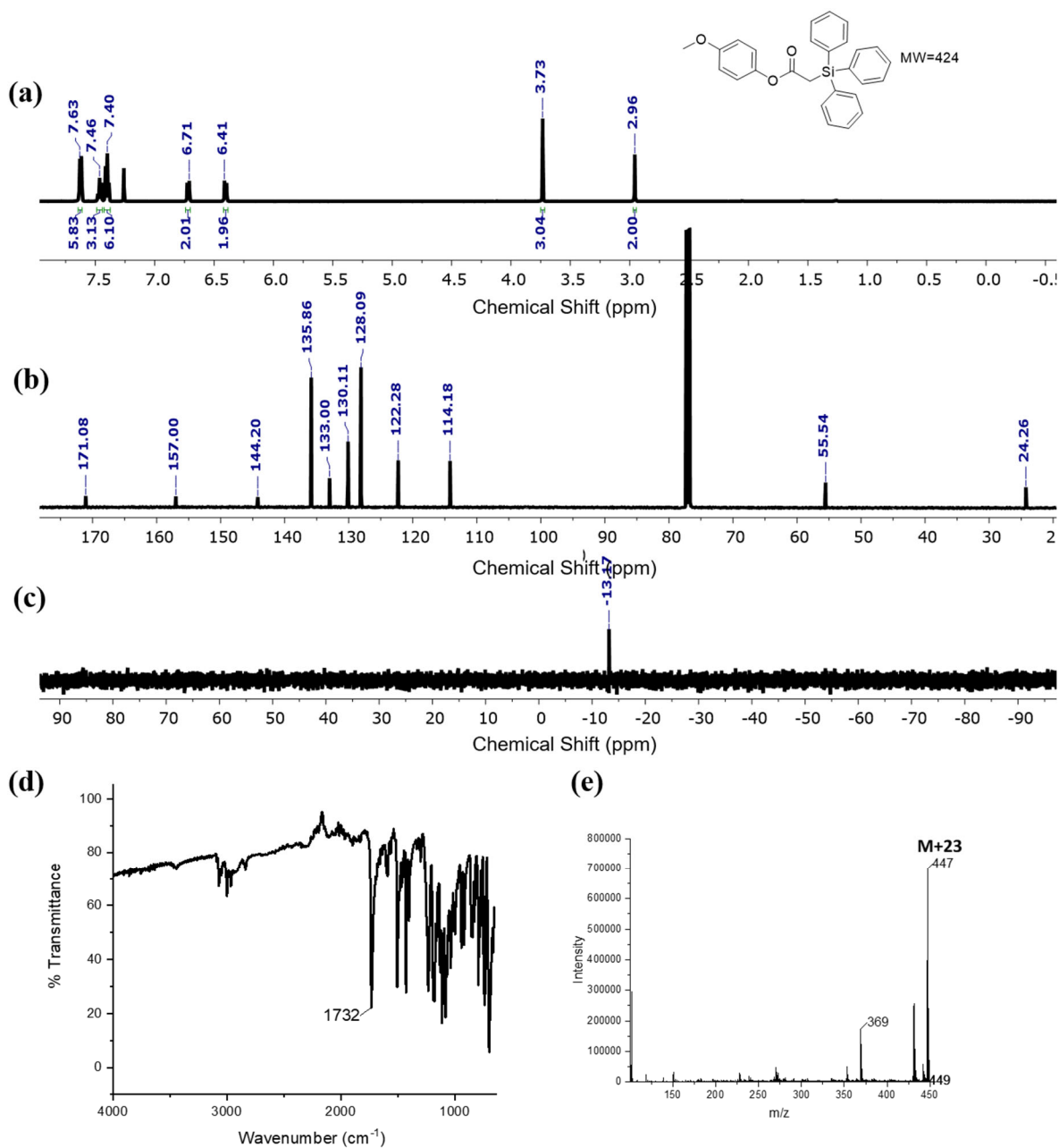
Figure A2.33. Table 2.3, entry TPhS 2. (a) ^{1}H NMR, (b) ^{13}C NMR, (c) ^{29}Si NMR, (d) FTIR, (e) mass spectroscopy.
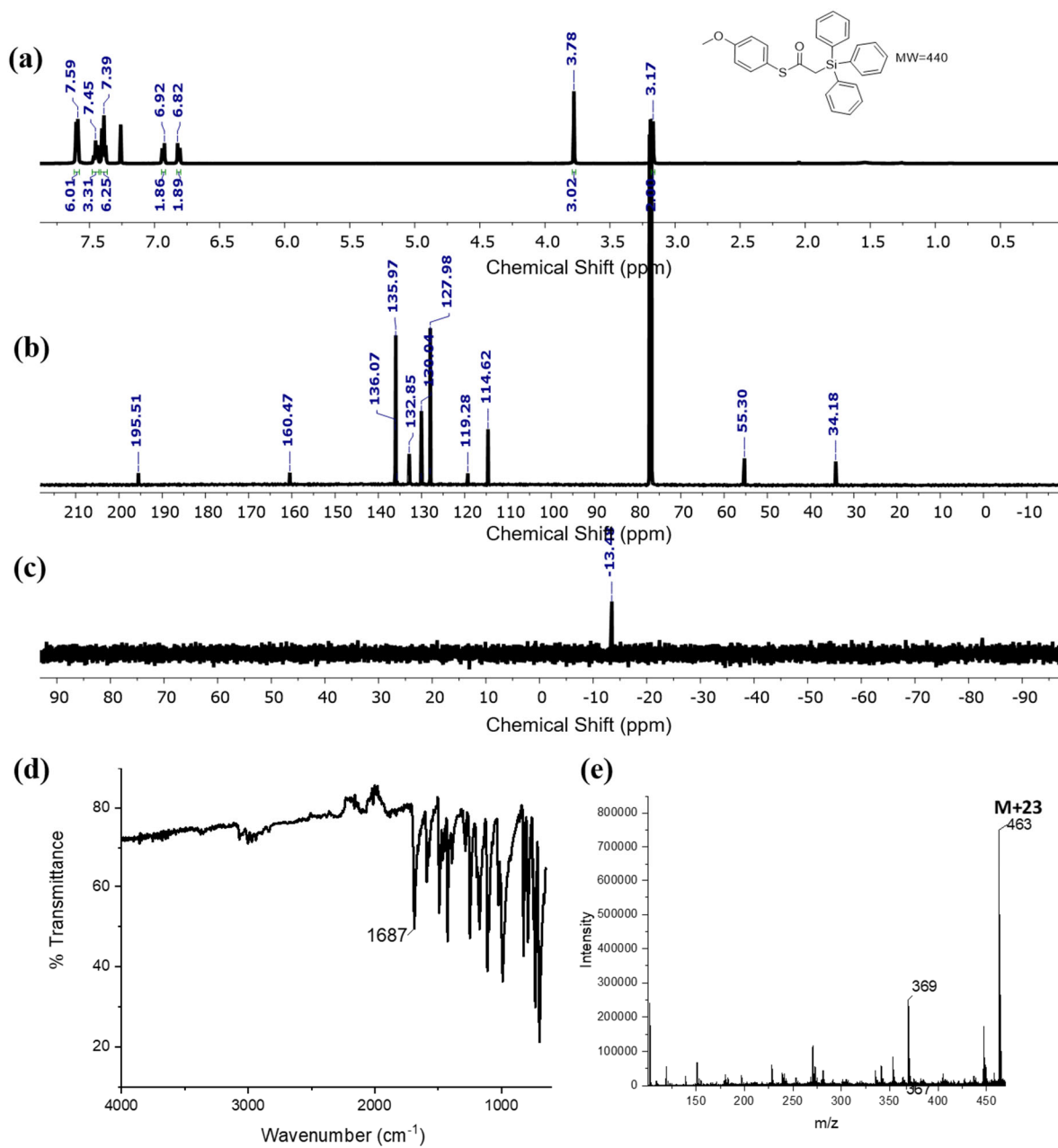
Figure A2.34. Table 2.3, entry TPhS 3. (a) ^{1}H NMR, (b) ^{13}C NMR, (c) ^{29}Si NMR, (d) FTIR, (e) mass spectroscopy.
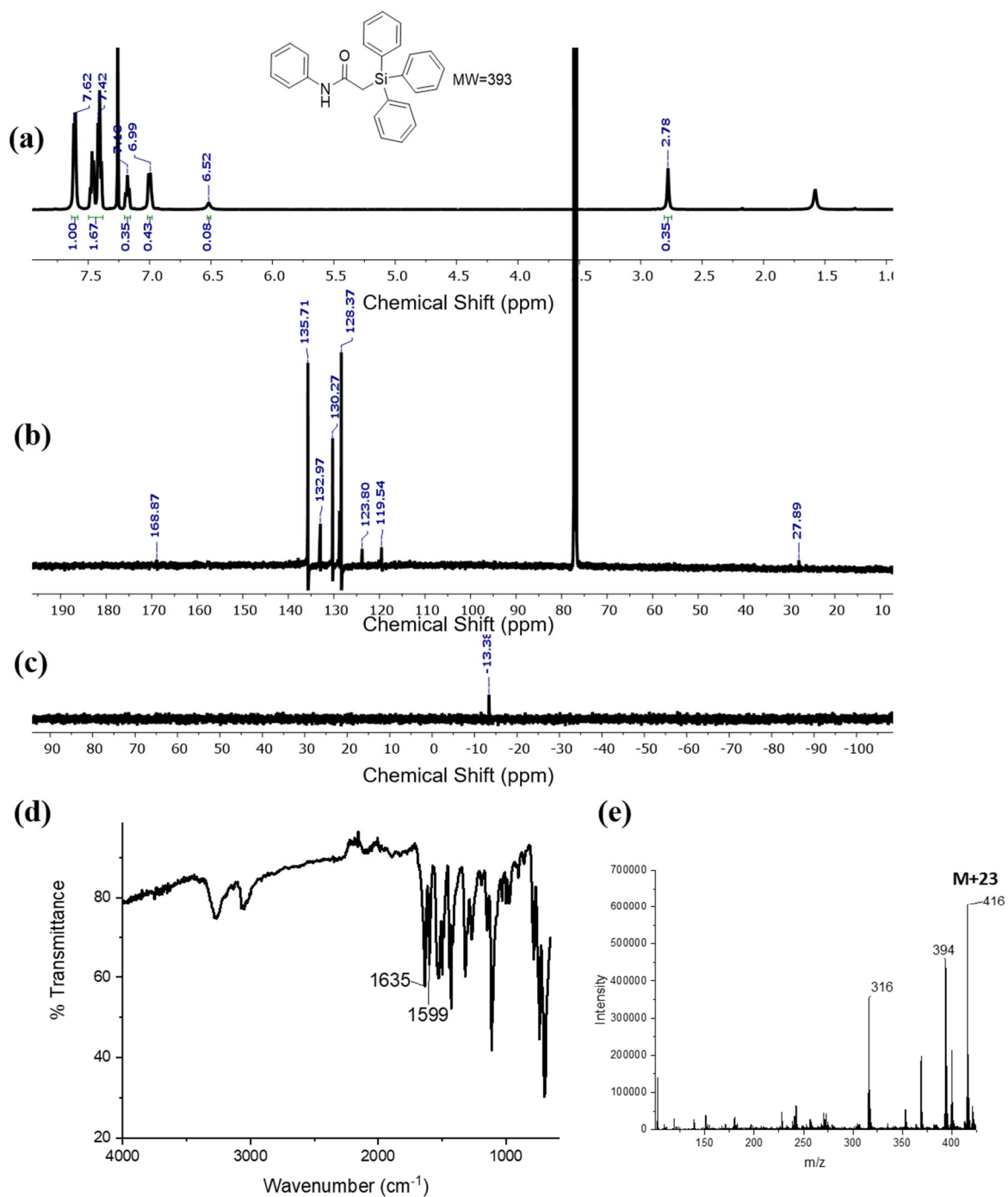
2.8   References

(20)   Blasco, E.; Sims, M. B.; Goldmann, A. S.; Sumerlin, B. S.; Barner-Kowollik, C. 50th Anniversary Perspective: Polymer Functionalization. Macromolecules 2017, 50 (14), 5215–5252. https://doi.org/10.1021/acs.macromol.7b00465.

(108)   Xiang, Y.; Burrill, D. J.; Bullard, K. K.; Albrecht, B. J.; Tragesser, L. E.; McCaffrey, J.; Lambrecht, D. S.; Pentzer, E. Polymerization of Silyl Ketenes Using Alkoxide Initiators: A Combined Computational and Experimental Study. Polym. Chem. 2017, 8 (35), 5381–5387. https://doi.org/10.1039/C7PY00858A.

(117)   Xiang, Y.; Mitchell, S.; Rheingold, A. L.; Lambrecht, D. S.; Pentzer, E. Oligomerization of Silyl Ketene: Favoring Chain Extension over Backbiting. Macromolecules 2019, 52 (16), 6126–6134. https://doi.org/10.1021/acs.macromol.9b00752.

(118)   Brady, W. T.; Saidi, K. Trimethylsilylketene. Cycloadditions of Ketenes and Aldehydes. J. Org. Chem 1979, 44 (5), 733–737.

(119)   Yang, H. W.; Romo, D. Studies of the Asymmetric [2+2] Cycloaddition of Silylketenes and Aldehydes Employing Ti-TADDOL Catalysts. Tetrahedron Lett. 1998, 39 (19), 2877–2880. https://doi.org/10.1016/S0040-4039(98)00422-5.

(120)   Concepcion, A. B.; Maruoka, K.; Yamamoto, H. Organoaluminum-Promoted Cycloaddition of Trialkylsilylketene with Aldehydes: A New, Stereoselective Approach to Cis-2-Oxetanones and 2(Z)-Alkenoic Acids. Tetrahedron 1995, 51 (14), 4011–4020. https://doi.org/10.1016/0040-4020(95)00142-U.

(121)   Dymock, B. W.; Kocienski, P. J.; Pons, J. View Article Online / Journal Homepage / Table of Contents for This Issue 3-(Trimethylsilyl)Oxetan-2-Ones via Enantioselective [2+2]

Cycloaddition of (Trimethylsily1)Ketene to Aldehydes Catalysed by Methylaluminoimidazolines. Chem. Commun. 1996, No. 3, 1053–1054.

(122)   Rossé, G.; Gerber, F.; Specklin, J. L.; Hubschwerlen, C. A Novel Synthesis of β-Sulfinyl- and β-Sulfonyl-Hydroxamic Acids via CsF-Mediated Ring Opening of Substituted β-Lactones. Synlett 2001, No. 4, 538–540. https://doi.org/10.1055/s-2001-12311.

(123)   Brady, W. T.; Cheng, T. C. Phenyl(Trimethylsilyl)Ketene. Some Ketene Reactions with Diazomethane. J. Organomet. Chem. 1977, 137 (3), 287–292. https://doi.org/10.1016/S0022-328X(00)81435-7.

(124)   Allen, A.; Tidwell, T. Trimethylsilylketene: Reactivity and Stabilization. Tetrahedron Lett. 1991, 32 (7), 847–850.

(125)   Green, I. X.; Tang, W.; Neurock, M.; Yates, J. T. Localized Partial Oxidation of Acetic Acid at the Dual Perimeter Sites of the Au/TiO2 Catalyst-Formation of Gold Ketenylidene. J. Am. Chem. Soc. 2012, 134 (33), 13569–13572. https://doi.org/10.1021/ja305911e.

(126)   Hurd, C. D.; Blunck, F. H. The Pyrolysis of Esters. J. Am. Chem. Soc. 1938, 60 (10), 2419–2425. https://doi.org/10.1021/ja01277a035.

(127)   DeWitt, C. H. The Ketenic Decomposition Of Ketones. Ketene And Methyl Ketene. J. Am. Chem. Soc. 1923, 45 (12), 3095–3101. https://doi.org/10.1021/ja01665a042.

(128)   Haller, I.; Srinivasan, R. Primary Processes in the Photochemistry of TetramethyI-1,3-Cyclobutanedione. J. Am. Chem. Soc. 1965, 87 (5), 1144–1145. https://doi.org/10.1021/ja01083a044.

(129)   Turro, N. J.; Leermakers, P. A.; Wilson, H. R.; Neckers, D. C.; Byers, G. W.; Vesley, G. F. Photochemistry of 1,3-Cyclobutanediones. Decomposition Modes and Chemical Intermediates. J. Am. Chem. Soc. 1965, 87 (12), 2613–2619. https://doi.org/10.1021/ja01090a017.

(130) Fisher, G. J.; MacLean, A. F.; Schnizer, A. W. Apparatus For The Preparation Of Ketene By The Pyrolysis Of Acetic Anhydride. J. Org. Chem. 1953, 18 (8), 1055–1057. https://doi.org/10.1021/jo50014a021.

(131) Hertler, W. R.; Sogah, D. Y.; Webster, O. W.; Trost, B. M. Group-Transfer Polymerization. 3. Lewis Acid Catalysis. Macromolecules 1984, 17 (7), 1415–1417. https://doi.org/10.1021/ma00137a021.

(132) Kojima, K.; Sawamoto, M.; Higashimura, T. Living Cationic Polymerization of Isobutyl Vinyl Ether by Hydrogen Iodide/Lewis Acid Initiating Systems: Effects of Lewis Acid Activators and Polymerization Kinetics. Macromolecules 1989, 22 (4), 1552–1557. https://doi.org/10.1021/ma00194a008.

(133) Corma, A.; García, H. Lewis Acids as Catalysts in Oxidation Reactions: From Homogeneous to Heterogeneous Systems. Chem. Rev. 2002, 102 (10), 3837–3892. https://doi.org/10.1021/cr010333u.

(134) Román-Leshkov, Y.; Davis, M. E. Activation of Carbonyl-Containing Molecules with Solid Lewis Acids in Aqueous Media. ACS Catal. 2011, 1 (11), 1566–1580. https://doi.org/10.1021/cs200411d.

(135) Ruden, R. A. Trimethylsilylketene. Acylation and Olefination Reactions. J. Org. Chem. 1974, 39 (24), 3607–3608. https://doi.org/10.1021/jo00938a041.

(136) Kita, Y.; Sekihachi, J. I.; Hayashi, Y.; Da, Y. Z.; Yamamoto, M.; Akai, S. An Efficient Synthesis of A-Silylacetates Having Various Types of Functional Groups in the Molecules. J. Org. Chem. 1990, 55 (3), 1108–1112. https://doi.org/10.1021/jo00290a058.

(137) Kita, Y.; Matsuda, S.; Kitagaki, S.; Tsuzuki, Y.; Akai, S. Chemistry of Silylketene: A One-Pot Synthesis of a-Silyl Ketones. Synlett 1991, 6, 401–402.

(138) Johnson, D. A.; Jennings, M. P. Tandem Copper-Catalyzed Conjugate Addition-Diastereoselective Protonation of (E)-α-Trialkylsilyl-β-Alkyl(Aryl)-α,β-Unsaturated Esters. Org. Lett. 2018, 20 (19), 6099–6103. https://doi.org/10.1021/acs.orglett.8b02527.

(139) Fessenden, R. J.; Fessenden, J. S. A Convenient Synthesis of α-Silyl Esters. J. Org. Chem. 1967, 32 (11), 3535–3537. https://doi.org/10.1021/jo01286a054.

(140) Larson, G. L.; Fuentes, L. M. α-Silylation of Lithium Ester Enolates. J. Am. Chem. Soc. 1981, 103 (9), 2418–2419. https://doi.org/10.1021/ja00399a052.

(141) Van Staden, L. F.; Gravestock, D.; Ager, D. J. New Developments in the Peterson Olefination Reaction. Chem. Soc. Rev. 2002, 31 (3), 195–200. https://doi.org/10.1039/a908402i.

(142) Larson, G. L.; Hernandez, D.; de Lopez-Cepero, I. M.; Torres, L. E. Reaction of α-Silyl Esters with Grignard Reagents: A Synthesis of β-Keto Silanes and Ketones. Preparation of the Douglas Fir Tussock Moth Pheromone. J. Org. Chem. 1985, 50 (25), 5260–5267. https://doi.org/10.1021/jo00225a053.

(143) Gennari, C.; Beretta, M. G.; Bernardi, A.; Moro, G.; Scolastico, C.; Todeschini, R. Lewis Acid Mediated Aldol Condensations Using Thioester Silyl Ketene Acetals. Tetrahedron 1986, 42 (3), 893–909.

(144) Ireland, R.; Wipf, P.; Armstrong, J. Stereochemical Control in the Ester Enolate Claisen Rearrangement. 1. Stereoselectivity in Silyl Ketene Acetal Formation. J. Org. Chem. 1991, 56 (2), 650–657. https://doi.org/10.1021/jo00002a030.

(145) Hattori, K.; Yamamoto, H. Highly Selective Generation and Application of (E)- and (Z)-Silyl Ketene Acetals from α-Hydroxy Esters. J. Org. Chem. 1993, 58 (20), 5301–5303. https://doi.org/10.1021/jo00072a005.

(146)   Rikkou-Kalourkoti, M.; Webster, O. W.; Patrickios, C. S. Group Transfer Polymerization. Encycl. Polym. Sci. Technol. 2013, 6, 527–543.

(147)   Valentí, E.; Pericàs, M. A.; Serratosa, F. Convenient Synthesis of Silylketenes from 1-Tert-Butoxy-2-Silylethynes. J. Org. Chem. 1990, 55 (1), 395–397. https://doi.org/10.1021/jo00288a081.

(148)   Pericas, M. A.; Serratosa, F.; Valenti, E. An Efficient Synthesis of Tert-Alkoxyethynes. Tetrahedron 1987, 43 (10), 2311–2316.

Part I: Silyl Ketenes as Building Blocks for Small Molecules and Polymers

Chapter 3

Group Transfer Polymerization of Silyl Ketene Monomers and

Additional Reactivity Experiments

3.1　Introduction

3.1.1　Group Transfer Polymerization Background

Group transfer polymerization (GTP) is a controlled polymerization technique developed by DuPont in the 1980s for acrylic monomers.[146] This technique commonly uses a silyl ketene acetal initiator and a catalyst to polymerize monomers, typically at ambient temperatures (Scheme 3.1).[131,149,150] The name of GTP comes from the silicon substituent on the initiator transferring to the end group upon termination, thus group transfer.[146,151] GTP proceeds through repeating Mukaiyama-Michael type reactions that are catalyzed by an additional catalyst, both associative and dissociative mechanisms have been proposed. It is also known that GTP is very sensitive to moisture and oxygen and air-free techniques are necessary for polymerization to occur.
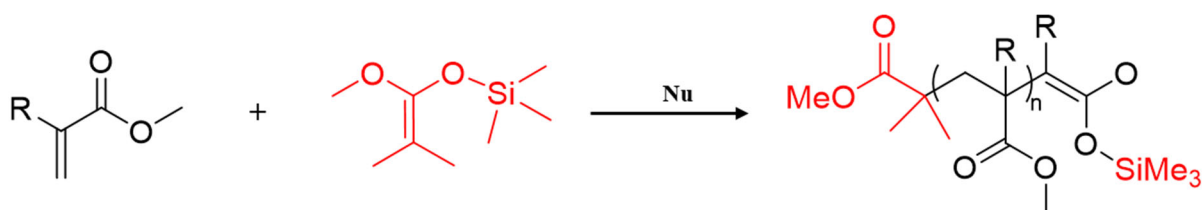
Scheme 3.1. General scheme for group transfer polymerization.

3.1.2　Components for Group Transfer Polymerization

Components for GTP include a monomer, an initiator, and a catalyst. Common monomers for GTP are acrylates or methacrylates; specifically, monomers that do not have an active hydrogen (Figure 3.1a).[146,151] For example, hydrogens on an alcohol or carboxylic acid are not ideal for GTP; however, these groups can be protected with a silyl substituent prior to polymerization and
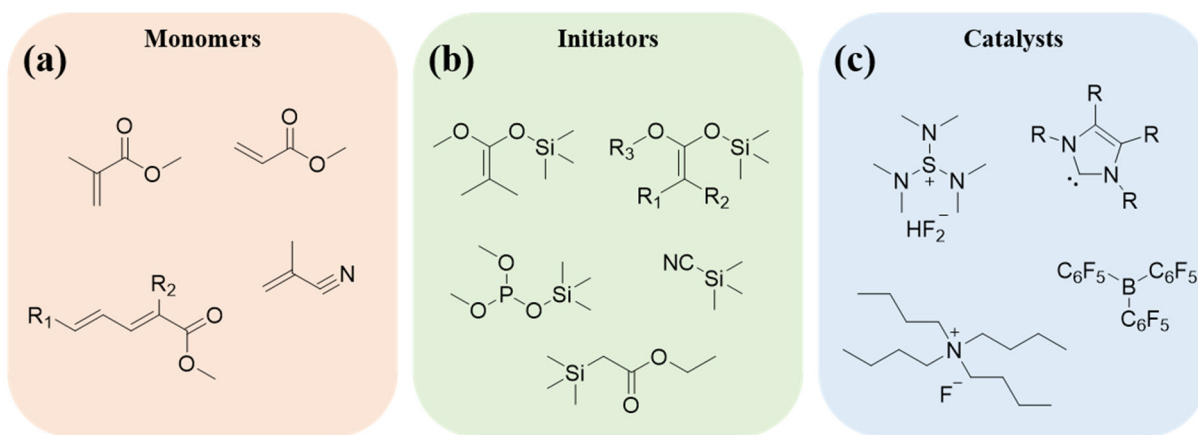
Figure 3.2. Components of GTP; (a) common monomers, (b) common initiators, and (c) various catalysts for GTP.

removed after polymerization. Acrylonitriles and acrylamides have also been used as monomers for GTP.[152,153] The polymerization conditions, such as choice of solvent, temperature, initiator, and catalysts, are dependent on the monomer of choice.

Initiators for GTP are typically silyl ketene acetals, most commonly used is methyl trimethylsilyl dimethylketene acetal (MTS) where all R-groups are methyl groups (Figure 3.1b).[146,151] If the R^1 and R^2 are large, the initiation step will be slowed and propagation is unlikely, for example if R^1 and R^2 are triisopropyl groups. The ether group (R^3) has little to no effect on the polymerization rate. Other initiators that have been used in GTP include trimethylsilyl cyanide, trimethyl(methylthio)silane, and dimethyl trimethylsilyl phosphite. Bifunctional initiators have also been developed for GTP to produce block copolymers.

A significant amount of research has been done on catalysts for GTP, as it plays an integral part in activating the initiator for polymerization. Catalyst type can be divided into two categories, (1) nucleophilic anions and (2) Lewis acids (Figure 3.1c).[146,151,154] Nucleophilic catalysts have been studied significantly and there are several generations of this type of catalyst used in GTP, such as

fluorides, azides, carboxylates, and bifluorides. Typically, these anions are accompanied by a larger cation, for example tetrabutylammonium. The most recent generation of nucleophilic catalysts are phosphines, phosphazene bases, and *N*-heterocyclic carbenes (NHCs). These types of catalysts are usually used in 1-0.1% vs initiator concentration and too much catalyst can halt the polymerization. Lewis acid catalysts are typically used with acrylate monomers where there is a 10% concentration vs. the monomer. Instead of the Lewis acid activating the initiator, the Lewis acid is more likely to activate the monomer due to their electrophilic nature.

The process of GTP is sensitive to moisture and reagents must be dried or anhydrous. Solvents typically used in GTP are toluene or tetrahydrofuran (THF), but other solvents have been used and is based on the catalyst for a specific system. For example, dichloromethane is commonly used for Lewis acid catalysts. In many experimental procedures, there is an induction period so the catalyst and initiator can interact to form the actual initiator or activated complex. However, this induction period many not be necessary depending on the mechanism of polymerization.

3.1.3 Associative vs. Dissociative Mechanism

As previously mentioned, there are two main mechanistic pathways for GTP, the associative or dissociative mechanism, usually the dissociative mechanism is the most widely accepted.[146,151] However, the most recent research involving NHC catalysts still has much debate as to which mechanism proceeds during polymerization, it is most likely due to the substituents on the backbone of the NHC.[155,156]

The dissociative pathway involves the catalysts' complexing with the initiators silyl group which then dissociates to generate an enolate.[156] The monomer is then added to react with the enolate that acts as the chain end and propagation occurs. Termination occurs when the enolate reacts with the dissociated initiator group to generate the end group (Scheme 3.2a). The associative

pathway follows a similar starting point, where the catalyst complexes to the initiator to form the activated initiator.[155] The monomer is then added to react with the activated initiator in a concerted like mechanism and the silyl group from the activated initiator is transferred to each incoming monomer and remains on the chain end. Termination occurs when the catalyst dissociates from the chain end so there is no activated complex (Scheme 3.2b).
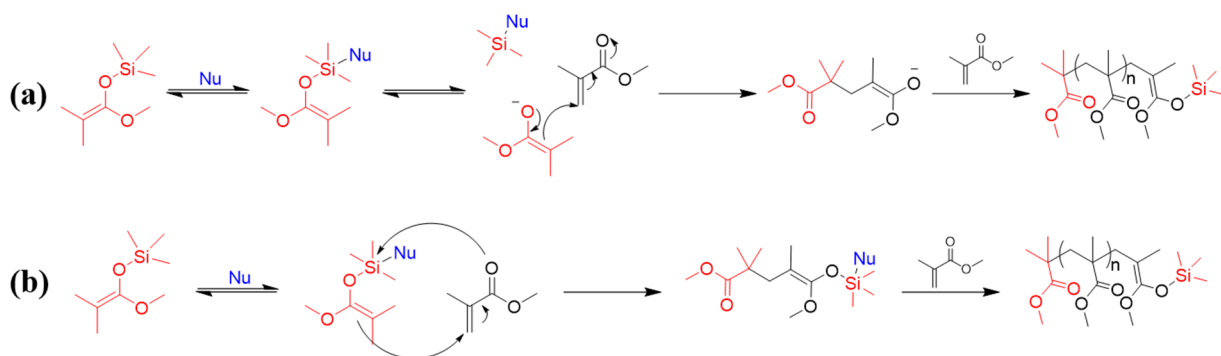
Scheme 3.2. Mechanistic pathways for GTP; (a) dissociative pathway and (b) associative pathway.

3.2   Approach

GTP is a great polymerization technique for the controlled polymerization of acrylates and methacrylates. Alternative monomers for GTP all contain some conjugated vinyl group, for example dienoates or acrylonitriles.[146] Silyl ketenes are uniquely different than these typical GTP monomers due to the cumulated double bond structure. However, silyl ketenes are similar to methacrylate's in that both compounds can easily produce enolates (Scheme 3.3), which can be polymerized by various polymerization techniques, for example anionic polymerization.[157,158] Therefore, silyl ketenes should be able to polymerization via GTP techniques. More specifically, the polymerization of silyl ketenes via GTP is hypothesized to produce the polyketone backbone
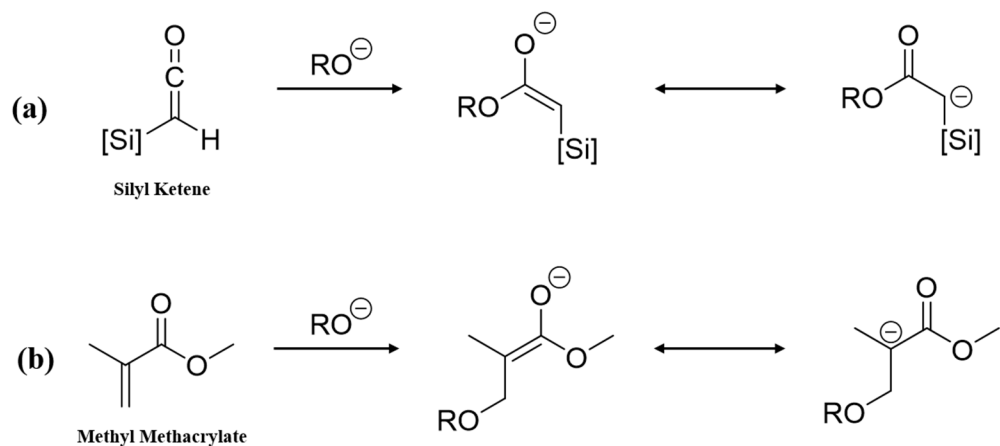
Scheme 3.3. (a) Enolate formation from silyl ketenes and (b) enolate formation from methyl methacrylate.
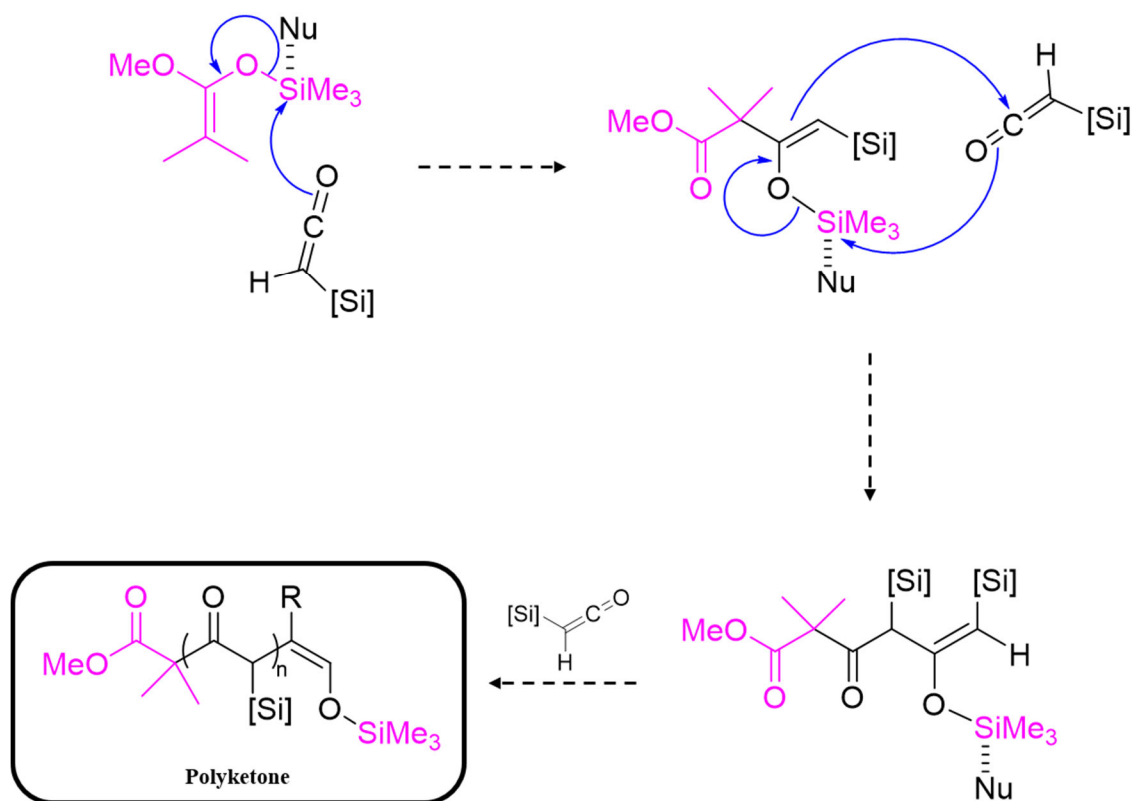
Figure 3.2. Proposed GTP of silyl ketene monomers.

(Figure 3.2). The hypothesis is that the initiator/catalyst can coordinate to the oxygen atom and react with the central carbon atom.

3.3   Examination of Protocol with Methyl Methacrylate

As previously mentioned, GTP is a very air-sensitive polymerization, so to ensure adequate technique, polymerization of methyl methacrylate (MMA) was performed. Each reagent needs to be thoroughly dried and degassed to help ensure the polymerization will be successful. MTS was chosen as the initiator, due to it being the most commonly studied GTP initiator. The catalyst of choice was an NHC due to recent literature on these compounds as catalyst and for their high silicophilicity or their ability to coordinate to silicon atoms. The NHC of choice, 1,3-diisopropylimidazolium chloride, is commercially available with the protonated carbene carbon atom.[155] Prior to use, the NHC needs to be deprotonated, which can be done by reacting the NHC with a base (sodium hydride) for three hours. Once the reaction reached completion, the reaction mixture was filtered under nitrogen and the solvent removed. The deprotonated NHC can then be diluted to the desired concentration for GTP (typically 1M) and can be stored in a glovebox. However, if a glovebox is unavailable, the NHC cannot be stored and needs to be deprotonated prior to every use.

For polymerization, the NHC and MTS were added to a round bottom flask with tetrahydrofuran (THF) and stirred for 10 minutes; this is to allow the initiator and catalyst to complex (Figure 3.3a). MMA is then added dropwise and a color change is immediately observed (Figure 3.3b). The reaction is monitored with ^{1}H NMR and FTIR to observe the C=C bond being consumed (Figure 3.3c/d). Once fully consumed, the polymerization is quenched and exposed to atmosphere. The resulting polymer, PMMA, is then purified via precipitation with methanol and THF and PMMA is obtained as a white solid. In comparison with literature, the theoretical average molecular
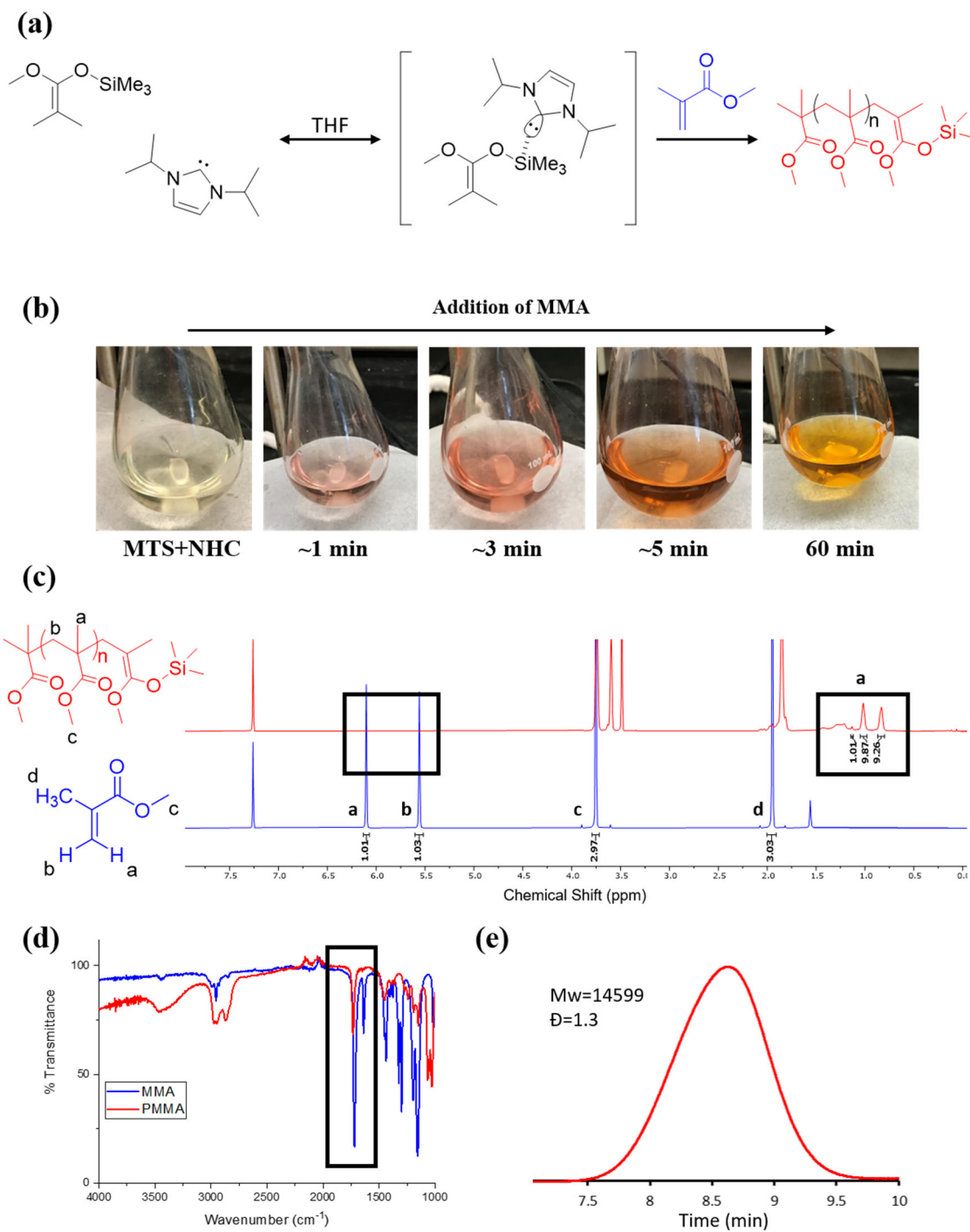
Figure 3.3. (a) Reaction scheme for the GTP of MMA with an NHC catalyst; (b) color change of reaction mixture as MMA is added; (c) ^{1}H NMR of MMA monomer (blue) and PMMA (red); (d) FTIR of MMA and PMMA; (e) GPC of PMMA.

Overall, the methodology used was successful and consistently produced PMMA.

3.4   Control Experiments

This developed methodology was then applied to silyl ketene monomers, with initial experiments using the same experimental procedure as MMA. TIPS (triisopropylsilyl) ketene was first used and full consumption of ketene was observed, however this was not reproducible, regardless of polymerization conditions. So to take a step back we needed to perform some baseline experiments; more specifically, performing the polymerization with the absence of catalyst or initiator.

3.4.1   Absence of Catalyst or Initiator

These baseline experiments were performed with both TIPS and TES ketene. The first control experiment examined the outcome of the polymerization with the absence of initiator (Scheme 3.4a). The NHC was added to a round bottom flask with THF, then TIPS or TES ketene was added dropwise. The reactions were monitored over time with FTIR and ^{1}H NMR to observe any ketene consumption or the formation of any products. For both TIPS and TES ketene after 4 hours the ketene peak was still observed in both FTIR and ^{1}H NMR, however there was formation of a secondary product. This is easily observed in the ^{29}Si NMR where two peaks are observed in the small molecule region, one indicating the silyl ketene peak and an additional small molecule peak. This was expected due to the high silicophilicity of the NHC, so the second peak is likely due to the NHC coordinating to the silyl group on the silyl ketene.[155,159]

The second control experiment examined the outcome of the polymerization conditions in the absence of catalyst (Scheme 3.4b). The initiator (MTS) was added to a round bottom flask with anhydrous THF, then TIPS or TES was added dropwise. Again, the reactions were monitored with FTIR and ^{1}H NMR. For both ketenes examined, no reaction was observed and no ketene was
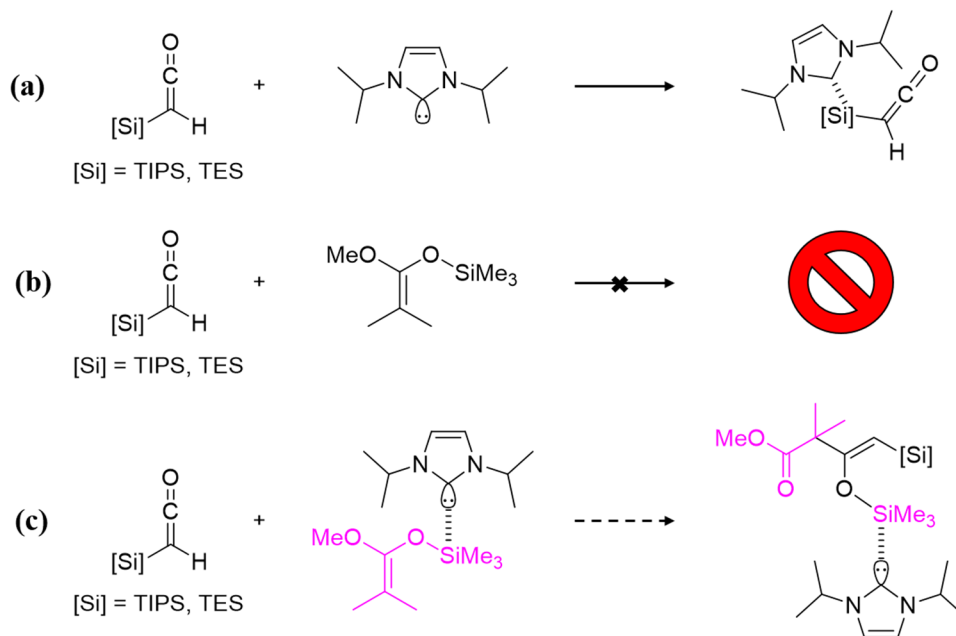
Scheme 3.4. (a) Control reaction in the absence of initiator; (b) control reaction in the absence of catalyst; (c) Control reaction with a 1:1 monomer to initiator ratio.

consumed. No reaction was expected to occur between the monomer and initiator without the presence of an additional catalyst.

To continue with the control experiments, an experiment with a smaller ratio of initiator to monomer (1:1 and 1:3) was performed (Scheme 3.4c). This is to examine the initiation step of the first monomer and observe if a small molecule forms or propagation is possible. Several attempts were made with both TIPS and TES ketene, however the results were inconsistent and varied with each reaction. Some reactions saw consumption of ketene and the formation of a small molecule and others did not exhibit any ketene consumption.

3.4.2 Why the inconsistency?

Unfortunately, there was inconsistency in the outcome of the reactions when all components were present, the monomer, initiator, and catalyst; regardless of consistent technique. The reaction

procedure was successful when MMA was used as the monomer, however the same was not observed with silyl ketenes, therefore the silyl ketene is likely causing the inconsistencies. In the test experiments, MMA was commercially purchased with an inhibitor. Prior to polymerization, MMA was degassed using freeze-pump-thaw and then dried over calcium hydride for ~2 hours. The mixture was then distilled to obtain thoroughly dried monomer and was stored under nitrogen; MMA could then be used in the GTP protocol. For silyl ketenes, however, each respective silyl ketene was synthesized in the three step synthesis and a thermal rearrangement. All silyl ketenes were stored at cool temperatures and under nitrogen gas once synthesized. The initial control experiments with silyl ketenes used the monomers as prepared for any GTP reactions. It was later realized that the silyl ketenes need to be degassed prior to use. Once this was done the outcome of the reactions became more consistent. It was also determined that the GTP of silyl ketenes was significantly more air-sensitive than the GTP of MMA, so ideally a glovebox is used.

3.5   GTP Component Scope Experiments

After the initial control experiments, some time elapsed, in which a glovebox was set up and the reactivity of silyl ketenes with LA and nucleophiles was examined (chapter 2). The following set of experiments examine various components of GTP and how each reacted with silyl ketene monomers, including initiator, catalyst, ratio, and silyl substituent.

3.5.1   Examination of Catalysts

The first component examined was various catalysts, mainly due to the large number of possible catalysts to choose from and the large number of recent studies involving new catalysts for GTP. For example, Takenaka *et al.* recently examined the use of organic acids as catalysts for GTP of alkyl crotonates.[160] From previous experiments and literature searches, five catalysts were chosen to examine, including both nucleophilic anions and Lewis acids; more specifically, boron
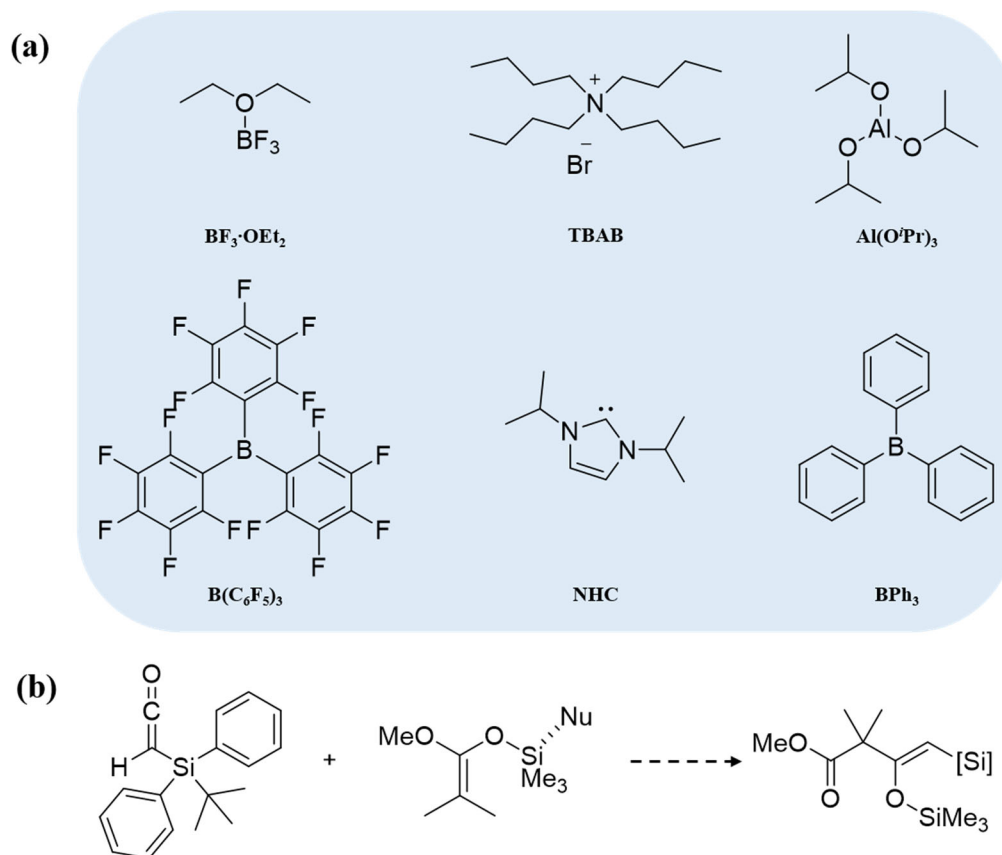
Figure 3.4. (a) Selected catalysts to examine with silyl ketenes; (b) reaction scheme for catalyst scope.

trifluoride diethyl etherate (BF$_3$·OEt$_2$), aluminum isopropoxide (Al(O^{i}Pr)$_3$), tris(pentafluorophenyl) borane (B(C$_6$F$_5$)$_3$), tetrabutylammonium bromide (TBAB), and NHC (1,3-diisopropylimidazolium chloride) (Figure 3.4a).[131,155,161] The remainder of the reagents were kept contant for comparison of the catalysts; the reaction used tert-butyldiphenylsilyl (TBDPS) ketene and MTS as the initiator (Figure 3.4a). The solvent was dependent on the identity of the catalyst, for example the reactions with LAs were performed in dichloromethane (DCM) and nucleophilic anions in THF.

The GTP protocol varied slightly from previous experiments now that a glovebox utilized. MTS and the selected catalyst were added into a round bottom flask in the glovebox and the silyl ketene was added into a separate vial, both were capped and removed from the glovebox. The solvent was added to both the round bottom flask and vial and the round bottom flask with MTS and the catalysts was stirred for ~10 minutes. The silyl ketene solution was then added dropwise to the round bottom flask and the reaction was monitored with FTIR (*when available, it was being fixed periodically). Once full ketene consumption was observed, the reactions were quenched with degassed methanol.

The selected catalysts did produce variable outcomes and both a 1:1 and a 1:10 ratio of initiator to monomer was examined (Table 3.1, entries 1-11). When TBAB was used no reaction was observed for both ratios and the silyl ketene remained unreacted (Table 3.1, entries 5 and 10). This eliminated TBAB as a contender for future experiments and was not use with additional silyl ketenes. For the remainder of the catalysts in a 1:1 ratio, Table 3.1, entries 1-4, a mixture of an

Table 3.1. Catalyst scope with TBDPS ketene and MTS initiator.

Entry	Catalyst	Monomer	Initiator	Solvent	Ratio	Outcome
1	$BF_3 \cdot OEt_2$	TBDPS	MTS	DCM	1:1	Mixture of SM/products*
2	$B(C_6F_5)_3$	TBDPS	MTS	DCM	1:1	Mixture of SM/products*
3	NHC	TBDPS	MTS	THF	1:1	Mixture of SM/products*
4	$Al(O^iPr)_3$	TBDPS	MTS	THF	1:1	Mixture of SM/products*
5	TBAB	TBDPS	MTS	THF	1:1	No ketene consumption
6	$BF_3 \cdot OEt_2$	TBDPS	MTS	DCM	1:10	α-silyl carbonyl
7	$B(C_6F_5)_3$	TBDPS	MTS	DCM	1:10	α-silyl carbonyl
8	NHC	TBDPS	MTS	THF	1:10	No ketene consumption
9	$Al(O^iPr)_3$	TBDPS	MTS	THF	1:10	α-silyl carbonyl
10	TBAB	TBDPS	MTS	THF	1:10	No ketene consumption
11	BPh_3	TBDPS	MTS	DCM	1:10	No ketene consumption

*starting material (SM)
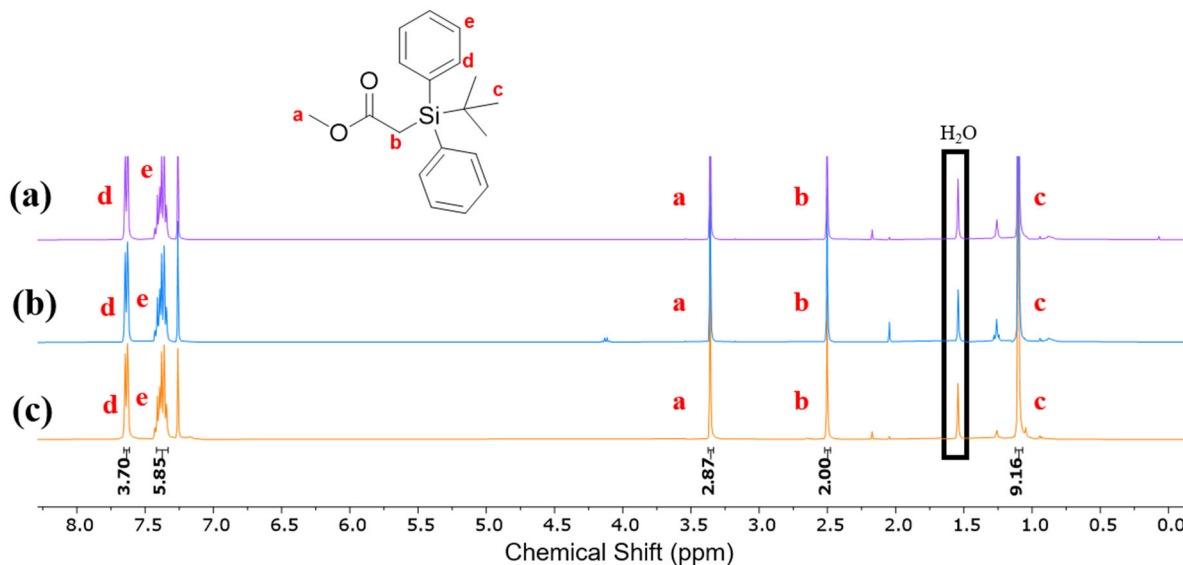
Figure 3.5. ^{1}H NMR of major product of 1:10 ratio MTS:TBDPS ketene with different catalysts: (a) BF$_3$·OEt$_2$ – Table 3.1, entry 6, (b) B(C$_6$F$_5$)$_3$ – Table 3.1, entry 7, and (c) Al(O^{i}Pr)$_3$ – Table 3.1, entry 9.

unidentified product and silyl ketene was obtained. When the ratio was increased to 1:10, Table 3.1, entries 6-9, the NHC catalyst (Table 3.1, entry 8) did not from any products and the silyl ketene remained unreacted. For the other three catalysts, Table 3.1, entries 6, 7, and 9, the major product was isolated via column chromatography and determined to be an α-silyl carbonyl (Figure 3.5), which was due to the use of methanol to quench the reaction. For additional comparison, BPh$_3$ was also examined to compare B(C$_6$F$_5$)$_3$. When B(C$_6$F$_5$)$_3$ was used an α-silyl carbonyl was formed (Table 3.1, entry 6), however when BPh$_3$ was used no reaction was observed and no ketene was consumed (Table 3.1, entry 11).

3.5.2   Examination of Silyl Substituents

The catalysts, BF$_3$·OEt$_2$, B(C$_6$F$_5$)$_3$, NHC, and Al(O^{i}Pr)$_3$, were then examined with methyldiphenylsilyl (MDPS) ketene and TIPS ketene (Table 3.2, entries 12-19). The reaction with

Table 3.2. Catalyst scope with various silyl ketenes and MTS initiator.

Entry	Catalyst	Monomer	Initiator	Solvent	Ratio	Outcome
12	$BF_3 \cdot OEt_2$	TIPS	MTS	DCM	1:10	α-silyl carbonyl
13	$B(C_6F_5)_3$	TIPS	MTS	DCM	1:10	α-silyl carbonyl
14	NHC	TIPS	MTS	THF	1:10	Mixture of SM/products*
15	$Al(O^iPr)_3$	TIPS	MTS	THF	1:10	No ketene consumption
16	$BF_3 \cdot OEt_2$	MDPS	MTS	DCM	1:10	α-silyl carbonyl
17	$B(C_6F_5)_3$	MDPS	MTS	DCM	1:10	α-silyl carbonyl
18	NHC	MDPS	MTS	THF	1:10	Mixture of SM/products*
19	$Al(O^iPr)_3$	MDPS	MTS	THF	1:10	α-silyl carbonyl
20	$B(C_6F_5)_3$	TES	MTS	DCM	1:10	Mixture of SM/products
21	$B(C_6F_5)_3$	TPhS	MTS	DCM	1:10	No ketene consumption

*starting material (SM)

TIPS and $Al(O^iPr)_3$ catalyst did not react and silyl ketene was not consumed (Table 3.1, entry 15), whereas the reaction with MDPS ketene produced an α-silyl carbonyl (Table 3.1, entry 19), the inconsistency led to not using $Al(O^iPr)_3$ further. Several of these reactions using other catalysts also produced the corresponding α-silyl carbonyl product (Table 3.1, entries 12, 13, 16, and 17). The formation of the α-silyl carbonyl product was the favorable product for mainly the LA catalysts, which have been shown in the previous chapter to catalyze the formation of an α-silyl carbonyl when a nucleophile is present.[162] When methanol is used to quench the reaction, it acts as a nucleophile to form the α-silyl carbonyl, regardless of the product formed prior to quenching the reactions. From this discovery, the use of methanol to quench the reactions ceased and alternatively the solvent was removed under reduced pressure and the reaction flask exposed to ambient conditions.
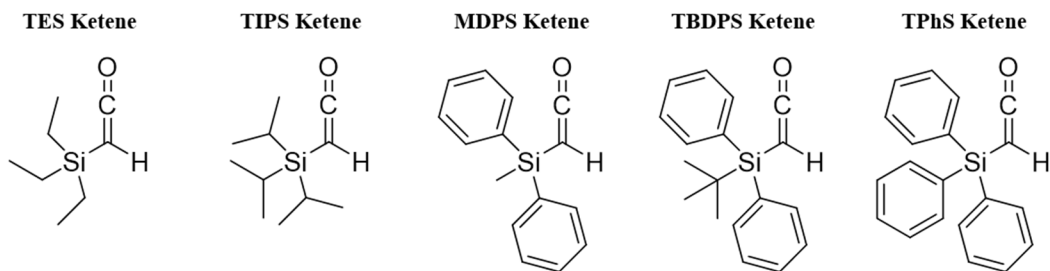
Figure 3.6. Silyl ketenes studied for GTP.

To further the scope of various silyl ketene substituents, TES and triphenylsilyl (TPhS) ketene were examined to have full comparison of the impact of steric bulk and electronics under GTP conditions (Figure 3.6). TES and TPhS ketene were reacted with MTS and $B(C_6F_5)_3$ in a 1:10 ratio (Table 3.2, entry 20 and 21). For TES ketene full consumption of ketene was observed and a mixture of oligomers/small molecules was obtained. It should also be noted that TES ketene reacted significantly faster than any other ketene examined and typically full consumption of ketene was observed in less than 1 hour. For TPhS ketene little ketene reacted and the majority of the reaction mixture was unreacted silyl ketene. Of the ketenes examined, only TPhS ketene was unsuccessful and the remainder of the ketenes exhibited some type of reaction when $B(C_6F_5)_3$ was used as catalyst. Due to variable reactivity, two silyl ketenes, TES and TBDPS, were chosen to examine so both types of silyl substituents would be studied.

3.5.3   Examination of Initiators

After examining various catalysts and silyl substituents, only low molar mass oligomers and small molecules were being produced. To ensure full examination of components, various initiators were also examined. Silyl ketene acetals are the most common initiators used for GTP, specifically MTS due to the small R-groups. However, since no high molar mass oligomers were being formed, a different type of initiator may be need for the GTP of silyl ketenes. After further

literature search, trimethylsilyl cyanide (TMS cyanide) and benzaldehyde have been used as initiators for GTP and were selected to use as initiators for silyl ketenes. TMS cyanide have been used similarly to silyl ketene acetals, however benzaldehyde initiators have been used for monomers have a silyl group to undergo aldol GTP.

Prior to use benzaldehyde was recrystallized and TMS cyanide was used as received, both compounds were stored in the glovebox. To start, two different catalysts were used to activate the selected initiators, $BF_3 \cdot OEt_2$ and $B(C_6F_5)_3$, with TBDPS ketene as the monomer (Table 3.3, entries 23-26). For comparison of the two catalysts, $B(C_6F_5)_3$ was much slower than $BF_3 \cdot OEt_2$ and needed to run overnight for full consumption of ketene, as well as Table 3.3, entry 23 still had some silyl ketene present according to ^1H NMR; so $BF_3 \cdot OEt_2$ was used for the remainder of the initiator scope. The outcome of these reactions with TBDPS ketene, Table 3.3, entries 23-26, were the similar, in which a low molar mass oligomer was formed with a molar mass of 1180 m/z according to ESI mass spectroscopy, regardless of the catalyst used. Unfortunately, the structure of which was not able to be determined, however a cyclic oligomer is hypothesized. A similar product was

Table 3.3. Initiator scope for GTP with TBDPS and TES ketenes.

Entry	Catalyst	Monomer	Initiator	Solvent	Ratio	Outcome
23	$B(C_6F_5)_3$	TBDPS	TMS cyanide	DCM	1:10	*SM/small molecules /oligomers
24	$B(C_6F_5)_3$	TBDPS	Benzaldehyde	DCM	1:10	Small molecules/oligomers
25	$BF_3 \cdot OEt_2$	TBDPS	TMS cyanide	DCM	1:10	Small molecules/oligomers
26	$BF_3 \cdot OEt_2$	TBDPS	Benzaldehyde	DCM	1:10	Small molecules/oligomers
27	$BF_3 \cdot OEt_2$	TES	TMS cyanide	DCM	1:10	Small molecules
28	$BF_3 \cdot OEt_2$	TES	Benzaldehyde	DCM	1:10	Small molecules
29	$BF_3 \cdot OEt_2$	TES	Benzaldehyde	DCM	1:50	Small molecules/oligomers
30	$BF_3 \cdot OEt_2$	TBDPS	Benzaldehyde	DCM	1:50	Small molecules/oligomers

*starting material (SM)

also formed when MTS was used with TBDPS, indicating that the product formed does not incorporate the initiator. The mass spectrum does show that there is higher molar mass (>1500) compound being formed however the low molar mass oligomer is favored (~1200).

Continuing the examination of TMS cyanide and benzaldehyde as initiators, these reactions were performed with TES ketene. For the 1:10 ratio of initiator to monomer, the TES reactions produced small molecules and no high molecular weight compound was detected through ESI (Table 3.2, entries 27 and 28). Again, the products formed were similar to the products formed when MTS was used, indicating that the product does not incorporate the initiator.

Out of curiosity, the ratio was increased from 1:10 to 1:50 initiator to monomer to see if the formation of this low molar mass oligomer could be overcome and higher molar mass oligomers obtained, indicating polymerization could occur. These higher ratio experiments were performed with a benzaldehyde initiator and BF$_3$·OEt$_2$ catalyst for both TES and TBDPS ketene (Table 3.3,
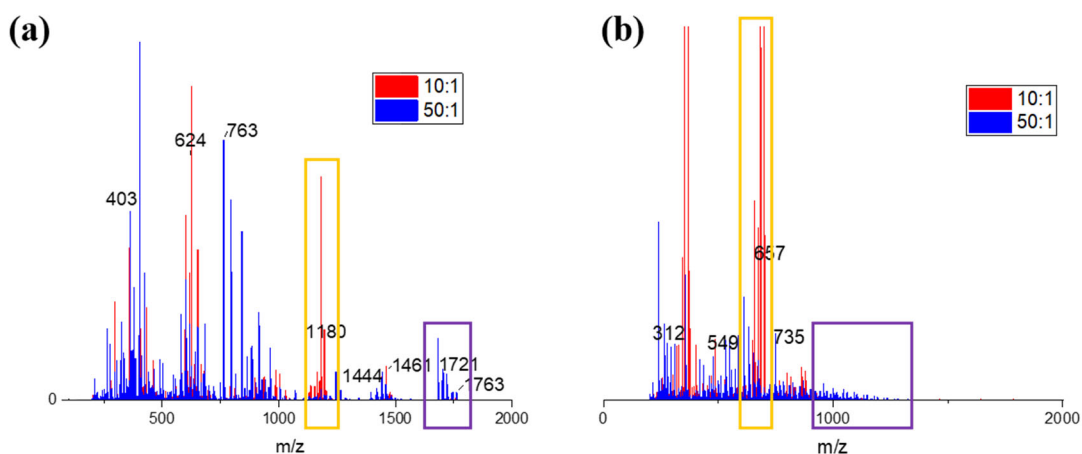
Figure 3.7. Comparison of 10:1 and 50:1 of silyl ketene to benzaldehyde; (a) TBDPS ketene and (b) TES ketene. Orange box – favored oligomer in 1:10; purple box – higher molecular oligomers.

entries 29 and 30). Interestingly, for both of the silyl ketenes higher molar mass oligomers were observed and the formation of the corresponding low molar mass oligomers was diminished. When comparing the mass spectrum for the 1:10 and 1:50 ratio experiments for both ketenes the diminished formation of the low molar mass oligomers can be easily observed (Figure 3.7). This was the first example of higher molar mass oligomers forming from the GTP of silyl ketenes. Additionally, the 1:50 ratio experiment of TBDPS, table 3.3, entry 30, formed a solid upon removal of the solvent from the reaction mixture.

3.5.4   Additional Polymerization Conditions

Additional polymerization conditions were also examined, including temperature of reaction and concentration. Concentration of the monomer has been shown to affect the polymerization rate, which can in turn affect the dispersity of the resulting polymer and possible side reactions.[155] Prior to examining the catalyst scope, concentration of monomer was examined at both 1M and 5M. The reactions were performed with TBDPS ketene and MTS initiator, both concentrations exhibited full consumption of ketene with no noticeable difference between the two concentrations. The subsequent reactions were performed in a 1 M concentration as a standard for all GTP of silyl ketenes. Concentration will play a larger role in the GTP of silyl ketenes when higher molar mass polymers are obtained.

Temperature was also examined, as temperature can impact the rate of reactions as well as promote product formation by decreasing activation energy.[36] In the case of GTP, majority of reactions are performed at room temperature, however lower temperatures can be used to favor polymerization. Four experiments were performed at various temperatures with variable times with a 1:10 ratio of initiator to monomer (Table 3.4). For Table 3.4, entry 31 the procedure varied slightly from previous runs, after the initiator and catalyst stirred for ~5 minutes, the reaction flask was cooled

to 0°C with an ice bath and the ketene was added dropwise. The solution was stirred for 30 minutes and then warmed to room temperature and stirred until full consumption of ketene was observed. A similar procedure was followed for Table 3.4, entry 32, but the reaction flask was cooled to -46°C with a dry ice/acetonitrile bath. Both of these reactions produced the same product, as well as took the same amount of time for full consumption of ketene to be observed. Table 3.4, entry 33 and 34 examine extended stirring times at 0°C, entry 33 stirred for 2 hours and was then warmed to room temperature and entry 34 was stirred for 3 hours and then warmed to room temperature. For entry 34, full consumption of ketene was observed after the 3 hours, however for entry 33 full consumption of ketene was not observed until 5 hours. Comparing these reactions to the room temperature experiment, the reaction products were the same, however reaction time was reduced from 24 hours to 3-5 hours. The temperature at which these polymerizations are performed is important, however more thorough studies need to be performed when high molar mass polymers can be obtained.

Table 3.4. Temperature studies for GTP.

Entry	Catalyst	Monomer	Initiator	Ratio	Solvent	Temperature
31	$B(C_6F_5)_3$	TBDPS	MTS	1:10	DCM	0°C → RT upon addition of monomer*
32	$B(C_6F_5)_3$	TBDPS	MTS	1:10	DCM	-46°C → RT upon addition of monomer*
33	$B(C_6F_5)_3$	TBDPS	MTS	1:10	DCM	0°C, warm to RT after 2 hours
34	$B(C_6F_5)_3$	TBDPS	MTS	1:10	DCM	0°C, warm to RT after 3 hours

*room temperature (RT)

3.6   Miscellaneous Experiments

Grignard reagents are good nucleophiles and commonly react with carbonyl containing compounds to form an alcohol and a new C-C bond.[163] Additionally, these reagents are good bases and can be used deprotonate alcohols or phenols to generate alkoxides. A Grignard was previously

used as a catalyst in the LA study generating α-silyl carbonyls, forming the product in <2 minutes (chapter 2). However, the yield was low compared to other LAs examined in the formation of α-silyl carbonyls. Since many of the catalysts overlap between these two studies, a Grignard reagent was used a catalyst for GTP. Ethylmagnesium bromide was used with MTS as the initiator and TBDPS ketene. Unfortunately, this reaction observed little consumption of ketene. Regardless, Grignard reagents may work better with different initiators for GTP and a more thorough study is needed to understand their reactivity with silyl ketenes.

Cationic polymerization is a polymerization technique where a cationic initiator generates a positive charge that is transferred through the propagating end.[164] Typical cationic initiators include strong acids, Lewis acids, and carbenium ions. Since many LAs are being used with GTP, cationic polymerization techniques were attempted. For example, a catalytic amount of a LA was added to a round bottom flask with MDPS ketene, along with a nucleophile. The order of how the reagents were added were examined, as well as various LAs. Unfortunately, each attempt was unsuccessful with minimal ketene being consumed, more research needs to be performed utilizing cationic polymerization techniques.

3.7   Summary

Overall, GTP is a powerful technique to polymerize silyl ketenes and has great potential in obtaining high molar mass polymers from silyl ketenes. However, similar to past students, the understanding of how silyl ketenes react in various polymerization conditions is limited, so an understanding of how silyl ketenes react with the various components of GTP is necessary. GTP techniques are also very air/moisture sensitive and proper techniques are needed to ensure potential polymerization. The components of GTP examined include catalyst identity, silyl substituent, initiator, and polymerization conditions. Six different catalysts were examined, ranging from

nucleophilic anions to LAs; in which $BF_3 \cdot OEt_2$, $B(C_6F_5)_3$, and NHC performed the most consistently and reacted with all silyl substituents to produce either an α-silyl carbonyl or a set of oligomers. The initiator identity scope, expanded from using the most common initiator for GTP, MTS, to using benzaldehyde and TMS-cyanide, both of which exhibited potential to form higher molar mass oligomers. For both the catalyst and initiator scope, several silyl ketenes were utilized, including TES, TIPS, MDPS, TBDPS, and TPhS ketene; each undergoing various reactivity. Additional parameters were examined, including temperature, ratio, and concentration, which will be of greater importance when an initiator/catalyst system are identified to produce high molar mass oligomers/polymers. There is still a significant amount of research that needs to be done with the GTP of silyl ketenes, including further initiator studies and polymerization conditions.

3.8   Appendix

General Considerations.   All purchased chemicals were used directly as received, unless otherwise stated. All reactions were performed under an inert atmosphere (nitrogen gas) or in a Vigortech glovebox with a nitrogen atmosphere. DCM and THF were obtained by passing the commercial grade solvent through a double filter column in a MBRAUN SPS compact system. All ^1H and ^{13}C NMR were collected on a Bruker Ascend III HD 500 MHz NMR instrument equipped with prodigy probe (CWRU) or a Bruker Advance Neo console 400 MHz NMR with an Ascend magnet and automated tuning 5mm broadband iProbe (TAMU); shifts are reported relative to the residual solvent peak, as noted. All NMR spectra were collected using $CDCl_3$ as the solvent unless otherwise noted. FTIR spectra were acquired using an Agilent Cary 630 FTIR in the ATR mode or a JASCO FT/IR-4000. ESI spectra were obtained on a THERMO Finniagn LCQ DECA ion trap mass spectrometer equipped with an external AP ESI ion source. THERMO DSQ II Series Single Quadrupole GC/MS.

Reagent Drying Procedure. All reagents need to be properly dried prior to use for all GTP experiments. Methyl methacrylate and MTS were degassed with freeze-pump-thawed three times, followed by stirring with calcium hydride for two hours. Each were then distilled at room temperature and the dry reagent stored under $N_2(g)$. Methanol was degassed with freeze-pump-thaw three times prior to use. Benzaldehyde was recrystallized with water prior to use. All silyl ketenes were synthesized as described in chapter 2 and then degassed with freeze-pump-thaw three times. All catalysts and TMS-cyanide were used as received. Once dried, all reagents were stored under $N_2(g)$ or in a glovebox. If stored outside of the glovebox, the reagents need to be dried immediately prior to use (up to 24 hours).

Deprotonation of NHC Catalyst. An oven dried round bottom flask was purged three times with vacuum and $N_2(g)$. 1,3-diisopropylimidazolium chloride (1 eq, 0.0013 mol) and NaH (1.4 eq, 0.0018 mol) was added to the flask, followed by anhydrous THF (3 mL). To the reaction mixture, potassium *tert*-butoxide (0.075 eq, 0.01 mL) was added and the reaction was then stirred at room temperature for three hours. After three hours, the reaction mixture was filtered under an inert atmosphere (cannula transfer, do not expose to atmosphere). Once filtered, the solvent was removed under reduced pressure. The deprotonated NHC could then be diluted to the desired concentration (typically 1 M) with THF and used as needed.

Group Transfer Polymerization of MMA. An oven dried Schlenk flask was purged three times with vacuum and $N_2(g)$. MTS (0.00049 mol, 0.1 mL) and NHC (0.1 mL of 1M solution) were added, followed by dry THF (30 mL). The solution was stirred for 10 minutes to allow the catalyst to coordinate to the initiator. MMA (8 mL) was then added dropwise over a period of 5 minutes. As monomer is added, a color change should be observed going from clear to pink. Monomer consumption was monitored via FTIR. Once full consumption was observed, the reaction was

quenched with degassed methanol. The resulting polymer was purified via recrystallization by dissolving PMMA in THF and then adding dropwise to cold methanol. PMMA was then dried under vacuum and spectra obtained.

Control experiments.   An oven dried round bottom flask was purged three times with vacuum and $N_2(g)$. MTS (0.002 mol) or NHC (0.002 mol) was added to the flask, followed by dry THF (3 mL). TIPS or TES ketene (0.002 mol) was then added. The reaction was monitored with FTIR and quenched after 4 hours. The crude spectra were obtained for all control experiments.

General Procedure for the GTP of Silyl Ketenes. An oven dried Schlenk flask and vial were loaded into a nitrogen filled glovebox. The desired initiator (1 mol) and catalyst (5 mol %) were added to the Schlenk flask and the flask was capped and sealed. The desired silyl ketene (1, 5, 10, or 50 mol) was added to the vial and capped and sealed. Both were then removed from the glovebox and were immediately attached to a Schlenk line. Half of the solvent was added to the Schlenk flask and half was added to the vial (1 M monomer in solvent). The initiator/catalyst solution was stirred for 10 minutes and then the silyl ketene solution was added dropwise at room temperature. Various color changes were observed, typically depending on the silyl ketene being used. The reaction was monitored with FTIR. When full consumption of silyl ketene was observed, the solvent was removed under reduced pressure, followed by the reaction flask being exposed to atmosphere. The crude ESI and NMR was collected for each reaction.

Variable Temperature Reactions. An oven dried Schlenk flask and vial were loaded into a nitrogen filled glovebox. The desired initiator (1 mol) and catalyst (5 mol %) were added to the Schlenk flask and the flask was capped and sealed. The desired silyl ketene (10 mol) was added to the vial and capped and sealed. Both were then removed from the glovebox and were

immediately attached to a Schlenk line. Half of the solvent was added to the Schlenk flask and half was added to the vial (1 M monomer in solvent). The initiator/catalyst solution was stirred for 10 minutes and the reaction flask cooled to the desired temperature. The silyl ketene solution was added and the reaction stirred for the desired length of time at a specified temperature. Various color changes were observed, typically depending on the silyl ketene being used. The reaction was monitored with FTIR. When full consumption of silyl ketene was observed, the solvent was removed under reduced pressure, followed by the reaction flask being exposed to atmosphere. The crude ESI and NMR was collected for each reaction.

GTP with Grignard Reagent Catalyst. An oven dried Schlenk flask and vial were loaded into a nitrogen filled glovebox. MTS (1 eq, 0.0001 mol) and ethyl magnesium bromide solution (0.01 eq, 0.011 mL) were added to the Schlenk flask and the flask was capped and sealed. TBDPS ketene (10 eq, 0.001 mol) was added to the vial and capped and sealed. Both were then removed from the glovebox and were immediately attached to a Schlenk line. Half of the THF was added to the Schlenk flask and half was added to the vial (1.1 mL THF). The MTS/Grignard reagent solution was stirred for 10 minutes and then the silyl ketene solution was added dropwise at room temperature. The reaction was monitored with FTIR. When full consumption of silyl ketene was observed, the solvent was removed under reduced pressure, followed by the reaction flask being exposed to atmosphere. The crude ESI and NMR was collected for the reaction.

General Procedure for Cationic Polymerization. In an oven dried round bottom flask, purged with $N_2(g)$ and vacuum. A LA (cat. 0.2, or 1.2 eq.) was dissolved in DCM (neat or 3 mL). The desired initiator (1 mol) and silyl ketene (20 mol) were added simultaneously. The solution was stirred at room temperature overnight. The reaction was monitored with FTIR.

Figure A3.1. Control experiment with TES ketene and NHC catalyst in a 1:1 ratio, (a) ^{29}Si NMR, (b) ^{1}H NMR.
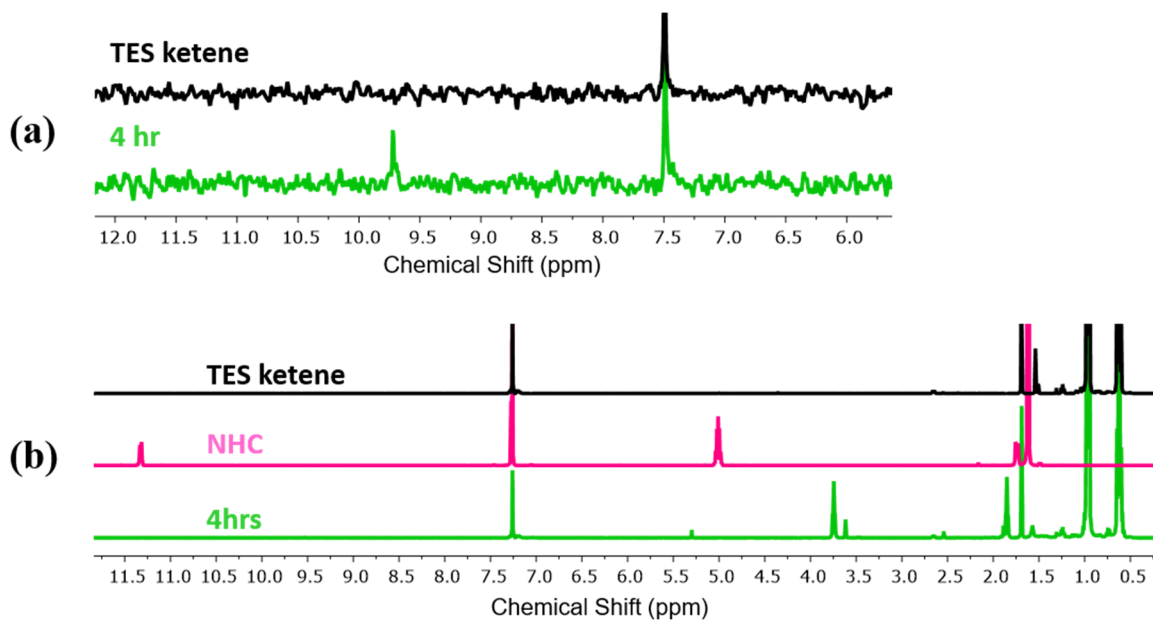
Figure A3.2. Control experiment with TES ketene and MTS initiator in a 1:1 ratio, (a) ^{29}Si NMR, (b) ^{1}H NMR.
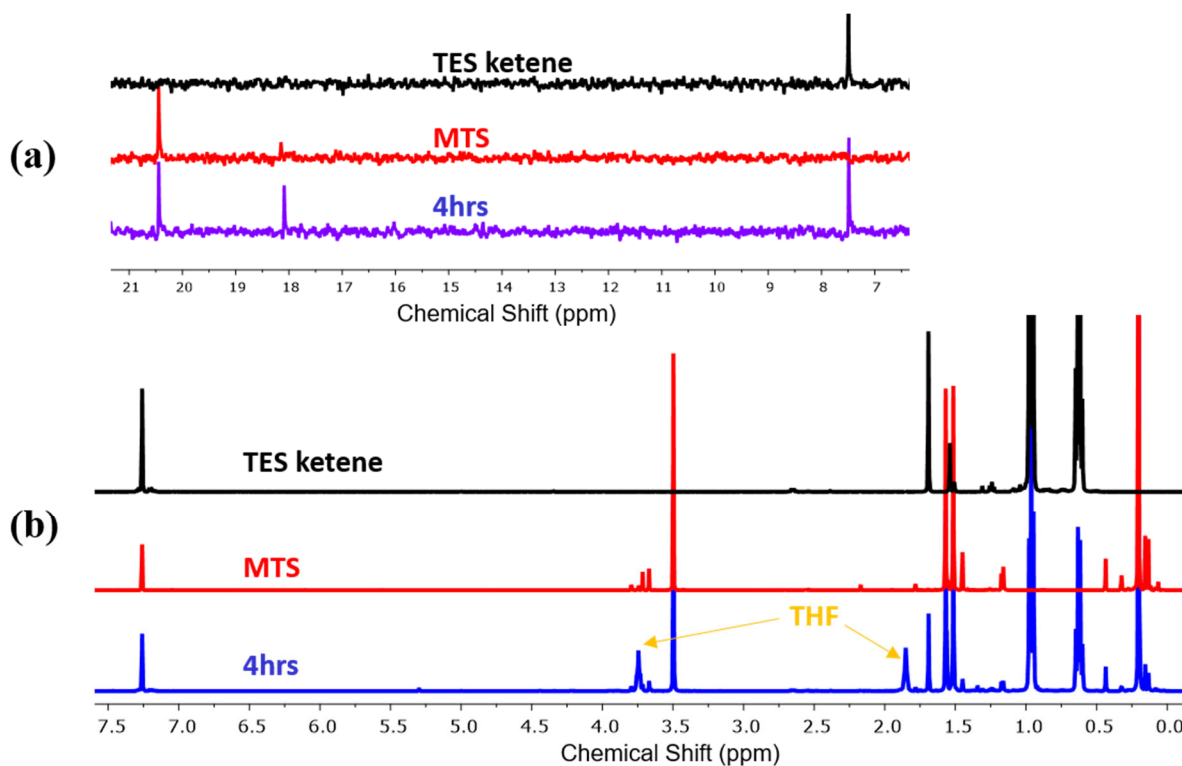
Figure A3.3. Control experiment of 1:1 TES ketene:MTS initiator with NHC catalyst, (a) FTIR, (b) ^{1}H NMR.
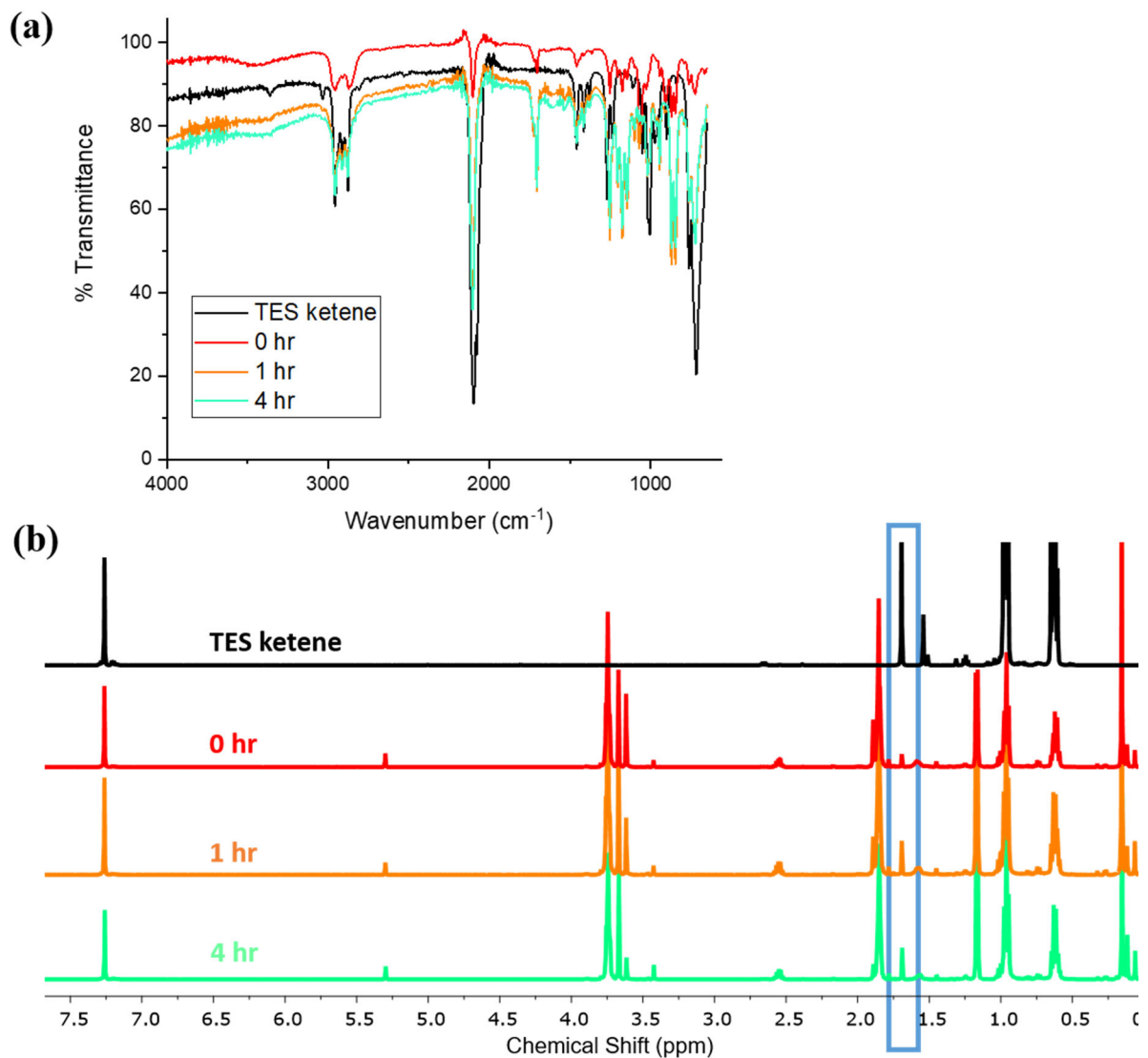
Figure A3.4. Catalyst scope: crude ^{1}H NMR of 1:1 TBDPS ketene:MTS (Table 3.1, entries 1-5), (a) TBAB, (b) BF$_3$·OEt$_2$, (c) B(C$_6$F$_5$)$_3$, (d) NHC, (e) Al(O^{i}Pr)$_3$.
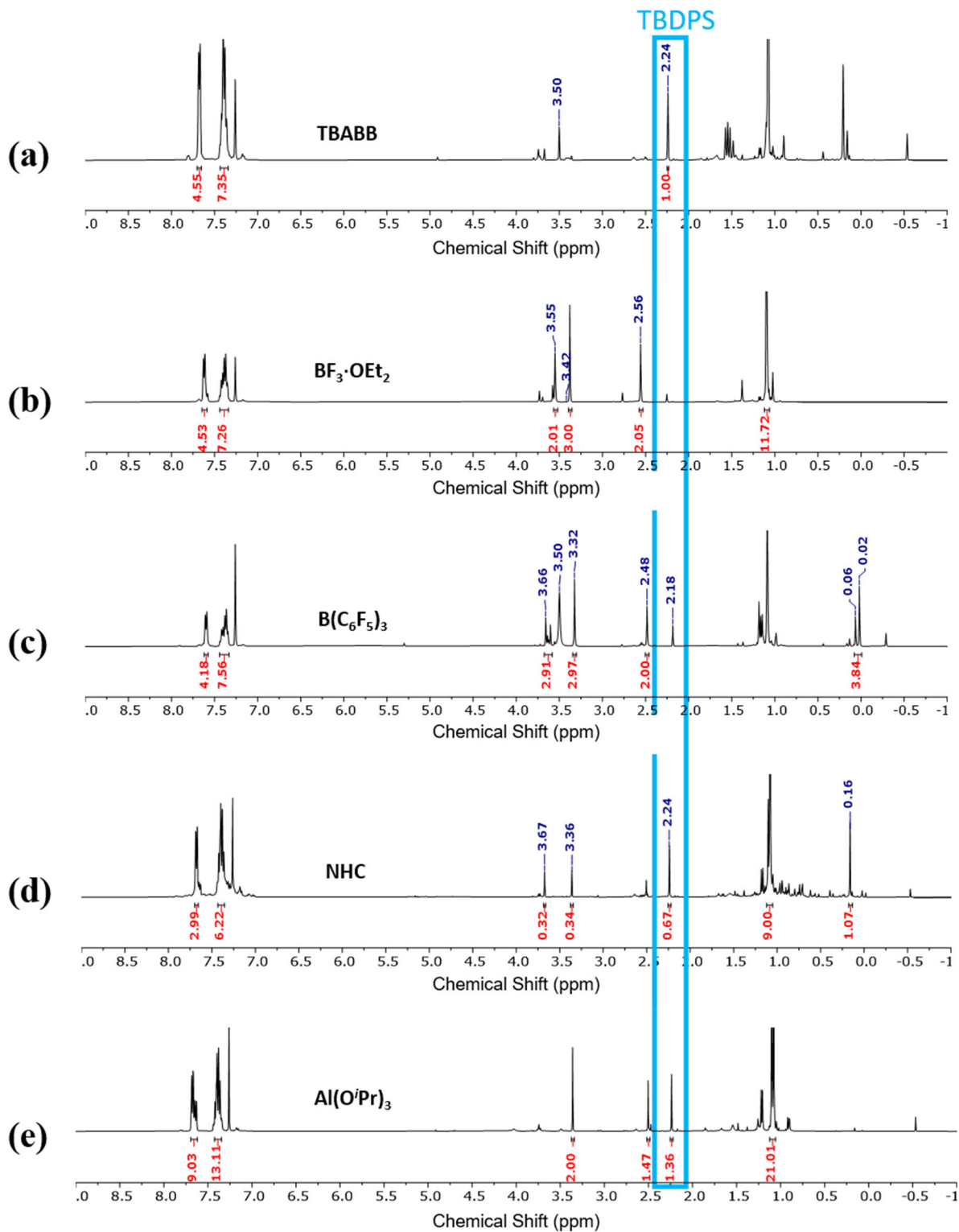
Figure A3.5. Catalyst scope: crude ^{1}H NMR of 1:10 MTS:TBDPS ketene (Table 3.1, entries 6-10), (a) TBAB, (b) $BF_3 \cdot OEt_2$, (c) $B(C_6F_5)_3$, (d) NHC, (e) $Al(O^iPr)_3$.
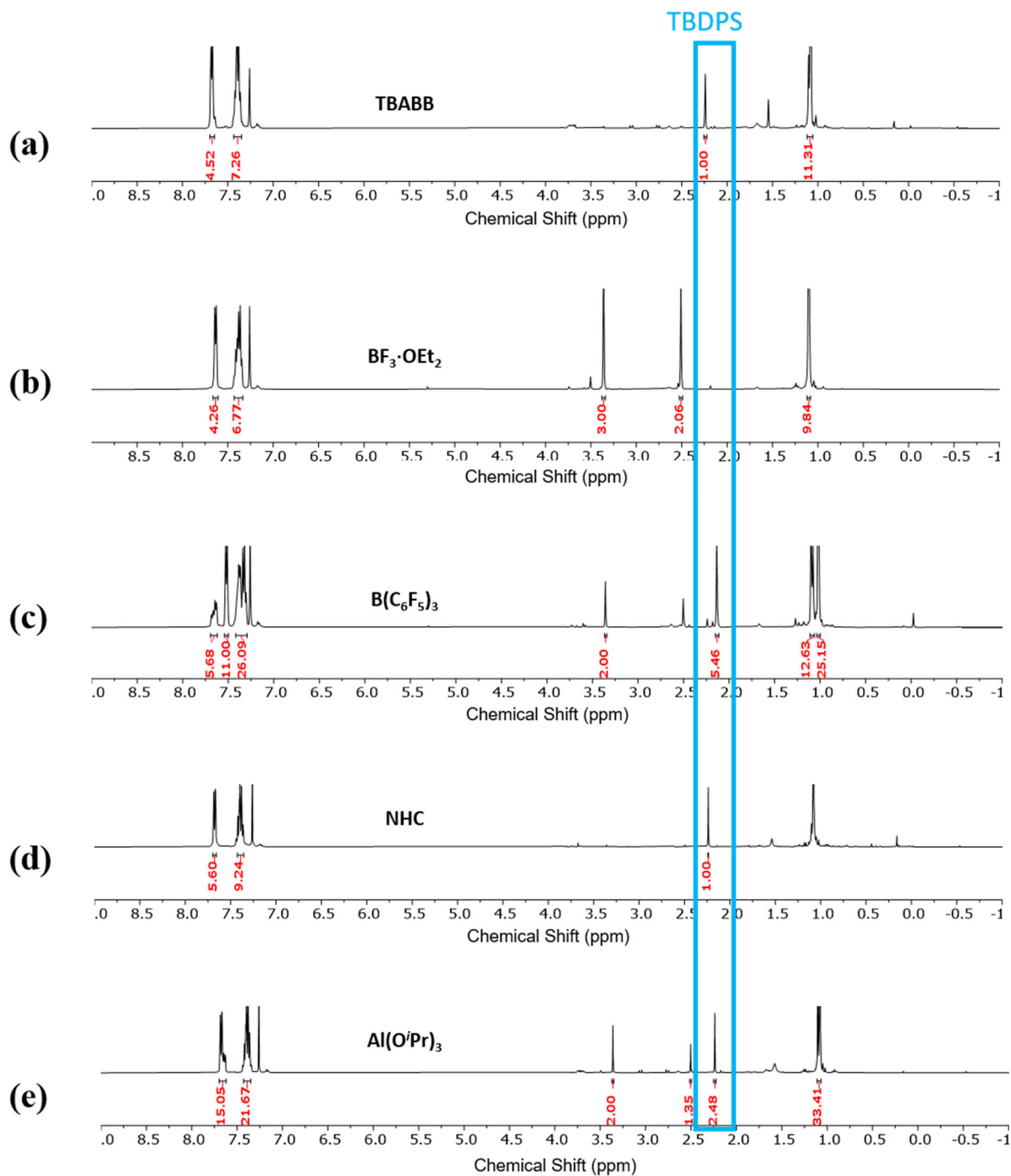
Figure A3.6. Catalyst scope: crude ^{1}H NMR of 1:10 MTS:TIPS ketene (Table 3.2, entries 12-15), (a) BF$_3$·OEt$_2$, (b) B(C$_6$F$_5$)$_3$, (c) NHC, (d) Al(O^{i}Pr)$_3$.
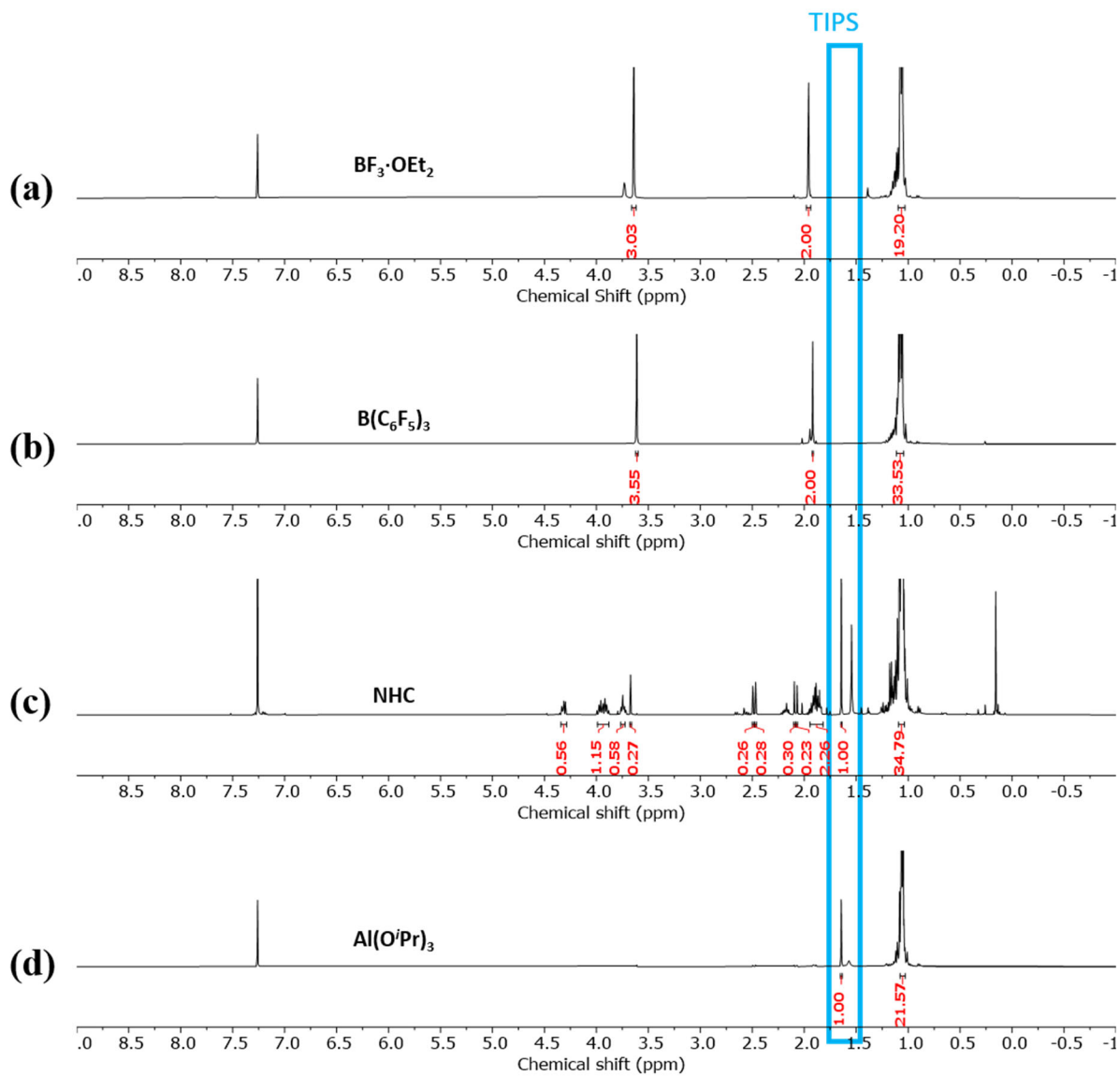
Figure A3.7. Catalyst scope: crude ^{1}H NMR of 1:10 MTS:MDPS ketene (Table 3.2, entries 16-19), (a) BF$_3$·OEt$_2$, (b) B(C$_6$F$_5$)$_3$, (c) NHC, (d) Al(O^{i}Pr)$_3$.
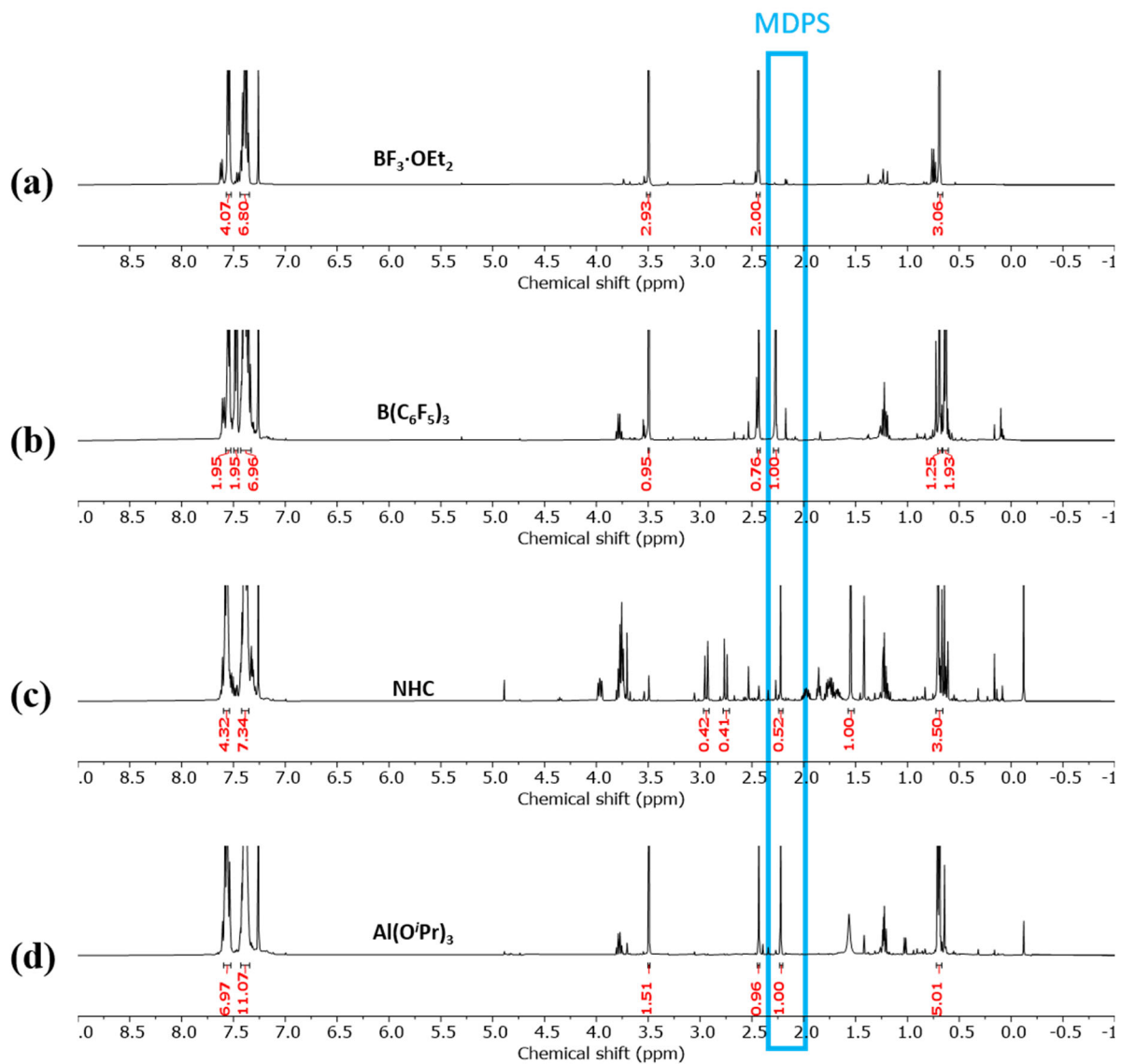
Figure A3.8. Catalyst scope: crude ^{1}H NMR of 1:10 MTS:TBDPS ketene comparing B(C$_6$F$_5$)$_3$ (Table 3.1 entry 7) and BPh$_3$ (Table 3.1 entry 11) catalysts.
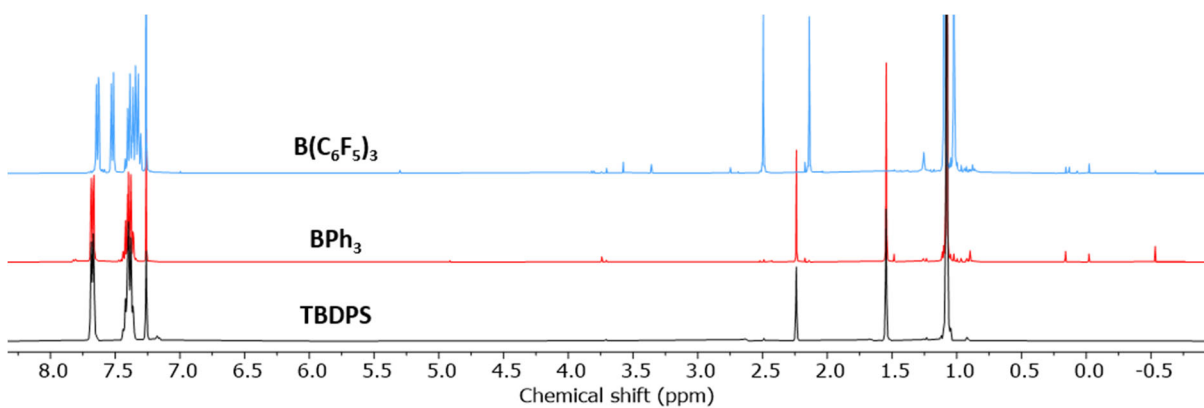
Figure A3.9. Catalyst scope: crude ^{1}H NMR of 1:10 TES or TPhS ketene to MTS using B(C$_6$F$_5$)$_3$, (a) TES ketene (Table 3.2, entry 20), (b) TPhS ketene (Table 3.2, entry 21).
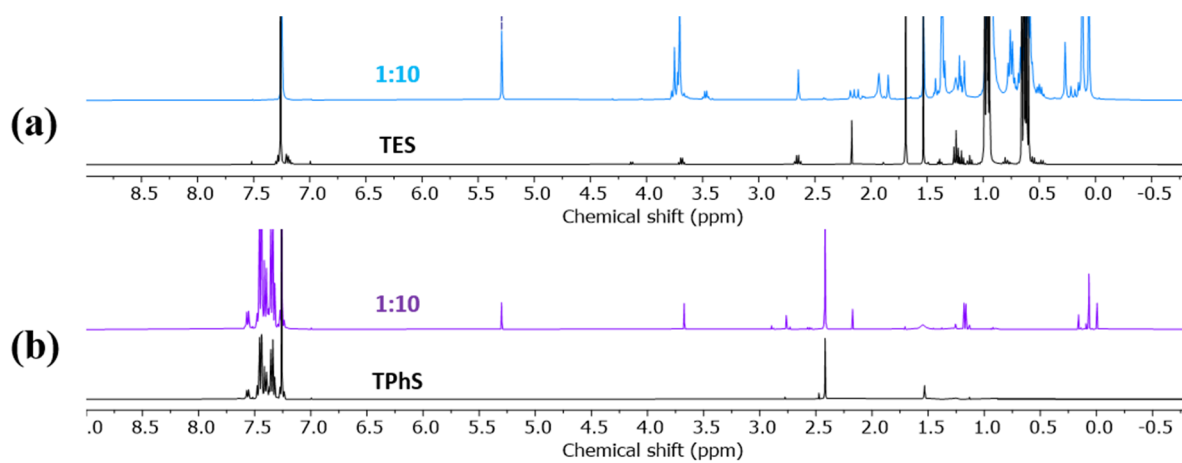
Figure A3.10. ESI mass spectrum of Table 3.1 entry 1 (BF$_3$·OEt$_2$, 1:1 MTS:TBDPS ketene).
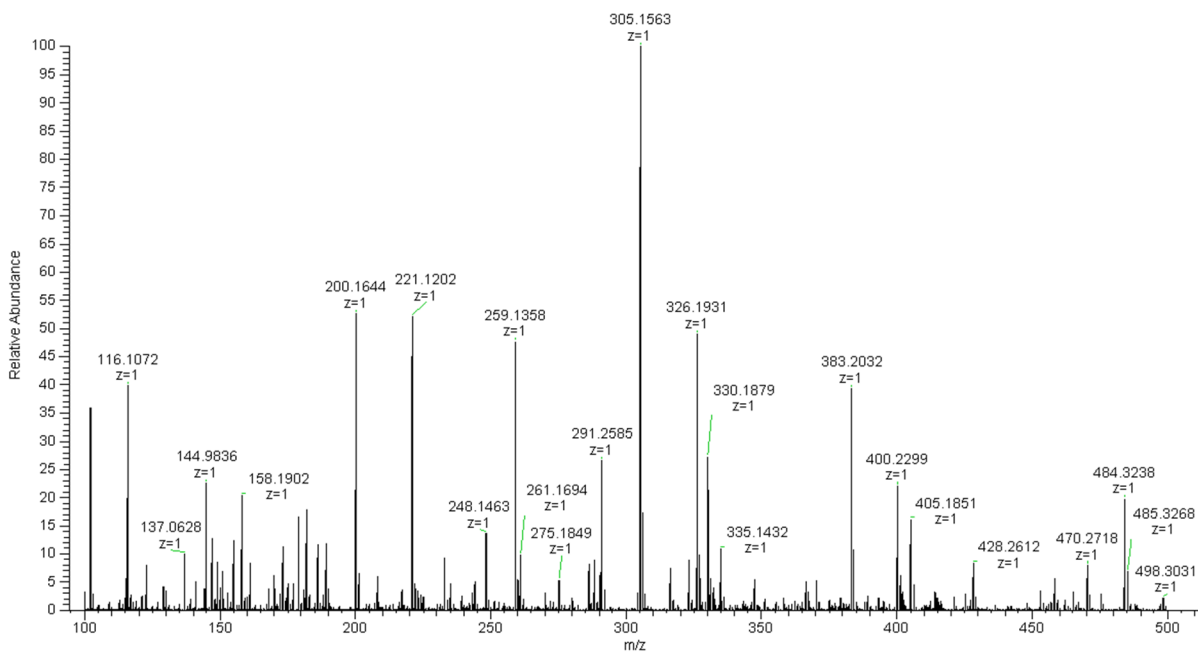
Figure A3.11. ESI mass spectrum of Table 3.1 entry 2 (B(C$_6$F$_5$)$_3$, 1:1 MTS:TBDPS ketene).

Figure A3.12. ESI mass spectrum of Table 3.1 entry 3 (NHC, 1:1 MTS:TBDPS ketene).

201027-143331 #70-95 RT: 0.31-0.42 AV: 26 SB: 17 0.13-0.20 NL: 1.84E8
T: FTMS + p ESI Full ms [100.0000-500.0000]
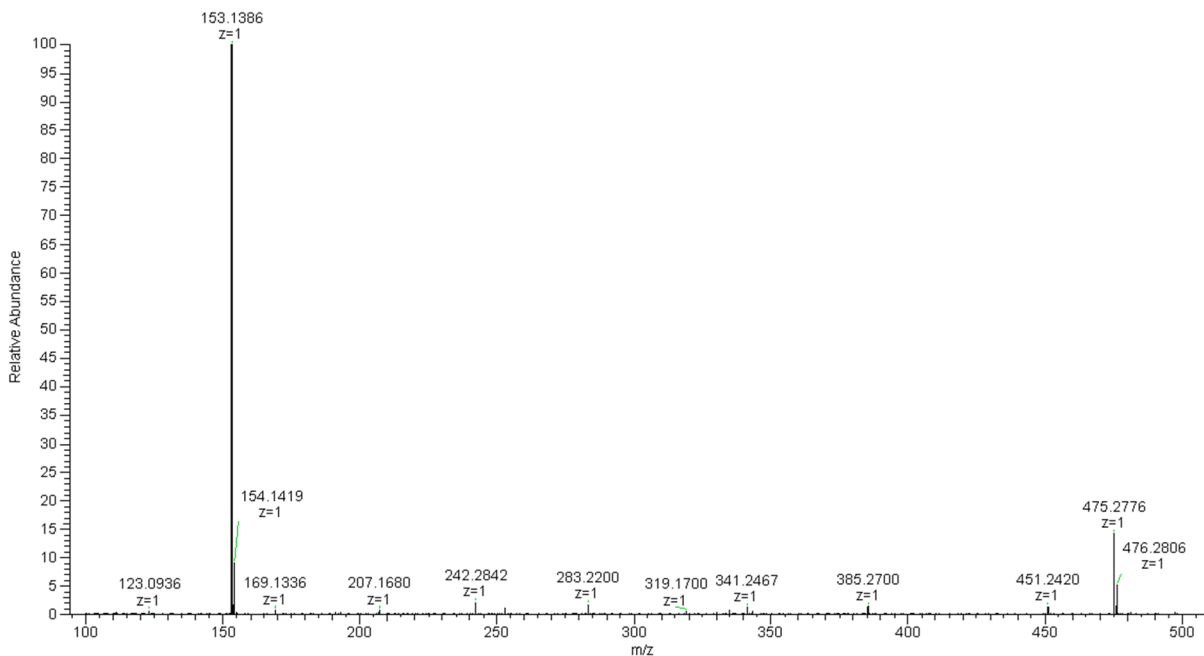
Figure A3.13. ESI mass spectrum of Table 3.1 entry 4 (Al(O^{i}Pr)$_3$, 1:1 MTS:TBDPS ketene).

201110-112103_1 #70-95 RT: 0.31-0.42 AV: 26 SB: 17 0.13-0.20 NL: 1.80E7
T: FTMS + p ESI Full ms [100.0000-500.0000]

120
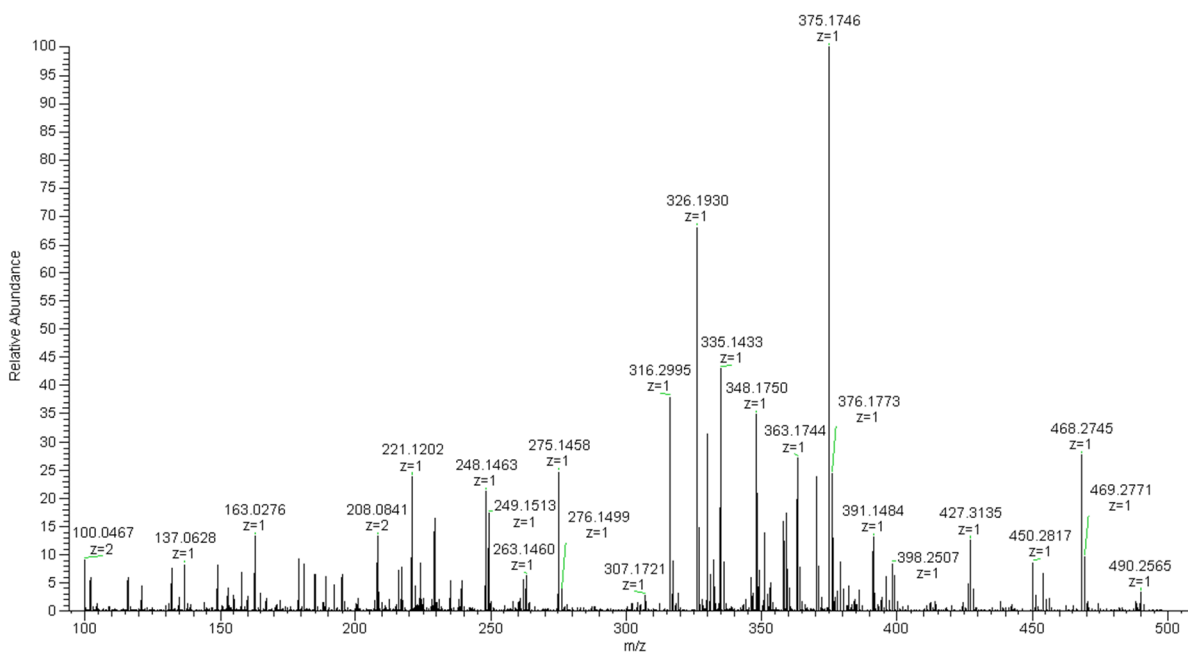
Figure A3.14. ESI mass spectrum of Table 3.1 entry 5 (TBAB, 1:1 MTS:TBDPS ketene).
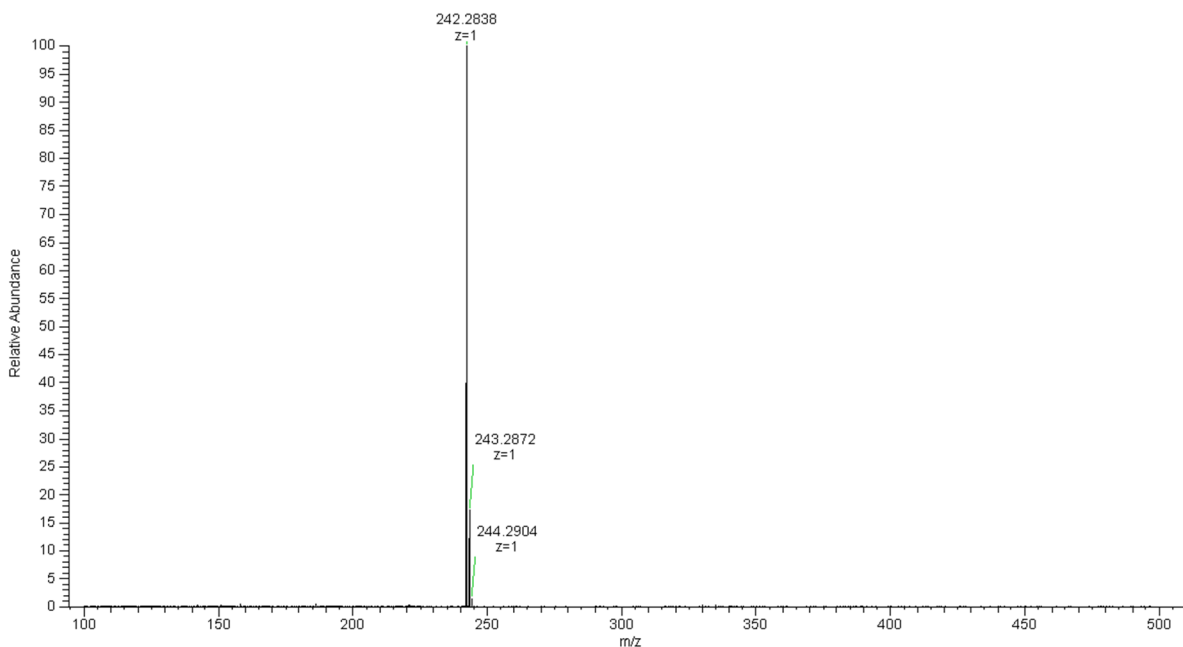
Figure A3.15. ESI mass spectrum of Table 3.1 entry 6 (BF$_3$·OEt$_2$, 1:10 MTS:TBDPS ketene).
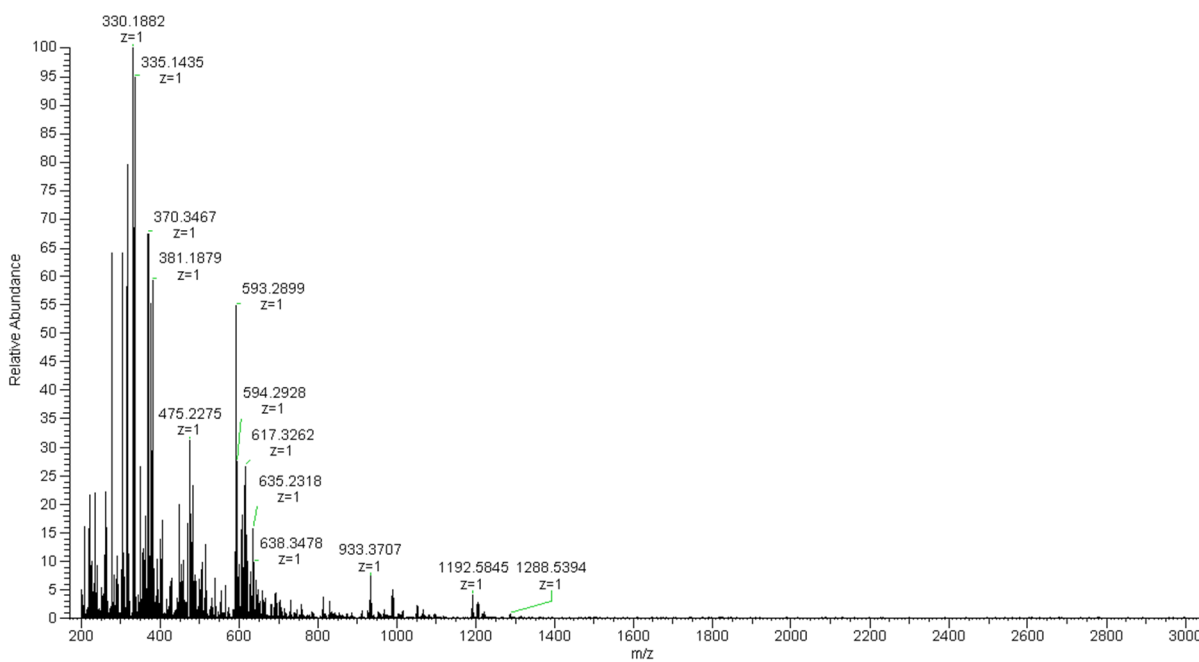
Figure A3.16. ESI mass spectrum of Table 3.1 entry 7 (B(C$_6$F$_5$)$_3$, 1:10 MTS:TBDPS ketene).
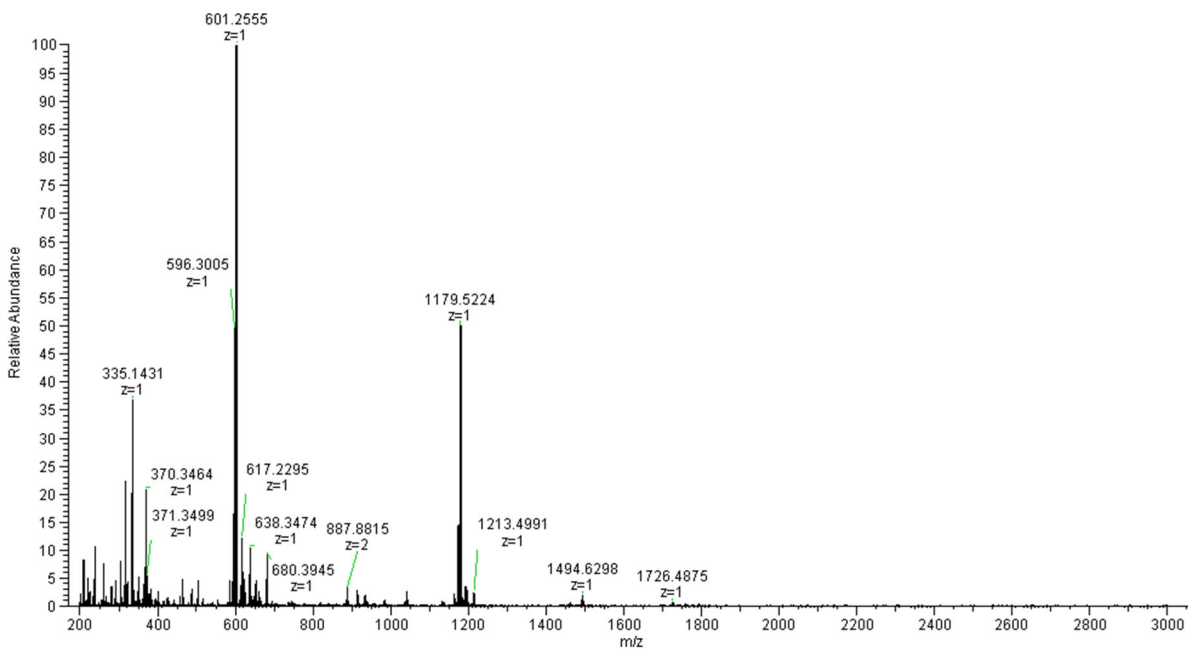
Figure A3.17. ESI mass spectrum of Table 3.1 entry 8 (NHC, 1:10 MTS:TBDPS ketene).

Figure A3.18. ESI mass spectrum of Table 3.1 entry 9 (Al(O*i*Pr)$_3$, 1:10 MTS:TBDPS ketene).
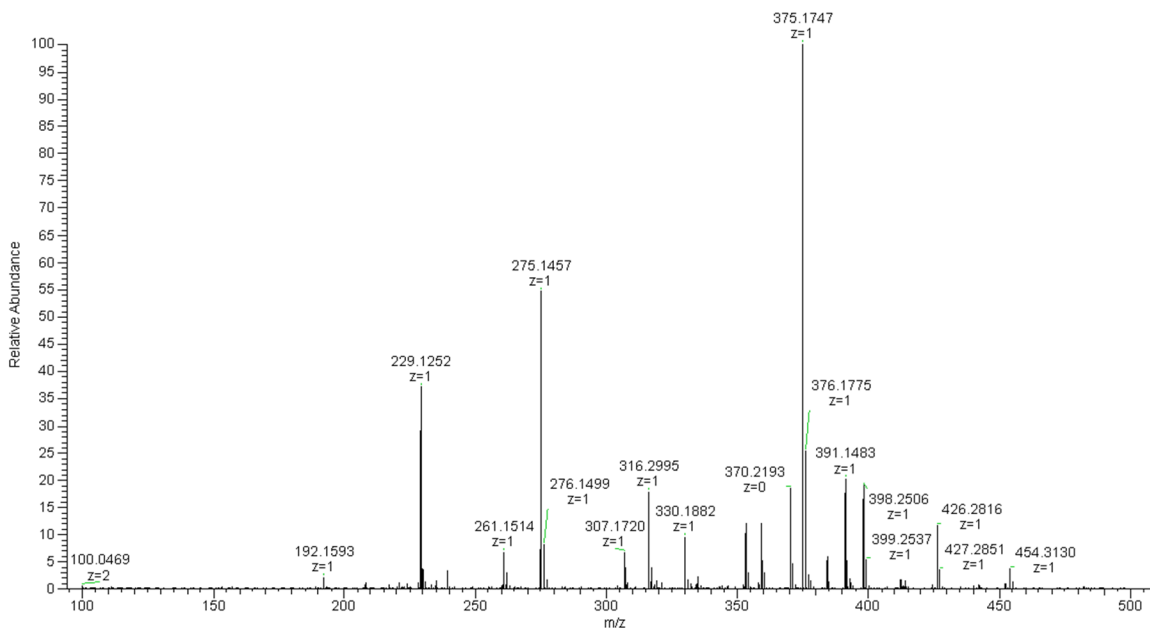
Figure A3.19. ESI mass spectrum of Table 3.1 entry 10 (TBAB, 1:10 MTS:TBDPS ketene).
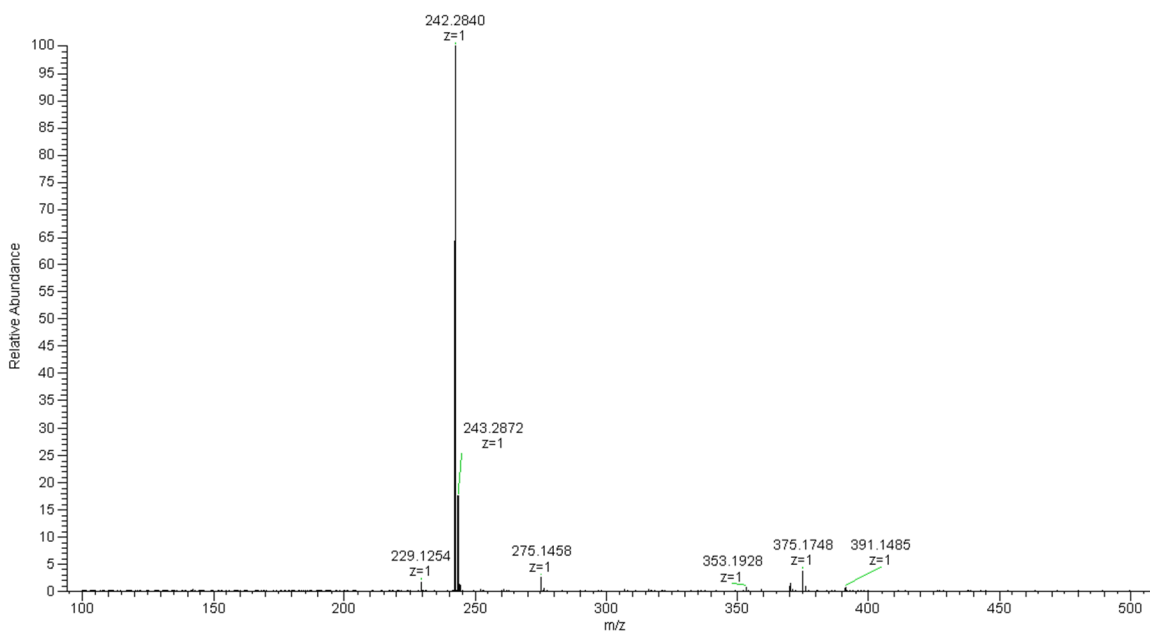
Figure A3.20. ESI mass spectrum of Table 3.2 entry 12 (BF$_3$·OEt$_2$, 1:10 MTS:TIPS ketene).

201103-114947 #70-95 RT: 0.31-0.42 AV: 26 SB: 17 0.13-0.20 NL: 3.24E7
T: FTMS + p ESI Full ms [200.0000-3000.0000]
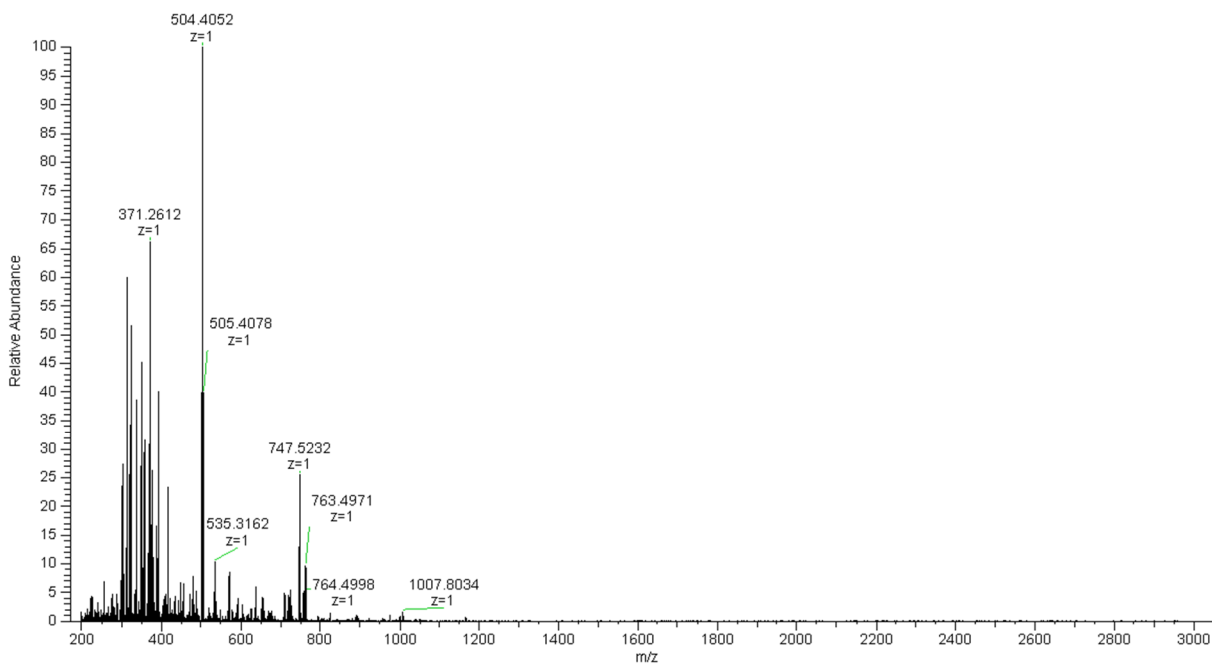
Figure A3.21. ESI mass spectrum of Table 3.2 entry 13 (B(C$_6$F$_5$)$_3$, 1:10 MTS:TIPS ketene).

201103-115148 #70-95 RT: 0.31-0.42 AV: 26 SB: 17 0.13-0.20 NL: 8.40E7
T: FTMS + p ESI Full ms [200.0000-3000.0000]

124
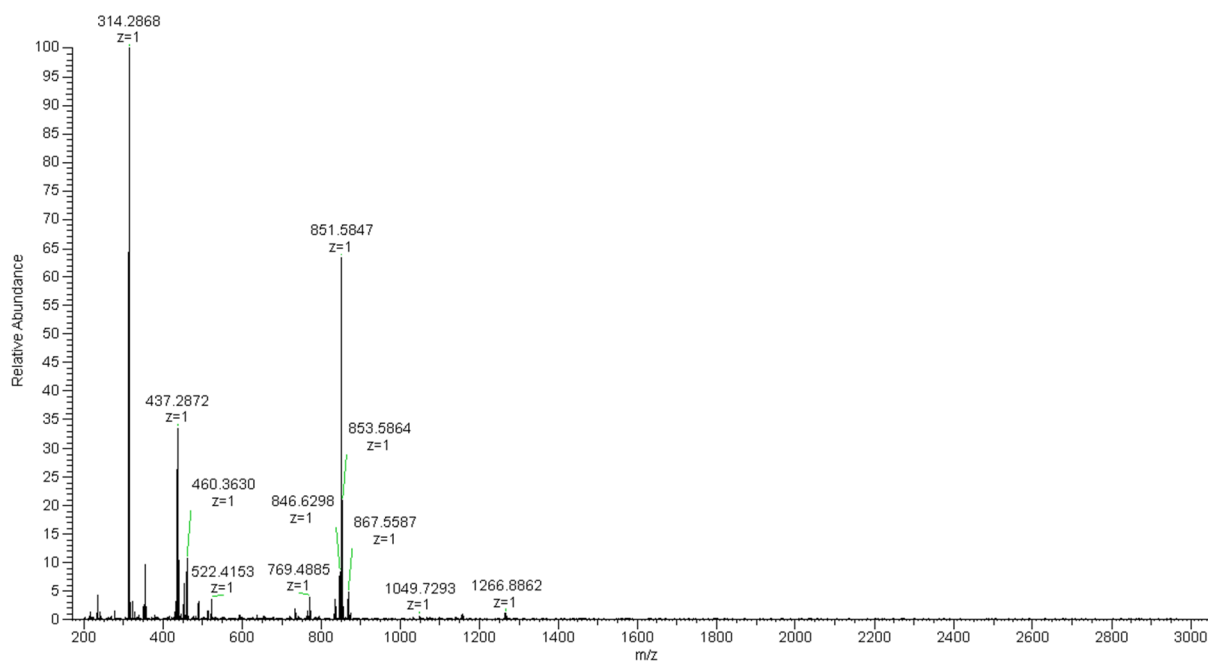
Figure A3.22. ESI mass spectrum of Table 3.2 entry 15 (Al(O^{i}Pr)$_3$, 1:10 MTS:TIPS ketene).

201112-115928 #70-95 RT: 0.31-0.42 AV: 26 SB: 17 0.13-0.20 NL: 1.17E8
T: FTMS + p ESI Full ms [200.0000-3000.0000]
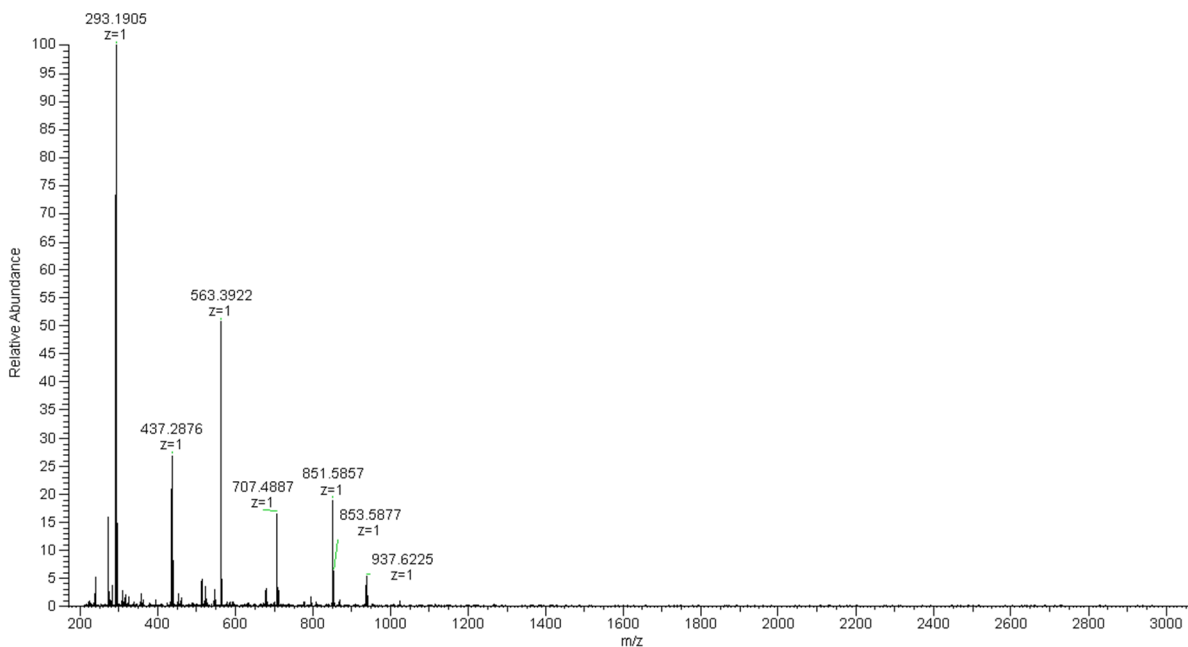
Figure A3.23. ESI mass spectrum of Table 3.2 entry 16 (BF$_3$·OEt$_2$, 1:10 MTS:MDPS ketene).

201106-123650 #70-95 RT: 0.31-0.42 AV: 26 SB: 17 0.13-0.20 NL: 1.28E7
T: FTMS + p ESI Full ms [200.0000-3000.0000]

125
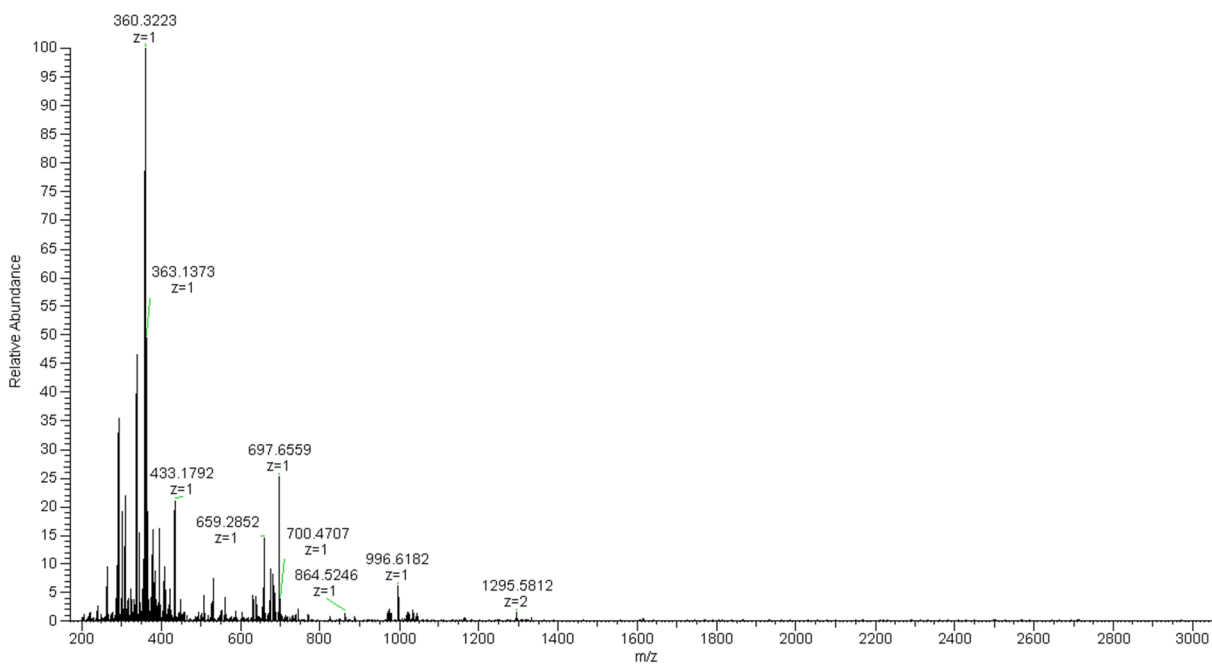
Figure A3.24. ESI mass spectrum of Table 3.2 entry 17 (B(C$_6$F$_5$)$_3$, 1:10 MTS:MDPS ketene).

201106-123827 #70-95 RT: 0.31-0.42 AV: 26 SB: 17 0.13-0.20 NL: 2.97E7
T: FTMS + p ESI Full ms [200.0000-3000.0000]
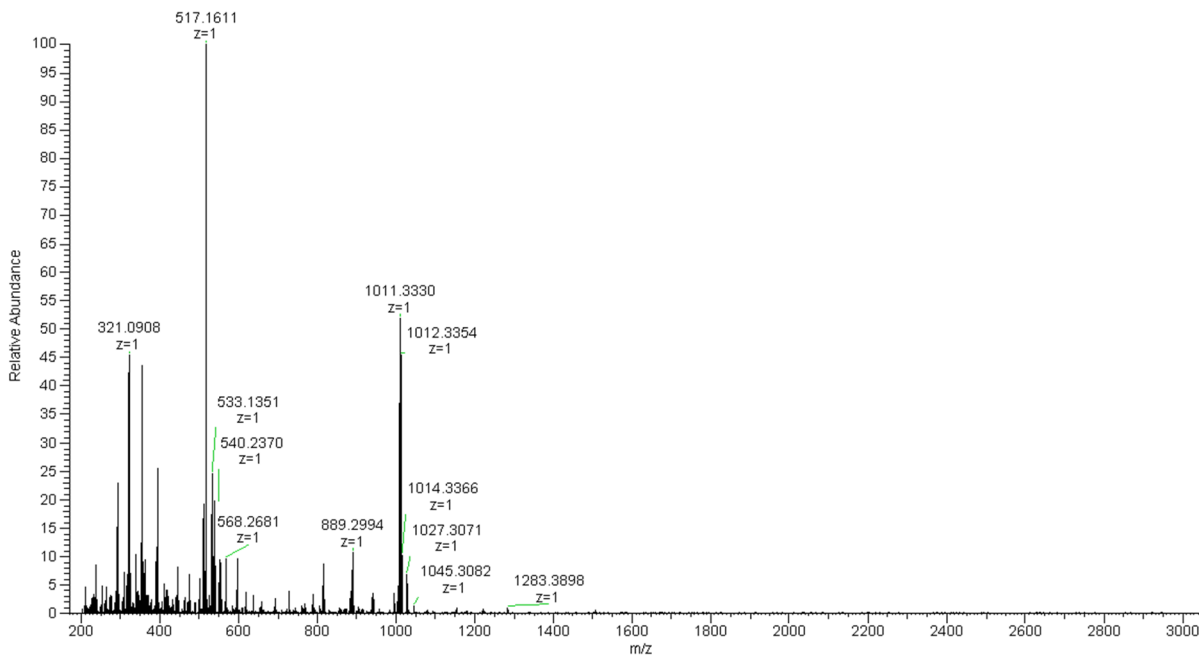
Figure A3.25. ESI mass spectrum of Table 3.2 entry 19 (Al(O^{i}Pr)$_3$, 1:10 MTS:MDPS ketene).

201112-120148 #222-346 RT: 0.99-1.54 AV: 125 SB: 17 0.13-0.20 NL: 8.67E6
T: FTMS + p ESI Full ms [200.0000-3000.0000]
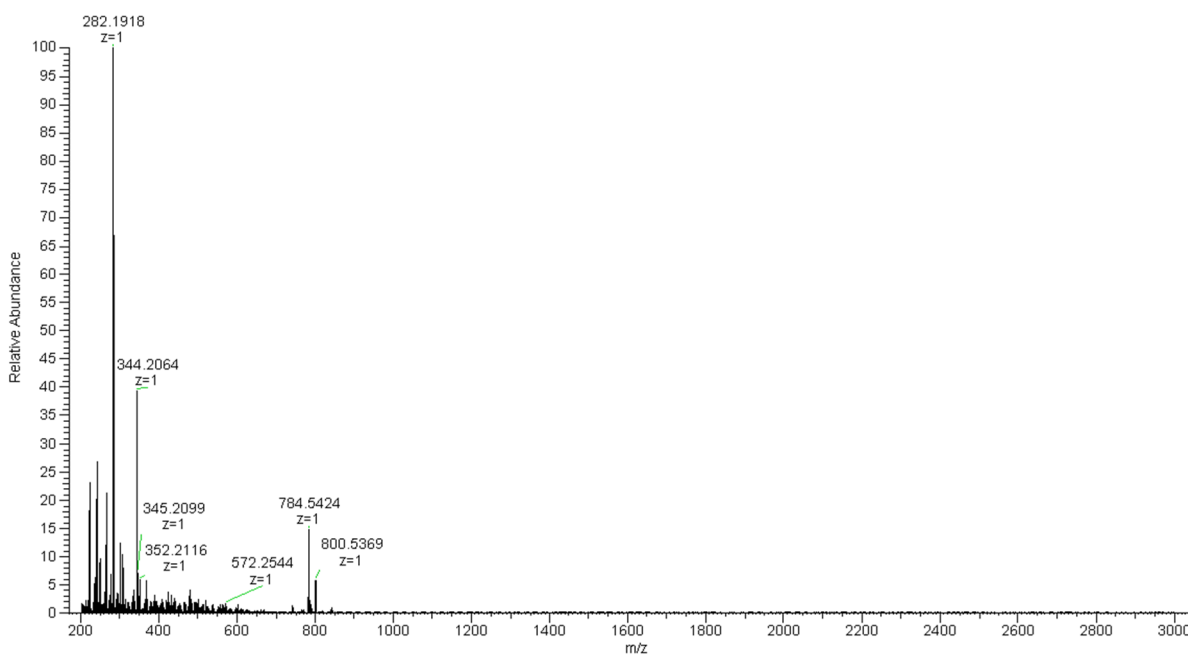
Figure A3.26. ESI mass spectrum of Table 3.2 entry 20 (B(C$_6$F$_5$)$_3$, 1:10 MTS:TES ketene).
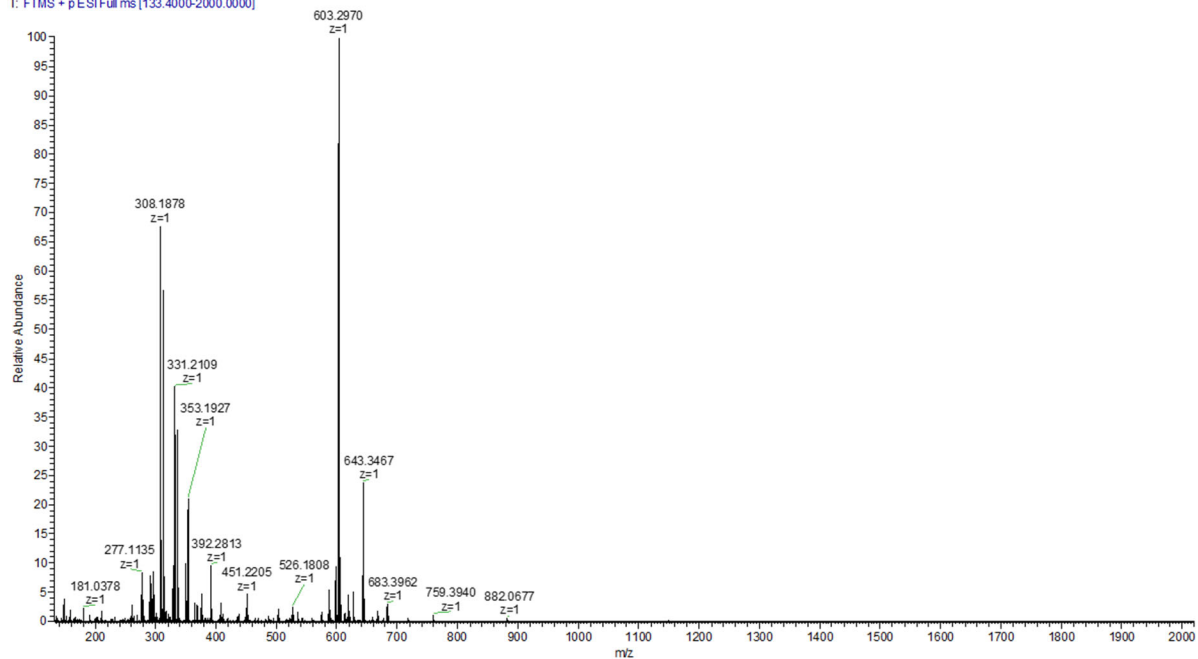
Figure A3.27. ESI mass spectrum of Table 3.2 entry 21 (B(C$_6$F$_5$)$_3$, 1:10 MTS:TPhS ketene).
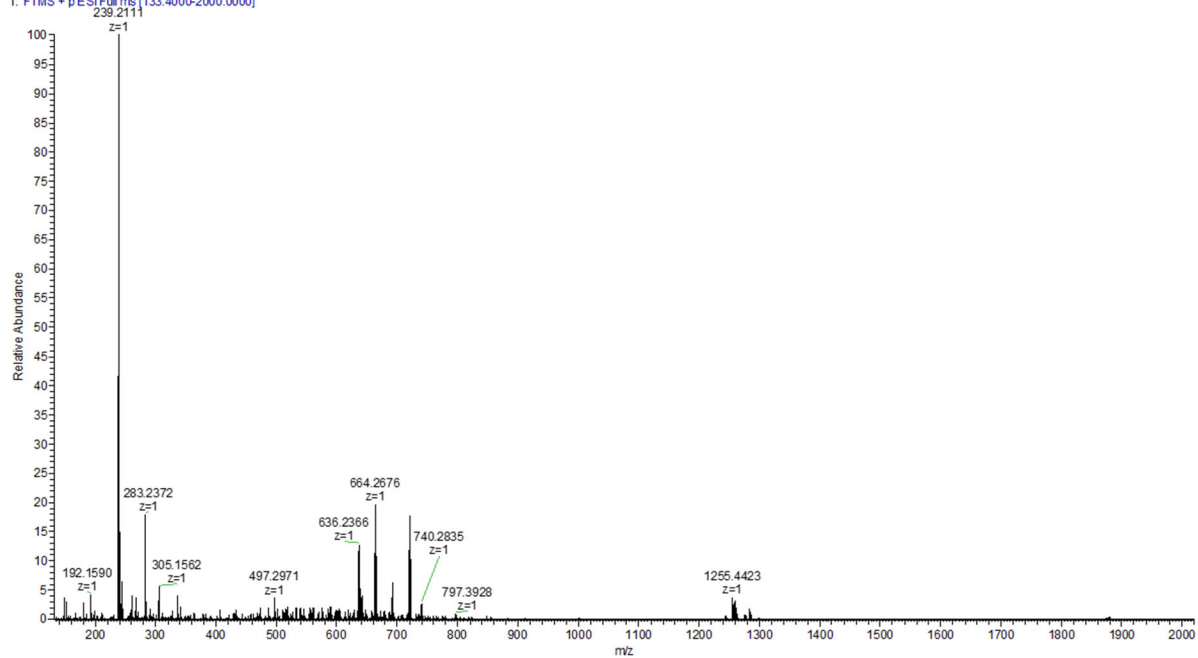
Figure A3.28. ESI mass spectrum of Table 3.3 entry 23 (B(C$_6$F$_5$)$_3$, 1:10 TMS cyanide:TBDPS ketene).
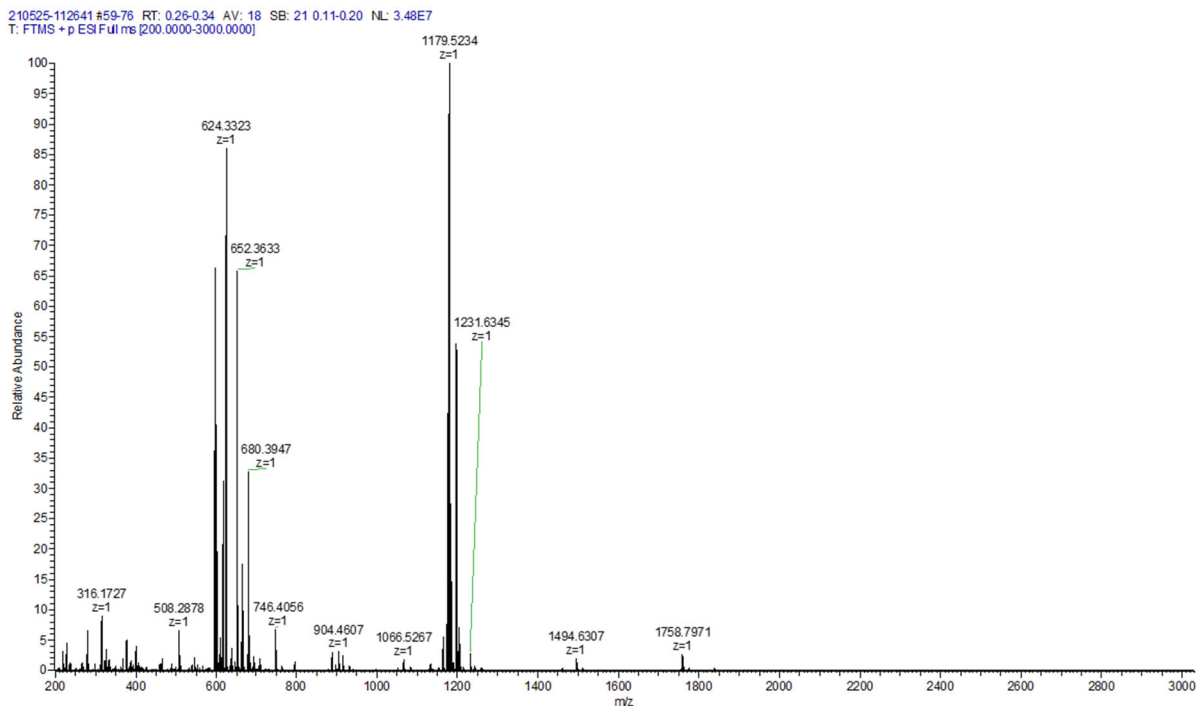
Figure A3.29. ESI mass spectrum of Table 3.3 entry 24 (B(C$_6$F$_5$)$_3$, 1:10 benzaldehyde:TBDPS ketene).
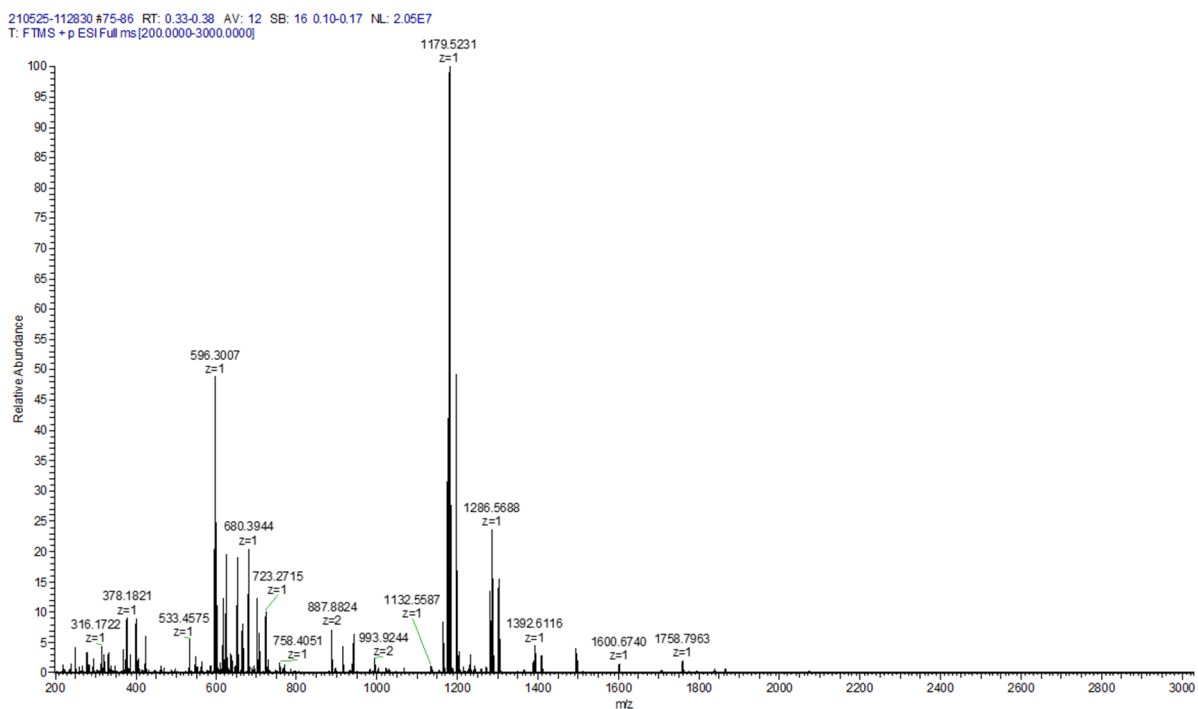
Figure A3.30. ESI mass spectrum of Table 3.3 entry 25 (BF$_3$·OEt$_2$, 1:10 TMS cyanide:TBDPS ketene).
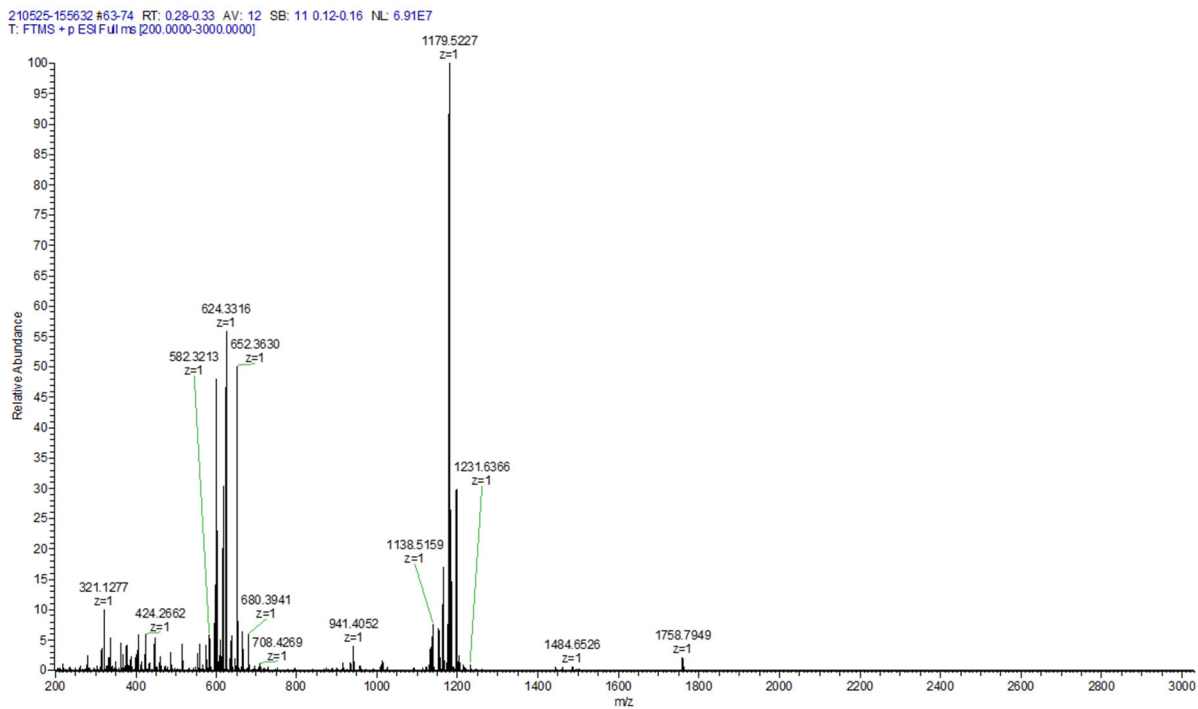
Figure A3.31. ESI mass spectrum of Table 3.3 entry 26 (BF$_3$·OEt$_2$, 1:10 benzaldehyde:TBDPS ketene).
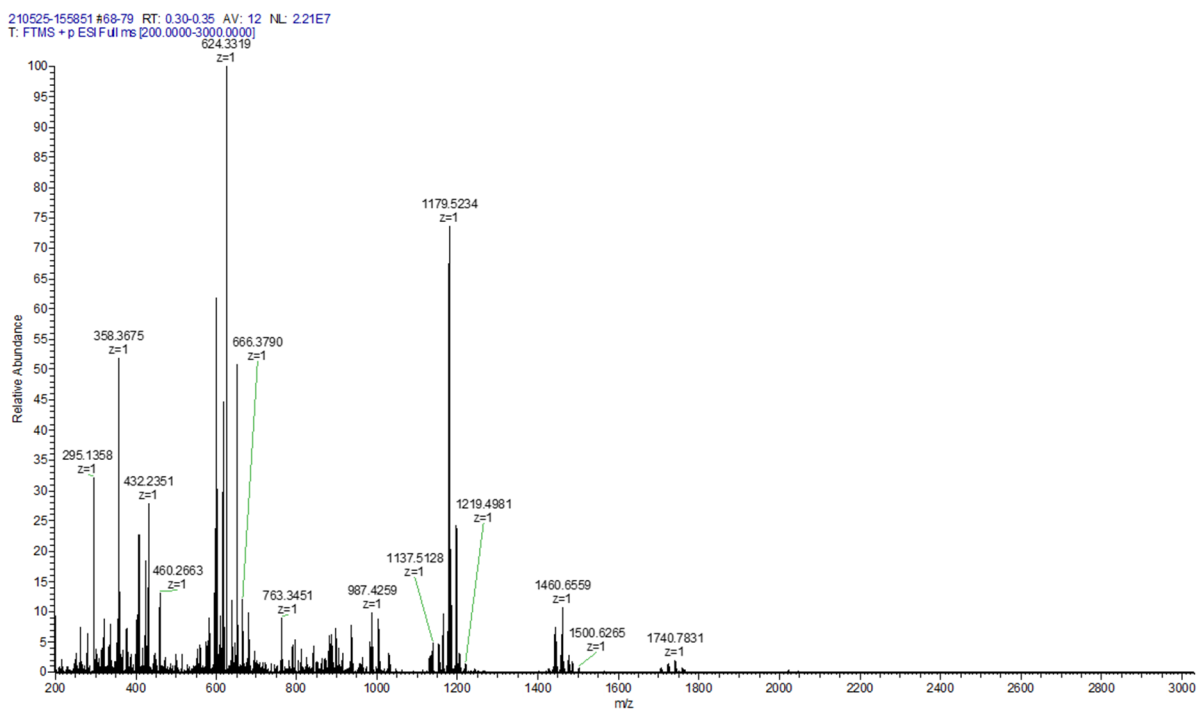
Figure A3.32. ESI mass spectrum of Table 3.3 entry 27 (BF$_3$·OEt$_2$, 1:10 TMS cyanide:TES ketene).
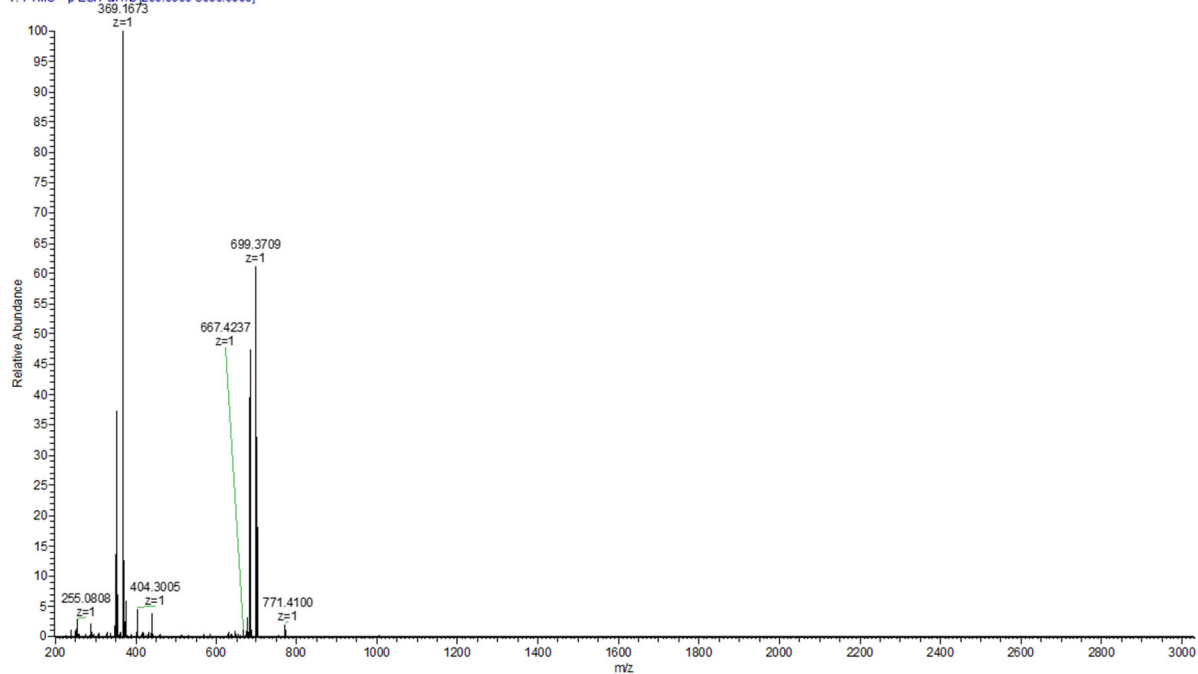
Figure A3.33. ESI mass spectrum of Table 3.3 entry 28 (BF$_3$·OEt$_2$, 1:10 benzaldehyde:TES ketene).
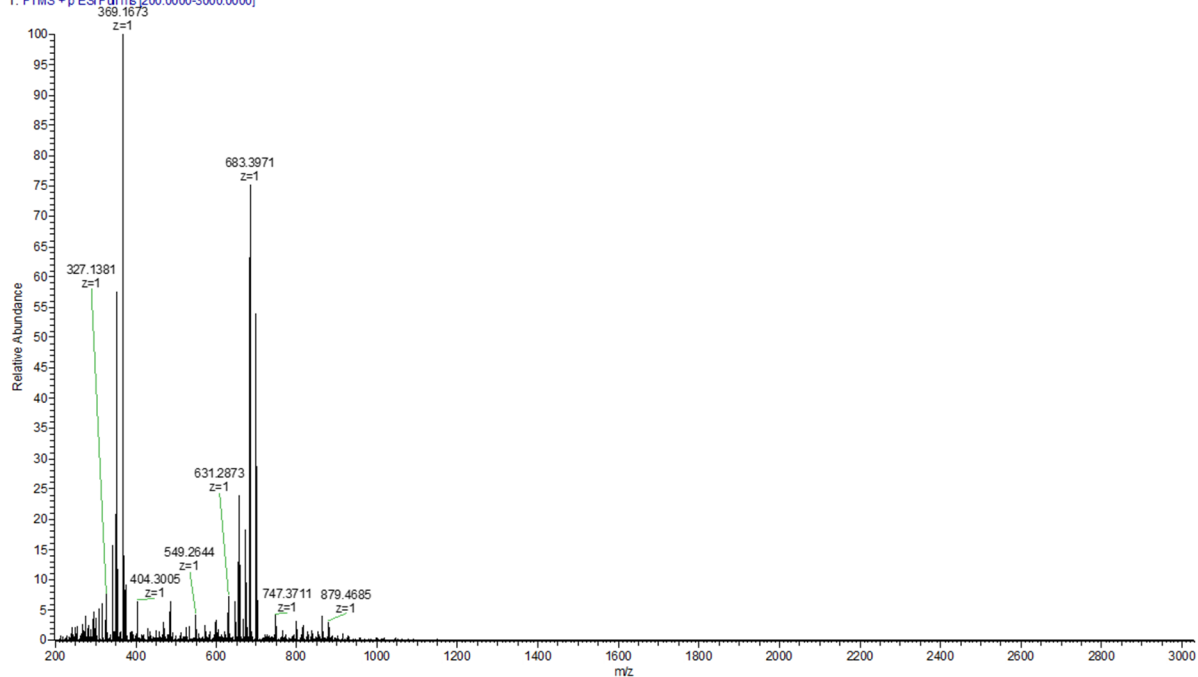
Figure A3.34. ESI mass spectrum of Table 3.3 entry 29 (BF$_3$·OEt$_2$, 1:50 benzaldehyde:TES ketene).
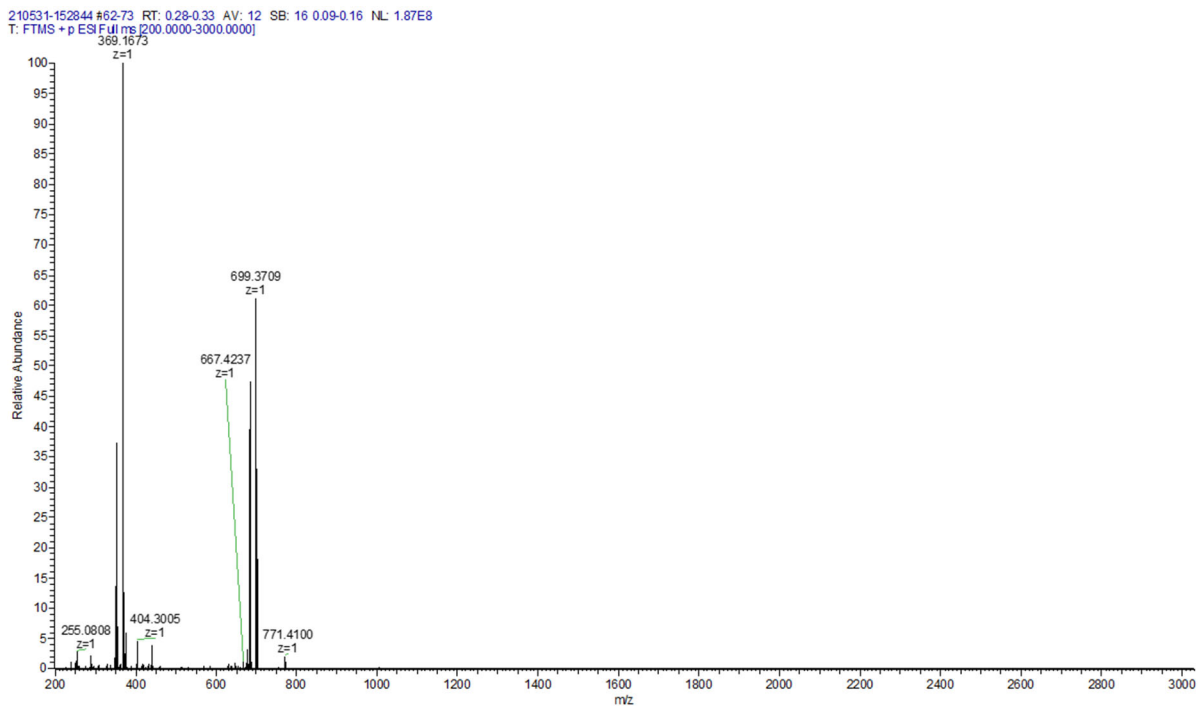
Figure A3.35. ESI mass spectrum of Table 3.3 entry 30 (BF$_3$·OEt$_2$, 1:50 benzaldehyde:TBDPS ketene).
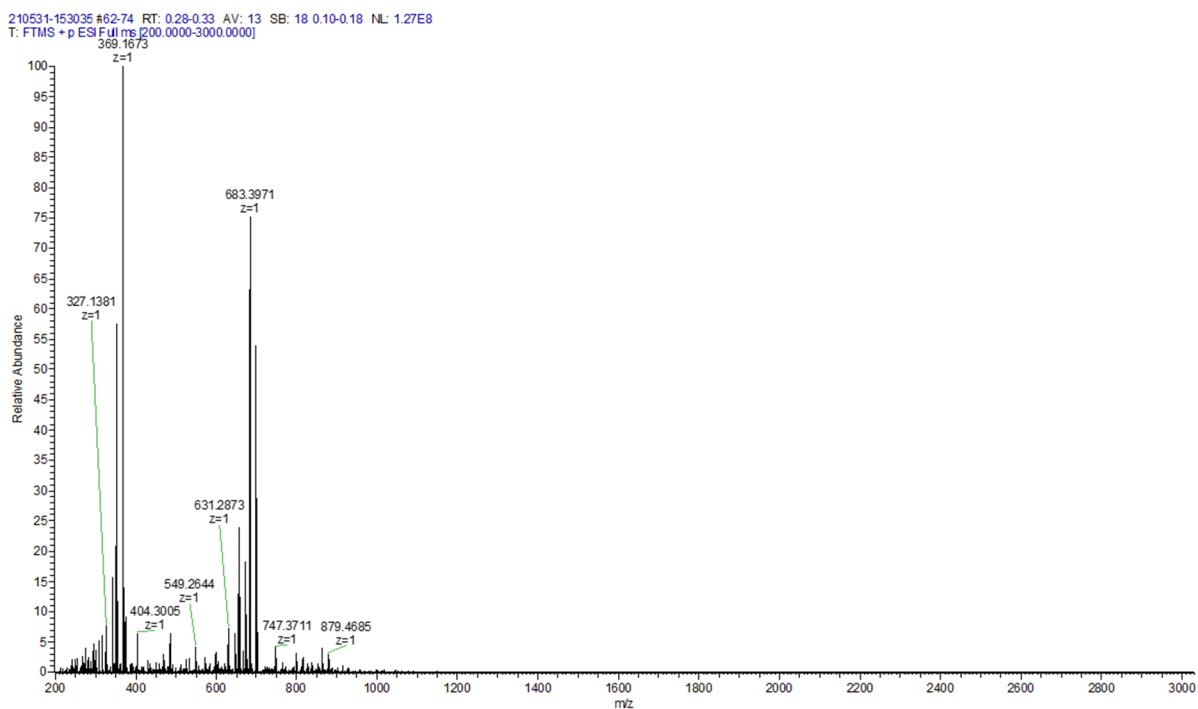
Figure A3.36. ESI mass spectrum of Table 3.4 entry 31 (B(C$_6$F$_5$)$_3$, 1:10 MTS:TBDPS ketene, 0°C to room temperature).
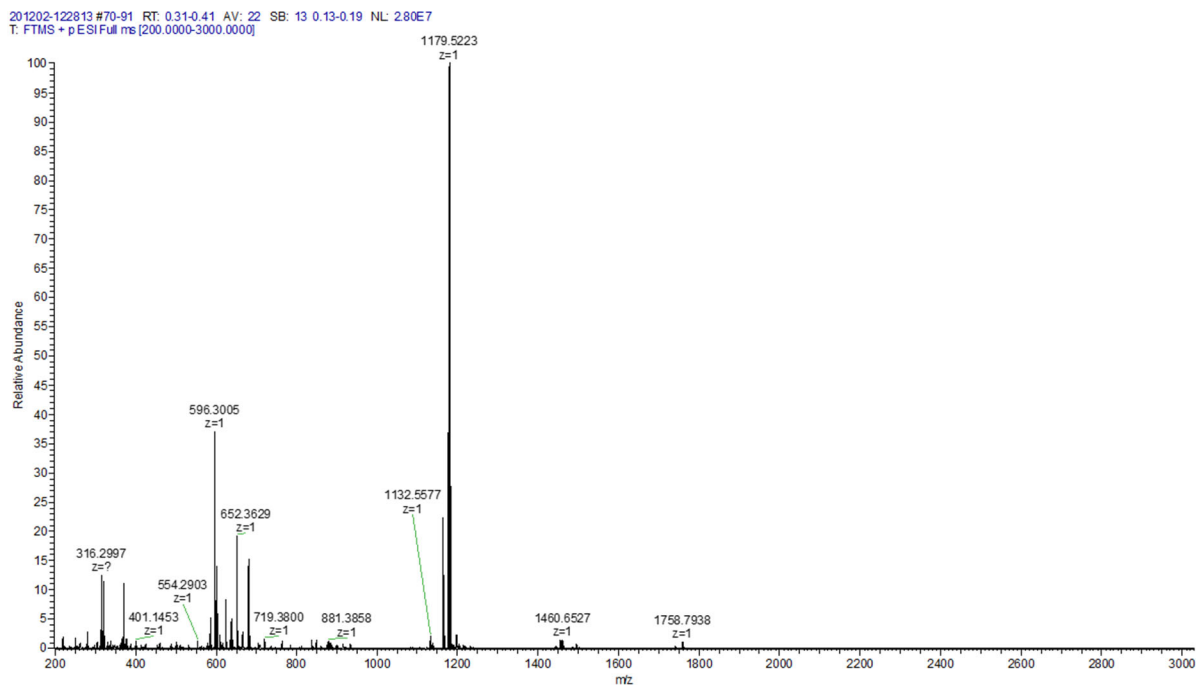
Figure A3.37. ESI mass spectrum of Table 3.4 entry 32 (B(C$_6$F$_5$)$_3$, 1:10 MTS:TBDPS ketene, -46°C to room temperature).
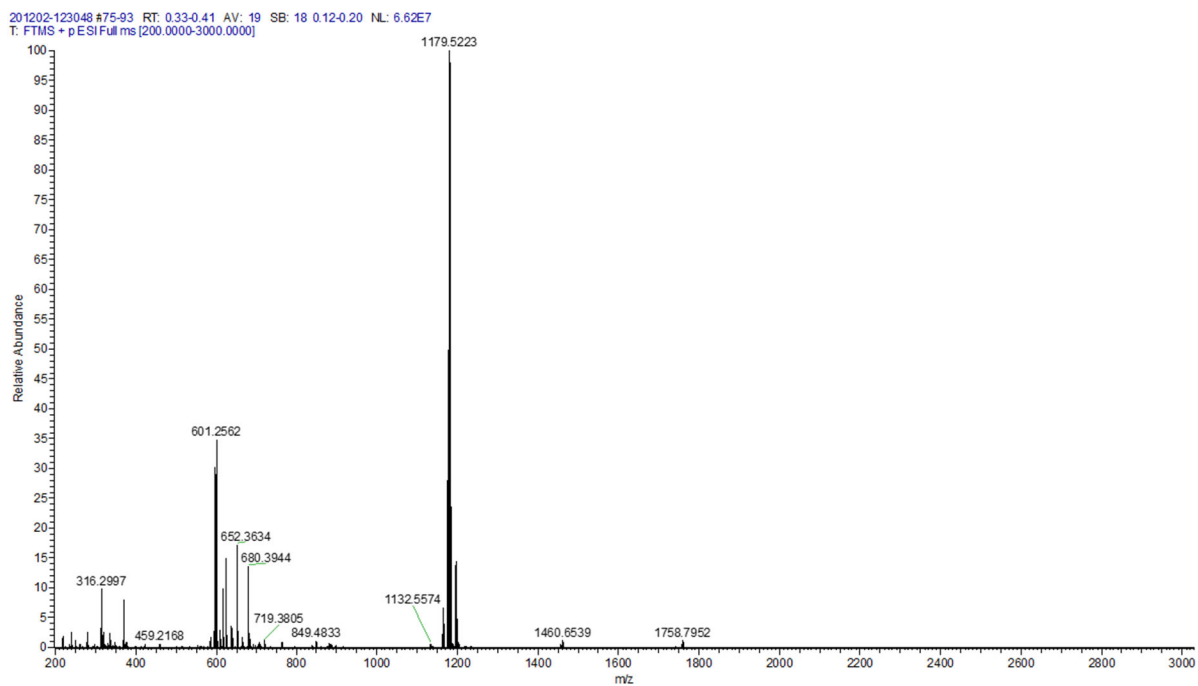
Figure A3.38. ESI mass spectrum of Table 3.4 entry 33 (B(C$_6$F$_5$)$_3$, 1:10 MTS:TBDPS ketene, 0°C for 2 hours then warm to room temperature).
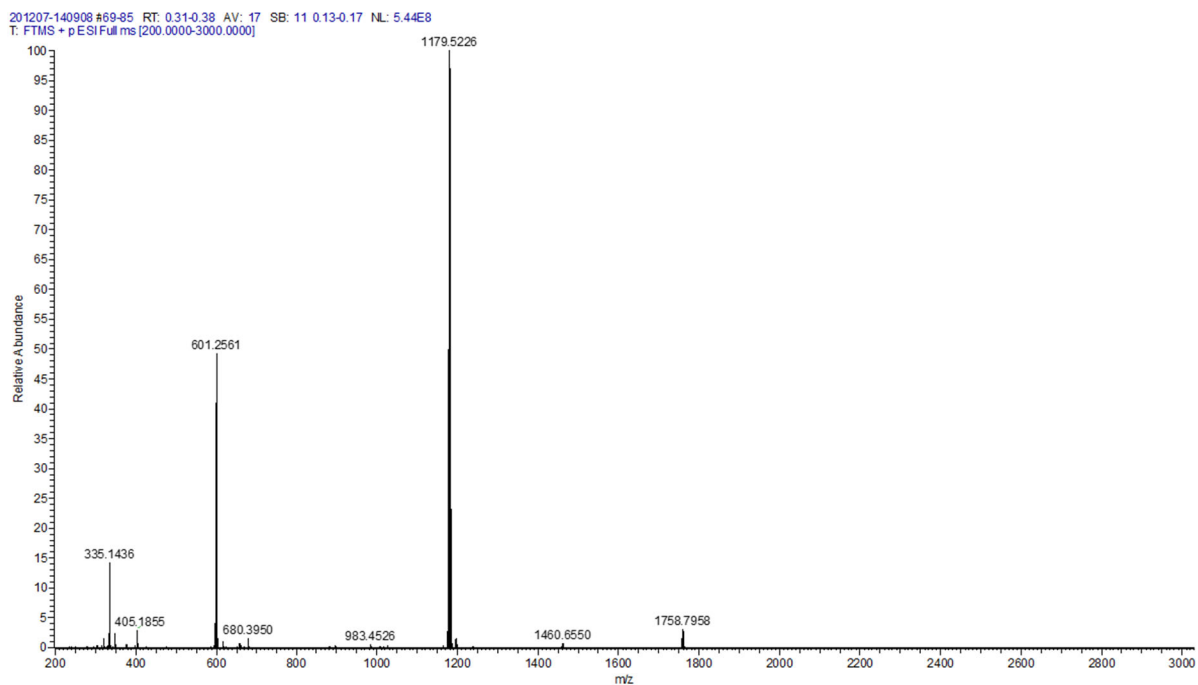
Figure A3.39. ESI mass spectrum of Table 3.4 entry 34 (B(C$_6$F$_5$)$_3$, 1:10 MTS:TBDPS ketene, 0°C for 3 hours then warm to room temperature).
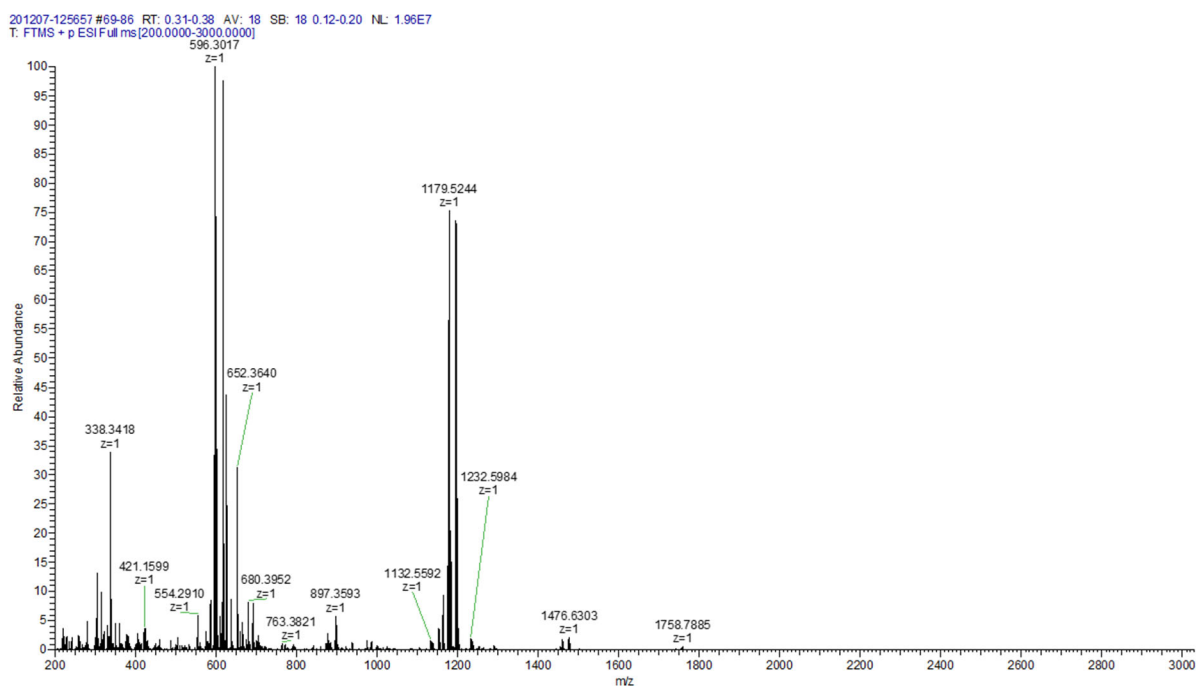
Figure A3.40. ESI mass spectrum of Grignard reagent catalyst with 1:10 MTS:TBDPS ketene.
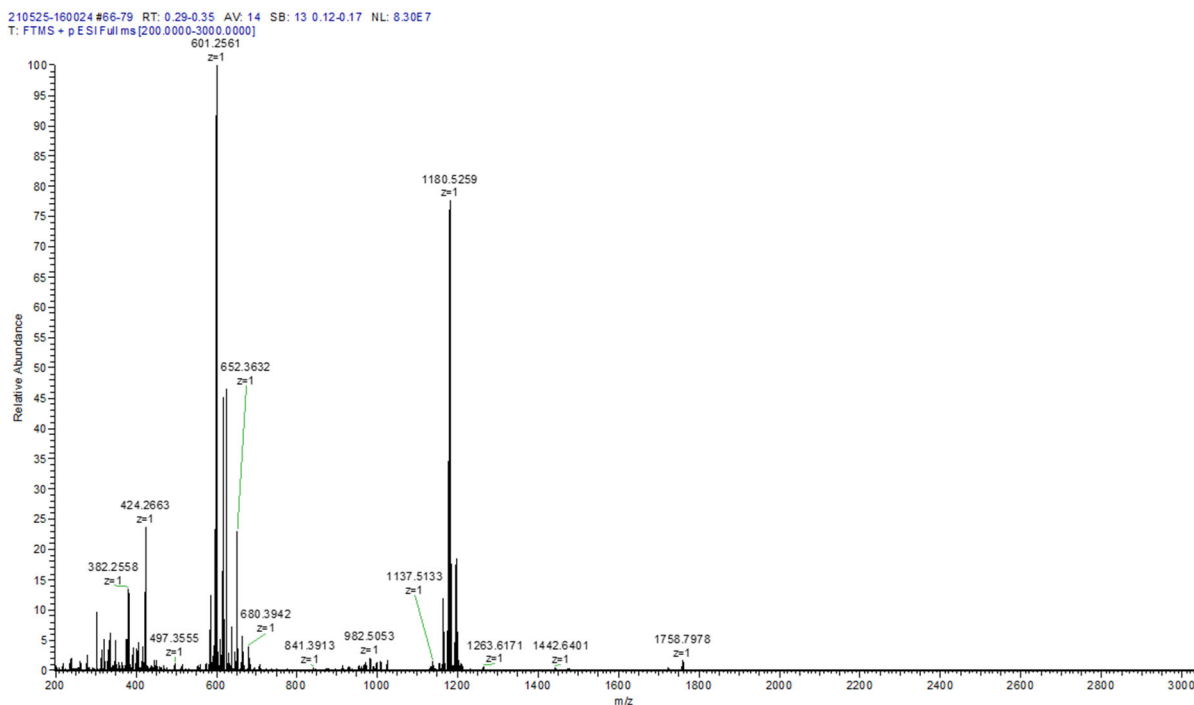
3.9   References

(36)   Odian, G. Principles of Polymerization, 4th ed.; John Wiley & Sons, Inc.: Hoboken, New Jersey, 2004.

(131)   Hertler, W. R.; Sogah, D. Y.; Webster, O. W.; Trost, B. M. Group-Transfer Polymerization. 3. Lewis Acid Catalysis. Macromolecules 1984, 17 (7), 1415–1417. https://doi.org/10.1021/ma00137a021.

(146)   Rikkou-Kalourkoti, M.; Webster, O. W.; Patrickios, C. S. Group Transfer Polymerization. Encycl. Polym. Sci. Technol. 2013, 6, 527–543.

Webster, O. W.; Hertler, W. R.; Sogah, D. Y.; Farnham, W. B.; RajanBabu, T. V. Group-Transfer Polymerization. 1. A New Concept for Addition Polymerization with Organosilicon Initiators. J. Am. Chem. Soc. 1983, 105 (17), 5706–5708. https://doi.org/10.1021/ja00355a039.

(150)   Sogah, D. Y.; Hertler, W. R.; Webster, O. W.; Cohen, G. M. Group Transfer Polymerization. Polymerization of Acrylic Monomers. Macromolecules 1987, 20 (7), 1473–1488. https://doi.org/10.1021/ma00173a006.

(151)   Webster, O. W. Group Transfer Polymerization: Mechanism and Comparison with Other Methods for Controlled Polymerization of Acrylic Monomers. Adv. Polym. Sci. 2004, 167, 1–34. https://doi.org/10.1007/b12303.

(152)   Zhang, J.; Wang, M.; Wang, J.; Shi, Y.; Tao, J.; Wang, D. Group Transfer Polymerization of Acrylonitrile in Bulk at Ambient Temperature. Polym. Bull. 2005, 54 (3), 157–161. https://doi.org/10.1007/s00289-005-0376-3.

(153)   Kikuchi, S.; Chen, Y.; Kitano, K.; Sato, S. I.; Satoh, T.; Kakuchi, T. B(C6F5)3-Catalyzed Group Transfer Polymerization of N,N-Disubstituted Acrylamide Using Hydrosilane: Effect of Hydrosilane and Monomer Structures, Polymerization Mechanism, and Synthesis of α-End-Functionalized Polyacrylamides. Macromolecules 2016, 49 (8), 3049–3060. https://doi.org/10.1021/acs.macromol.6b00190.

(154)   Fuchise, K.; Chen, Y.; Satoh, T.; Kakuchi, T. Recent Progress in Organocatalytic Group Transfer Polymerization. Polym. Chem. 2013, 4 (16), 4278–4291. https://doi.org/10.1039/c3py00278k.

(155)   Raynaud, J.; Gnanou, Y.; Taton, D. Group Transfer Polymerization of (Meth)Acrylic Monomers Catalyzed by N-Heterocyclic Carbenes and Synthesis of All Acrylic Block Copolymers: Evidence for an Associative Mechanism. Macromolecules 2009, 42 (16), 5996–6005. https://doi.org/10.1021/ma900679p.

(156)   Scholten, M. D.; Hedrick, J. L.; Waymouth, R. M. Group Transfer Polymerization of Acrylates Catalyzed by N-Heterocyclic Carbenes. Macromolecules 2008, 41 (20), 7399–7404. https://doi.org/10.1021/ma801281q.

(157)   Muller, A. H. Group Transfer and Anionic Polymerization: A Critical Comparison. Makromol. Chemie. Macromol. Symp. 1990, 32, 87–104.

(158)   Vlček, P.; Lochmann, L. Anionic Polymerization of (Meth)Acrylate Esters in the Presence of Stabilizers of Active Centres. Prog. Polym. Sci. 1999, 24 (6), 793–873. https://doi.org/10.1016/S0079-6700(99)00017-9.

(159)   Raynaud, J.; Liu, N.; Fèvre, M.; Gnanou, Y.; Taton, D. No Matter the Order of Monomer Addition for the Synthesis of Well-Defined Block Copolymers by Sequential Group Transfer Polymerization Using N-Heterocyclic Carbenes as Catalysts. Polym. Chem. 2011, 2 (8), 1706–1712. https://doi.org/10.1039/c1py00077b.

(160)   Imada, M.; Takenaka, Y.; Tsuge, T.; Abe, H. Kinetic Modeling Study of the Group-Transfer Polymerization of Alkyl Crotonates Using a Silicon Lewis Acid Catalyst. Polym. Chem. 2020, 11 (37), 5981–5991. https://doi.org/10.1039/d0py00353k.

(161)   Fuchise, K.; Tsuchida, S.; Takada, K.; Chen, Y.; Satoh, T.; Kakuchi, T. B(C6F5)3-Catalyzed Group Transfer Polymerization of n-Butyl Acrylate with Hydrosilane through in Situ Formation of Initiator by 1,4-Hydrosilylation of n -Butyl Acrylate. ACS Macro Lett. 2014, 3 (10), 1015–1019. https://doi.org/10.1021/mz5004689.

(162)   Mitchell, S. M.; Xiang, Y.; Matthews, R.; Amburgey, A. M.; Pentzer, E. B. Lewis Acid-Activated Reactions of Silyl Ketenes for the Preparation of α-Silyl Carbonyl Compounds. J. Org. Chem. 2019, 84 (22), 14461–14468. https://doi.org/10.1021/acs.joc.9b01859.

(163)   Seyferth, D. The Grignard Reagents. Organometallics 2009, 28, 1598–1605. https://doi.org/10.1021/om900088z.

(164)   Aoshima, S.; Kanaoka, S. A Renaissance in Living Cationic Polymerization. Chem. Rev. 2009, 109 (11), 5245–5287. https://doi.org/10.1021/cr900225g.

Part I: Silyl Ketenes as Building Blocks for Small Molecules and Polymers

Chapter 4

Summary and Future Directions of Silyl Ketene Monomers

Portions of this chapter appear in the following manuscript that was recently submitted to JOC:

Competition of Deprotonation and Nucleophilic Addition: Computational Insight into Silyl Ketenes as Molecular Building Blocks; Krista Schoonover,[1] Ian Baxter,[2] Sarah Mitchell,[3] Amanda Dumi,[4] Emily Pentzer,[1,3] and Daniel S. Lambrecht[*2,4]; JOC, submitted.

4.1   Summary

The work presented in part one of this thesis explores the reactivity and polymerization of silyl ketenes. The reactivity of silyl ketenes was explored via the formation of α-silyl carbonyls from various nucleophiles catalyzed by a Lewis acid (LA).[162] More specifically, alcohols, thiols, and amines were reacted with a silyl ketene to form α-silyl esters, α-silyl thioesters, and α-silyl amides respectively. The alcohol based nucleophiles examined steric bulk and electronics of the nucleophiles and their impact on the reaction. Overall, little difference was observed between alkyl alcohols versus the phenols. Of the phenol-based nucleophiles, compounds bearing electro-donating substituents performed slightly better, producing higher isolated yields. The amine nucleophiles performed similarly to the alcohol nucleophiles, whereas the thiol nucleophiles produced low yields and products were difficult to purify. The silyl substituent scope was also examined, exploring how steric bulk and electronics affected the reaction. No trend was observed between the silyl substituents, as all silyl groups performed with similar reaction times and yield, showing the robustness of the LA catalyst. This works provides knowledge on how LAs can be used to activate silyl ketenes for reaction with nucleophiles, informing the reactivity pathways of silyl ketenes.

Additionally, this thesis examined group transfer polymerization (GTP) of silyl ketenes, examining catalysts, initiators, silyl substituents, and reaction conditions. It was determined, that the GTP of silyl ketenes is extremely air sensitive. Several catalysts were examined to activate the initiator, including LAs and nucleophilic anions, of which $BF_3 \cdot OEt_2$, $B(C_6F_5)_3$, and *N*-heterocyclic carbenes performed the best. Catalysts $Al(O^iPr)_3$, tetrabutylammonium bromide, and triphenylborane had one or more reactions of unreacted silyl ketene and will not be used in future experiments. Three initiators were also examined, including methyl trimethylsilyl dimethylketene acetal (MTS),

benzaldehyde, and trimethysilyl cyanide, each producing cyclic oligomers. Several polymerization conditions were also examined, including monomer:initiator ratio, reaction temperature, and concentration, all of which must be further examined to determine proper initiator/catalyst combination. Thus far, the 1:50 of benzaldehyde to silyl ketene produced a higher molecular weight oligomer with reduced formation of a cyclic oligomer observed in the 1:10 ratio. Regardless, work is ongoing for the GTP of silyl ketenes and is promising to obtain high molar mass polymers.

4.2   Future Directions

4.2.1   Future of Group Transfer Polymerization

The work presented in this thesis, provides a foundation for GTP of silyl ketenes and the ability to obtain high molar mass polymers is possible. Formation of cyclic oligomers are favored at a 1:10 initiator:monomer ratio, however the more recent experiments that used a 1:50 ratio resulted in lower yields of the cyclic oligomers. Further characterization of the 1:50 ratio experiments need to be obtained, including MALDI and GPC to determine the molar mass and the presence of polymers. Additional higher ratio experiments need to be explored, due to the major difference between the 1:10 and 1:50, higher molar mass polymers could be obtained.

Another intriguing pathway to explore is a wider initiator scope, examining additional potential initiators. There was a noticeable difference observed when benzaldehyde or trimethylsilyl cyanide was used, with only benzaldehyde producing a solid product, which could be due to the cyclic oligomer not forming and a higher molar mass being obtained (~1700 m/z). Future work could expand the scope of benzaldehyde derivative initiators (Figure 4.1a), incorporating electron-withdrawing or electron-donating groups or di-functional initiators. Silyl ketene acetals are the most commonly used initiator in GTP, specifically MTS. Interestingly, α-silyl carbonyls have

been used as precursors for the formation of silyl ketene acetals (Figure 4.1b).[165] Therefore, an initiator could be prepared from a given silyl ketene then used to polymerize the selected ketene. Future work should also explore the kinetics of polymerizing silyl ketenes via group transfer polymerization. Examining how temperature, solvent, and concentration play a role in the rate of polymer formation. Also, appropriate conditions should be identified to determine catalyst/initiator combination that will produce polymers of defined stereochemistry.
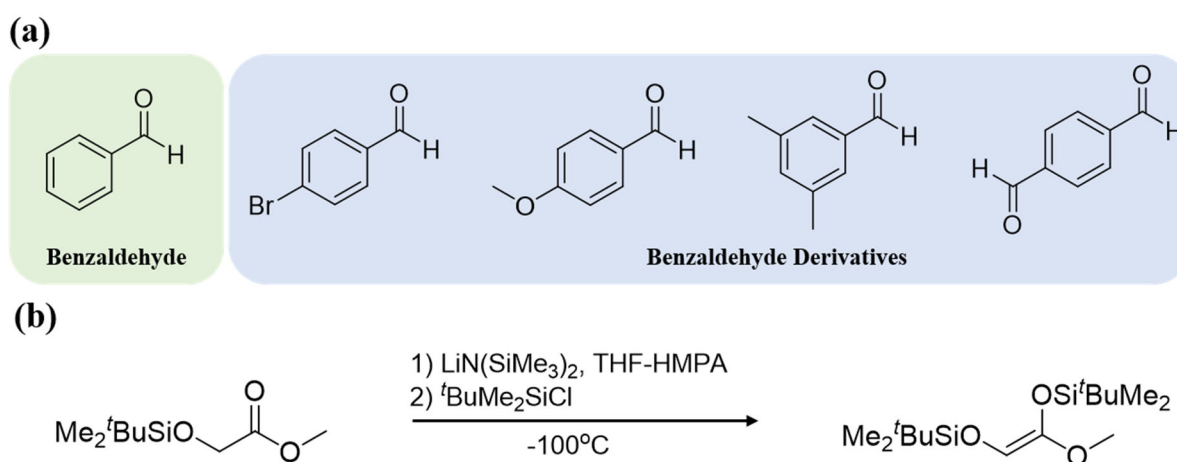
Figure 4.1. (a) Potential benzaldehyde derivative initiators, (b) formation of silyl ketene acetal from an α-hydroxy ester.

4.2.2   Future of Cationic Polymerization

Cationic polymerization is a technique that typically polymerizes alkenes and heterocyclic compounds using protic acids or LAs and Friedel-Craft catalysts.[164] This technique has previously been extended to ketenes, for example dimethylketene was polymerized with the cationic initiator, aluminum tribromide, to produce a crystalline polyketone (Scheme 4.1).[99] In this work, cationic polymerization was attempted with GTP catalysts, however the conditions tested did not lead to polymerization. Future work can further evaluate cationic initiators and various LAs to obtain

polymers of silyl ketenes. For example, a wider range of LAs such as AlBr$_3$, AlEt$_3$, zinc complexes, and boron complexes can be examined or use of cocatalyst systems such as BF$_3$/H$_2$O or AlCl$_3$/H$_2$O.
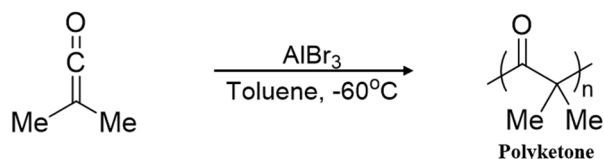
Scheme 4.1. Cationic polymerization of dimethyl ketene to produce crystalline polyketone.

4.2.3 Anionic Polymerization

Anionic polymerization was the significant initial focus in the Pentzer lab for the polymerization of silyl ketenes, with research supporting that polymers of high molar mass can be obtained using alkoxide initiators. However, the polymers obtained contained all possible polymeric backbone functional groups (ester, acetal, and ketone), and polymerization competed with backbiting and side reactions.[108] Further, it was determined that in addition to the nucleophilic addition of the alkoxide to the central carbon of ketene, in certain monomer/initiator pairs, the alkoxide would act as a base and deprotonate the terminal ketene carbon, leading to formation of an alkynoate which could then react. Additional initiators were studied and differences in the ratio of deprotonation and nucleophilic addition was determined (Figure 4.2a).[117] A trend was observed that selective nucleophilic addition could be obtained and was correlated to the pK$_{aH}$ of the initiators, where nucleophilic addition was favored with less basic initiators. For example, when a lithium thiolate (pK$_{aH}$ = 15) was used, 100% nucleophilic addition was observed (Figure 4.2a). Using this knowledge of how pK$_{aH}$ of the initiator impacts reactivity patterns can lead to better selection of

(a)
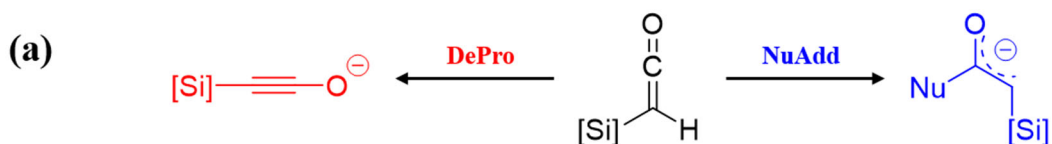
Entry	Nucleophile	pK$_{aH}$	Time	% conv	DePro:NuAdd
1	tBuO⁻	30	0.16	100	100:0
2	PhO⁻	18	10	100	40:60
3	CH3COO⁻	12	420	50	0:100
4	PhCH2S⁻	15	30	100	0:N/A
5	PhCH2S⁻	15	10	100	0:100

(b)
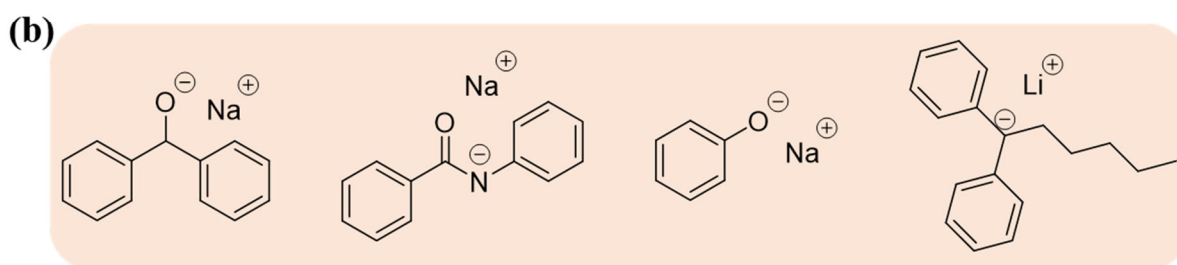
Figure 4.2. (a) Nucleophilic addition vs. deprotonation of silyl ketenes that can be correlated to pK$_{aH}$, (reproduced from Xiang *et al.*); (b) Dual functional initiators previously used for the controlled polymerization of isocyanates that are of interest for the polymerization of silyl ketenes.

anionic initiators that will undergo a controlled polymerization (further expanded in section 4.2.4 Combining Experimental and Computational Studies).

Unlike ketenes, polymerization of isocyanates has been thoroughly studied; specifically, dual functional initiators have led to the controlled polymerization of isocyanates. Since isocyanates and silyl ketenes are isoelectronic, initiators can be selected based on successful polymerization of isocyanates. Looking at the pK$_{aH}$ of these initiators can also lead to a better selection of initiators to evaluate. Currently, another Pentzer lab member is examining lithium diphenylhexane, sodium

benzanilide, sodium phenoxide, and sodium benzhydroxide (pK_{aH} value of 35, 25, 18, and 14 respectively) as initiators for the polymerization of silyl ketenes (Figure 4.2b). The identity of the counterions has been shown to impact the propagation, as based on their interaction with the charged chain end, the formation of low molecular weight oligomers is favored by steric hinderance, which can prevent approach of another monomer unit and favor intrachain backbiting due to local concentration of oligomeric functional groups. Examining the counterion (lithium, sodium, or potassium cations) of the initiators could lead to high the formation of higher molar mass polymers.

4.2.4 Combining Experimental and Computational Studies

The combination of computational studies and experimental studies can lead to better selection for possible initiators. As mentioned above, the pK_{aH} correlates to the whether nucleophilic addition or deprotonation will occur. Through computational calculations an initiator can be predicted to favor either deprotonation or nucleophilic addition, which can lead to the controlled inititation of silyl ketenes. Currently, the Lambrecht group at Florida Gulf Coast University is performing computational experiments to determine the activation energy required and relative produce energies of nucleophilic addition and deprotonation product using select initiators (Figure 4.3a). An ideal candidate would greatly favor nucleophilic addition and disfavor deprotonation. This

could greatly streamline the selection of potential initiators to evaluate experimentally and lead to more controlled polymerizations of silyl ketenes.

To better guide the development of these calculations, experimental results were obtained with 3 of the calculated initiators, 4-methoxyphenol, 4-nitrophenol, and 3-nitrophenol, were performed
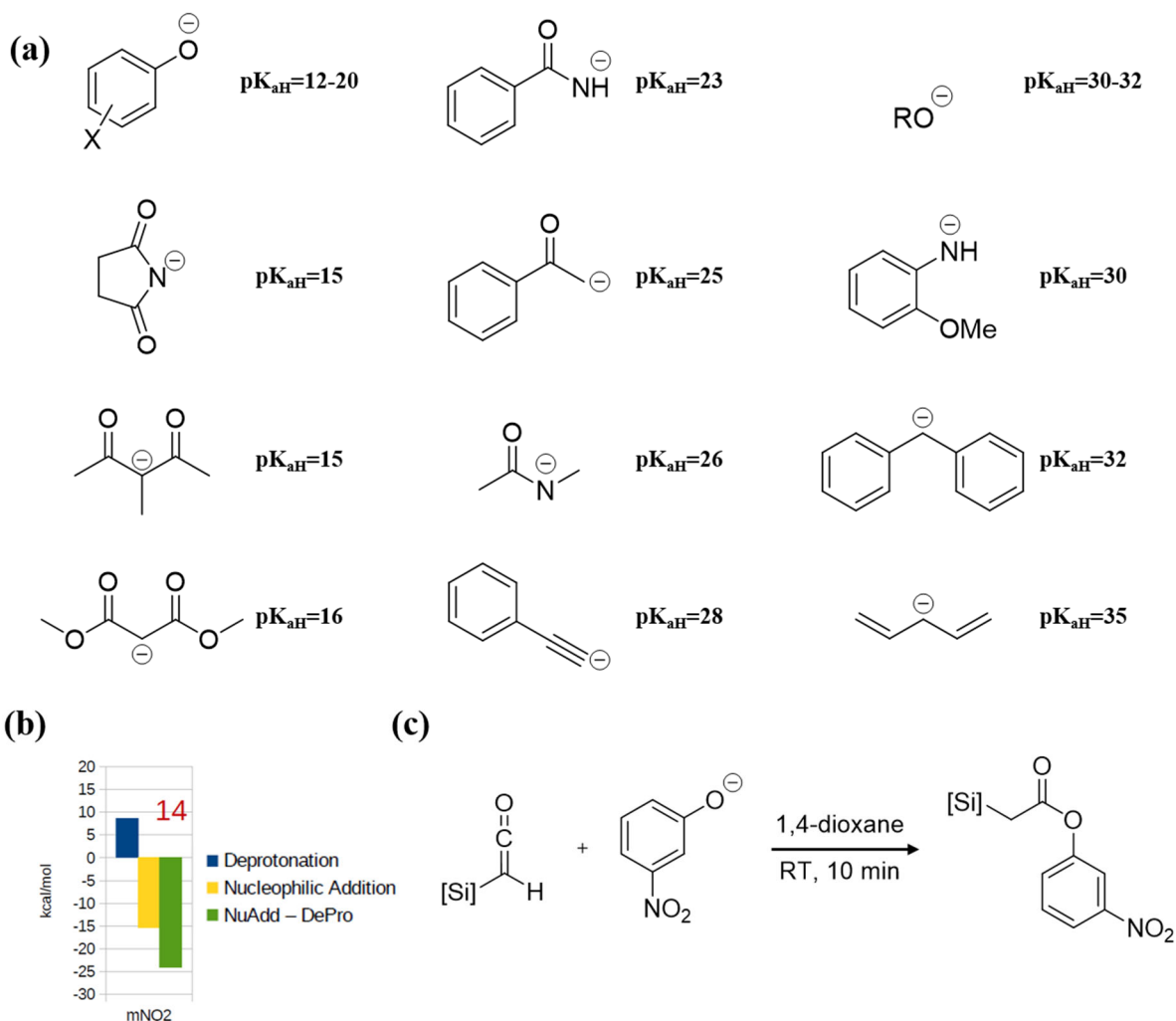
Figure 4.3. (a) Possible initiators and the pK_{aH} of their conjugate acid in DMSO, (b) DFT calculation of the favorability of the deprotonation (blue) and nucleophilic addition (yellow) product and the difference (green), (c) Experimental reaction of 3-nitrophenoxide to validate calculations.

to confirm the predicted outcome. For example, it was predicted that 3-nitrophenoxide would favor nucleophilic addition when reacted with tert-butyldiphenylsilyl ketene (Figure 4.3b). When performed experimentally, characterization of the crude reaction mixture by ^{1}H NMR confirmed that only the nucleophilic addition product was formed, which is an α-silyl carbonyl, and no deprotonation product was detected (Figure 4.3c). This was further confirmed with 4-methoxyphenol and 4-nitrophenol, where 4-methoxyphenol exhibited both deprotonation and nucleophilic addition products and 4-nitrophenol only exhibited nucleophilic addition products; both of these outcomes were predicted through calculations. Thus, combining computational and experimental studies can lead to predictive reactivities. Future work exploring the combination of computational and experimental work involves calculating the energy necessary to initiate a silyl ketene with the dual functional initiators (Figure 4.2b). Thus, through evaluating the activation energy of the reaction pathways, in addition to the thermodynamic favorability of the different products can be used to guide experiment, facilitating rapid materials development with saved cost and resources.

4.3 References

(99)   Natta, G.; Mazzanti, G.; Pregaglia, G.; Binaghi, M.; Peraldo, M. Crystalline Polymers of Dimethylketene. J. Am. Chem. Soc. 1960, 82 (17), 4742–4743. https://doi.org/10.1021/ja01502a073.

(108) Xiang, Y.; Burrill, D. J.; Bullard, K. K.; Albrecht, B. J.; Tragesser, L. E.; McCaffrey, J.; Lambrecht, D. S.; Pentzer, E. Polymerization of Silyl Ketenes Using Alkoxide Initiators: A Combined Computational and Experimental Study. Polym. Chem. 2017, 8 (35), 5381–5387. https://doi.org/10.1039/C7PY00858A.

(117)   Xiang, Y.; Mitchell, S.; Rheingold, A. L.; Lambrecht, D. S.; Pentzer, E. Oligomerization of Silyl Ketene: Favoring Chain Extension over Backbiting. Macromolecules 2019, 52 (16), 6126–6134. https://doi.org/10.1021/acs.macromol.9b00752.

(164)   Aoshima, S.; Kanaoka, S. A Renaissance in Living Cationic Polymerization. Chem. Rev. 2009, 109 (11), 5245–5287. https://doi.org/10.1021/cr900225g.

(165)   Hattori, K.; Yamamoto, H. Highly Selective Generation and Application of (E)- and (Z)-Silyl Ketene Acetals from α-Hydroxy Esters. J. Org. Chem. 1993, 58 (20), 5301–5303. https://doi.org/10.1021/jo00072a005.

Part II: The Incorporation of Redox Small Molecules into Deep Eutectic Solvents for the Development of New Electrolytes

Chapter 5

Introduction to Redox Active Small Molecules and Deep Eutectic Solvents for the Development of New Electrolytes

5.1 Current World Energy Needs

The energy needs of the world have been a great topic of interest in recent decades, mainly due to the shift away from using fossil fuels to more renewable/sustainable sources, such as wind and solar. Renewable energy, unlike fossil fuels, needs to be harvested when available, so energy storage is vital to new technologies. There are four types of energy storage systems, including thermal, mechanical, chemical, and electro-chemical energy storage (Figure 5.1.a).[166] Many criteria are used for the selection of energy storage systems, for example large scale, high efficiency, low cost, and so on (Figure 5.1b).[167] A common application of electro-chemical energy storage is battery energy storage systems, which can exhibit high energy densities and high
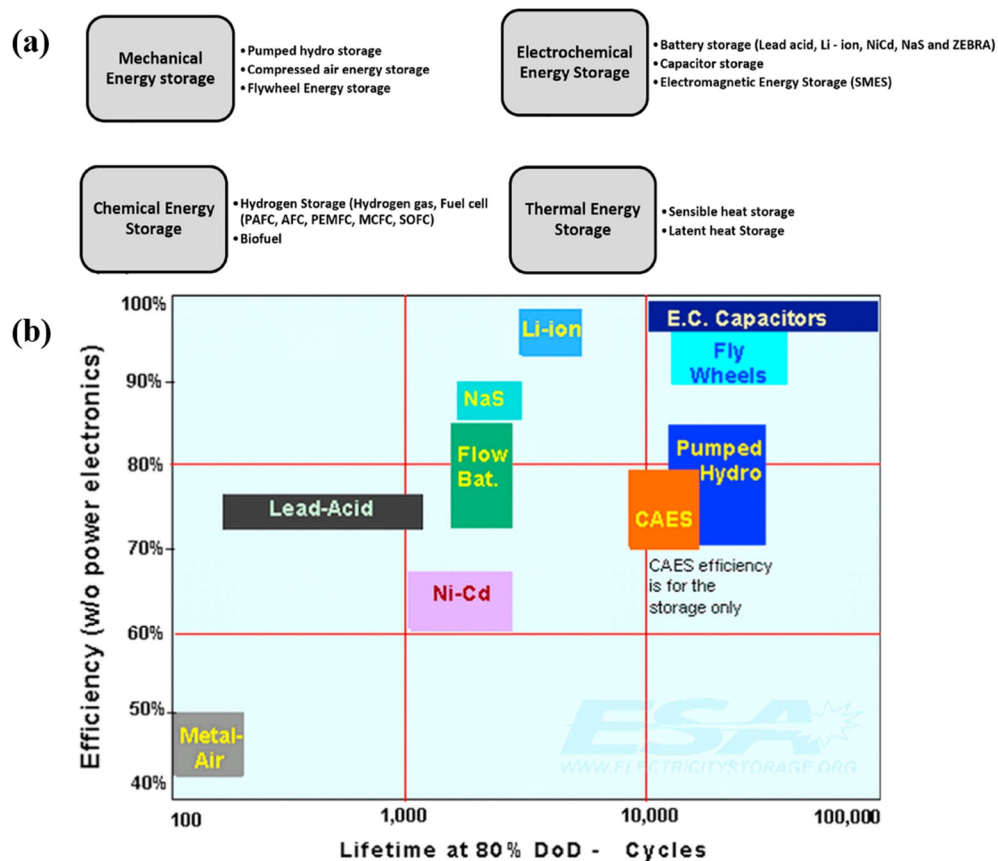
Figure 5.1. (a) types of energy storage and systems (Reproduced from reference 166), (b) efficiency and lifetime of common energy storage systems (Reproduced from reference 167).

voltages. A lot of recent research around new electrolytes and electrode materials has been done to improve efficiency, energy density, life/safety of battery, and to decrease cost. The major types of batteries are lithium-ion, lead acid, and flow batteries.

5.2 Redox Flow Batteries

Redox flow batteries (RFB) are an intriguing sub-class of energy storage systems, that have the potential to overcome drawbacks that are prevalent in other energy storage systems, for example potential phase transformations in lithium ion batteries.[168–171] RFBs are modular in nature so the entire system can be systematically and modularly altered to improve performance without change to the rest of the system. Components that can be changed include electrolyte solutions, separation membranes, and redox active species. RFBs provide the opportunity for successful scale-up of the technology, improved stability, improved efficiency, and potentially low costs.

5.2.1 Components of Redox Flow Batteries

Typical RFBs consist of two electrolyte reservoirs (catholyte and anolyte), pumps, collectors, electrodes, and a separator (Figure 5.2).[168,169] The electrolyte reservoirs contain the redox-active species dissolved in a liquid, which are called the anolyte and catholyte depending on what side of the membrane they are on. The anolyte and catholyte are pumped through the electrochemical cell, which is where the electrochemical reaction takes place and consists of the collectors, electrodes, and separator. The separator is ideally an ion-conductive structure with limited crossover and separates the two electrolyte chambers. Crossover is when ions of either the anolyte or catholyte pass through the separator and reduces efficiency of RFBs. The electrodes are used for charge transfer, typically they are made of a porous carbon material that sandwich the electrolyte chambers and are connected to the current collectors. As the anolyte and catholyte are
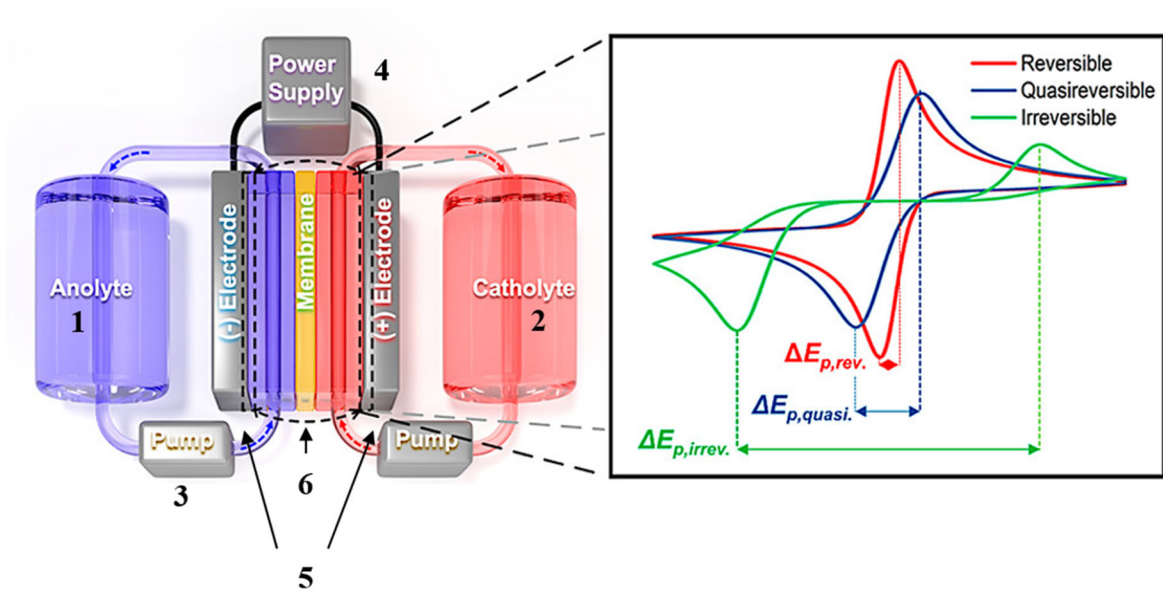
Figure 5.2. Components of a redox flow battery; anolyte reservoir (1), catholyte reservoir (2), pumps (3), connectors (4), electrodes (5), and separator (6). (Reproduced from reference 168)

pumped through the electrochemical cell, oxidation and reduction of the catholyte and anolyte, respectively, takes place and energy is stored as the charge/discharge process repeats.

The main feature of RBFs that allow for large scaling of the systems is the ability to decouple the energy/power from the electrochemical reactions taking place in the anolyte and catholytes. So the energy density and power density are directly determined by the amount of electrolyte in the system and the size of the electrochemical cell, respectively. This can be greatly impact the design of a system, including other parameters such as life of the system, safety features, flexible design, and scalability. Other parameters that are used to evaluate the performance of RFBs are the capacity, Coulombic efficiency, voltage efficiency, and energy efficiency of the of system.

5.2.2 Current Electrolytes for Redox Flow Batteries

The redox-active species are a crucial component in RFBs and directly impacts the cyclabilty, energy density, cell voltage, and cost; both inorganic and organic species have been used in RFBs.

More traditional RFBs use inorganic species, such as vanadium, iron, chromium, zinc, bromine, and lead acid. An example of a traditional RBF is an all vanadium system, which uses four oxidation states for vanadium (V^{2+}, V^{3+}, V^{4+}, and V^{5+}) and uses vanadium dissolved in sulfate-chloride electrolytes.[172] The electrolyte was stable over various temperatures and exhibited improved reaction kinetics compared to previous vanadium RFBs in sulfate systems (sulfuric acid). However, these inorganic systems do have many drawbacks including high costs and slow reaction kinetics.

Alternatively, organic RBFs have been recently explored due to their potential to be cost effective and have a high-energy density (increased solubility of redox active species).[171] Organic RFBs are also attractive for being synthetically tunable; which can allow for a systematic approach to understanding how the chemical structure relates to the properties and performance of the RFB.
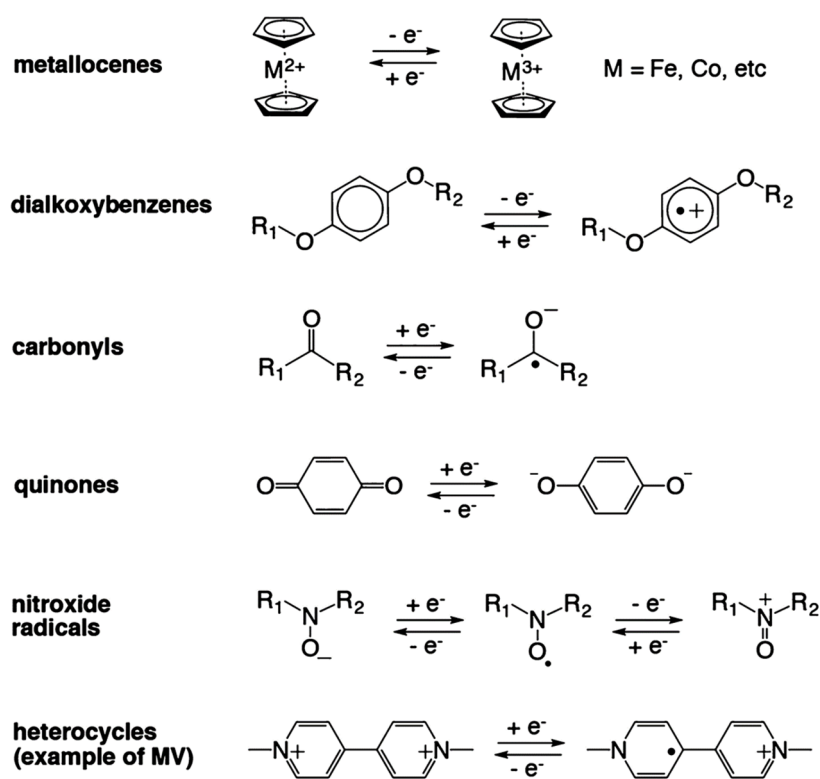
Figure 5.3. Organic small molecule redox active species. (Reproduced from reference 171)

Current organic redox-active species being investigated for use in RFBs include metallocenes, dialkoxybenzenes, quinones, heterocycles, and nitroxide radicals; all of which can be synthetically modified to alter electrochemical properties and solubility (Figure 5.3).[171] These redox active species have a wide range of redox potentials and have been used in nonaqueous and aqueous RFBs.[173] The advantages of using aqueous RFBs includes the use of a nonflammable electrolyte, inexpensive supporting electrolyte materials, and high conductivity/well-developed membranes. Unfortunately, these aqueous electrolytes have a narrow electrochemical window (1.23 V), which limits the redox active species that can be utilized. Nonaqueous RFBs use organic solvents that can increase the electrochemical window up to 4.0V. These nonaqueous systems are also advantageous higher flexibility with choice of solvent and redox active species.   There are some major challenges regarding organic RBFs for example, safety reasons (flammable solvents), lower conductivities, and lack of research on membranes.

5.3   What are deep eutectic solvents?

Recently, deep eutectic solvents (DES) have gained attention for possible use as electrolytes in RFB. A DES is a eutectic mixture that is comprised of a hydrogen bond donor (HBD) and a hydrogen bond acceptor (HBA) to form an intricate H-bond network; the melting point of the mixture is greatly depressed compared to the individual components.[174,175] For example, ethaline is a common DES, with a composition of choline chloride and ethylene glycol (Scheme 5.1). DESs
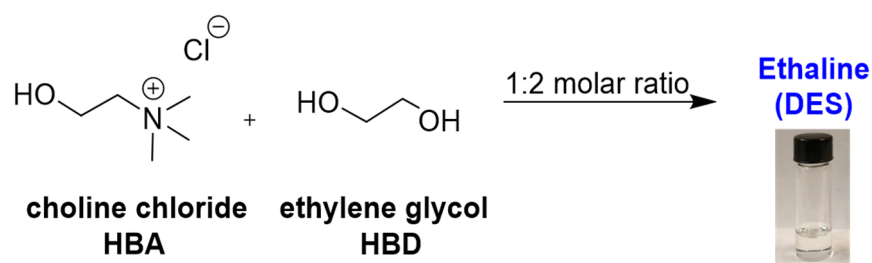
Scheme 5.1. Composition of ethaline, a common DES.

are a relatively new type of liquid that are considered "greener" alternatives to ionic liquids (ILs), namely due to low-cost and the individual components being biodegradable and non-toxic.[174–177] These mixtures are also attractive for their low vapor pressures, easy preparation, and can be easily tailored for various properties.

5.3.1 Components of DES

A DES is typically formulated with two or three components with one HBD and one HBA. HBDs used in DESs are typically small molecules that vary in functional groups that contain H-bonding moieties, including alcohols, amines, carboxylic acids, and sugars (Figure 5.4a).[178–181] HBAs are generally halide salts, for example quaternary ammonium-based salts, such as choline chloride (Figure 5.4b).[182,183] Each component of a specific DES are mixed together in a desired ratio at elevated temperatures to form a homogenous eutectic mixture. DESs can be categorized into two categories, metal-free ("all organic") DES and those that contain a metal salt. Those that contain a metal salt can be further categorized into whether the metal salt is hydrated or not.
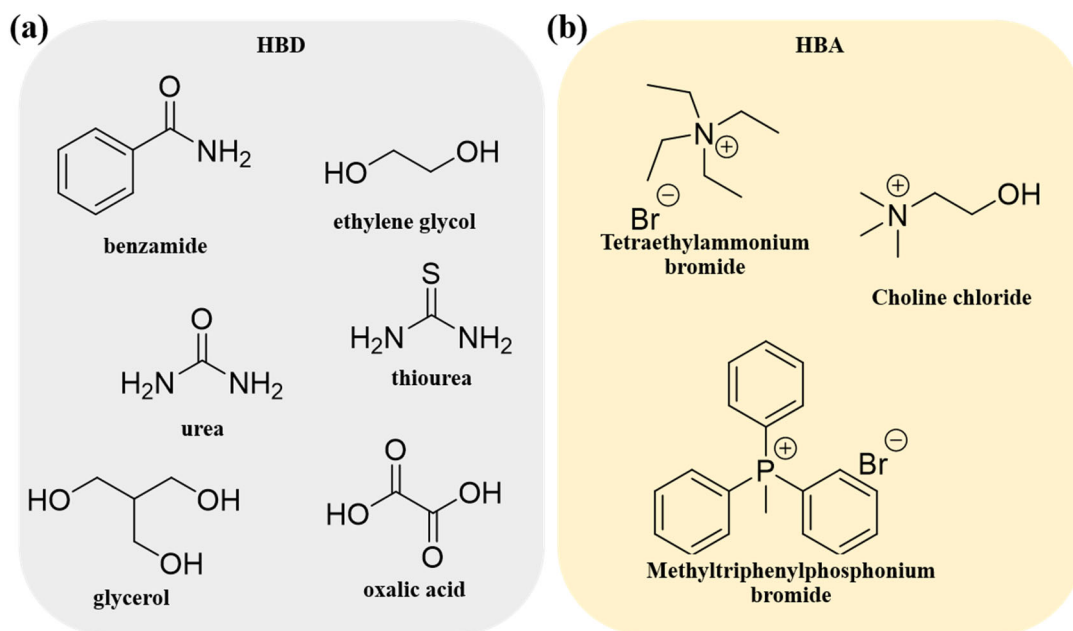
Figure 5.4. Common (a) HBD for DES and (b) HBA for DES.

5.3.2 Properties of DES

A large variety of HBDs and HBAs can be used to form DES, leading the ability to easily tune the physio-chemical and physical properties of a DES, for example the density, viscosity, conductivity, and polarity of the mixture.[174,175,180,184,185] Bahadori and coworkers performed a study to examine the physical properties and electrochemical stability of seven different DESs.[186] Each was formed with either choline chloride or *N,N*-diethylethanol ammonium chloride as the HBA and either malonic acid, oxalic acid, triethanolamine, trifluoracetamide, or Zn(NO₃) hexahydrate as the HBD. The identity of the HBD did not affect the density and ionic conductivity, but both properties were temperature dependent. In contrast, the viscosity measurements were dependent on the identity of the HBD, with the amide HBD exhibiting the lowest viscosity. There have been other examples of viscosity, density, and ionic conductivity of a DES being dependent on the identity of the HBD and HBA, as well as the ratio between the two.[174,175,180] The ability to
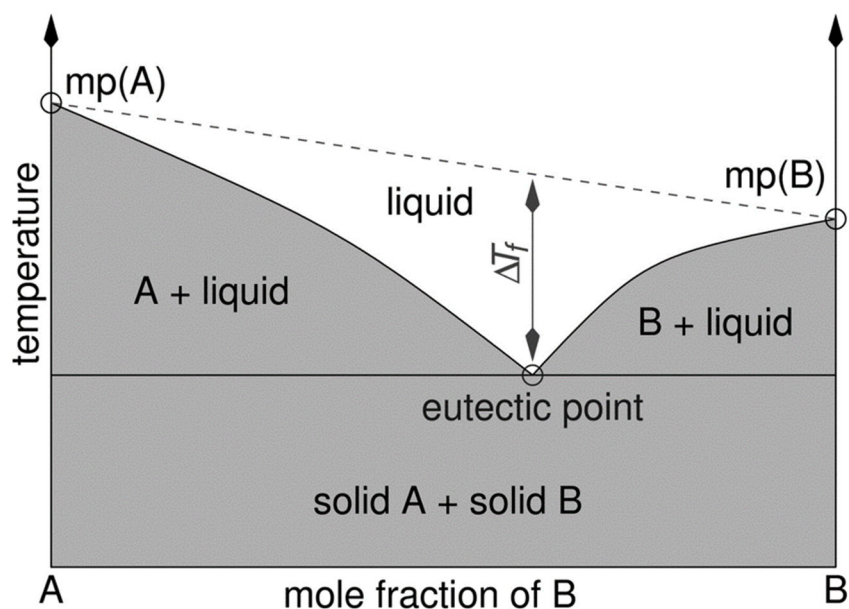
Figure 5.5. Phase diagram for a two-component eutectic mixture. (Reproduced from reference 174).

tailor the properties of a DES to a specific application makes these mixtures very attractive for various applications.

The phase behavior of a DES is dependent on the ratio of HBD to HBA and how they interact with each other.[174] The freezing point of the eutectic mixture is proportional to the interaction between the HBD and HBA, therefore the larger the interaction, the larger the freezing point depression of the mixture. Figure 5.5 shows a typical phase diagram for a DES.[174] The electrochemical behavior of DES electrolytes can also be tailored from the components of the DES and the ratio between the components as well. For example the electrochemical window (voltage window where system is stable) is different for ethaline (1:2 choline chloride:ethylene glycol) and reline (1:2 choline chloride:urea).[187,188] It has also been shown that the electrode material can also influence the electrochemical potentials.[189] There have been many other properties of DESs studied, including surface tension and polarity of the DES.

DES are considered a "greener" option than ionic liquids, both have low vapor pressure but ILs can be toxic.[174] The components of DES are typically non-toxic material, with the exception of some metal-containing DES. Currently the toxicity of DESs are analyzed based on the individual components, with little research has been done on the toxicity of a DES (i.e., mixture).[176] Hayyan *et al*. explored the toxicity and cytotoxicity of choline chloride based DESs, the HBAs used were ethylene glycol, urea, glycerol, and triethylene glycol.[176] For the two cell lines used to examine for the toxicity of each DES, all no affect was observed and the DES determined to be benign to the bacteria. In contrast, the cytotoxicity for each DES was found to be higher than the individual components. Each DES also exhibited different toxicity and cytotoxicity, which was dependent on the chemical structure of each component.

Table 5.1. Applications of DES overview (Reproduced from reference 190).

Application	DES property of most interest	Examples
Catalysis	Solvation strength; recyclability of DES by liquid−liquid extractions; lowered reactivity by H-bond network toward enzymes in biocatalysis	Acid-catalyzed dehydration of hexoses to 5 hydroxymethylfurfural; catalytic conversion of lignocellulosic biomass
Drug solubilization	Solvation strength; low toxicity	Dissolution of several poorly soluble drugs (i.e., benzoic acid); solvents for nucleic acids (DNA, RNA reversible secondary structures)
Material synthesis	Low/negligible vapor pressures; thermal decomposition pathway; liquid heterogeneity	Ionothermal synthesis of aluminophosphate and organophosphonate materials
Extractions	Low/negligible vapor pressures; solvation strength	Starch extraction from plants; various micro extraction techniques possible
Gas separations	Density and free volume for gas solubility	CO_2 and SO_2 capture from flue gas
Electrochemical energy storage	Electrochemical stability; conductivity and viscosity; solvate structure and coordination strength; solubility of redox-active species; suppressed flammability	All-iron redox flow battery in ChCl + EG, hybrid-ion flow batteries; ferrocene in metal-free DES and redox-active DES based on viologens in EG or malonic acid
Other electrochemical processes	Solvation strength; electrode−electrolyte interface	Electrodeposition of conductive polymers for sensing; electrochromic devices

5.3.3. Current Applications of DES

Regardless of DESs being relatively new, there have been numerous applications of DESs, ranging from solvents for catalysis to gas separations to electrochemical processes (Table 5.1).[190] One of the first applications of DESs was a solvent for metal electrodeposition, which is the process of depositing metal ions onto a surface to generate a coating via reduction of a metal.[191] DESs can overcome some of the drawbacks of other aqueous and organic electrolytes, for example, high solubility of metal oxides in DESs can lead to less material needed (lower costs) and reduced passivation. Metals, including chromium, aluminum, copper, zinc, and nickel, have been studied in DESs for metal electrodeposition. DESs have been useful in metal electropolishing, which also has advantages compared to aqueous electrolytes.

DESs have been used in synthetic applications, where the DES is used as an alternative solvent to typical volatile organic solvents or ionic liquids. One of the first examples was the use of a choline

chloride/zinc chloride DES being used as the solvent for a Diels-Alder cycloaddition.[192] Other reactions that utilized DESs included *N*-alkylation of amines, polymerizations, and ionothermal syntheses. DESs have also been found to have significant use in catalysis reactions both as a solvent and a catalyst. For example, Singh *et al*. prepared reline (1:2 choline chloride:urea) to use as a solvent and a catalyst in an *N*-alkylation reaction of aniline with an alkyl bromide.[193] This reaction was compared to a lipase catalyst in a traditional organic solvent. Overall the yields and reaction times were comparable, however the DES had a higher recyclability than the lipase catalyst. Further, the DES acted as both the solvent and catalyst, making the reaction more cost-effective. Overall, the applications of DESs stretch a large variety of fields, significantly more than stated above; such as battery technology, power systems, biomass processing, genomics of nucleic acids, nanomaterials, etc.

5.4   DESs Potential as Electrolytes

One of the most intriguing applications for DESs are their potential to act as electrolytes due to their low flammability, good conductivity, and tailorable electrochemical windows.[194] As previously mentioned, RFBs are an energy storage system that can be built on large-scales. To make a viable electrolyte for RFBs they must be easy to produce on a large scale, cost effective, and safe/environmentally friendly, and thus DESs fit into these criteria as potential electrolytes for RFBs. Indeed, some studies have addressed using DESs as an electrolyte, for example, Lloyd *et al*. examined an anhydrous $CuCl_2$ in ethaline as an electrolyte for RFBs; high solubility was obtained however poor mass transport led to poor performance RBFs.[195] Their work allowed for proof of concept that DES can be used as an electrolyte for RFBs.   In a similar vein, Cong et al. used a used an all organic approach and developed an electrolyte where a redox active species a component in the eutectic.[194] The DESs were based on phthalimide, urea, and LiTFSI, where

phthalimide was the redox active species. The concept of the eutectic mixture consisting of the redox active species provides potential to achieve higher energy densities.

5.5   Redox Active Small Molecules

As previously mentioned, all organic systems show great potential and benefits in redox flow batteries, as well as potential redox active species in DESs. There are many examples of organic redox active species, including TEMPO, pthalimide, quinones, and viologens.[196] Overall, a worthy goal is to identify redox active small molecules that would be great candidates to incorporate into DESs, which could then be used as electrolytes in RFBs.

5.5.1   TEMPO derivatives

TEMPO ((2,2,6,6-tetramethylpiperidin-1-yl)oxyl) is a stable organic nitroxide radical that has been used in various chemical and biochemical applications, namely utilized as catalysts in various reactions. The high stability of the persistent radical is attributed to the unpaired electron being delocalized through the N-O bond and the steric shielding provided by the methyl groups in the 2 and 6 positions.[197,198] Many TEMPO derivatives have been synthesized (adding to the 4 position, distal to the nitroxide radical) to tune TEMPO for various applications, typically using 4-hydroxy TEMPO (4HT) as the building block (Figure 5.6). The hydroxyl group is a synthetic handle that
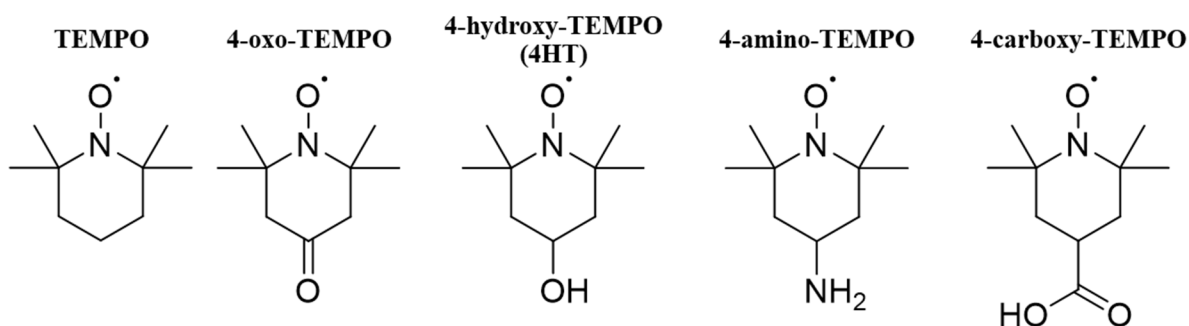
Figure 5.6. Structure of TEMPO and common TEMPO derivatives.

allows multiple synthetic routes to be used to incorporate various functional groups and to increase solubility.

5.5.2 Electrochemistry of TEMPO Derivatives

TEMPO is also regularly used in electrochemistry as a redox active unit. TEMPO exhibits a well-defined single-electron transfer and has the potential to exhibit a second electron transfer due to the oxygen atom being able to be reduced and oxidized (Scheme 5.2). Nishide *et al.* performed cyclic voltammetry of TEMPO in acetonitrile and observed a single reversible electron transfer at a half-wave potential of +0.63 V vs. Ag/AgCl.[197] The anodic peak corresponded to the oxidation of the nitroxide radical to the oxoammonium cation and the cathodic peak corresponded to the reduction of the oxoammonium cation back to the neutral radical. The redox behavior of TEMPO as well as TEMPO derivatives has also been studied in aqueous[199–201] and non-aqueous[202–204] media. 4HT is a commonly used TEMPO derivative in electrolytes, because the hydroxyl group has been shown to increase the solubility compared to TEMPO.

TEMPO derivatives can also be tuned to alter the redox potential of the redox reaction. For example, Chang *et al.* compared 4HT to a TEMPO derivative modified with a 1-methyl-imidazolium chloride salt, where the derivatives were studied in an aqueous NaCl electrolyte.[200] The half-cell potential for 4HT was +0.56 V vs. Ag quasi-reference electrode, where the half-cell potential for the imidazolium functionalized TEMPO was +0.71 V vs. Ag quasi-reference
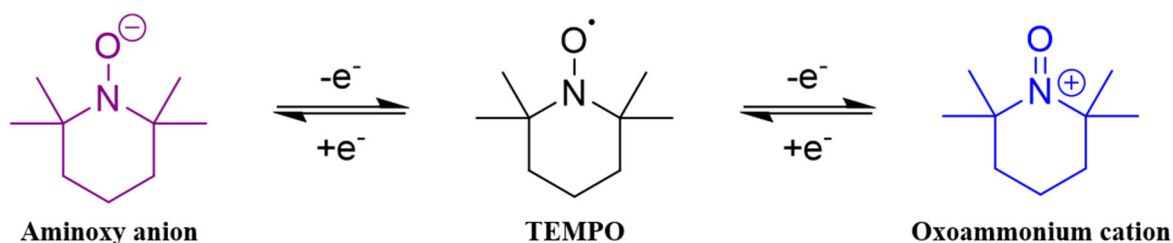
Scheme 5.2. Two potential electron transfers with TEMPO derivatives.

electrode. This shift demonstrated that chemical modification can shift the redox potential, which may be attributed to the electron-withdrawing character of the imidazolium functionality. Janoschka *et al.* performed a similar study comparing different 4HT and a trimethyl ammonium chloride TEMPO derivative and observed a similar effect, where 4HT had a more positive redox couple.[205]

5.5.3 Phenothiazine Derivatives

Another common redox active molecule that has potential in RFBs is phenothiazine (2,3,5,6-dibenzo-l,4-thiazine or PHZ); this is a heterocyclic thiazine that has been prevalent since before 1900, and it has been used in many applications, including dyes, pharmaceuticals, and insecticides (Figure 5.7a).[206,207] The most notable application of PHZ derivatives are in psychopharmacology as treatments for various diseases including Parkinson's and Alzheimer's diseases. Similar to TEMPO, PHZ can be easily synthetically modified to tune the redox behavior and solubility of the derivative (Figure 5.7b).[208,209] It has been shown that when substituents are added to the nitrogen the solubility increases and when substituents are added to the 3 and 7 position the molecule is more electrochemically stable.
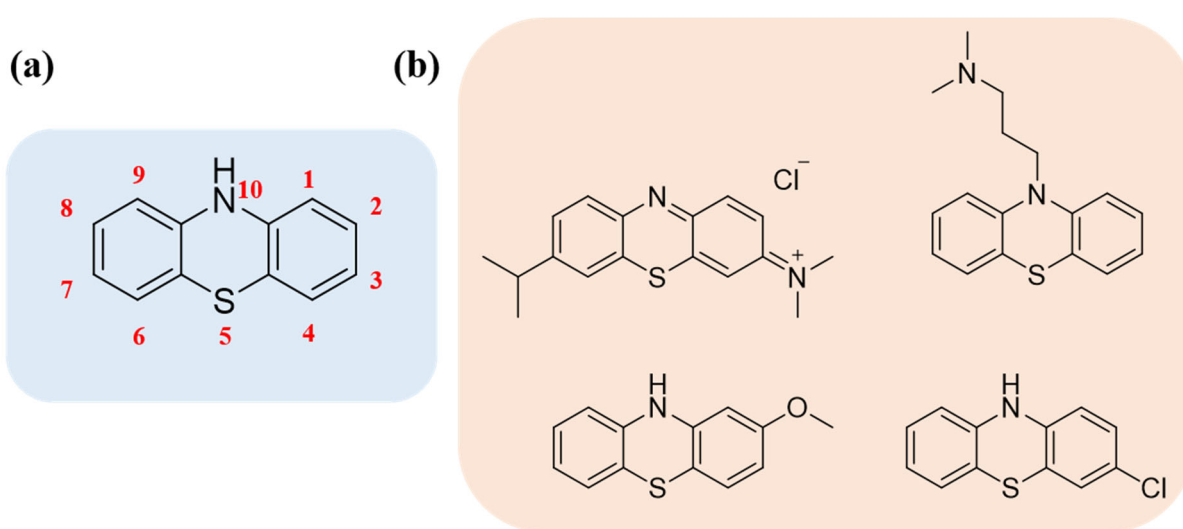
Figure 5.7. (a) Structure of phenothiazine and (b) phenothiazine derivatives.

5.5.4 Electrochemistry of Phenothiazine Derivatives

PHZ exhibits a single reversible electron transfer in most electrolytes, including aprotic and acidic electrolytes. The oxidation of PHZ produces a radical cation, which is reversible and reduction of the radical cation produces the neutral PHZ species (Scheme 5.3). A second electron transfer is possible is some aprotic solvents, however the CV needs to have a larger sweep width to observe this.[206,207] This second electron transfer starts from the radical cation to produce a dication, where a positive charge is present on both the sulfur and nitrogen atoms. The formation of the dication is also reversible, and the molecule can return to the radical cation; however, the dication can irreversibly react with water. Some factors explored to stabilize the cationic radicals include the identity/position of substituents, acidity of electrolyte, and presence of various salts.

There are many potential ways to modify phenothiazine to impact the solubility and redox behavior of the unit. Buhrmester *et al*., for example, examined five PHZ derivatives and their potential as redox small molecules.[210] The derivatives had varied the substituents at the 10 and 3 positions on
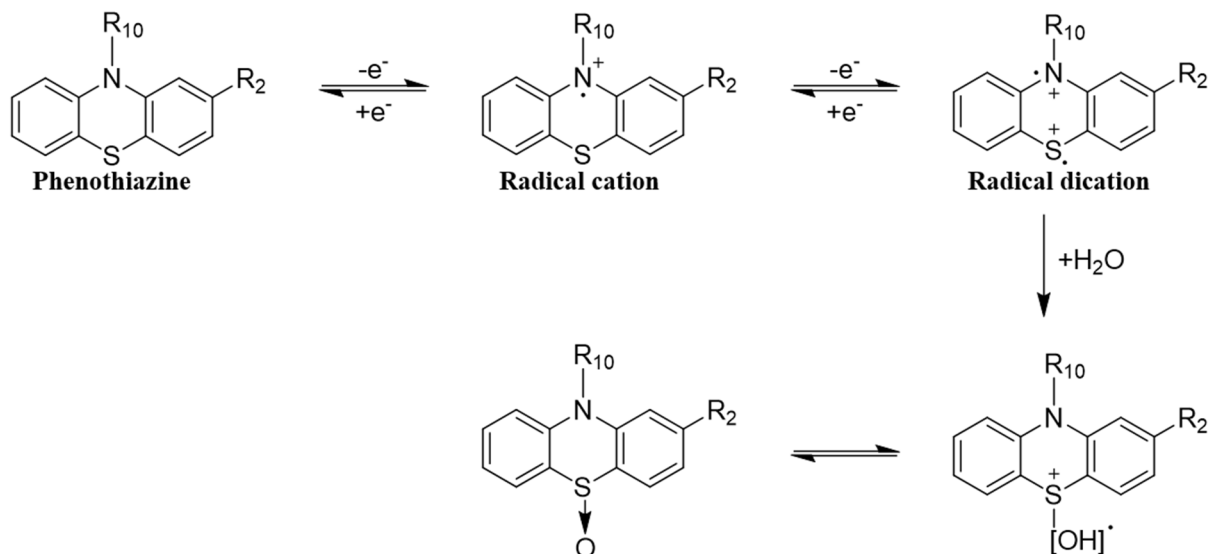
Scheme 5.3. Two potential electron transfers with phenothiazine derivatives and a potential degradation pathway.

the parent compound. They found that 10-methyl-PHZ had a low redox potential, however if the methyl group is changed to an electron-withdrawing group (chlorine atom) a higher redox potential could be obtained. Kowalski *et al*. demonstrated that if a larger sweep width is applied to 10-ethyl-PHZ in 1M LiTFSI in propylene carbonate, a second redox reaction is observed.[208] They further demonstrated that if substituents are added to the 3 and 7 positions, the stability of the dication is increased.

5.6   Summary

Overall, the future of energy storage will rely on technological developments across many systems. New methods that are sustainable and efficient need to be developed for the growing energy needs. Organic RFBs have great potential to accomplish these goals. Traditional RFBs involve inorganic redox active species that are expensive and can exhibit slow kinetics, such as an all vanadium battery. New electrolytes need to be identified that have the potential to incorporate organic species in high solubility. DESs are a new class of liquid that is considered "greener" than ionic liquids with great potential to be electrolytes.

The overarching goal of this project is to synthetically modify organic redox active species so they can be incorporated into DESs, with the ultimate application as electrolyte in a RFB, ideally acting as both the anolyte and catholyte. Whereas many organic redox active species have been studied in other electrolytes, few have been studied in DES. TEMPO and phenothiazine are chosen as the model redox active units because of their synthetic feasibility and well defined performance in non-DES electrolytes and will be discussed in the following chapters. The chemical modification of TEMPO is shown to influence both the solubility and the redox potential of the derivative, making these great compounds to study as potential additives in DESs. A library of TEMPO derivatives was synthesized and were then incorporated into ethaline. The physical properties of

the solutions were evaluated, as well as the electrochemical behavior. Similarly, the chemical modification of PHZ derivatives have been shown to influence the solubility and the redox behavior of the derivative. A library of PHZ derivatives was also synthesized and the electrochemical behavior of the derivatives were evaluated in ethaline.

5.7   References

(166) Olabi, A. G.; Onumaegbu, C.; Wilberforce, T.; Ramadan, M.; Abdelkareem, M. A.; Al – Alami, A. H. Critical Review of Energy Storage Systems. Energy 2021, 214, 118987. https://doi.org/10.1016/j.energy.2020.118987.

(167) Guney, M. S.; Tepe, Y. Classification and Assessment of Energy Storage Systems. Renew. Sustain. Energy Rev. 2017, 75 (October 2016), 1187–1197. https://doi.org/10.1016/j.rser.2016.11.102.

(168) MacHado, C. A.; Brown, G. O.; Yang, R.; Hopkins, T. E.; Pribyl, J. G.; Epps, T. H. Redox Flow Battery Membranes: Improving Battery Performance by Leveraging Structure-Property Relationships. ACS Energy Lett. 2021, 6 (1), 158–176. https://doi.org/10.1021/acsenergylett.0c02205.

(169) Wang, H.; Sayed, S. Y.; Luber, E. J.; Olsen, B. C.; Shirurkar, S. M.; Venkatakrishnan, S.; Tefashe, U. M.; Farquhar, A. K.; Smotkin, E. S.; McCreery, R. L.; Buriak, J. M. Redox Flow Batteries: How to Determine Electrochemical Kinetic Parameters. ACS Nano 2020, 14 (3), 2575–2584. https://doi.org/10.1021/acsnano.0c01281.

(170) Zhang, C.; Zhang, L.; Ding, Y.; Guo, X.; Yu, G. Eutectic Electrolytes for High-Energy-Density Redox Flow Batteries. ACS Energy Lett. 2018, 3 (12), 2875–2883. https://doi.org/10.1021/acsenergylett.8b01899.

(171)   Wei, X.; Pan, W.; Duan, W.; Hollas, A.; Yang, Z.; Li, B.; Nie, Z.; Liu, J.; Reed, D.; Wang, W.; Sprenkle, V. Materials and Systems for Organic Redox Flow Batteries: Status and Challenges. ACS Energy Lett. 2017, 2 (9), 2187–2204. https://doi.org/10.1021/acsenergylett.7b00650.

(172)   Li, L.; Kim, S.; Wang, W.; Vijayakumar, M.; Nie, Z.; Chen, B.; Zhang, J.; Xia, G.; Hu, J.; Graff, G.; Liu, J.; Yang, Z. A Stable Vanadium Redox-Flow Battery with High Energy Density for Large-Scale Energy Storage. Adv. Energy Mater. 2011, 1 (3), 394–400. https://doi.org/10.1002/aenm.201100008.

(173)   Luo, J.; Hu, B.; Hu, M.; Zhao, Y.; Liu, L. Status and Prospects of Organic Redox Flow Batteries toward Sustainable Energy Storage. ACS Energy Lett. 2019, 4, 2220–2240. https://doi.org/10.1021/acsenergylett.9b01332.

(174)   Smith, E. L.; Abbott, A. P.; Ryder, K. S. Deep Eutectic Solvents (DESs) and Their Applications. Chem. Rev. 2014, 114 (21), 11060–11082. https://doi.org/10.1021/cr300162p.

(175)   Zhang, Q.; Vigier, K. D. O.; Royer, S.; Jerome, F. Deep Eutectic Solvents: Syntheses, Properties and Applications. Chem. Soc. Rev. 2012, 41, 7108–7146. https://doi.org/10.1039/c2cs35178a.

(176)   Hayyan, M.; Ali, M.; Hayyan, A.; Al-saadi, M. A.; Alnashef, I. M.; Mirghani, M. E. S.; Kola, O. Are Deep Eutectic Solvents Benign or Toxic ? Chemosphere 2013, 90 (7), 2193–2195. https://doi.org/10.1016/j.chemosphere.2012.11.004.

(177)   Haerens, K.; Matthijs, E.; Chmielarz, A.; Bruggen, B. Van Der. The Use of Ionic Liquids Based on Choline Chloride for Metal Deposition : A Green Alternative ? J. Environ. Manage. 2009, 90 (11), 3245–3252. https://doi.org/10.1016/j.jenvman.2009.04.013.

(178)   Constantin, V.; Adya, A. K.; Popescu, A. M. Density, Transport Properties and Electrochemical Potential Windows for the 2-Hydroxy-N,N,N-Trimethylethanaminium Chlorides

Based Ionic Liquids at Several Temperatures. Fluid Phase Equilib. 2015, 395, 58–66. https://doi.org/10.1016/j.fluid.2015.03.025.

(179)   Yadav, A.; Kar, J. R.; Verma, M.; Naqvi, S.; Pandey, S. Densities of Aqueous Mixtures of (Choline Chloride + Ethylene Glycol) and (Choline Chloride + Malonic Acid) Deep Eutectic Solvents in Temperature Range 283.15–363.15 K. Thermochim. Acta 2015, 600, 95–101. https://doi.org/10.1016/j.tca.2014.11.028.

(180)   Abbott, A. P.; Capper, G.; Davies, D. L.; Rasheed, R. K.; Tambyrajah, V. Novel Solvent Properties of Choline Chloride / Urea Mixtures. Chem. Commun. 2003, 70–71.

(181)   Sas, O. G.; Fidalgo, R.; Domínguez, I.; Macedo, E. A.; González, B. Physical Properties of the Pure Deep Eutectic Solvent, [ChCl]:[Lev] (1:2) DES, and Its Binary Mixtures with Alcohols. J. Chem. Eng. Data 2016, 61 (12), 4191–4202. https://doi.org/10.1021/acs.jced.6b00563.

(182)   Khalid, M.; Hayyan, M.; Abdulhakim, M.; Akib, S. Glycerol-Based Deep Eutectic Solvents: Physical Properties. J. Mol. Liq. 2016, 215, 98–103. https://doi.org/10.1016/j.molliq.2015.11.032.

(183)   Ibrahim, R. K.; Hayyan, M.; Alsaadi, M. A.; Ibrahim, S.; Hayyan, A.; Hashim, M. A. Diethylene Glycol Based Deep Eutectic Solvents and Their Physical Properties. Stud. Univ. Babes-Bolyai Chem. 2017, 62 (4), 433–450. https://doi.org/10.24193/subbchem.2017.4.37.

(184)   Abbott, A. P.; Boothby, D.; Capper, G.; Davies, D. L.; Rasheed, R. K. Deep Eutectic Solvents Formed between Choline Chloride and Carboxylic Acids : Versatile Alternatives to Ionic Liquids. J. Am. Chem. Soc. 2004, 126 (9), 9142–9147. https://doi.org/10.1021/ja048266j.

(185)   Kareem, M. A.; Mjalli, F. S.; Hashim, M. A.; Alnashef, I. M. Phosphonium-Based Ionic Liquids Analogues and Their Physical Properties. J. Chem. Eng. Data 2010, 55, 4632–4637.

(186)   Bahadori, L.; Chakrabarti, M. H.; Mjalli, F. S.; Alnashef, I. M.; Manan, N. S. A.; Hashim, M. A. Physicochemical Properties of Ammonium-Based Deep Eutectic Solvents and Their Electrochemical Evaluation Using Organometallic Reference Redox Systems. Electrochim. Acta 2013, 113, 205–211. https://doi.org/10.1016/j.electacta.2013.09.102.

(187)   Brett, C. M. A. Deep Eutectic Solvents and Applications in Electrochemical Sensing. Curr. Opin. Electrochem. 2018, 10, 143–148. https://doi.org/10.1016/j.coelec.2018.05.016.

(188)   Chakrabarti, M.; Mjalli, F.; AlNashef, I.; Hashim, M. A.; Hussain, M. A.; Bahadori, L.; Low, C. Prospects of Applying Ionic Liquids and Deep Eutectic Solvents for Renewable Energy Storage by Means of Redox Flow Batteries. Renew. Sustain. Energy Rev. 2014, 30, 254–270. https://doi.org/10.1016/j.rser.2013.10.004.

(189)   Shen, X.; Sinclair, N.; Wainright, J.; Akolkar, R.; Savinell, R. F. Evaluating and Developing a Reliable Reference Electrode for Choline Chloride Based Deep Eutectic Solvents. J. Electrochem. Soc. 2020, 167 (8), 086509. https://doi.org/10.1149/1945-7111/ab913c.

(190)   Gurkan, B.; Squire, H.; Pentzer, E. Metal-Free Deep Eutectic Solvents: Preparation, Physical Properties, and Significance. J. Phys. Chem. Lett. 2019, 10 (24), 7956–7964. https://doi.org/10.1021/acs.jpclett.9b01980.

(191)   Hansen, B. B.; Spittle, S.; Chen, B.; Poe, D.; Zhang, Y.; Klein, J. M.; Horton, A.; Adhikari, L.; Zelovich, T.; Doherty, B. W.; Gurkan, B.; Maginn, E. J.; Ragauskas, A.; Dadmun, M.; Zawodzinski, T. A.; Baker, G. A.; Tuckerman, M. E.; Savinell, R. F.; Sangoro, J. R. Deep Eutectic Solvents: A Review of Fundamentals and Applications. Chem. Rev. 2021, 121 (3), 1232–1285. https://doi.org/10.1021/acs.chemrev.0c00385.

(192)   Abbott, A. P.; Capper, G.; Davies, D. L.; Rasheed, R. K.; Tambyrajah, V. Quaternary Ammonium Zinc- or Tin-Containing Ionic Liquids: Water Insensitive, Recyclable Catalysts for Diels-Alder Reactions. Green Chem. 2002, 4 (1), 24–26. https://doi.org/10.1039/b108431c.

(193)   Singh, B.; Lobo, H.; Shankarling, G. Selective N-Alkylation of Aromatic Primary Amines Catalyzed by Bio-Catalyst or Deep Eutectic Solvent. Catal. Letters 2011, 141 (1), 178–182. https://doi.org/10.1007/s10562-010-0479-9.

(194)   Cong, G.; Lu, Y. C. Organic Eutectic Electrolytes for Future Flow Batteries. Chem 2018, 4 (12), 2732–2734. https://doi.org/10.1016/j.chempr.2018.11.018.

(195)   Lloyd, D.; Vainikka, T.; Kontturi, K. The Development of an All Copper Hybrid Redox Flow Battery Using Deep Eutectic Solvents. Electrochim. Acta 2013, 100, 18–23. https://doi.org/10.1016/j.electacta.2013.03.130.

(196)   Li, M.; Rhodes, Z.; Cabrera-Pardo, J. R.; Minteer, S. D. Recent Advancements in Rational Design of Non-Aqueous Organic Redox Flow Batteries. Sustain. Energy Fuels 2020, 4 (9), 4370–4389. https://doi.org/10.1039/d0se00800a.

(197)   Nishide, H.; Iwasa, S.; Pu, Y. J.; Suga, T.; Nakahara, K.; Satoh, M. Organic Radical Battery: Nitroxide Polymers as a Cathode-Active Material. Electrochim. Acta 2004, 50 (2-3 SPEC. ISS.), 827–831. https://doi.org/10.1016/j.electacta.2004.02.052.

(198)   Winsberg, J.; Hagemann, T.; Janoschka, T.; Hager, M. D.; Schubert, U. S. Redox-Flow Batteries : From Metals to Organic Redox- Active Materials. Angew. Chemie - Int. Ed. 2017, 56, 686–711. https://doi.org/10.1002/anie.201604925.

(199)   Liu, T.; Wei, X.; Nie, Z.; Sprenkle, V.; Wang, W. A Total Organic Aqueous Redox Flow Battery Employing a Low Cost and Sustainable Methyl Viologen Anolyte and 4-HO-TEMPO Catholyte. Adv. Energy Mater. 2016, 6. https://doi.org/10.1002/aenm.201501449.

(200)   Chang, Z.; Henkensmeier, D.; Chen, R. Shifting Redox Potential of Nitroxyl Radical by Introducing an Imidazolium Substituent and Its Use in Aqueous Fl Ow Batteries. J. Power Sources 2019, 418 (February), 11–16. https://doi.org/10.1016/j.jpowsour.2019.02.028.

(201)   Winsberg, J.; Stolze, C.; Schwenke, A.; Muench, S.; Hager, M. D.; Schubert, U. S. Aqueous 2,2,6,6-Tetramethylpiperidine-N-Oxyl Catholytes for a High-Capacity and High Current Density Oxygen-Insensitive Hybrid-Flow Battery. ACS Energy Lett. 2017, 2 (2), 411–416. https://doi.org/10.1021/acsenergylett.6b00655.

(202)   Takechi, K.; Kato, Y.; Hase, Y. A Highly Concentrated Catholyte Based on a Solvate Ionic Liquid for Rechargeable Flow Batteries. Adv. Mater. 2015, 27 (15), 2501–2506. https://doi.org/10.1002/adma.201405840.

(203)   Li, Z.; Li, S.; Liu, S.; Huang, K.; Fang, D.; Wang, F.; Peng, S. Electrochemical Properties of an All-Organic Redox Flow Battery Using 2,2,6,6-Tetramethyl-1-Piperidinyloxy and N-Methylphthalimide. Electrochem. Solid-State Lett. 2011, 14 (12), A171. https://doi.org/10.1149/2.012112esl.

(204)   Park, S.; Shim, J.; Yang, J.; Shin, K.; Jin, C.; Suk, B.; Lee, Y.; Jeon, J. Electrochemistry Communications Electrochemical Properties of a Non-Aqueous Redox Battery with All-Organic Redox Couples. Electrochem. commun. 2015, 59, 68–71. https://doi.org/10.1016/j.elecom.2015.07.013.

(205)   Janoschka, T.; Martin, N.; Hager, M. D.; Schubert, U. S. An Aqueous Redox-Flow Battery with High Capacity and Power : The TEMPTMA / MV System. Angew. Chemie - Int. Ed. 2016, 55, 14427–14430. https://doi.org/10.1002/anie.201606472.

(206) Paduszek, B.; Kalinowski, M. K. Redox Behaviour of Phenothiazine and Phenazine in Organic Solvents. Electrochim. Acta 1983, 28 (5), 639–642. https://doi.org/10.1016/0013-4686(83)85057-9.

(207) Puzanowska-Tarasiewicz, H.; Kuźmicka, L.; Karpińska, J.; Mielech-Łukasiewicz, K. Efficient Oxidizing Agents for Determination of 2,10-Disubstituted Phenothiazines. Anal. Sci. 2005, 21 (10), 1149–1153. https://doi.org/10.2116/analsci.21.1149.

(208) Kowalski, J. A.; Casselman, M. D.; Kaur, A. P.; Milshtein, J. D.; Elliott, C. F.; Modekrutti, S.; Attanayake, N. H.; Zhang, N.; Parkin, S. R.; Risko, C.; Brushett, F. R.; Odom, S. A. A Stable Two-Electron-Donating Phenothiazine for Application in Nonaqueous Redox Flow Batteries. J. Mater. Chem. A 2017, 5 (46), 24371–24379. https://doi.org/10.1039/c7ta05883g.

(209) Attanayake, N. H.; Kowalski, J. A.; Greco, K. V.; Casselman, M. D.; Milshtein, J. D.; Chapman, S. J.; Parkin, S. R.; Brushett, F. R.; Odom, S. A. Tailoring Two-Electron-Donating Phenothiazines to Enable High-Concentration Redox Electrolytes for Use in Nonaqueous Redox Flow Batteries. Chem. Mater. 2019, 31 (12), 4353–4363. https://doi.org/10.1021/acs.chemmater.8b04770.

(210) Buhrmester, C.; Moshurchak, L.; Wang, R. L.; Dahn, J. R. Phenothiazine Molecules. J. Electrochem. Soc. 2006, 153 (2), A288. https://doi.org/10.1149/1.2140615.

Part II: The Incorporation of Redox Small Molecules into Deep Eutectic Solvents for the Development of New Electrolytes

Chapter 6

Feasibility of TEMPO-Functionalized Imidazolium, Ammonium and Pyridinium Salts as Redox Active Carriers in Ethaline Deep Eutectic Solvent for Energy Storage

Portions of this chapter appear in the following manuscript:

Contributions:
Sarah Mitchell – Synthesis, characterization, and solubility studies
Brian Chen – Physical property measurements and initial CVs
Nicholas Sinclair – Flow cell experiments

6.1   Introduction

DESs are a eutectic mixture comprised of a HBD and HBA in which the melting point is depressed compared to the individual components. A commonly reported DES is ethaline, a 1:2 molar ratio of choline chloride (ChCl) and ethylene glycol (EG). Of DES, ethaline has a relatively low viscosity (36 cP at 25°C), and is thus more attractive for processes involving flow of the liquid.[211] For this reason, ethaline was chosen for initial studies to evaluate DES as electrolytes for redox flow batteries (RFB). Organic RFBs utilize redox-active organic small molecules as the redox active species, which can ideally be easily tuned via synthesis and scaled.[173] Incorporating, redox active small molecules into a DES would be a new approach to developing active electrolyte/redox couple for RFBs, laying the foundation for further tuning combinations of redox active small molecules and DES.

A common redox active organic small molecule is (2,2,6,6-tetramethylpiperidin-1-yl)oxyl (TEMPO), a stable organic radical that has a well-defined single-electron transfer (Scheme 6.1).[197,198] Nishide *et al*. performed the cyclic voltammetry (CV) of TEMPO in acetonitrile and observed a reversible single-electron redox reaction at a half-wave potential ($E_{1/2}$) of +0.63 V vs. Ag/AgCl.[197] This peak corresponded to the oxidation of the nitroxide radical to oxoammonium cation and the reverse. TEMPO is also attractive due to the variety of commercially available derivatives available and synthetic tunability. Multiple studies have also shown through CV that derivatives of TEMPO exhibit different redox behavior (shifting the oxidation and reduction
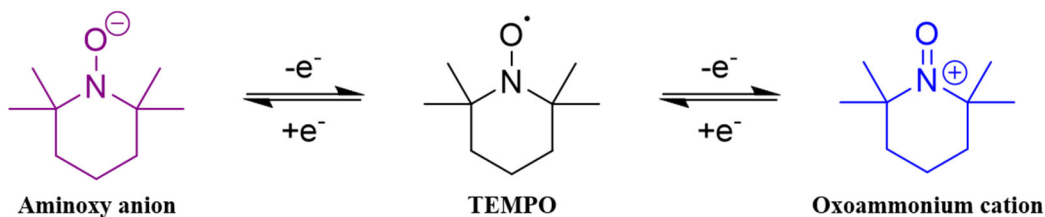
Scheme 6.1. Two electron transfer of TEMPO.

peaks), and that adding various functional groups leads to changes in solubility.[200,205] For example, 4-Hydroxy-TEMPO (4HT) is a commercially available TEMPO derivative that has been reported to have appreciable solubility in aqueous electrolytes.[199] Comparison of the electrochemical behavior of 4HT to other TEMPO derivatives reveals the oxidation and reduction peaks shift. Therefore, modification of the chemical composition of TEMPO can influence the solubility and redox potential of an electrolyte.

6.2 Approach

TEMPO derivatives were synthesized using a modular approach, to easily access a family of different compounds from a single intermediate that could be produced in large quantities. Derivatives synthesized focused on cationic structure and anion identity. To form redox active electrolytes using DES, the TEMPO derivatives were incorporated into ethaline (1:2 ChCl:EG) at various concentrations. (Figure 6.1) Maximum solubility was examined for each derivative in
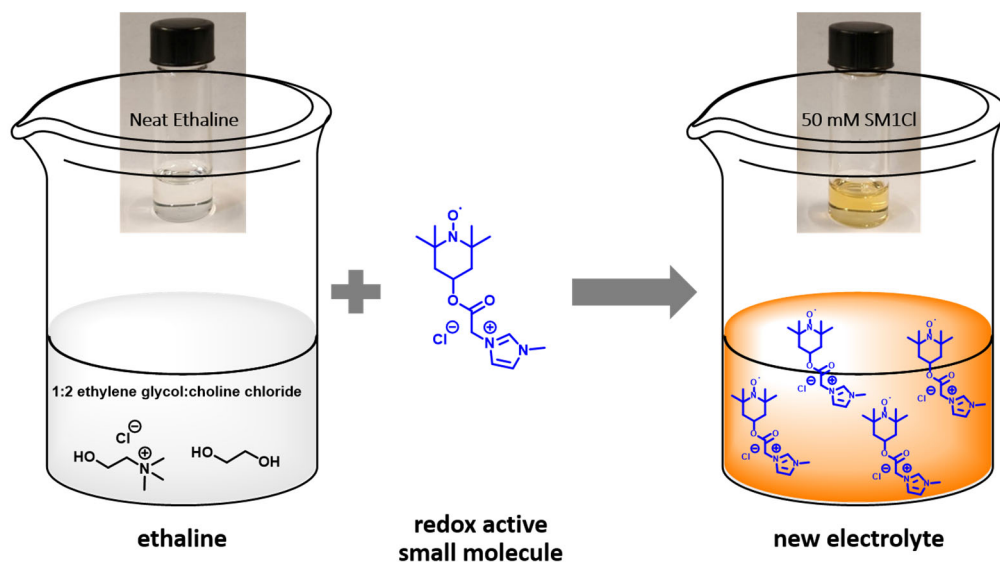
Figure 6.1 Approach for developing of DESs (specifically ethaline) as electrolytes by incorporating redox active small molecules based on TEMPO salts.

ethaline using UV-vis spectroscopy. Of the derivatives synthesized, three were chosen to examine the impact on the physical properties and electrochemical behavior in the solutions. Specifically, the imidazolium, ammonium, and pyridinium chloride salts (compounds **1**, **2**, and **3**, respectively) were compared with TEMPO and 4HT. This approach gives insight to the feasibility of incorporating redox active organic small molecules into DESs for electrolytes and highlights the need for improved electrochemical stability of redox active small molecules in DES.

6.3   Synthesis of TEMPO Salt Derivatives

The TEMPO salt derivatives were derived from commercially available 4HT, which contains a hydroxyl group in the 4 position. 4HT was converted into an α-chloro acetate intermediate through a Steglich esterification with dicyclohexylcarbodiimide (DCC) coupling agent and chloroacetic acid; the intermediate prepared on multi-gram scale. (Scheme 6.2a) Nucleophilic displacement of the chloride atom with nitrogen-based nucleophiles formed the desired TEMPO salt derivatives. For compounds **1**, **2**, and **3** the intermediate was reacted with 1-methyl imidazolium (Scheme 6.2b), trimethylamine (Scheme 6.2c), and pyridine (Scheme 6.2d) to form an imidazolium, ammonium, and pyridinium TEMPO salts, respectively. The reaction time varied depending on the nucleophile and took anywhere from 3-5 days for completion, as monitored by thin layer chromatogrphy. Triethylamine was also reacted with the intermediate to examine how steric bulk affected the solubility, yielding compound **4**. (Scheme 6.2e) An alternative counter anion was also examined by performing anion exchange of compound **2** with lithium bis(trifluoromethanesulfonyl)imide, replacing the Cl$^-$ ion with TFSI$^-$ forming compound **5**. (Scheme 6.2f) Additionally, a diTEMPO compound was synthesized with α,α'-dibromo-*p*-xylenes as the linker; 4HT was reacted with sodium hydride in tetrahydrofuran, then the linker was added to produce the diTEMPO compound **6**. (Scheme 6.2g)
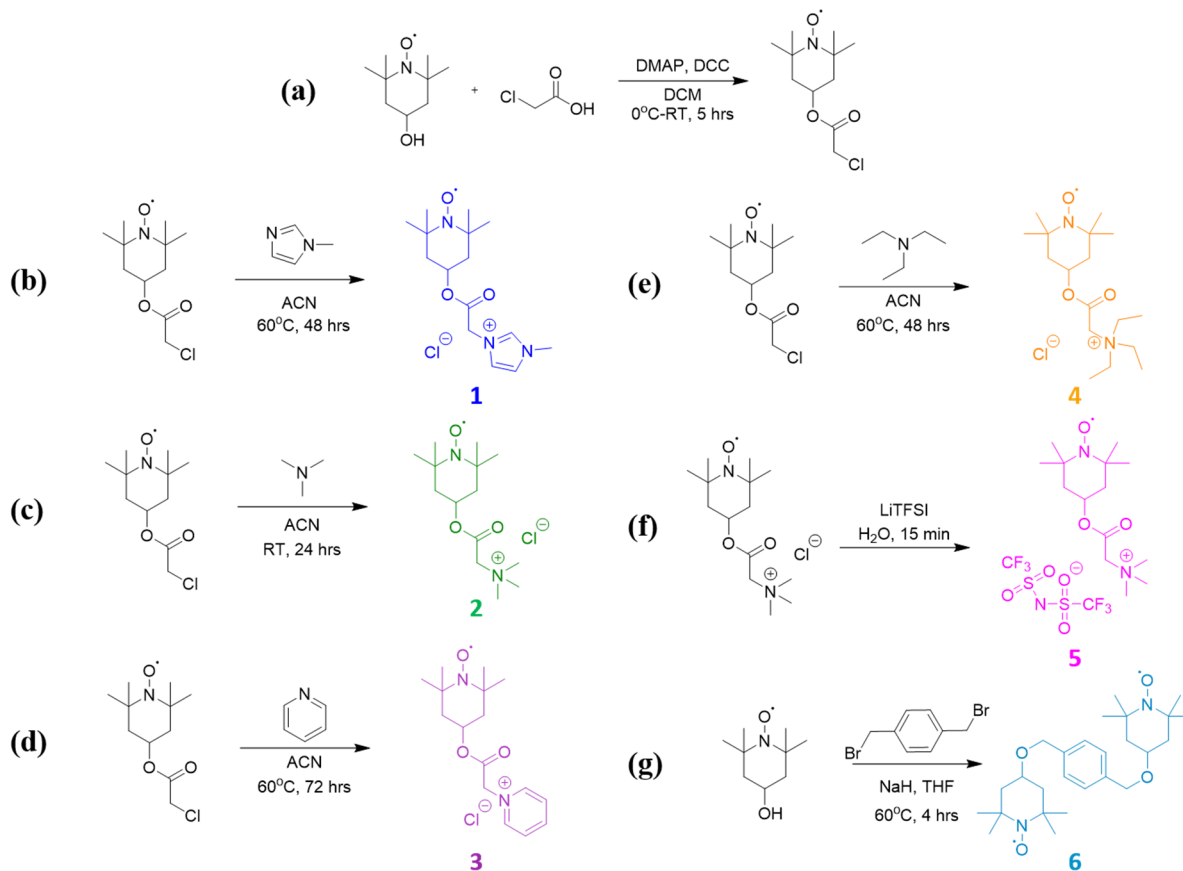
Scheme 6.2. Synthesis of TEMPO derivatives. (a) Steglich esterification of 4HT to form the chloroacetic intermediate. (b) Synthesis of compound **1**. (c) Synthesis of compound **2**. (d) Synthesis of compound **3**. (e) Synthesis of compound **4**. (f) Synthesis of compound **5**. (g) Synthesis of compound **6**.

6.4   Solubility Study of TEMPO Salt Derivatives

The maximum solubility of each of the TEMPO derivatives, TEMPO, and 4HT in ethaline was determined using UV-vis absorption spectroscopy. A calibration curve was generated from five solutions of known concentration in DMSO. A saturated sample was made for each derivative by continually adding the compounds to ethaline until solids remained in the vial after briefly heating the sample. (Figure A6.1) TEMPO exhibited the lowest maximum solubility of 0.17 M, whereas

4HT exhibited the highest solubility of 1.93 M. The TEMPO salts of varied cationic identity (compounds **1-4**) exhibited moderate solubility, being more soluble than TEMPO but less soluble than 4HT. For the different cations, the solubility decreased from compound **2** (1.35 M) > compound **1** (0.94 M) > compound **4** (0.92 M) > compound **3** (0.85 M) for the trimethyl ammonium, imidazolium, triethyl ammonium, and pyridinium salts, respectively. For the different counter anions, the solubility drastically decreased from 1.35 M for compound **2** to 0.32 M for compound **5**, or simply changing the anion from Cl to TSFI. This indicates that the anion plays a significant role in the solubility of the compound and may contributes to integration of the salt into th H-bond network of the DES. The diTEMPO compound had no measurable solubility in ethaline, which our group has also observed with alkylated TEMPO derivatives, indicating that for incorporation into a DES the small molecule must exhibit HBD functionalities.

6.5   Physical Properties of TEMPO Salt/Ethaline Solutions

The main advantage of using TEMPO salts over 4HT, regardless of solubility, is to address the challenge of crossover within a RFB, which has been shown to be suppressed when a charge is introduced or size of the molecule is increased. Compounds **1**, **2**, and **3** were chosen to continue examining the impact the incorporation of TEMPO derivatives into ethaline solutions due to their higher maximum solubility. Similar concentrations were evaluated so comparisons could be made and the water content was determined to be <400 ppm prior to use.

6.5.1   Density

The measured densities were obtained in a temperature range of 25-55 °C for TEMPO, 4HT, **1**, **2**, and **3**. (Figure 6.2) When TEMPO or 4HT was incorporated into ethaline, the density of the solution decreased as the concentration of the compound increased. This suggests that there was an increase in molar free volume of the solutions. Solutes with H-bonding capability are generally
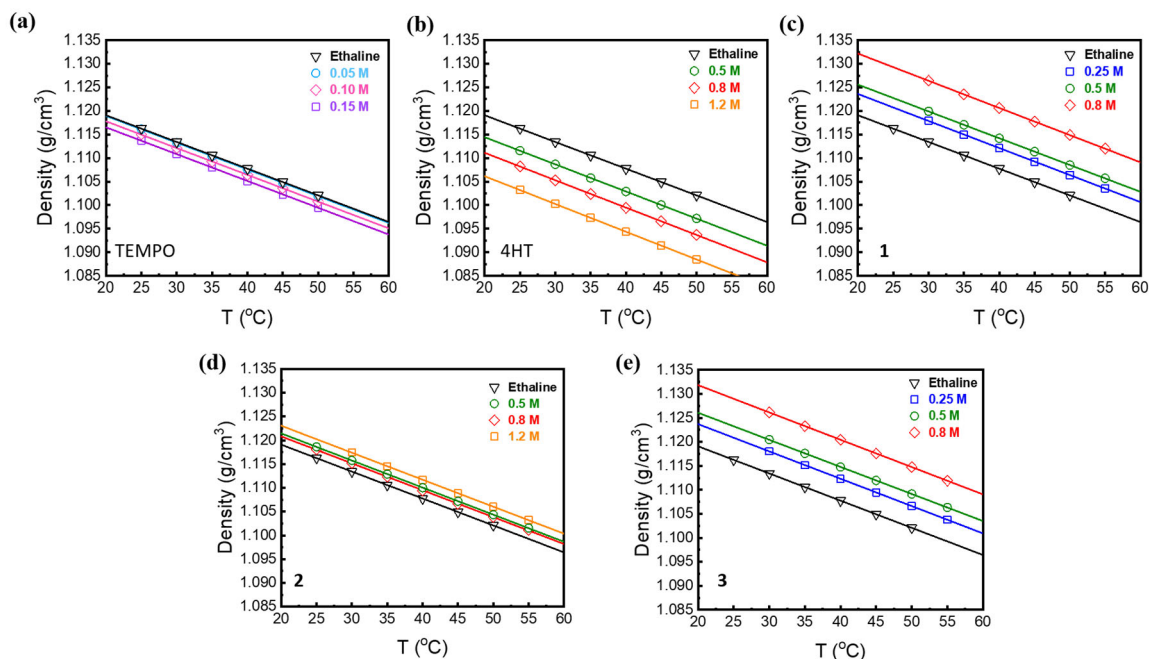
Figure 6.2. Measured densities for TEMPO derivative/ethaline solutions with temperature dependence for (a) TEMPO, (b) 4HT, (c) compound **1**, (d) compound **2**, (e) compound **3**. Solid lines represent the linear fits.

expected to increase the density of solutions; however due to the high solubility of 4HT in ethaline the hydrogen bond network of the solution may be altered in a way that increases the molar volume. The opposite was observed with the addition of compounds **1**, **2**, and **3**, in which the density of the solutions increased; this reflects the differences of how the TEMPO salts are incorporated into the DES. Compounds **1** and **3** consist of an aromatic cation structure with promotes tighter packing which leads to higher densities, and compound **2** contained an ammonium cation and had the least impact on the density of solution.

6.5.2 Viscosity

The measured viscosities of the TEMPO salt/ethaline solutions were obtained in a temperature range of 25-55 °C for TEMPO, 4HT, **1**, **2**, and **3**. (Figure 6.3) Unlike the density measurements,
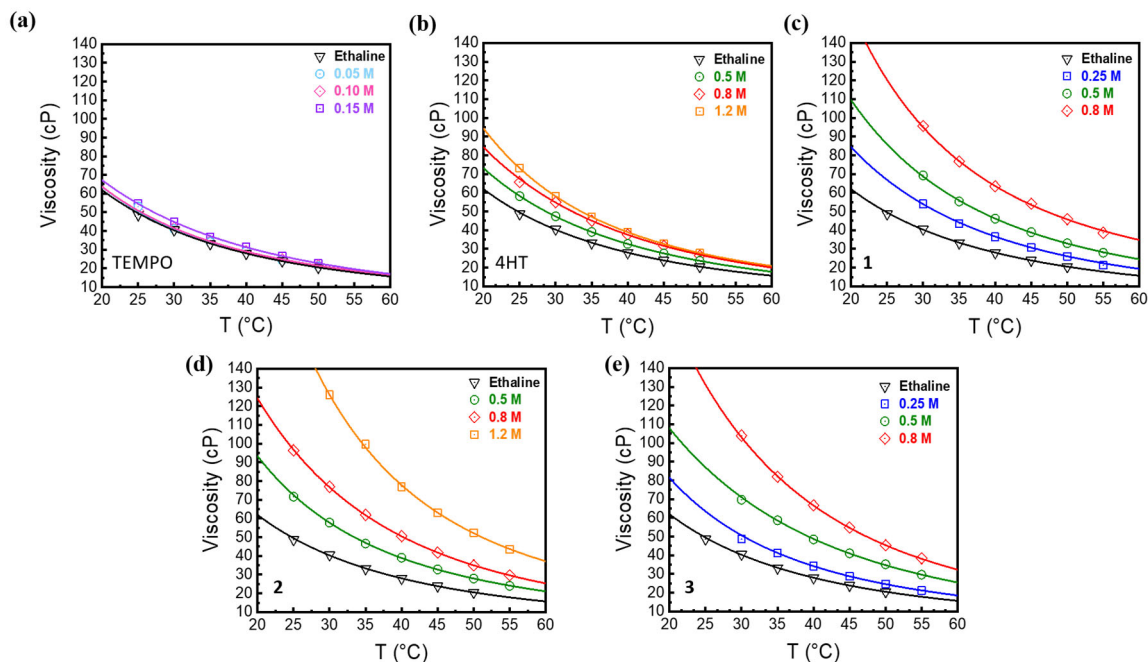
Figure 6.3. Measured viscosities for TEMPO derivative/ethaline solutions with temperature dependence for (a) TEMPO, (b) 4HT, (c) compound **1**, (d) compound **2**, (e) compound **3**. Solid lines represent VFT fits.

the viscosity of all the solutions increased regardless of the TEMPO derivative. Interestingly, the density of the 4HT/ethaline solutions decrease where viscosity of the solutions increases. This suggests that despite the increased molar volume, the H-bond dynamics are slowed. Compared to the TEMPO salts, the viscosity increase for the 4HT/ethaline solutions is small. Of the TEMPO salts, compound **2** had the lowest increase in viscosity, whereas compounds **1** and **3** exhibited similar increases in viscosity, which again can be contributed to the aromaticity of the cations. Hole theory rationalizes why the TEMPO salts exhibited an increase in the viscosity of the solutions,[212] where the probability of finding holes of a suitable radius for movement of ions/molecules in solution is hindered due to the densified liquid structure.[213]

6.5.3 Ionic Conductivity

The measured ionic conductivities of the TEMPO salt/ethaline solutions were obtained in a temperature range of 25-55 °C for TEMPO, 4HT, **1**, **2**, and **3** (Figure 6.4). An opposite trend was observed compared to the viscosities of the solutions for all of the TEMPO derivatives in which the ionic conductivities of solutions decreased; therefore, as the viscosity of the solution increases the ionic conductivity decreases. As well as, when the concentration of the TEMPO derivative is increased the conductivity of the solution is decreased. The TEMPO salts exhibited a lower conductivity compared to TEMPO and 4HT, ideally an electrolyte with increased salt content would increase the ionic conductivity.[214] In the case with ethaline, increasing the concentration of compounds **1**, **2**, and **3** resulted in stronger ionic associations between the ChCl and the TEMPO salts.
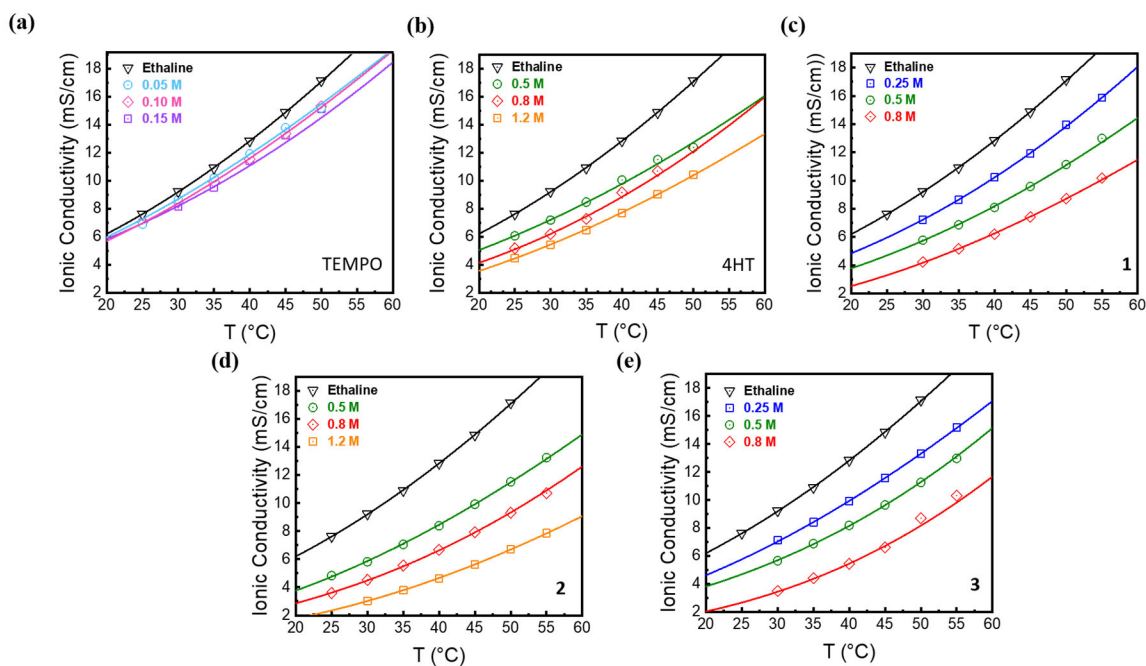
Figure 6.4. Measured ionic conductivities for TEMPO derivative/ethaline solutions with temperature dependence for (a) TEMPO, (b) 4HT, (c) compound **1**, (d) compound **2**, (e) compound **3**. Solid lines represent VFT fits.

6.6   Electrochemical Characteristics

The redox behavior of 50 mM TEMPO in ethaline is shown in Figure 6.5, two single-electron reductions are observed at +0.70 and -0.58 V vs. Ag/AgCl (denoted as E1 and E2). The E1 reduction exhibited a corresponding oxidation peak at +0.78 V, which resulted in a half wave potential of +0.74 V vs. Ag/AgCl. This redox couple likely corresponds to the formation of the oxoammonium cation through the reduction of TEMPO, which would be consistent with Nishide and coworkers study of TEMPO in acetonitrile.[197] The 80 mV separation of the reduction and oxidation peaks are roughly equal anodic and cathodic current densities which suggest that the E1 redox reaction is reversible, which was reported in literature for studies performed in acetonitrile. The negative shift of 60 MV in the redox potential of TEMPO to form an oxoammonium cation in ethaline as compared to acetonitrile can be attributed to the increased polarity of the solvent.[215] Comparing the CV of TEMPO in ethaline to the CV of TEMPO in acetonitrile shows an additional
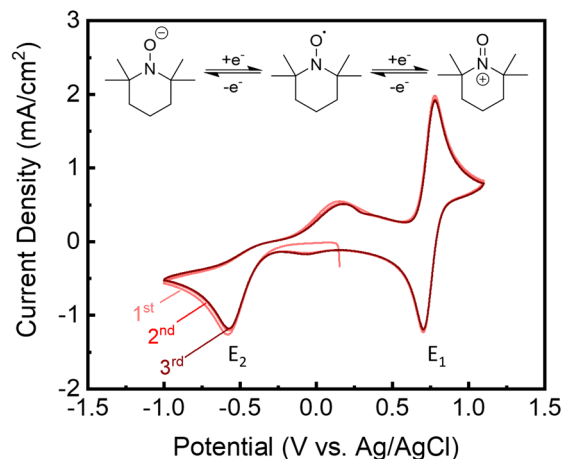
Figure 6.5. CV of 50 mM TEMPO in ethaline (1:2 ChCl:EG). Showing the first 3 cycles with a 100 mV s^{-1} scan rate. Performed with a glass carbon working electrode and a coiled Pt wire counter electrode wrapped around a Ag/AgCl reference electrode.   The inset is the electrochemical reduction of TEMPO to an oxoammonium cation (E1) and the oxidation of TEMPO to an aminoxyl anion (E2).

redox peak at -0.58 C (E2) in ethaline, which is due to the aminoxyl anion formation. (Figure 6.5) This observation is consistent with TEMPO-based redox species reported in various electrolytes ranging from methanol to phosphate buffer upon cathodic polarization.[215–217] This E2 electron transfer appears irreversible or quasi-reversible with a reduced anodic current intensity on the oxidative scan.

There is an additional third reduction peak with a very low intensity at -0.07 V, which could appear for two reasons. One is due to hydroxyl formation with the aminoxyl anion though water
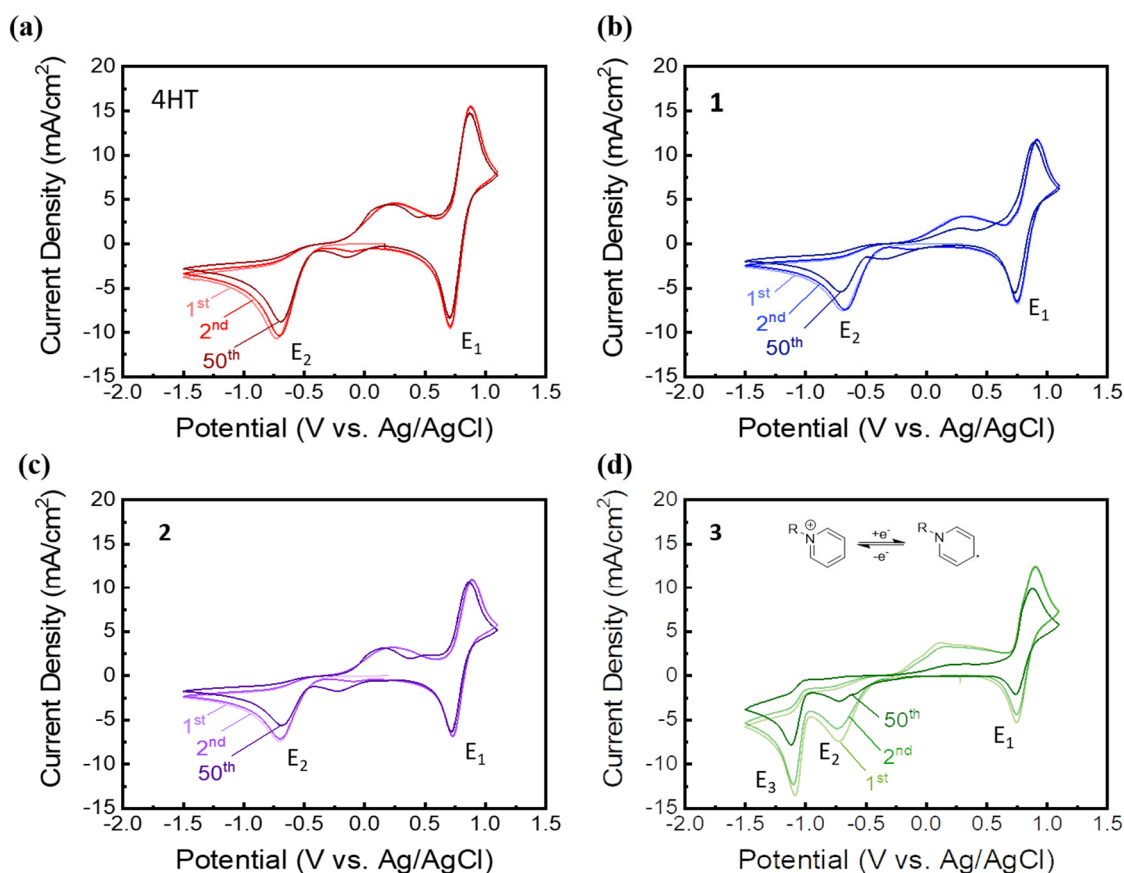
Figure 6.6. CVs of (a) 4HT, (b) compound **1**, (c) compound **2**, (d) compound **3** at 0.5 M in ethaline. Each shows the 1st, 2nd, and 50th cycles at a scan rate of 100 mV s⁻¹. CVs performed with a glass carbon working electrode and a coiled Pt wire counter electrode wrapped around a Ag/AgCl reference electrode.

hydrolysis, however this would be a small chance due to the water content being low (140 ppm). The second reason could be from the anion interacting with EG through H-bonding which would slow the redox reaction. This additional peak is observed for all TEMPO derivatives in ethaline. Figure 6.6 shows the 1st, 2nd and 50th CV cycles for 4HT, **1**, **2**, and **3**; in which the two, single-electron redox reactions of TEMPO, E1 and E2, are observed for all derivatives. The CV of compound **3** exhibited an additional reduction between E1 and E2 (Figure 6.6d) which is likely due to the pyridinium unit undergoing a reduction reaction where the pyridinyl radical (inset) forms at -1.09 V, which is more negative to the aminoxyl anion formation of TEMPO at -0.73 V.[218]

Preliminary assessment of the reversibility of the solutions was performed by repeating the CV for 50 cycles. Compound **3** and TEMPO solutions showed reduced reduction currents after the 50 cycles, as well as small changes in the oxidative currents of aminoxyl anion and pyridinyl radical. The other compounds; 4HT, **1** and **2**; exhibited greater redox stability over 50 cycles with minimal change in current density. (Figure 6.6a-c) The diffusion coefficients of the compounds were estimated by isolating the redox couple of the TEMPO radical and the oxoammonium cation through restricting the potential window to 0.5-1.1 V vs. Ag/AgCl. The estimated diffusion coefficients are summarized in Table A6.5. The observed trend was opposite of the viscosities was the solution, where 4HT had the largest diffusion coefficient ($4 \cdot 10^{-8}$ cm^2 s^{-1}) and the lowest viscosity. This can be explained by the lack of charge in the compound promoting stronger association with ethaline. Of the TEMPO salts, the diffusivity for compound **2** ($2 \cdot 10^{-8}$ cm^2 s^{-1}) was twice the diffusivity than compounds **1** and **3**, indicating the solvation of the TEMPO salts has significant impact on the transport properties of the solution.

To better understand the redox behavior and stability of these compounds in ethaline, flow-cell experiments were repeated with a Pt microelectrode, specifically focusing on 4HT.[219,220] The purpose of the flow-cell experiment is to obtain known concentrations of the oxidized and reduced version of 4HT so the E1 and E2 redox reactions could be studied independently in a symmetric cell configuration. The concentrations of the various redox active species for the positive and negative electrolytes were evaluated at 50% state of charge (SOC) by performing CVs, in which supports that the 4HT oxidation reaction involves one electron. Similar experiments were repeated by replacing the negative electrolyte with 4HT producing $4HT/4HT^-$ redox couple, while the positive electrolyte remained $4HT/4HT^+$. The data supported that there was a loss of active $4HT^+$, which could be caused by the formation of an electrochemically inactive compound, making the electron transfer irreversible.

To further understand the loss of active $4HT^+$, an experiment was performed where a flow cell was used to charge a solution of 4HT in aqueous KCl was charged to 50% SOC and the negative electrolyte was $K_3Fe(CN)_6$. The positive electrolyte was dosed with urea, ethylene glycol, or choline chloride, which are all common components of DESs. The objective was to determine if any of these components could be the cause for the loss of active $4HT^+$. The urea doped sample had little effect on the reduction current, whereas EG and ChCl had larger effects on the reduction current. Both EG and ChCl contain primary alcohol groups, which have been reported to react with $TEMPO^+$ in aqueous systems (Scheme 6.3).[221] Therefore, it is possible that the presence of
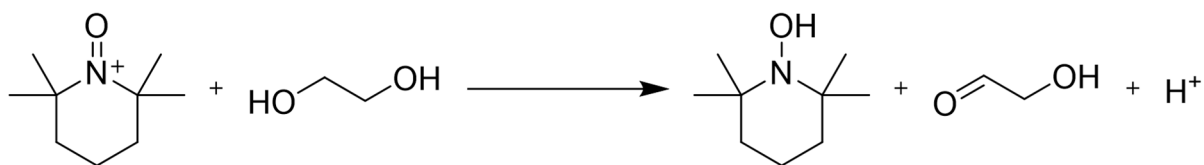
Scheme 6.3. Possible electrochemical deactivation reaction of $TEMPO^+$ in ethylene glycol.

a primary alcohol the HBD or HBA could oxidize to an aldehyde in the presence of a TEMPO derivative.

6.7　Summary

DESs have great potential for energy storage mainly due to their low vapor pressures and ability to incorporate redox active species thus increasing energy density. I have successfully synthesized a variety of TEMPO salts examining cationic identity, anionic identity, and linkers. Each was incorporated into ethaline (1:2 ChCl:EG) and exhibited higher maximum solubility than TEMPO in ethaline, but lower maximum solubility than commercially available 4HT. The TEMPO salts containing imidazolium, ammonium, and pyridinium functionality, compounds **1**, **2**, and **3** respectively, were used to examine the impact on the physical properties of the solutions; including density, viscosity, and ionic conductivity. This study provided valuable information on the electrochemical behavior of TEMPO derivatives (compounds **1**, **2**, and **3**) in DESs. Each of the TEMPO derivatives exhibited two, single-electron reactions corresponding to oxoammonium and aminoxyl anion formations. Compound **3** also exhibited a third electron transfer due to the pyridinium cation. Compounds **1**, **2**, and 4HT exhibited redox stability over 50 cycles at 100 mV s^{-1}, while TEMPO and compound **3** exhibited a reduced reductive current for all redox couples. Further flow cell experiments showed that stability of the $4HT/4HT^+$ redox couple decreases over time. We hypothesize that this is due the primary alcohols present in the DES to be oxidized to aldehydes in the presence of TEMPO derivatives. This unfortunately limits of the potential for this specific system to be used for RFBs; regardless this work provided insight into how chemical modification of redox active small molecules impacts their solubility in DES, physical properties of the solutions, and their redox performance in DES. Future research is needed to understand the

interactions between the DES components and the dissolved redox species. As well as, research looking at alternative DESs and alternative redox active small molecules.

6.8   Appendix

General considerations.   TEMPO (Sigma Aldrich, 99%), 4-hydroxy-TEMPO used for synthesis (Sigma Aldrich, 97%), chloroacetic acid (Sigma Aldrich, 99%), 4-dimethylaminopyridine (Sigma Aldrich, 98%), 1-methylimidazole (Sigma Aldrich, 99%), N,N'-dicyclohexylcarbodiimide (ACROS organics, 99%), acetonitrile (Alfa Aesar, 99.8%), ferric chloride hydrate (97%), trimethylamine (Fisher, 1M solution), and pyridine (Fisher) were all used without further purification. All solvents for chemical synthesis were purchased from Fisher, unless otherwise stated. Dichloromethane (DCM) and tetrahydrofuran (THF) were obtained by passing commercial grade solvent through a column of activated neutral alumina in a Dow-Grubbs solvent system from Pure Process Technology (Nashua, NH). Choline Chloride, ChCl, ((2-hydroxyethyl)trimethyl)trimethylammonium chloride) (Acros Organics, 99%) was dried in a vacuum oven for over 12 hours at 150°C before use. Ethylene glycol (Acros Organics, anhydrous, 99%) was used without further purification. 4-hydroxy-TEMPO used in ethaline solutions (Alfa Aesar, 98%) was recrystallized using hexane at 50°C. Each synthesized TEMPO derivative was dried in a vacuum oven for over 12 hours at 80°C. Heat shrink tubing (NTE Electronics, 47-20306-CL) was used in preparation of reference and counter electrodes. An argon-filled glovebox (VTI Super, > 1 ppm water and oxygen) was used to handle all DES samples and DES constituents. Pt wire (Alfa Aesar, 0.3 mm dia., 99.9%) for cyclic voltammetry. Elemental analysis was used to confirm the purity of the synthesized TEMPO derivatives, compounds **1**, **2**, and **3**. ^{1}H Nuclear magnetic resonance (NMR), ^{13}C NMR, Fourier transform infrared spectroscopy (FTIR), and electron spray ionization (ESI) was performed for each synthesized TEMPO derivative. Due the

TEMPO derivatives being paramagnetic, phenylhydrazine was added to each NMR sample to obtain the spectra. All ^{1}H, ^{13}C, ^{29}Si NMR were collected on Bruker Ascend III HD 500MHz NMR instrument equipped with prodigy probe and shifts are reported relative to residual solvent peak. All NMR spectra were collected using CDCl$_3$ as the solvent unless otherwise noted. FTIR spectra were acquired using an Agilent Cary 630 FT-IR in ATR mode. ESI spectra were obtained on THERMO Finnigan LCQ DECA ion trap mass spectrometer equipped with an external AP ESI ion source. All UV-Vis spectra was obtained on a Cary 5000 UV-Vis-NIR. For Karl Fischer titrations measurements, a Metrohm Coulometric KF 899 D was used. Densities were measured with an oscillating U-tube density meter (Anton Paar DMA 4500) from 25 – 55°C with an uncertainty of ±0.0005 g cm-3. Viscosities were measured by a microchannel viscometer (MicroVISC, Rheosense) at a temperature range of 25 – 55°C. Approximately 10-45 μL of solution was injected into the microchannel with a flow rate between 10-450 μL min-1 for all measurements. At each temperature, the viscosity was measured in triplicate and the variability was observed to be 5 %. The ionic conductivities were measured by electrochemical impedance spectroscopy (EIS) using a potentiostat equipped with frequency response analyzer (BioLogic SP 240). A two-electrode cell (Biologic MCM-CC) with parallel, non-platinized Pt electrodes was used as for the conductivity measurements. A 0.1 M KCl(aq) solution was used to determine the conductivity cell constant (1.38 cm-1). About 600 μL of sample was loaded into the conductivity cell inside an argon-filled glovebox. The voltage amplitude was set at 10 mV and the applied frequency range was 100 kHz to 100 Hz from 25 – 55°C. For every sample, EIS was repeated three times. The bulk resistance of each sample was determined from the real intercept of Nyquist plot where the imaginary impedance is plotted with respect to the real part of the impedance (Figure A7.9).

Synthesis of TEMPO-Chloroacetate Intermediate.[222,223] An oven-dried round bottom flask (RBF) was purged with vacuum and N_2. 4HT (2.18g, 0.025mol) and chloroacetic acid (1.20g, 0.025mol) were added to the flask, followed by dichloromethane (DCM) (30mL). The flask was cooled to 0°C with an ice water bath under N_2. 4-Dimethylaminopyrdine (DMAP, 0.39g, 0.006mol) and N,N'-dicyclohexylcarbodimide (DCC, 2.62g, 0.025mol) were dissolved with DCM (15mL) and the solution added dropwise. Once added, the reaction was warmed to room temperature and stirred for 5 hrs at 400rpm. Upon completion, the reaction was cooled to 0°C with an ice water bath, the white precipitate was filtered with a Buchner funnel. The filtrate was washed with 1M HCl (25mL), saturated $NaHCO_3$ (25mL), and saturated NaCl (25mL) (chilling and filtering organic layer between each wash). The organic layer was dried over magnesium sulfate and solvent removed under reduced pressure using the rotary evaporator. The product was purified through column chromatography, eluted with a 9:1 hexane: ethyl acetate. Solvent was removed under reduced pressure and the product dried under vacuum. Product was an orange solid, with a 77% yield (2.5g).

Synthesis of Compound 1.[222,223] In an oven-dried RBF, TEMPO-chloroacetate intermediate (1.0 g, 0.004 mol) was dissolved in acetonitrile (30 mL). 1-methylimidazole was added slowly. The reaction was heated to 60°C and stirred at 400 rpm for 48hrs. Reaction was monitored with thin layer chromatography (TLC). Upon completion, the reaction was cooled with an ice water bath and diethyl ether (30 mL) was added. The precipitate was filtered and washed with acetone (40mL) and diethyl ether (40mL) successively. The product obtained was a red powder and dried under vacuum in 83 % yield (1.1g).

Synthesis of Compound 2. In an oven-dried RBF, TEMPO-chloroacetate intermediate (0.79g, 0.0032 mol) was dissolved in dry THF (20 mL). A solution of 1M trimethylamine in THF (2.23mL,

0.046mol) was added slowly. The reaction was stirred at room temperature at 400 rpm for 24hrs under N_2(g). Reaction was monitored with TLC. Once complete the reaction was cooled with an ice water bath and diethyl ether (30 mL) was added. The precipitate was filtered and washed with acetone (50 mL) successively. The product obtained was a red powder in 57% yield (0.56g) and dried under vacuum.

Synthesis of Compound 3. In an oven-dried RBF TEMPO-chloroacetate intermediate (3.0g, 0.012 mol) was dissolved in acetonitrile (70 mL). Pyridine (1.2 mL, 0.015 mol) was added slowly. The reaction was heated to 60°C and stirred at 400 rpm for 72 hrs. Reaction was monitored with TLC. Once complete the reaction was cooled with an ice water bath and ethyl acetate (100mL) was added. The precipitate was filtered and washed with acetone (50mL) and diethyl ether (50mL) successively. The product obtained was a red powder in 49 % yield (1.95g) and dried under vacuum.

Synthesis of Compound 4. In an oven-dried RBF, TEMPO-chloroacetate intermediate (1.0 g, 0.004 mol) was dissolved in acetonitrile (30mL). Triethylamine was added slowly. The reaction was heated to 60°C and stirred at 400 rpm for 48hrs. Reaction was monitored with thin layer chromatography (TLC). Upon completion, the reaction was cooled with an ice water bath and diethyl ether (30 mL) was added. The precipitate was filtered and washed with acetone (40mL) and diethyl ether (40mL) successively. The product obtained was a red powder and dried under vacuum in 61 % yield.

Synthesis of Compound 5. In a RBF, compound **2** (0.2g, 0.00065 mol) was added and dissolved in deionized H_2O (15 mL). Add lithium bis(trifluoromethanesulfonyl)imide (0.93g, 0.0032 mol) to a vial and dissolve in 5 mL H_2O. Added solution dropwise to RBF at room temperature. Once

fully added, stir for 5 minutes (precipitate forms). Filter precipitate and water with water. Dry under reduced pressure and the product obtained was an orange powder in 81% yield.

Synthesis of Compound 6. An oven-dried round bottom flask (RBF) was purged with vacuum and N_2 three times. 4HT (0.4 g, 0.0023 mol) was added and dissolved in THF (12 mL). The RBF was vented and cooled to 0°C with an ice bath. NaH (0.1 g, 0.00077 mol) was added and the reaction stirred for 20 minutes. The reaction was warmed to room temperature and α, α'-dibromo-*p*-xylene was added. The RBF was warmed to 60°C for 4 hours. Monitor reaction with thin layer chromatography. Quench with 20 ml H_2O, wash aqueous layer three times with 15 mL ethyl acetate. Combine organic layers and wash with 20 mL saturated aqueous NaCl. Dry organic layer with Mg_2SO_4, filter, and remove solvent under reduced pressure. Purify with column chromatography. Column was built with 100% hexanes and flushed with a hexanes:ethyl acetate solvent system. Product was dried and an orange solid was obtained in 66% yield.

Preparation of Ethaline and Redox Active DESs. Ethaline was prepared by mixing 1:2 molar ratio of choline chloride (10.12 g) : ethylene glycol (9.03 g) stirring at 80°C and 300 rpm for 30 minutes in a 20 mL glass vial. The hot plate was turned off and the solution was cooled slowly to room temperature. If not cooled slowly, crystals would form in the DES which were determined by NMR to be choline chloride. To prepare the redox-active DES, the TEMPO derivatives were dissolved in ethaline to produce the desired concentration. Water content of the ethaline stock solution and the redox-active DES solutions prepared from TEMPO, 4HT and compounds **1**, **2**, and **3** at concentrations ranging from 0.25-1.2 M were measured by a Karl Fischer titration and reported in Table A6.1.

Maximum Solubility Measurements. Solubility limits of TEMPO and TEMPO derivatives in ethaline were determined by calibration curves obtained from UV-Vis (Figure A6.7 and A6.8).

Five solutions of pre-determined concentration were made for each compound in DMSO. The UV-vis spectra were obtained from 200-800 nm. The calibration curves were plotted at a specific absorption wavelength for each compound. To make the concentrated samples, each TEMPO derivative was added to ethaline (0.5mL) and heated on a hot plate. This process was repeated till solid remained present in solution. The saturated samples were cooled to room temperature and stood for at least one hour. A solution was made with DMSO and UV-vis obtained from 200-800 nm. The solubility limit was obtained as in Table A6.1.

Electrochemical Characterization. Unless noted otherwise, cyclic voltammetry (CV) was performed in a 3-electrode cell inside an Argon purged glovebox (VTI Super, 1> ppm water and oxygen) to determine the electrochemical windows (EW) and study the redox potentials and reversibility of DESs with TEMPO functionality. A glassy carbon disc electrode (BASi MF-2012, 3 mm dia, surface area = 0.0707 cm2) was used as the working electrode. Pt wire was used as the counter electrode, and Ag/AgCl wire was the reference electrode. The Ag/AgCl wire reference electrode was prepared using chronoamperometry as described in Shen et al., where the chloride containing solution for AgCl deposition was ethaline.[224] The step potential for AgCl deposition was +1.5 V versus a graphite rod. With the exception of the microelectrode experiments, the electrodes were arranged in a T-cell configuration for CVs (Figure A7.12). The fabricated Ag/AgCl reference electrode was first wrapped with Teflon tape and then isolated from the coiled Pt counter electrode around it with heat-shrink tubing. The Pt-wire counter electrode was wound around the first layer of heat-shrink tubing along the length of the Ag/AgCl wire, and then coiled eight times near the tip of the exposed Ag/AgCl wire. The counter and reference electrodes were then placed over the working electrode with approximately 0.5 cm distance between the reference and the working electrode. About 200 μL of solution was injected into the liquid reservoir over the

working electrode (created by heat-shrink tube) for each CV measurement. Before each measurement, the glassy carbon disk electrode was polished with 0.05 μm alumina suspension (BASi, CF-1050) and ultrasonicated with deionized (DI) water. All CV measurements are iR-compensated (85%). For the iR-compensation, EIS was performed with 100 kHz single-frequency and a voltage amplitude of 20 mV. EW was determined using a scan rate of 10 mV s-1 from -2.5 V to +1.5 V vs. Ag/AgCl. 50 cycles were performed to confirm redox reversibility within the potential region of interest that is identified from the initial EW measurements. The CV measurements for studying the redox reactions were started from open circuit potential and then scanned to the negative direction to -1.5 V and then scanned to the positive direction to +1.1 V vs. Ag/AgCl. CV was performed for 50 cycles between -1.5 V to +1.1 V vs. Ag/AgCl. Diffusion coefficients of redox active solutes were measured using CV at a restricted potential range from +0.5 V to +1.1 V. Like the EW measurements, voltammetry measurements for measuring diffusion coefficient were started from open circuit potential and scanned to the positive direction that includes the redox potentials of TEMPO and derivatives in ethaline. Scan rates of 5, 10, 20, 50, 100, and 200 mV s^{-1} were used for application of the Randles-Sevcik (Figure A7.11). Flow cell testing was performed using an in house 2.5 cm^2 flow cell design. The cell uses a flow through electrode configuration. Graphite current collectors were machined in-house from impervious graphite (Graphite Store). Morgan Advanced Materials WDF 3 mm thick felt compressed to 2.5 mm was used as the flow through electrode. The felts were heat treated at 400 °C for 4 hours prior to use in the flow cell to improve their wettability. Polyvinyl-alcohol hydrogel coated Daramic 175 (200 μm wetted thickness) was used as a porous separator.[225] This separator was developed in house. The Daramic was soaked in 2-propanol for 10 minutes to remove residual oil remaining after manufacture and then dried in air prior to use. Charging of the electrolyte was performed with

a constant current of 20 mA/cm2 at 22°C to ensure that at 0% SOC the cell over potential was less than 200 mV. A constant electrolyte flow rate of 40 mL/min was used. A 20 ml sample takes approximately 1.3 hours to charge to 50% SOC under these conditions with a final over potential of approximately 400 mV. All 'dry' flow cell experiments were performed in a nitrogen purged, dry glove box with an approximate dew point of -75 °C. The voltammetry of the positive and negative electrolytes following a flow cell experiments was performed on with 100 μm diameter platinum microdisk purchased from BASi. A platinum mesh counter electrode was used. A chloridized silver wire placed directly into the electrolyte was used as reference for all three electrode experiments. Aqueous microelectrode voltammetry was performed using a similar working and counter electrode but with a commercial Ag/AgCl reference electrode purchased from BASi. Microelectrode CVs and flow cell experiments were performed with a Solartron 1280B Potentiostat. For the microelectrode CVs, the following equation holds at sufficiently slow scan rates: $i_{ss} = 4nFDCr$ where i_{ss} is the steady state current determined from the voltammetry, n is the number of electrons transferred, F is Faraday's constant, D is the diffusion coefficient of the active species, C is the bulk concentration of the active species and r is the radius of the micro-disk. For a viscous electrolyte such as used here, the diffusion coefficient of the reacting species is small enough that true steady-state behavior is only observed at very slow scan rates, on the order of 0.5 mV/s.
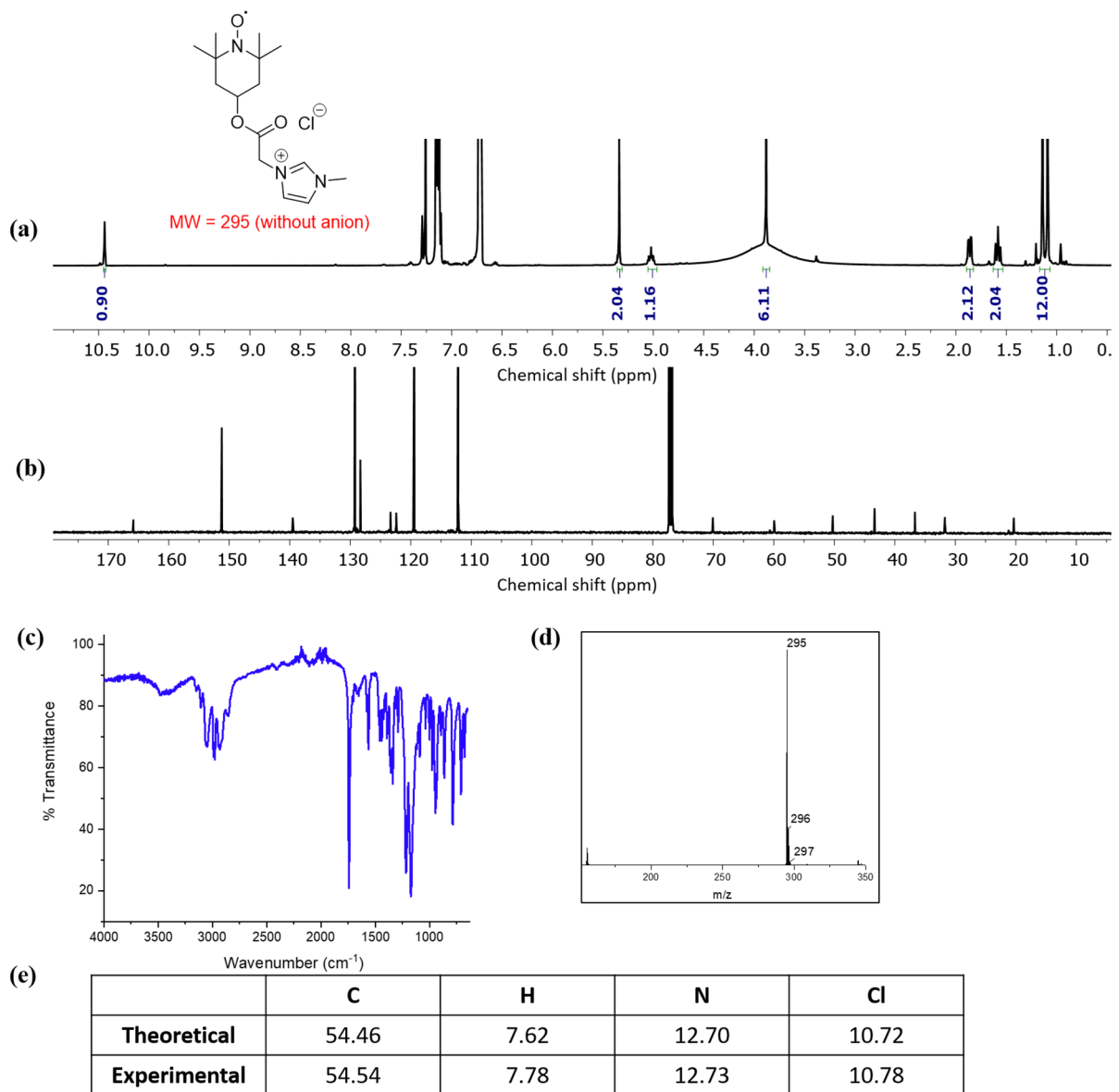
Figure A6.1. Chemical characterization of compound **1**. (a) ¹H NMR, (b) ¹³C NMR, (c) FTIR, (d) ESI, (e) elemental analysis.
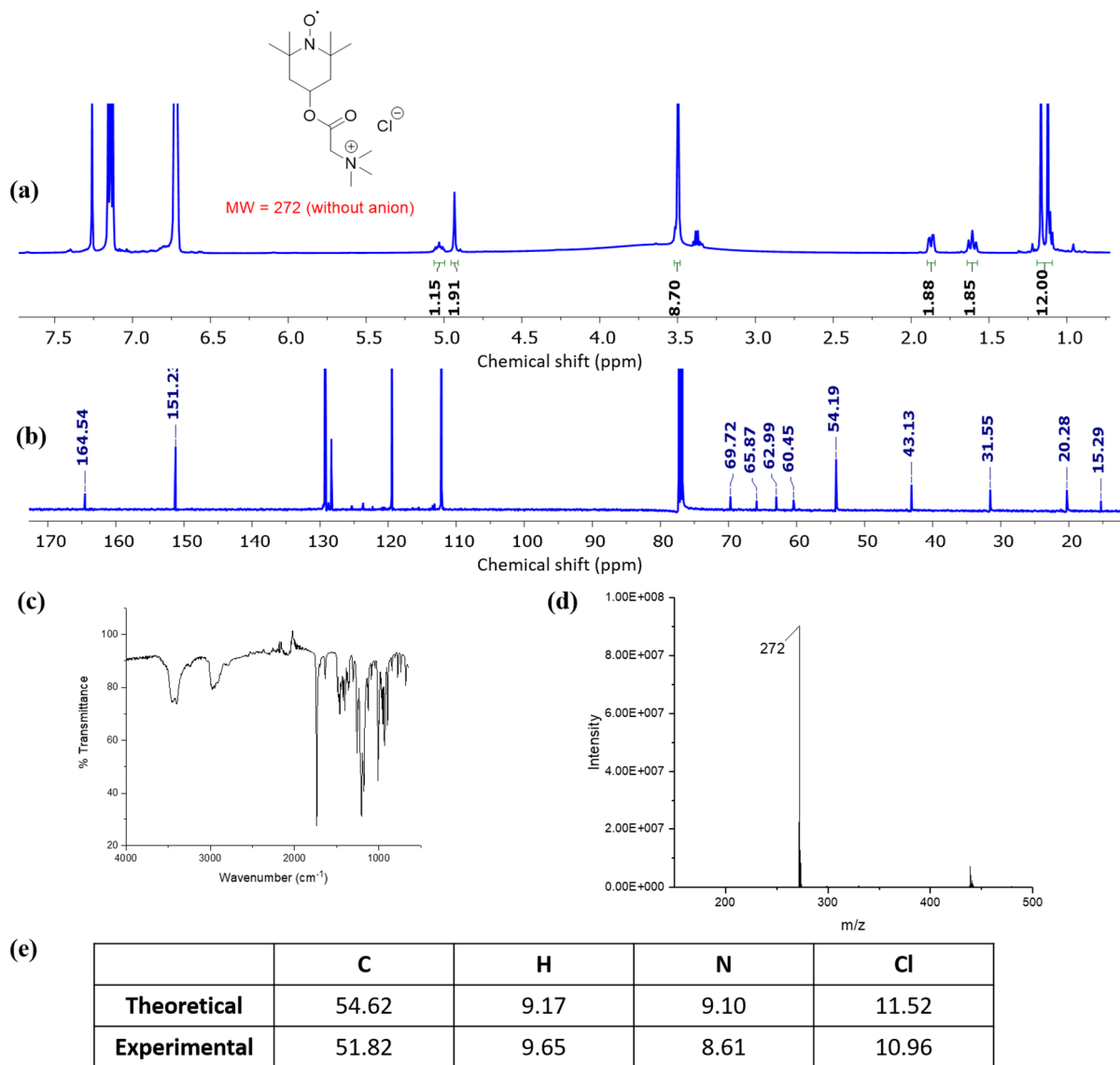
Figure A6.2. Chemical characterization of compound **2**. (a) ^{1}H NMR, (b) ^{13}C NMR, (c) FTIR, (d) ESI, (e) elemental analysis.
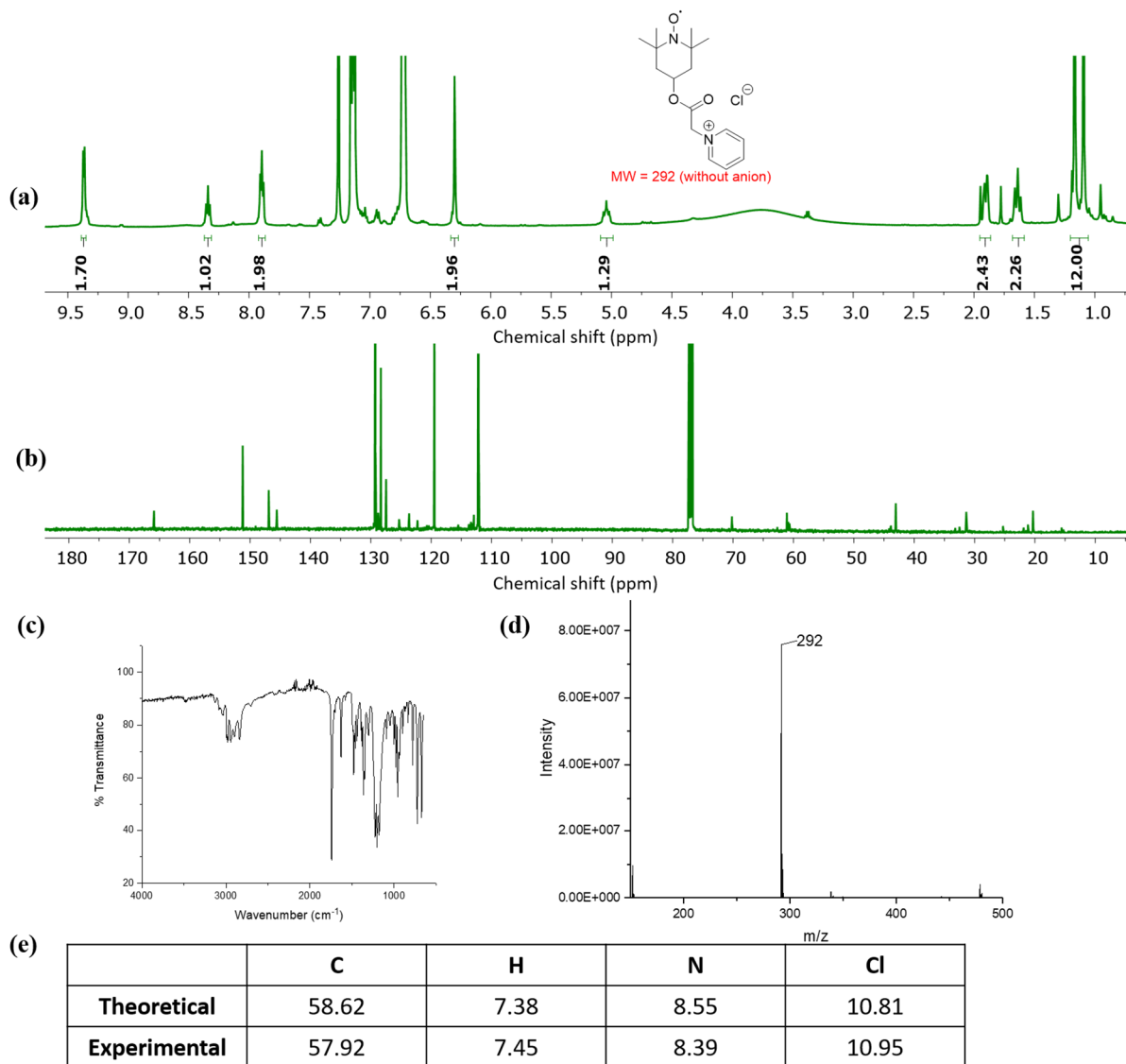
Figure A6.3. Chemical characterization of compound **3**. (a) ^{1}H NMR, (b) ^{13}C NMR, (c) FTIR, (d) ESI, (e) elemental analysis.

	C	H	N	Cl
Theoretical	58.62	7.38	8.55	10.81
Experimental	57.92	7.45	8.39	10.95
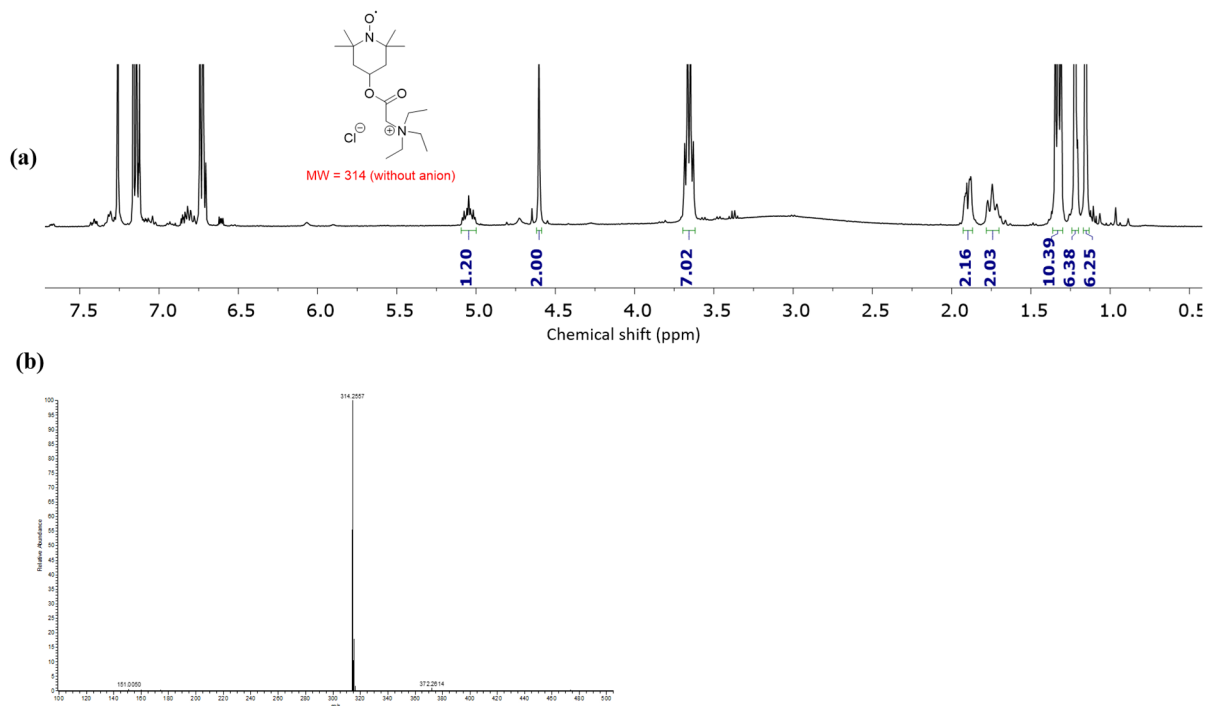
Figure A6.4. Chemical characterization of compound **4**. (a) ^{1}H NMR, (b) ESI.
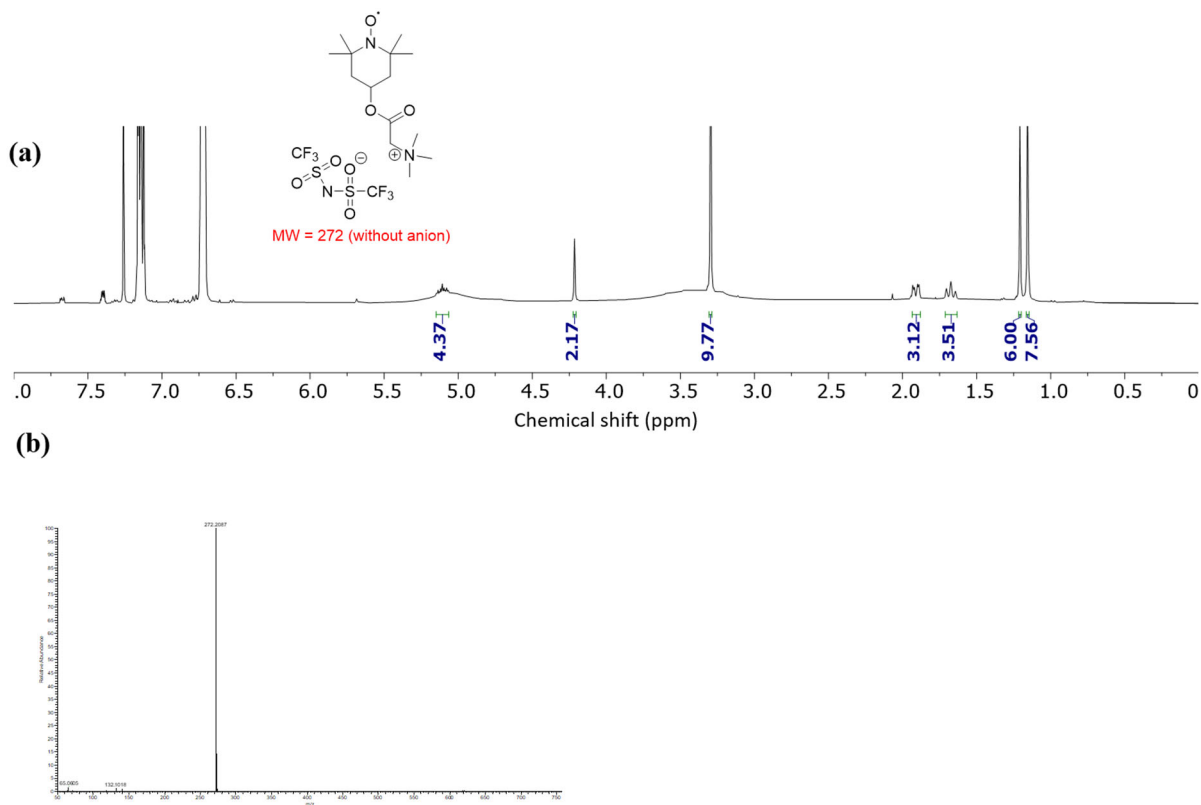
Figure A6.5. Chemical characterization of compound **5**. (a) ^{1}H NMR, (b) ESI.
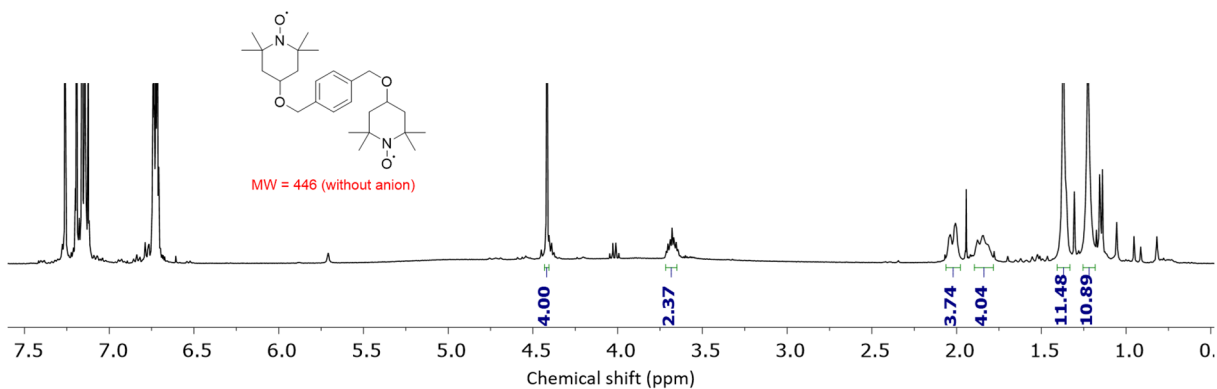
Figure A6.6. ^{1}H NMR of compound **6**.

Table A6.1. Solubility, melting point (T_m), decomposition temperature ($T_{0.05}$ loss; temperature corresponding to 5 wt% mass loss during TGA), and water content for ethaline solutions.

Compound	MW (g/mol)	Solubility in ethaline (mol/L)	T_m (°C)	$T_{0.05}$ loss (°C)	Solutions studied in ethaline (mol/L)	Water content (ppm)
TEMPO	156	0.17	36-38	--	0.05 0.10 0.15	136.6 120.7 113.2
4HT	172	1.93	69-71	155.5	0.5 0.8 1.2	178.6 148.1 74.0
1	330	0.94	209-212	244.5	0.25 0.5 0.8	210.8 141.6 117.5
2	307	1.35	165-174	199.1	0.5 0.8 1.2	274.2 260.7 387.2
3	327	0.85	200-204	224.8	0.25 0.5 0.8	77.6 105.2 114.8
4	349	0.92	--	--	--	--
5	552	0.32	--	--	--	--
6	446	insoluble	--	--	--	--
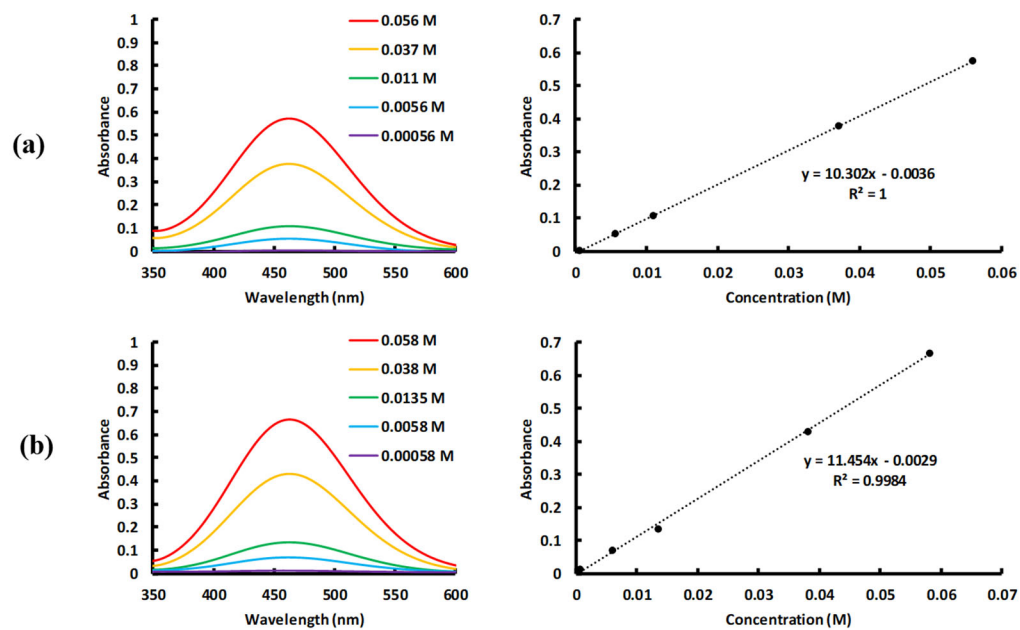
Figure A6.7. UV-vis spectra of known concentrations of commercial TEMPO derivatives in DMSO; (a) TEMPO and (b) 4HT. Used to form calibration curve to determine maximum solubility of derivative in ethaline.
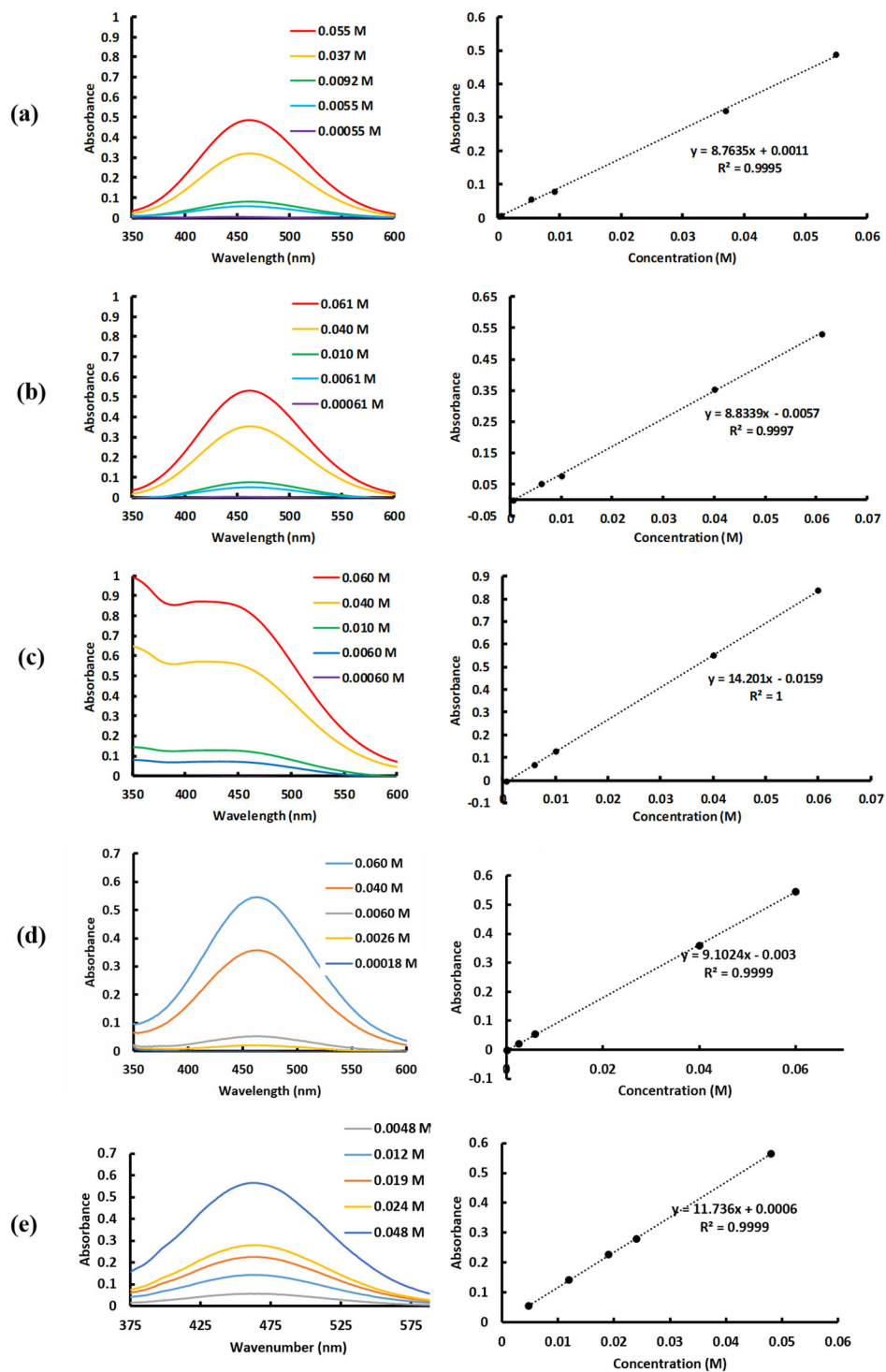
Figure A6.8. UV-vis spectra of known concentrations of synthesized TEMPO derivatives in DMSO; (a) compound **1**, (b) compound **2**, (c) compound **3**, (d) compound **4**, (e) compound **5**. Used to form calibration curve to determine maximum solubility of derivative in ethaline.

Table A6.2. Linear fit parameters for the temperature dependence of the measured densities for TEMPO derivative/ethaline solutions ($R^2 > 0.999$ for all solutions). The equation $\rho = A + BT$ was used to determine the linear line fit where ρ (g cm^{-3}) is the density at temperature T (K) and A and B are fitting parameters.

$\rho = A + BT$			
Compound	Concentration (M)	A (g cm^{-3})	B x 10^{-4} (g cm^{-3} °C^{-1})
TEMPO	0.05	1.13029	-5.675
	0.10	1.12917	-5.682
	0.15	1.12790	-5.688
4HT	0.5	1.12594	-5.755
	0.8	1.12273	-5.808
	1.2	1.11793	-5.887
1	0.25	1.13520	-5.762
	0.5	1.13695	-5.684
	0.8	1.14371	-5.767
2	0.5	1.13284	-5.698
	0.8	1.13213	-5.658
	1.2	1.13442	-5.677
3	0.25	1.13510	-5.696
	0.5	1.13736	-5.643
	0.8	1.14321	-5.692

Table A6.3. VFT fit parameters for temperature dependence of the measured viscosities for TEMPO derivative/ethaline solutions ($R_2 > 0.998$ for all solutions). The temperature dependence of viscosity was obtained by the Vogel-Fulcher-Tamann (VFT) model; $\eta = \eta_o \exp (B_\eta/T - T_o))$, where η (cP) is the viscosity at temperature T (K), η_o (cP) is the pre-exponential factor, B_η (K) is activation temperature, and T_o (K) is the ideal glass transition temperature.

$\eta = \eta_o \exp (B_\eta/(T-T_o))$				
Compound	Concentration (M)	η_o (cP)	B_η (K)	T_o (K)
TEMPO	0.05	0.58	-455.88	195.80
	0.10	0.56	-474.46	192.69
	0.15	0.08	-1075.37	134.81
4HT	0.5	0.25	-688.30	171.84
	0.8	0.12	-921.71	151.55
	1.2	0.58	-485.13	197.77
1	0.25	0.16	-811.43	163.13
	0.5	0.37	-634.29	181.30
	0.8	1.67	-366.28	212.33
2	0.5	0.66	-462.21	199.73
	0.8	0.14	-883.75	162.50
	1.2	0.68	-512.27	204.84
3	0.25	0.52	-487.13	196.46
	0.5	0.04	-1409.80	114.18
	0.8	0.12	-970.29	158.76

Table A6.4. VFT fit parameters for temperature dependence of the measured ionic conductivities for TEMPO derivative/ethaline solutions ($R_2 > 0.990$ for all solutions). T_o is the same as in Table A6.3. The VFT model, $\sigma = \sigma_o \exp (B\sigma/(T - T_o))$, was used to express temperature dependence of conductivity where σ is the conductivity (mS/cm) for temperature T (K), σ_o (mS/cm) is the pre-exponential, B_σ (K) is the activation temperature and T_o (K) is the ideal glass transition temperature obtained from the viscosity VFT fit.

$\sigma = \sigma_o \exp (B_\sigma/ (T-T_o))$			
Compound	**Concentration (M)**	σ_o **(mS cm^{-1})**	B_σ **(K)**
TEMPO	0.05	340.88	393.55
	0.10	411.77	429.59
	0.15	1747.82	902.01
4HT	0.5	533.98	564.86
	0.8	1902.82	867.42
	1.2	311.36	425.97
1	0.25	1296.52	725.90
	0.5	611.88	568.28
	0.8	243.94	368.80
2	0.5	367.59	427.25
	0.8	1589.92	824.71
	1.2	331.21	461.07
3	0.25	400.13	430.63
	0.5	7163.30	1347.60
	0.8	4152.81	767.82
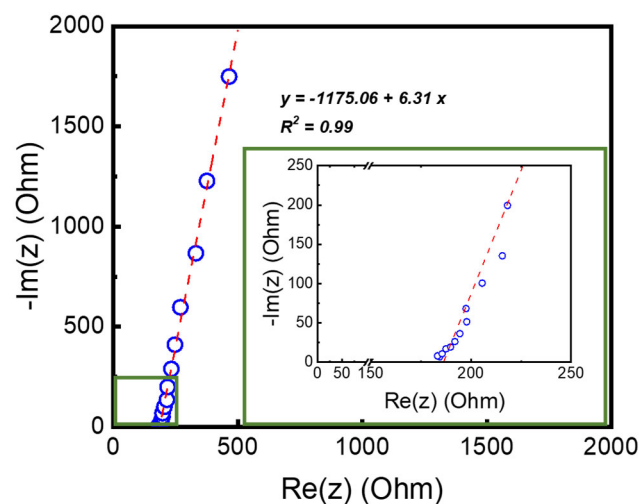
Figure A6.9. Nyquist plot for ethaline from electrochemical impedance spectroscopy. Voltage frequency range is 100 kHz - 100 Hz. Inset displays the x-intercept of the linear fit representing the bulk resistance for conductivity calculations. The x-intercept of the fitted line was taken as R_b, the resistance of the bulk solution. The ionic conductivity was then calculated using, $\sigma = d/R_bA =$ Cell Constant/R_b where d (cm) is the distance between the two parallel Pt electrodes, R_b (ohm) is the bulk resistance of the solution and A (cm^2) is the area of the Pt electrode. The ratio d/A constitutes the cell constant.

Table A6.5. Measured diffusion coefficients (D), cathodic ($E_{cathodic}$), anodic (E_{anodic}) limits, electrochemical windows (EW), oxidation (E_{ox}), and reduction (E_{red}) potentials of TEMPO derivatives for E1. All potentials are vs. Ag/AgCl and with a cut-off current density of 0.5 mA cm^{-2}. D was calculated using Randles-Sevcik equation from the 1st CV cycle (Figure A6.10) of 0.5 M solutions.

Compound	D x 10^{-8} (cm^2 s^{-1})	E_{anodic} (V)	$E_{cathodic}$(V)	EW (V)	E_{ox} (ox)	E_{red} (V)
4HT	4.37	+1.27	-1.96	3.23	+0.88	+0.71
1	1.48	+1.29	-1.99	3.28	+0.91	+0.74
2	2.43	+1.22	-1.71	2.93	+0.88	+0.73
3	1.44	+1.24	-1.27	2.51	+0.91	+0.75
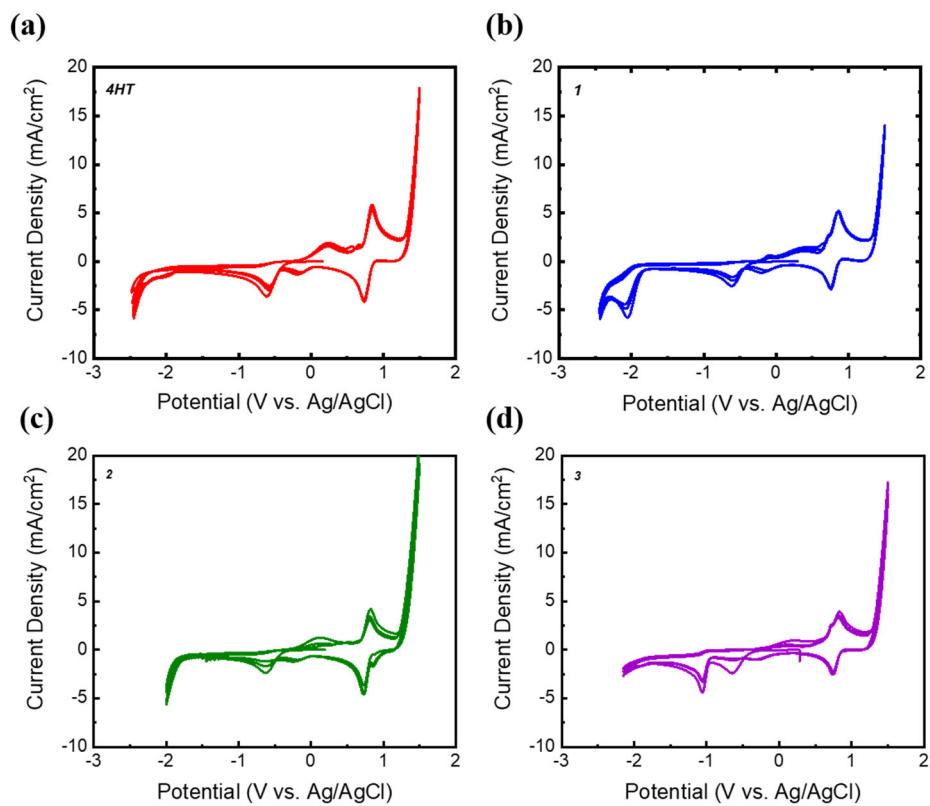
Figure A6.10. Electrochemical windows of 0.5 M concentration (a) 4HT, (b) compound **1**, (c) compound **2**, and (d) compound **3** dissolved in ethaline. Three full cycles are shown at a scan rate of 10 mV s⁻¹.
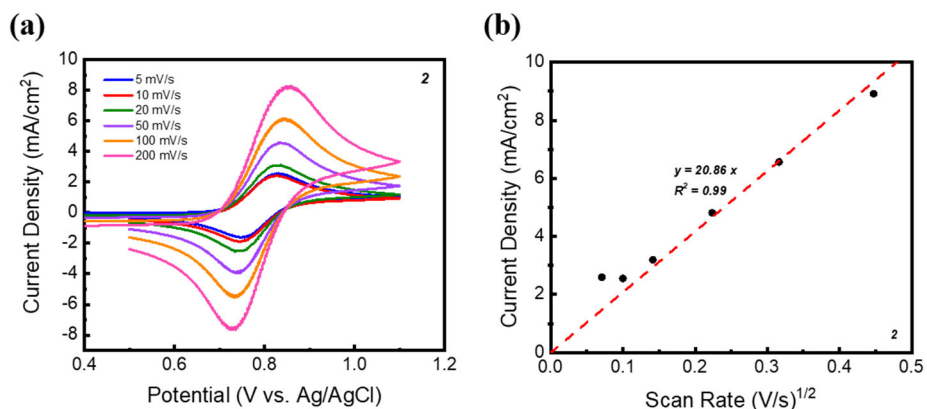
Figure A6.11. (a) CV of compound 2 (0. 5M in ethaline) at various scan rates; (b) Current density vs. square root of scan rate. The dashed line demonstrates the linear fit for the estimation of the diffusion coefficients according to Randles-Sevcik equation: $i_p = 0.4463nFAC (nFvD/RT)^{1/2}$ where A (cm^2) is the electro-active surface area of the working electrode (A = 0.0707 cm^2), C (mol cm^{-3}) is the bulk concentration of the redox-active small molecule salt, v (V s^{-1}) is the scan rate, D (cm^2 s^{-1}) is the diffusion coefficient of the redox active solute and i$_p$ (mA cm^{-2}) is the peak current density.
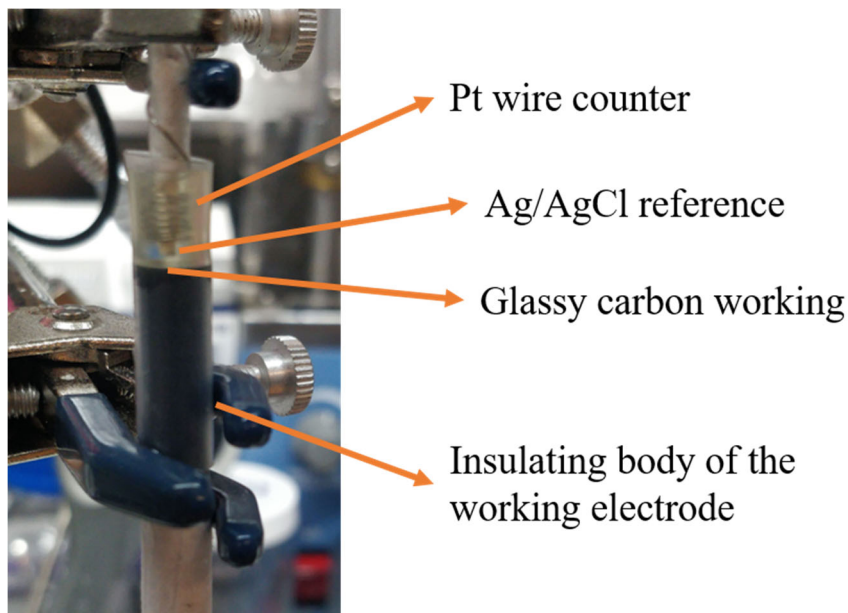
Figure A6.12. T-cell used for cyclic voltammetry. Shown is a Pt-wire coil counter electrode around the Ag/AgCl reference (separated by an insulator) on top of the disc glassy carbon working electrode. The liquid is housed in the reservoir on top of the working electrode created by heat shrink tube around the insulator body of the working electrode.

6.9   References

(173)   Luo, J.; Hu, B.; Hu, M.; Zhao, Y.; Liu, L. Status and Prospects of Organic Redox Flow Batteries toward Sustainable Energy Storage. ACS Energy Lett. 2019, 4, 2220–2240. https://doi.org/10.1021/acsenergylett.9b01332.

(197)   Nishide, H.; Iwasa, S.; Pu, Y. J.; Suga, T.; Nakahara, K.; Satoh, M. Organic Radical Battery: Nitroxide Polymers as a Cathode-Active Material. Electrochim. Acta 2004, 50 (2-3 SPEC. ISS.), 827–831. https://doi.org/10.1016/j.electacta.2004.02.052.

(198)   Winsberg, J.; Hagemann, T.; Janoschka, T.; Hager, M. D.; Schubert, U. S. Redox-Flow Batteries : From Metals to Organic Redox- Active Materials. Angew. Chemie - Int. Ed. 2017, 56, 686–711. https://doi.org/10.1002/anie.201604925.

(199)   Liu, T.; Wei, X.; Nie, Z.; Sprenkle, V.; Wang, W. A Total Organic Aqueous Redox Flow Battery Employing a Low Cost and Sustainable Methyl Viologen Anolyte and 4-HO-TEMPO Catholyte. Adv. Energy Mater. 2016, 6. https://doi.org/10.1002/aenm.201501449.

(200)   Chang, Z.; Henkensmeier, D.; Chen, R. Shifting Redox Potential of Nitroxyl Radical by Introducing an Imidazolium Substituent and Its Use in Aqueous Fl Ow Batteries. J. Power Sources 2019, 418 (February), 11–16. https://doi.org/10.1016/j.jpowsour.2019.02.028.

(205)   Janoschka, T.; Martin, N.; Hager, M. D.; Schubert, U. S. An Aqueous Redox-Flow Battery with High Capacity and Power : The TEMPTMA / MV System. Angew. Chemie - Int. Ed. 2016, 55, 14427–14430. https://doi.org/10.1002/anie.201606472.

(211)   Abbott, A. P.; Harris, R. C.; Ryder, K. S. Application of Hole Theory to Define Ionic Liquids by Their Transport Properties. J. Phys. Chem. B 2007, 111, 4910–4913. https://doi.org/10.1021/jp0671998.

(212)   Abbott, A. P. Application of Hole Theory to the Viscosity of Ionic and Molecular Liquids. ChemPhysChem 2004, 5 (8), 1242–1246. https://doi.org/10.1002/cphc.200400190.

(213)   Cardellini, F.; Germani, R.; Cardinali, G.; Corte, L.; Roscini, L.; Spreti, N.; Tiecco, M. Room Temperature Deep Eutectic Solvents of (1S)-(+)-10-Camphorsulfonic Acid and Sulfobetaines: Hydrogen Bond-Based Mixtures with Low Ionicity and Structure-Dependent Toxicity. RSC Adv. 2015, 5 (40), 31772–31786. https://doi.org/10.1039/c5ra03932k.

(214)   Reber, D.; Figi, R.; Kühnel, R. S.; Battaglia, C. Stability of Aqueous Electrolytes Based on LiFSI and NaFSI. Electrochim. Acta 2019, 321, 134644. https://doi.org/10.1016/j.electacta.2019.134644.

(215)   Manda, S.; Nakanishi, I.; Ohkubo, K.; Kawashima, T.; Matsumoto, K. I.; Ozawa, T.; Fukuzumi, S.; Ikota, N.; Anzai, K. Effect of Solvent Polarity on the One-Electron Oxidation of Cyclic Nitroxyl Radicals. Chem. Lett. 2007, 36 (7), 914–915. https://doi.org/10.1246/cl.2007.914.

(216)   Park, S. K.; Shim, J.; Yang, J. H.; Shin, K. H.; Jin, C. S.; Lee, B. S.; Lee, Y. S.; Jeon, J. D. Electrochemical Properties of a Non-Aqueous Redox Battery with All-Organic Redox Couples. Electrochem. commun. 2015, 59, 68–71. https://doi.org/10.1016/j.elecom.2015.07.013.

(217)   Stoyanovsky, A. D.; Stoyanovsky, D. A. 1-Oxo-2,2,6,6-Tetramethylpiperidinium Bromide Converts α -H N,N- Dialkylhydroxylamines to Nitrones via a Two-Electron Oxidation Mechanism. Sci. Rep. 2018, 8 (May), 15323. https://doi.org/10.1038/s41598-018-33639-w.

(218)   Lucio, A. J.; Shaw, S. K. Pyridine and Pyridinium Electrochemistry on Polycrystalline Gold Electrodes and Implications for CO2 Reduction. J. Phys. Chem. C 2015, 119 (22), 12523–12530. https://doi.org/10.1021/acs.jpcc.5b03355.

(219)   Escalante-García, I. L.; Wainright, J. S.; Thompson, L. T.; Savinell, R. F. Performance of a Non-Aqueous Vanadium Acetylacetonate Prototype Redox Flow Battery: Examination of Separators and Capacity Decay. J. Electrochem. Soc. 2015, 162 (3), A363–A372. https://doi.org/10.1149/2.0471503jes.

(220)   Hoyt, N. C.; Hawthorne, K. L.; Savinell, R. F.; Wainright, J. S. Plating Utilization of Carbon Felt in a Hybrid Flow Battery. J. Electrochem. Soc. 2016, 163 (1), A5041–A5048. https://doi.org/10.1149/2.0061601jes.

(221)   Angelin, M.; Hermansson, M.; Dong, H.; Ramstrom, O. Direct, Mild, and Selective Synthesis of Unprotected Dialdo-Glycosides. European J. Org. Chem. 2006, No. 19, 4323–4326. https://doi.org/10.1002/ejoc.200600288.

(222)   Wu, X.-E.; Ma, L.; Ding, M.; Gao, L. TEMPO-Derived Task-Specific Ionic Liquids for Oxidation of Alcohols. Synlett 2005, 4, 607–610. https://doi.org/10.1055/s-2005-862396.

(223)   Miao, C.; Wang, J.; Yu, B.; Cheng, W.; Sun, J.; Chanfreau, S.; He, L.-N.; Zhang, S.-J. Synthesis of Bimagnetic Ionic Liquid and Application for Selective Aerobic Oxidation of Aromatic Alcohols under Mild Conditions. Chem. Commun. 2011, 47, 2697–2699. https://doi.org/10.1039/c0cc04644b.

(224)   Shen, D.; Steinberg, K.; Akolkar, R. Avoiding Pitfalls in the Determination of Reliable Electrochemical Kinetics Parameters for the Cu 2+ → Cu 1+ Reduction Reaction in Deep Eutectic Solvents. J. Electrochem. Soc. 2018, 165 (14), E808–E815. https://doi.org/10.1149/2.1011814jes.

(225)   Selverston, S.; Nagelli, E.; Wainright, J. S.; Savinell, R. F. All-Iron Hybrid Flow Batteries with In-Tank Rebalancing. J. Electrochem. Soc. 2019, 166 (10), A1725–A1731. https://doi.org/10.1149/2.0281910jes.

Part II: The Incorporation of Redox Small Molecules into Deep Eutectic Solvents for the Development of New Electrolytes

Chapter 7

Synthesis of Phenothiazine Derivatives as a Redox Active Species in

Deep Eutectic Solvents for Energy Storage

Contributions:
Sarah Mitchell – Synthesis, characterization, and solubility studies
Nicholas Sinclair – Electrochemical behavior

7.1 Introduction

The concept of incorporating redox active small molecules into deep eutectic solvents (DESs) for the development of new electrolytes can be applied to many redox active species, both inorganic and organic. This chapter will discuss the potential of phenothiazine (PHZ) as a redox active moiety in DES and the synthesis of PHZ derivatives. PHZ is a heterocyclic thiazine composed of three fused rings (Figure 7.1) that has been used in multiple applications ranging from pharmaceuticals to insecticides.[207,226–228] The structure of PHZ allows for easy synthetic modification of the parent compound, which can tune both the redox behavior and solubility. For example, when substituents are added to the nitrogen atom (R_{10}) only solubility is affected and when substituents are added to the R_3 and R_7 position the electrochemical behavior is affected (e.g., redox potential).[208,209] The tunability of PHZ makes it an attractive candidate for a redox active species to incorporate into DES.

Similar to TEMPO, PHZ has the potential to undergo a two electron transfer.[206,207,229–231] In most electrolytes, PHZ exhibits a single reversible electron transfer, where oxidation generates a radical cation and reduction regenerates the neutral PHZ species.[207,208] However, in CV when a larger sweep width is used, a second electron transfer is possible in aprotic solvents (Scheme 7.1). This second electron transfer forms a radical dication from the radical cation, where a positive charge
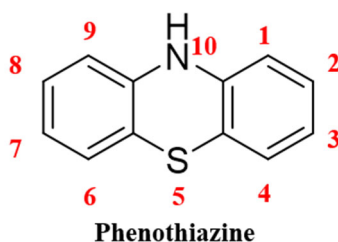
Figure 7.1. Structure of phenothiazine and numerical labels for positions of derivatization.
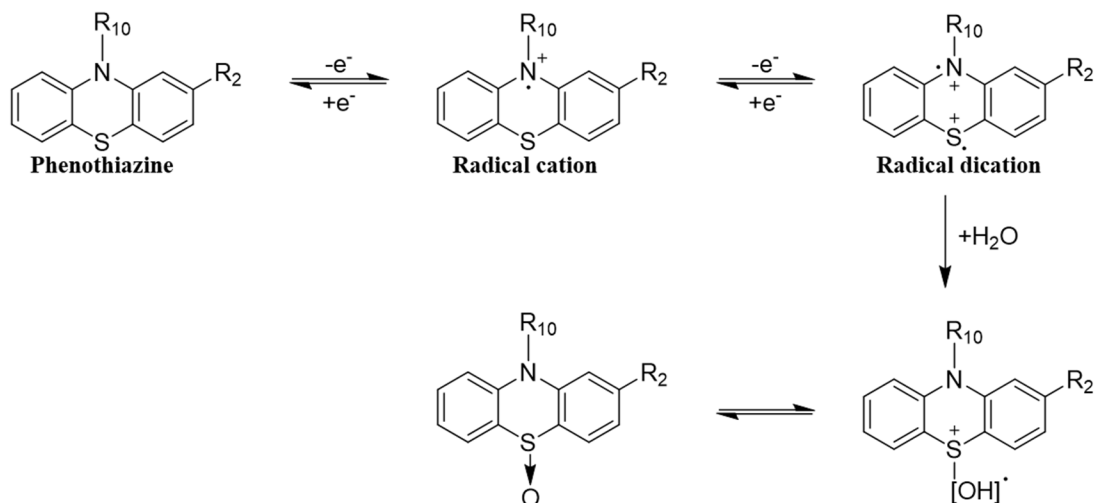
Scheme 7.1. Redox behavior of PHZ. Formation of radical cation then radical dication, followed by the irreversible reaction of the radical dication with water.

is on both the sulfur and nitrogen atoms. The radical dication can react with water, where the sulfur atom forms an irreversible bond with the oxygen atom (e.g., gets irreversibly oxidized). Both cationic radicals can be stabilized by substituents, acidity of the electrolyte, and addition of various salts.[207]

7.2   Approach

A similar approach from the TEMPO study described in Chapter 6 was used to synthesize a library of PHZ derivatives to alter their solubility.[232] However, unlike TEMPO, the redox properties of the species can be tuned, so the electrochemistry of the molecules was examined first, without attempts to maximize solubility.   The derivatives selected to synthesize vary the substituent identity and the position of the substituents to gather insight into how the derivatives impact the electrochemistry and solubility. Also, the amount of each derivative was streamlined for initial experiments, so minimal amount of a derivative was initially required. If a derivative performed

well electrochemically, then solubility studies were performed. Overall, this approach provides

insight into the feasibility of PHZ derivatives as a redox active species in a DES.

7.3   Synthesis of Phenothiazine Derivatives

PHZ is commercially available and was the starting material for all PHZ derivatives. Substituents

were initially added in the R_{10} position, i.e., off of the nitrogen atom. The first two compounds

synthesized were ethyl-phenothiazine (EPT, Scheme 7.2a) and methoxyethyl-phenothiazine

(MEPT, Scheme 7.2b), each following a similar synthetic route.[230] For EPT, PHZ was dissolved

in a round bottom flask with dry tetrahydrofuran (THF). Sodium hydride was added and the

reaction was stirred for ~30 minutes. Ethylbromide was then added, the reaction was heated to

60°C, and stirred overnight. The product was easily purified via column chromatography and an

off-white solid was obtained. Similarly, for MEPT, PHZ was dissolved in a round bottom flask

with dry dimethylformamide (DMF). Sodium hydride was added and the reaction was stirred for

~30 minutes. 2-Chloroehtyl methyl ether was added, the reaction flask heated to 60°C, and stirred
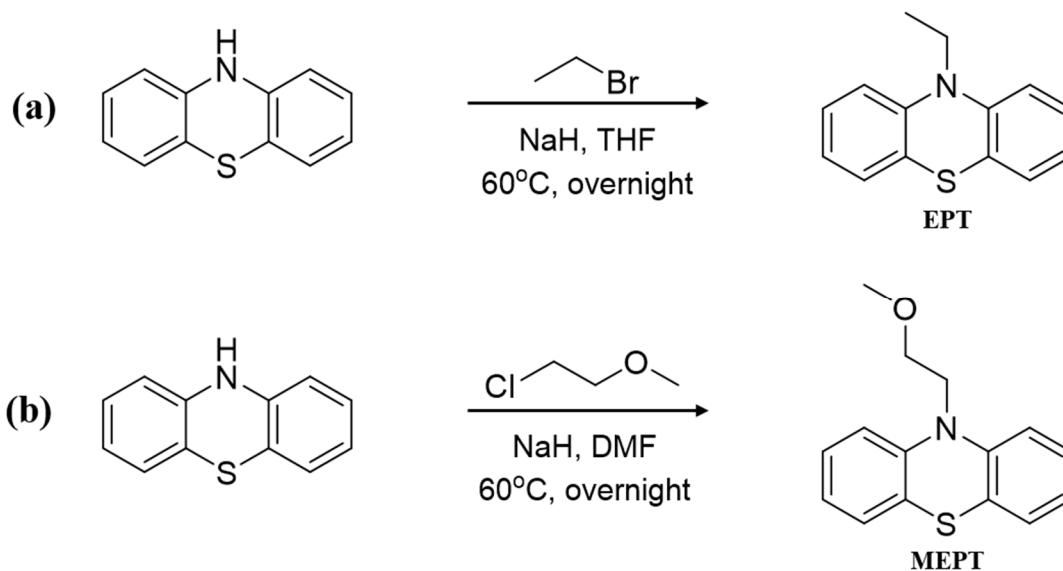
Scheme 7.2. Synthesis of (a) EPT and (b) MEPT.

overnight. The product was then purified via column chromatography and an off-white solid was again obtained. Both EPT and MEPT were synthesized on the gram scale, demonstrating ease of accessibility.

The next PHZ derivatives of interest were those with substituents at the R_3 and R_7 positions, specifically addition of methoxy groups. To add methoxy groups, a brominated intermediated was first synthesized (MEPT-Br, Scheme 7.3a).[208] MEPT was dissolved in a round bottom flask with dry dichloromethane (DCM) and cooled to 0°C in an ice water bath. A solution of *N*-bromosuccinimde (NBS) in DCM was then added dropwise. The reaction was stirred for 60 minutes and monitored with thin layer chromatography. After complete consumption of MEPT, MEPT-Br was purified via column chromatography and a blue solid was obtained. This reaction was consistent and could be run on the gram scale. This reaction was also performed with EPT to form EPT-Br following the same approach (Scheme 7.3b).

Substition of the bromides for methoxy groups was more difficult and many reaction conditions were evaluated. The general procedure for the synthesis of dimethoxy-MEPT (DMeMEPT) is shown in Scheme 7.3a: MEPT-Br was added to a round bottom flask with a 5 M solution of sodium methoxide in methanol and dry pyridine at room temperature.[208,209,233–235] Then the reaction was
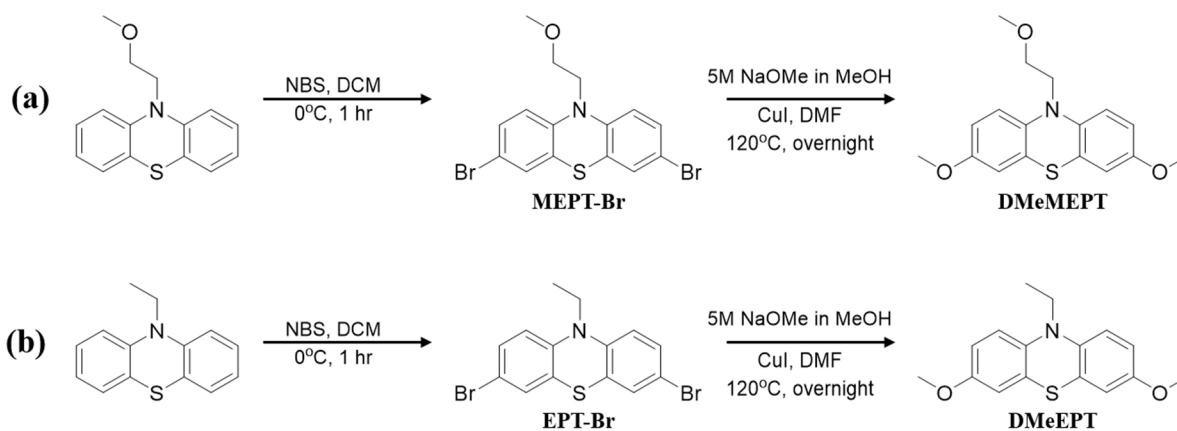
Scheme 7.3. Synthesis of (a) DMeMEPT and (b) DMeEPT.

heated to 120°C, CuI was added, and the reaction was stirred for 4 hours. This product has been difficult to purify and appears to degrade on the column, however crude ESI mass spec confirms that the product has been synthesized. The same limitations were met during the synthesis of EPT-Br (Scheme 7.3b).

Another set of PHZ derivatives selected to synthesize contain hydrogen bonding (H-bonding) groups, specifically an alcohol and amine, as pendant groups on the nitrogen atom. Synthesis of ethanol-PHZ (PHZ-OH) was a two-step process (Scheme 7.4). PHZ was dissolved in a round bottom flask with dry DMF. Sodium hydride was added and the reaction was stirred for 30 minutes. Methyl 3-bromopropionate was added, the reaction was heated to 60°C, and stirred overnight. The intermediate was purified via column chromatography then dissolved in diethyl ether and reacted with lithium aluminum hydride (LiAlH$_4$) to reduce the ester to an alcohol.[236] The reaction was stirred overnight at room temperature and quenched by the dropwise addition of water. PHZ-OH was obtained as an off-white solid and was purified by washing with diethyl ether.
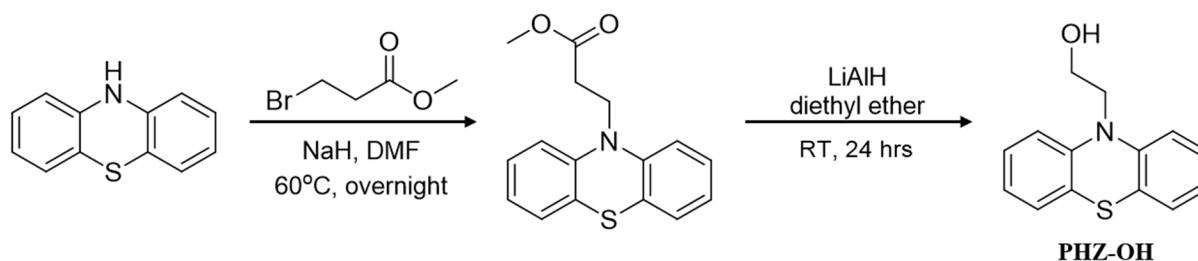
Scheme 7.4. Formation of PHZ-OH from the reduction of an ester.

Synthesis of propylamine-PHZ (PHZ-NH$_2$) was less straightforward, since amines are notoriously more difficult to work with and many reaction conditions were examined. The first route explored to obtain PHZ-NH$_2$ utilized a protected amine. A reaction to modify PHZ was prepared by
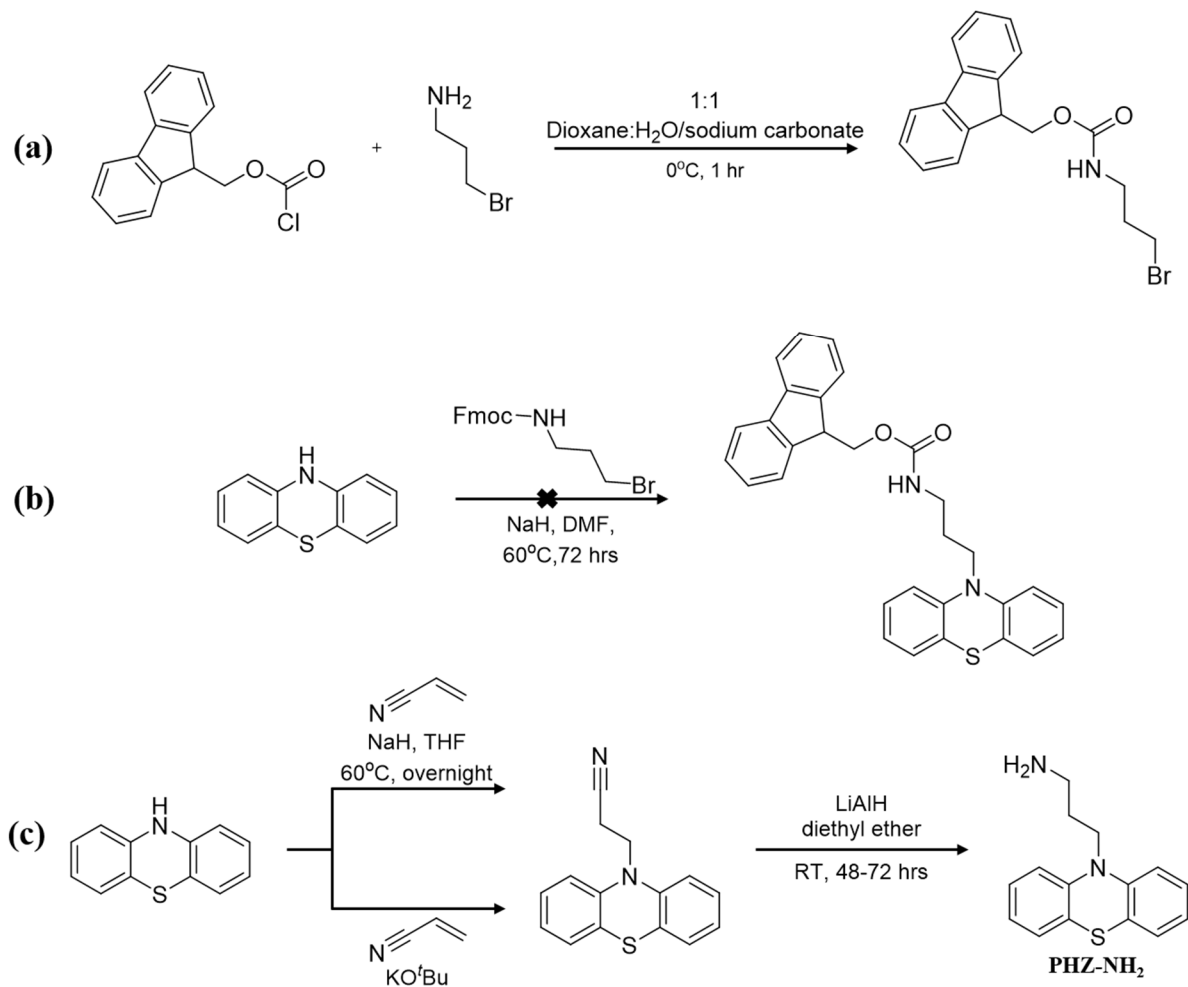
Scheme 7.5. Routes to prepare PHZ-NH$_2$. (a) Preparation of Fmoc protected amine (b) Use of Fmoc protected amine, (c) Formation and reduction of nitrile intermediate.

dissolving 9-Fluorenylmethoxycarbonyl (Fmoc) chloride in a 1:1 solution of 1,4-dioxane and sodium carbonate/water, cooling the solution to 0 °C, and adding 3-bromopropylamine, then stirring the reaction for 1 hour (Figure 7.5a).[237] The Fmoc protected amine was purified by recrystallization. To add the Fmoc protected amine to PHZ, initially sodium hydride deprotonation of PHZ was attempted, however this was unsuccessful (Scheme 7.5b). We hypothesize that the steric demands of the Fmoc group prevents the reaction from proceeding.

An alternative route to prepare PHZ-NH$_2$ was more similar to the synthesis of PHZ-OH, where an intermediate is formed and then the pendant group is reduced; to prepare PHZ-NH$_2$ the intermediate contained a pendant nitrile (Scheme 7.5c). To form this nitrile containing intermediate, two different pathways could be performed. In the first pathway, PHZ was dissolved in dry THF in a round bottom flask and sodium hydride was added. Once the solution stirred for 30 minutes, acrylonitrile was added and the reaction was stirred overnight at room temperature.[238] Here a Michael type addition took place. The nitrile containing intermediate was purified via column chromatography. The second pathway to form the nitrile intermediate is as follows: PHZ and acrylonitrile were added to round bottom flask and dissolved in THF. Potassium *tert*-butoxide was then added and the reaction stirred for 10-30 minutes.[239] The intermediate could then be purified via column chromatography. Both pathways led to the successful synthesis the nitrile intermediate. To form the final product, PHZ-NH$_2$, the nitrile intermediate was dissolved in diethyl ether and reacted with lithium aluminum hydride; the reaction was stirred for 24-48 hours and the product was purified.[240]

A variety of additional PHZ derivatives were synthesized, guided by initial evaluation of the electrochemical behavior of the derivatives discussed above. The first being an amide containing PHZ derivative. Several pathways were evaluated, the first used potassium tert-butoxide and acrylamide with PHZ to form PHZ-amide (Scheme 7.6a).[239] This pathway was attempted several times, each altering the reaction conditions (reaction time, temperature, solvent vs. neat). Though ESI mass spec confirms the product, the PHZ-amide product could not be purified and thus the electrochemical properties were not studied. We hypothesized that the acidity of the N-H bonds of acrylamide may prevent the reaction from taking place. Thus, a similar pathway was attempted with *N,N*-dimethylacrylamide, however similar issues with product purification were observed
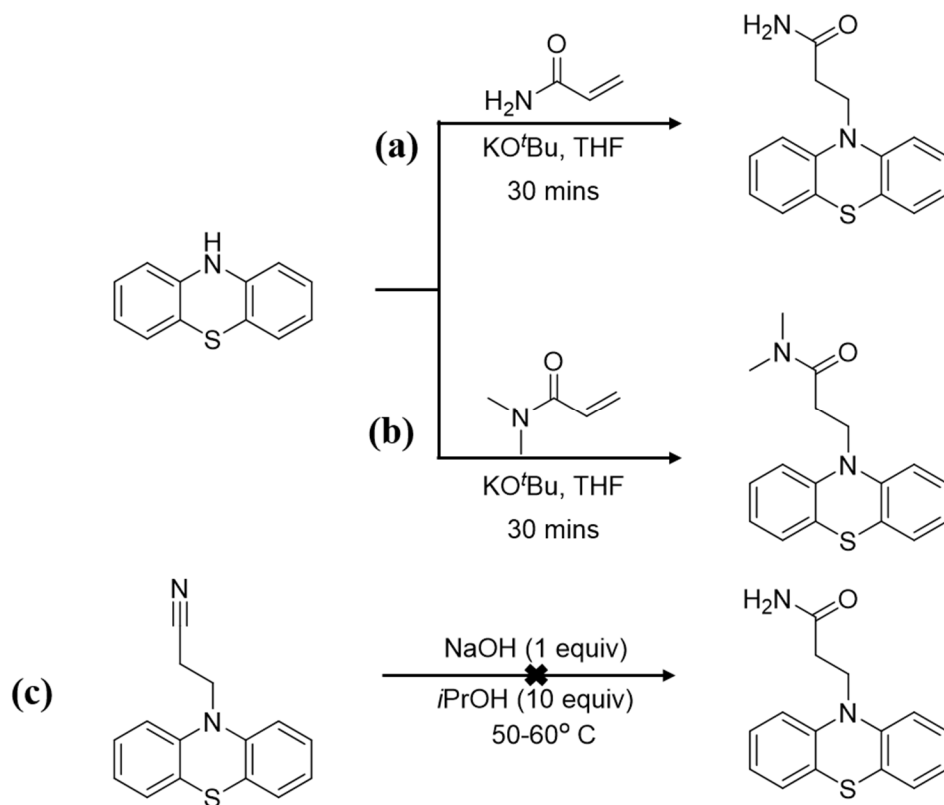
Scheme 7.6. Synthesis of PHZ-amide derivatives. (a) With pendant primary amide, (b) With pendant *N,N*-dimethyl amide, (c) Alternative route to pendant primary amide.

(Scheme 7.6b). An alternative pathway to form the PHZ-amide started from the nitrile intermediate and used sodium hydroxide in isopropanol, however this pathway was unsuccessful and the product was not formed, as indicated by only starting material in ^{1}H NMR (Scheme 7.6c).[241]

The final PHZ derivative synthesis was PHZ-diethanolamine (Scheme 7.7a). Here, the goal is to increase the H-bonding capabilities of the molecule by incorporation of a tertiary nitrogen and two primary alcohols. PHZ was added round bottom flask and dissolved in dry THF.[242] Sodium hydride was added and the reaction stirred for 30 minutes. 1-bromo-3-chloropropane was added, the reaction was heated to 60°C and stirred for 4 hours. The intermediate was purified via liquid-
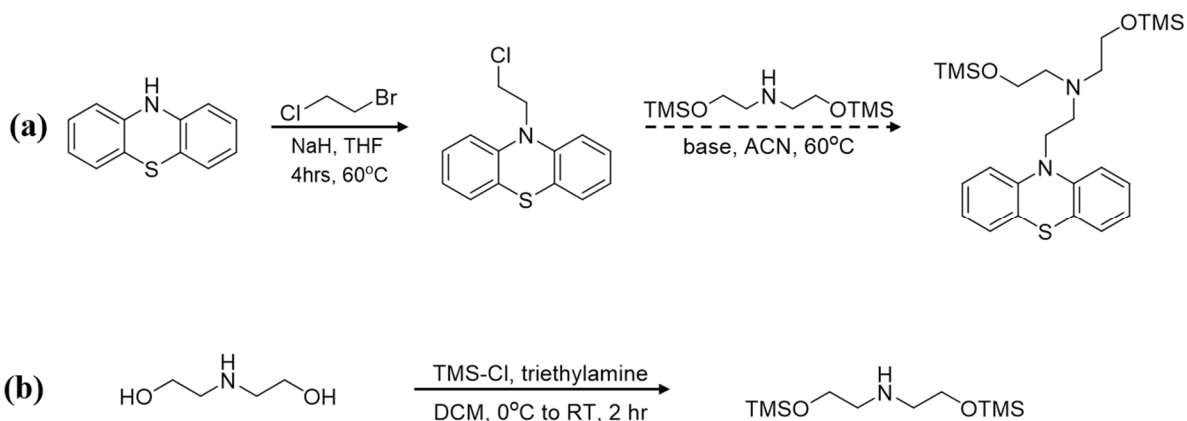
Scheme 7.7. (a) Synthesis of PHZ-diethanolamine and (b) protection of alcohol.

liquid extraction then solvent was removed under reduced pressure. Prior to adding the diethanolamine, the alcohol groups were protected. This was done by reacting diethanolamine with trimethylsilyl chloride and triethylamine in DCM (Scheme 7.7b).[243,244] The alcohols are converted to trialkylsilanes so they could be easily converted back to an alcohol groups. Ongoing work leverages the secondary amine for nucleophilic substation of the chloride with the use of a base.

7.4   Solubility Study of Phenothiazine Derivatives

Similar to the TEMPO derivatives, the maximum solubility of PHZ in DES was determined using UV-vis absorption spectroscopy.[232] A calibration curve was made from five solutions of known concentration in DMSO and a saturated sample of PHZ was made with ethaline (1:2 choline chloride:ethylene glycol). The maximum solubility of PHZ was determined to be 1.008 M. This same process was attempted for EPT and MEPT, however even with very low concentrations of the derivatives the UV-vis was too saturated to obtain valuable data for the calibration curve. However, in the saturated samples with ethaline, visibly EPT was minimally soluble in ethaline and MEPT-Br was insoluble in ethaline; which was expected for these two derivatives both lacking

H-bonding moieties. Of the H-bonding derivatives evaluated (PHZ-OH and PHZ-NH$_2$), PHZ-OH exhibited moderate solubility, however the sample needed longer times to dissolve. On the other hand, PHZ-NH$_2$ was extremely soluble and was a contributing factor synthesizing additional nitrogen containing derivatives. As expected these derivatives exhibited higher solubility due to the H-bonding moieties in the R$_{10}$ position on the parent compound.

7.5   Electrochemical Characteristics

The redox behavior of PHZ in an ethaline solution of (1:4 choline chloride:ethylene glycol) was examined using cyclic voltammetry (CV, Figure 7.2). Of note, this composition of ethaline was chosen due to its lower viscosity than the 1:2 ratio mixture.   This work was performed by collaborators (Nicholas Sinclair, Case Western Reserve University Department of Chemical
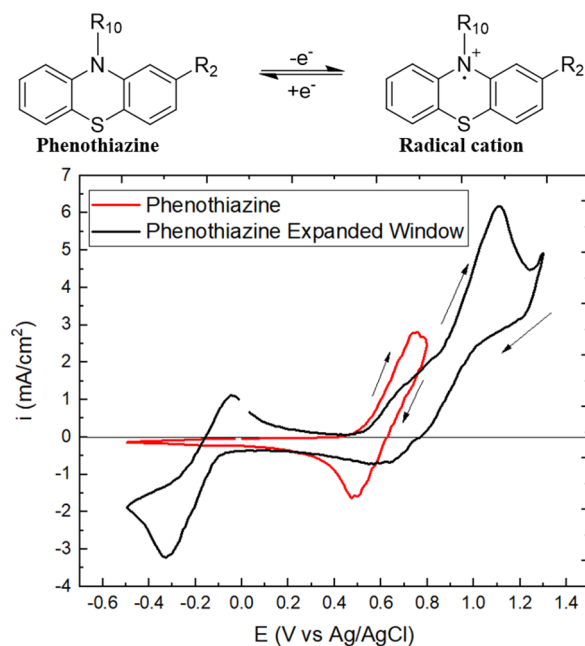
Figure 7.2. Cyclic voltammetry of 0.1 M PHZ in 1:4 choline chloride:ethylene glycol. Sweep width: red (-0.5-0.8 V) and black (-0.5-1.3 V), scan rate 100 mV/s, 1.6 mm Pt disk (W), Ag/AgCl (R).

Engineering). A similar trend was observed as in literature, that if a larger sweep width was used, two electron transfers occur when performed in acetonitrile or propylene carbonate.[208,209] The red curve in Figure 7.2 used a sweep width of -0.5-0.8 V vs Ag/AgCl and a single electron transfer at 0.5 V vs Ag/AgCl was observed, which is associated with the oxidation of PHZ to a radical cation and reduction of the reverse reaction. When expanded to a sweep width of -0.5-1.3 V vs Ag/AgCl, two electron transfers are observed, one at 1.0 and the other at -0.3 V vs Ag/AgCl, where the latter is reversible.

Figure 7.3 shows the CV data for select PHZ derivatives in the 1:4 ChCl:EG, including PHZ, EPT, MEPT, and PHZ-NH$_2$. Perhaps surprisingly, each derivative exhibited different electrochemical behavior, supporting the idea of synthetically modifying PHZ to tune the electrochemical
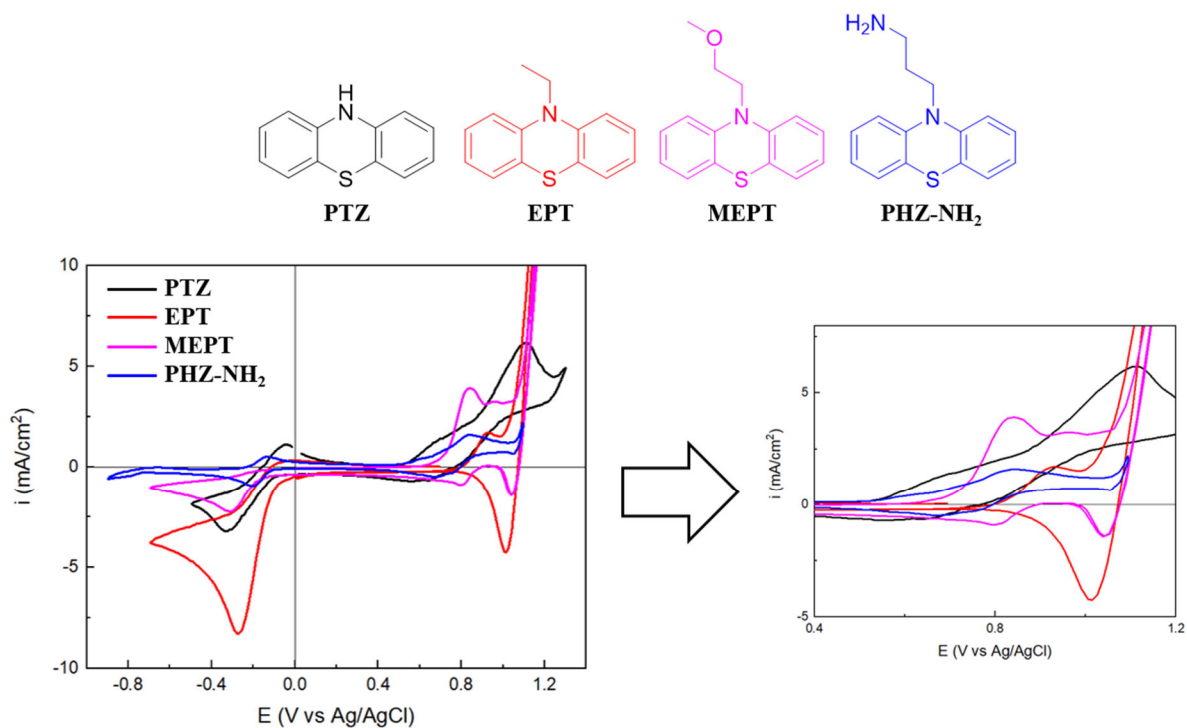
Figure 7.3. Cyclic voltammetry of select PHZ derivatives (0.1 M) in 1:4 choline chloride:ethylene glycol. Scan rate 100 mV/s, 1.6 mm Pt disk (W), Ag/AgCl (R).
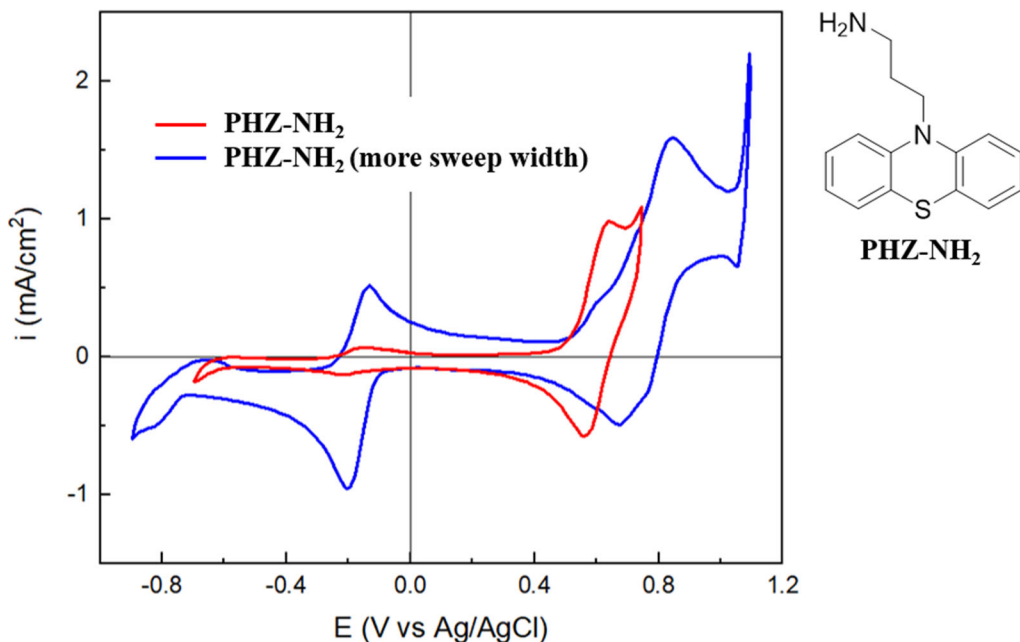
Figure 7.4. Cyclic voltammetry of select PHZ-NH$_2$ at a small (red) and large (blue) sweep width at 0.1 M in 1:4 choline chloride:ethylene glycol. Scan rate 100 mV/s, 1.6 mm Pt disk (W), Ag/AgCl (R).

properties of the derivative. Of the four derivatives, PHZ-NH$_2$ was the most interesting, due to the extremely reversible negative redox couple (-0.2 V vs Ag/AgCl).

Of the PHZ derivatives examined, PHZ-NH$_2$ was the first compound that exhibited a reversible negative couple. More thorough studies PHZ-NH$_2$ were performed to identify the species formed. Figure 7.4 shows the comparison of PHZ-NH$_2$ with small and large sweep width. When the sweep width was expanded, the negative redox couple at -0.3 V vs Ag/AgCl was observed. This electrochemical behavior and high solubility of PHZ-NH$_2$ led to the development of additional nitrogen containing PHZ derivatives. Ongoing work addresses the electrochemical behavior of these PHZ derivatives.

7.6 Summary

In summary, PHZ derivatives were synthesized modifying PHZ at the R_{10}, R_3, and R_7 positions to evaluate the impact on solubility and electrochemical behavior. Thus far, PHZ-NH$_2$ is the most promising derivative for use as a redox active unit in the DES ethaline, as it exhibits a highly reversible negative redox, and it is the first derivative to do so. The promising performance of PHZ-NH$_2$ led to the synthesis of additional nitrogen containing PHZ derivatives, specifically PHZ-amides, which must be purified before they can be evaluated. Current work is also examining the use of PHZ derivatives as one component in a mixed system, so two redox active small molecules will be present.

7.7 Appendix

General Considerations. All purchased chemicals were used directly as received, unless otherwise stated. All reactions were performed under an inert atmosphere. DCM and THF were obtained by passing the commercial grade solvent through a double filter column in a MBRAUN SPS compact system. Diethyl ether was passed through a basic alumina column and stored over molecular sieves. All ^{1}H and ^{13}C NMR were collected on a Bruker Advance Neo console 400 MHz NMR with an Ascend magnet and automated tuning 5mm broadband iProbe, with CDCl$_3$ as the solvent unless otherwise noted. FTIR spectra were acquired using a JASCO FT/IR-4000 with ATR attachment. ESI spectra were obtained on a Thermo Scientific Q Exactive Focus or a Thermo Scientific DSQ II GC-MS.

Synthesis of EPT. An oven-dried round bottom flask was purged with N$_2$(g) and vacuum three times. Phenothiazine (2 g, 0.01 mol) and anhydrous THF (30 mL) was added and the phenothiazine dissolved. Sodium hydride (0.26 g, 0.011 mol) was added and the reaction stirred for 30 minutes with a vent needle to allow for hydrogen gas evolution. The vent needle was

removed and ethylbromide (0.82 mL, 0.011 mol) was added to the reaction flask. The solution was heated to 60°C and stirred overnight. Upon completion, the reaction was quenched with water (30 ml) and washed 3 times with hexanes (20 mL). The organic layers were combined and dried with magnesium sulfate, the solvent was removed under reduced pressure. The product was purified by recrystallization with ethanol.

Synthesis of MEPT. An oven-dried round bottom flask was purged with $N_2(g)$ and vacuum three times. Phenothiazine (1.99 g, 0.0099 mol) and anhydrous DMF (20 mL) was added and the phenothiazine dissolved. Sodium hydride (0.29g, 0.012 mol) was added and the reaction stirred for 30 minutes with a vent needle to allow for hydrogen gas evolution. The vent needle was removed and 2-chloroethyl methyl ether (1.09 mL, 0.012 mol) was added to the reaction flask. The solution was heated to 60°C and stirred overnight. Upon completion, the reaction was quenched with water (20 ml) and washed 3 times with ethyl acetate (20 mL). The organic layers were combined and washed with 20 mL saturated aqueous NaCl. The organic layers were dried with magnesium sulfate and solvent removed under reduced pressure. The product was then purified via column chromatography.

Synthesis of MEPT-Br. An oven-dried round bottom flask was purged with $N_2(g)$ and vacuum three times. In the flask, MEPT (0.5 g, 0.0019 mol) was dissolved in anhydrous DCM (15 mL) and the mixture cooled to 0°C with an ice water bath. A solution of *N*-bromosuccinimide (1.03 g, 0.0058 mol) and DCM (5mL) was then added dropwise. The reaction was stirred for 60 minutes and monitored with thin layer chromatography. Once, complete consumption of MEPT was observed the reaction was quenched with aqueous sodium thiosulfate (0.8 g in 20 mL water). The solution was diluted with 20 mL DCM and washed with 30 mL water and 30 mL saturated aqueous NaCl. The organic layer was dried with magnesium sulfate and solvent removed under

reduced pressure. MEPT-Br was purified via column chromatography and a blue solid was obtained.

Synthesis of DMeMEPT. An oven-dried round bottom flask was purged with $N_2(g)$ and vacuum three times. MEPT-Br (0.5 g, 0.0012 mol), a 5 M solution of sodium methoxide in methanol (2.5 mL, 0.012 mol), and dry pyridine (15 mL) was added. The mixture was then heated to 120°C. CuI (0.46 g, 0.0024 mol) was added and the reaction was stirred for 4 hours. The reaction was quenched with 20 mL brine and 20 mL DCM. The brine layer was washed with 20 mL DCM. The organic layers were combined, dried with sodium sulfate, and the solvent was removed under reduced pressure.

Synthesis of PHZ-OH. An oven-dried round bottom flask was purged with $N_2(g)$ and vacuum three times. In the flask, phenothiazine (2 g, 0.01 mol) was dissolved in anhydrous DMF (30 mL). Sodium hydride (0.29 g, 0.012 mol) was added and the reaction stirred for 30 minutes with a vent needle to allow for hydrogen gas evolution. The vent needle was removed and methyl 3-bromopropionate (1.31 mL, 0.012 mol) was added, the reaction was heated to 60°C, and stirred overnight. Upon completion, the reaction was quenched with water (50 ml) and washed 3 times with ethyl acetate (20 mL). The organic layers were combined and dried with magnesium sulfate, solvent was removed under reduced pressure. The intermediate was purified via column chromatography. In an oven-dried round bottom flask purged with $N_2(g)$ and vacuum (3x), the intermediate (0.3 g, 0.0011 mol) was dissolved in diethyl ether (6 mL). Lithium aluminum hydride (LiAlH$_4$) (0.12 g, 0.0032 mol) was added and the reaction was stirred overnight at room temperature. Upon full consumption of the intermediate, the reaction was quenched by the dropwise addition of water. The solution was diluted with ether (20 mL) and washed with 25 mL 15% aqueous NaOH. The water layer was washed with ether (2 x 20 mL). The organic layers

were combined and washed with 20 mL water and dried with magnesium sulfate. The solvent was removed under reduced pressure to obtain the product.

Protection of Fmoc Amine Procedure. In a round bottom flask, 9-fluorenylmethoxycarbonyl chloride (1.42 g, 0.0055 mol) was dissolved in a 1:1 solution of 1,4-dioxane (15 mL) and sodium carbonate/water (1.68 g in 15 mL water). The reaction flask was cooled to 0 °C with an ice water bath and 3-bromopropylamine (1 g, 0.0046 mol) was added and the reaction stirred for 1 hour. The reaction was quenched with 50 mL ethyl acetate and the layers were separated. The water layer was washed with 20 mL ethyl acetate. The organic layers were combined and washed with 25 mL saturated aqueous $NaHCO_2$ and then dried with magnesium sulfate. The solvent was removed under reduced pressure. The Fmoc protected amine was purified by recrystallization in 4:6 DCM:hexanes.

Synthesis of PHZ-CN (1). An oven-dried round bottom flask was purged with $N_2(g)$ and vacuum three times. In the flask, phenothiazine (0.5 g, 0.0025 mol) was dissolved in anhydrous THF (10 mL). Sodium hydride (0.072 g, 0.003 mol) was added and the reaction stirred for 30 minutes with a vent needle to allow for hydrogen gas evolution. The vent needle was removed and acrylonitrile (0.20 mL, 0.003 mol) was added, the reaction stirred overnight at room temperature. Upon completion, the reaction was quenched with water (20 ml) and washed 2 times with ethyl acetate (20 mL). The organic layers were combined and washed with 20 mL saturated aqueous NaCl. The organic layers were dried with magnesium sulfate and solvent removed under reduced pressure. The intermediate was purified via column chromatography.

Synthesis of PHZ-CN (2). In an oven-dried round bottom flask under $N_2(g)$, phenothiazine (1 g, 0.005 mol) and acrylonitrile (1 mL, 0.015 mol) were dissolved in anhydrous THF (2mL). Potassium *tert*-butoxide (0.1 g, 5 mol %) was added and the reaction stirred for 10-30 minutes at

room temperature. Once complete the reaction was stored in the fridge overnight and purified via column chromatography.

Synthesis of PHZ-NH$_2$.   In an oven-dried round bottom flask purged with N$_2$(g) and vacuum (3x), PHZ-CN (0.5 g, 0.002 mol) was dissolved in diethyl ether (20 mL). LiAlH4 (0.23 g, 0.006 mol) was added and the reaction was stirred for 24-48 hours at room temperature. Upon full consumption of PHZ-CN, the reaction was quenched by the dropwise addition of water. The solution was diluted with ether (20 mL) and washed with 25 mL 15% aqueous NaOH. The water layer was washed with ether (2 x 20 mL). The organic layers were combined and washed with 20 mL water and dried with magnesium sulfate. The solvent was removed under reduced pressure to obtain the product.

Synthesis of PHZ Amides.   In an oven-dried round bottom flask under N$_2$(g), phenothiazine (1 g, 0.005 mol) and acrylamide (1.07 g, 0.015 mol) were dissolved in THF. Potassium *tert*-butoxide (0.1 g, 5 mol %) was added and the reaction stirred for 10-30 minutes at room temperature. Remove solvent under reduced pressure and dissolve in minimal DCM. Precipitate in hexanes and filter and dry solid.

Protection of Alcohol Procedure.   In an oven-dried round bottom flask purged with N$_2$(g) and vacuum (3x), diethaneolamine (1 mL, 0.01 mol) and anhydrous DCM (15 mL) was added to the flask. Triethylamine (3.65 mL, 0.026 mol) was added and the flask cooled to 0°C with an ice bath. Trimethylsilyl chloride (2.65 mL, 0.02 mol) was added dropwise and the reaction was warmed to room temperature and stirred for 2 hours. The reaction was quenched with 20 mL water and 20 mL DCM. The water layer was washed with DCM (2 x 10 mL). The organic layers were combined and washed with 20 mL water and 20 mL saturated aqueous NaHCO$_3$ and then dried with sodium sulfate. The solvent was removed under reduced pressure.

Synthesis of PHZ diethanolamine Intermediate. In an oven-dried round bottom flask purged with $N_2(g)$ and vacuum (3x), phenothiazine (1 g, 0.005 mol) was dissolved in anhydrous THF (20 mL). 1-Bromo-3-chloropropane (0.5 mL, 0.006 mol) was added and the reaction was heated to 60°C for 4 hours. Upon completion, the reaction was quenched with water (20 ml) and washed 2 times with ethyl acetate (20 mL). The organic layers were combined and washed with 20 mL saturated aqueous $NaHCO_3$. The organic layers were dried with sodium sulfate and solvent removed under reduced pressure.

Maximum Solubility Measurements. Solubility limit of phenothiazine in ethaline were determined by calibration curves obtained from UV-Vis. Five solutions of pre-determined concentration were made for each compound in DMSO. The UV-vis spectra were obtained from 200-800 nm. The calibration curves were plotted at a specific absorption wavelength for each compound. To make the concentrated sample, phenothiazine was added to ethaline (0.5mL) and heated on a hot plate. This process was repeated till solid remained present in solution. The saturated samples were cooled to room temperature and stood for at least one hour. A solution was made with DMSO and UV-vis obtained from 200-800 nm.
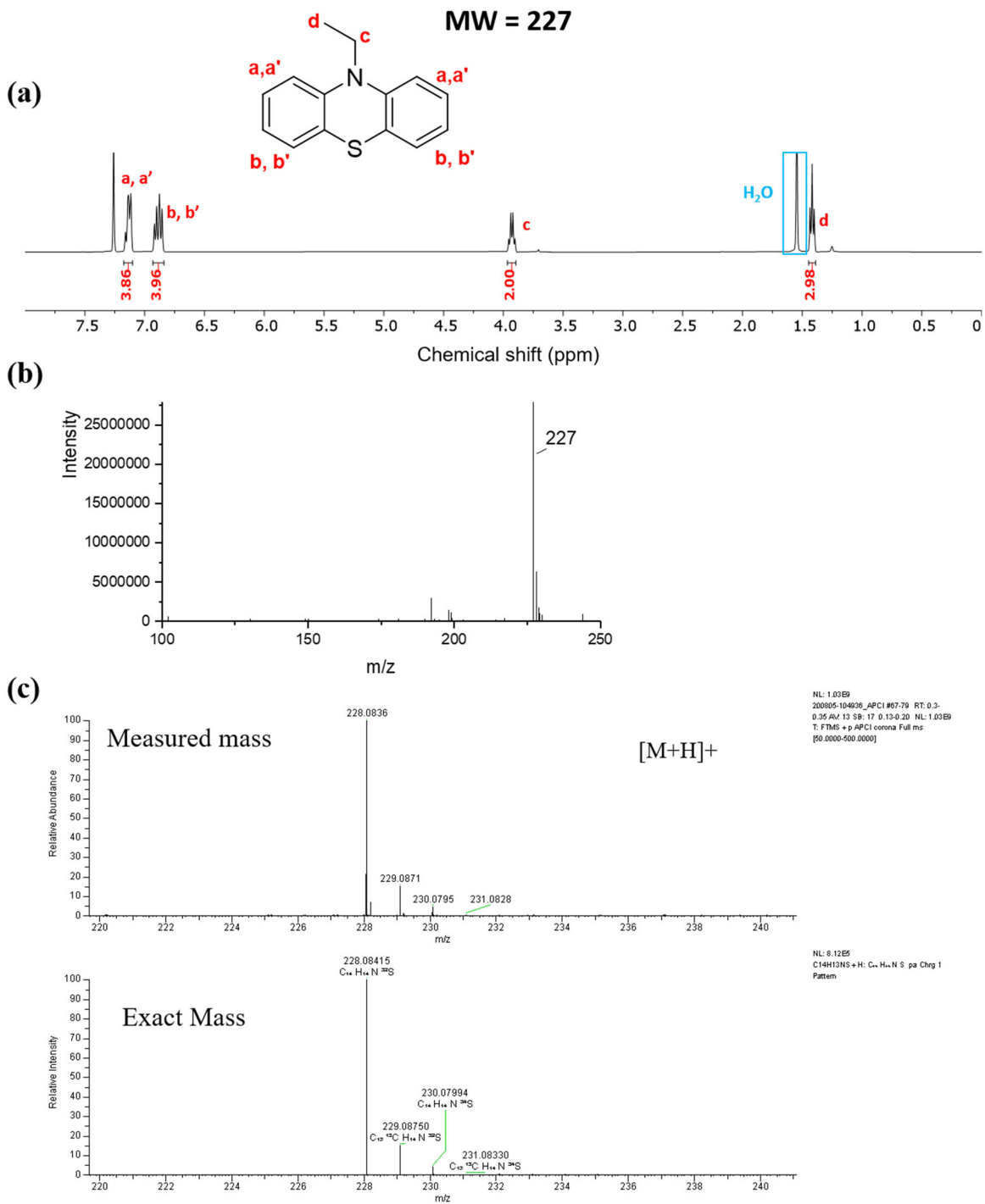
Figure A7.1. Characterization of EPT, (a) ^{1}H NMR, (b) ESI mass spec, (c) high resolution mass spec.
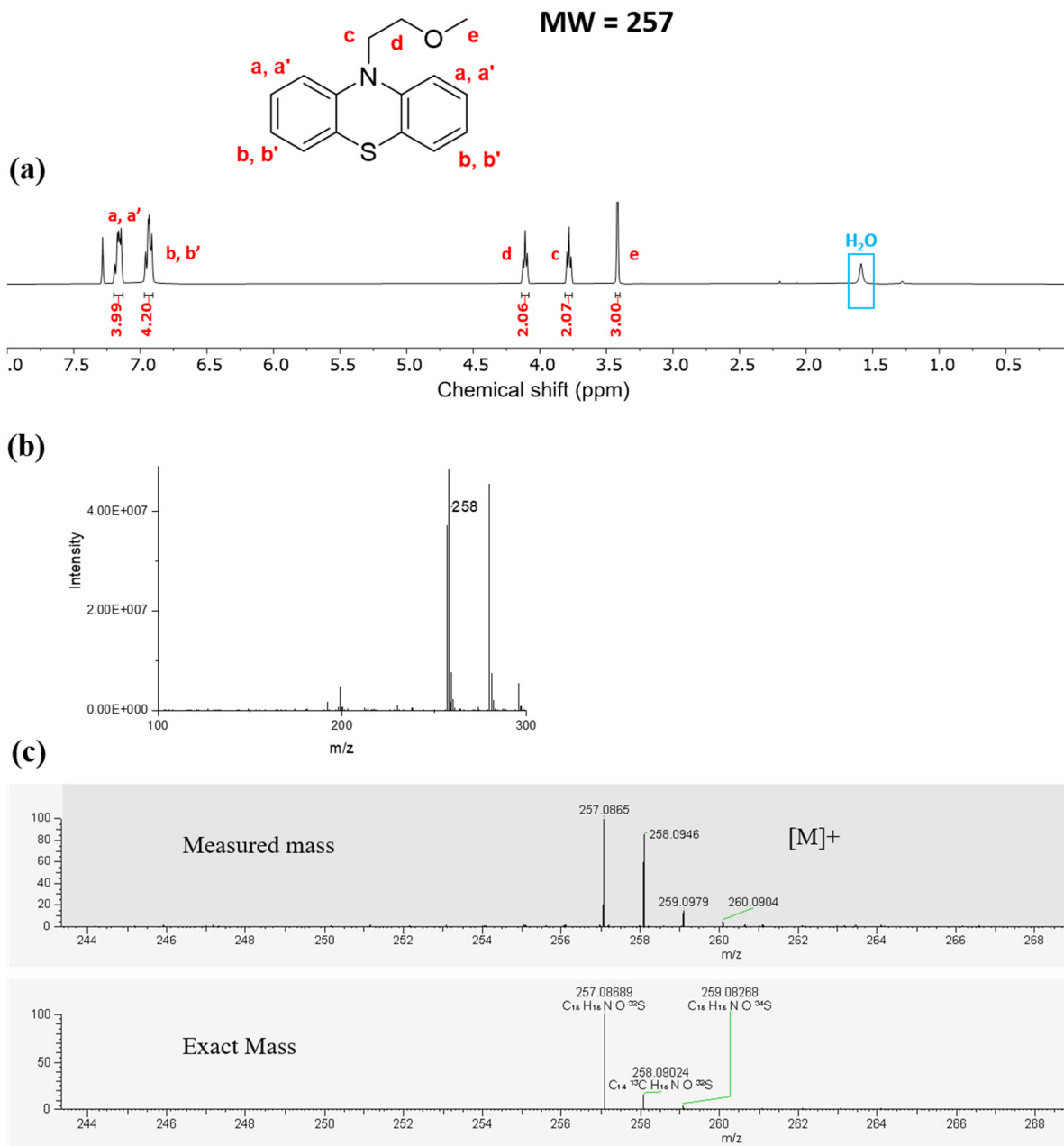
Figure A7.2. Characterization of MEPT, (a) ^{1}H NMR, (b) ESI mass spec, (c) high resolution mass spec.
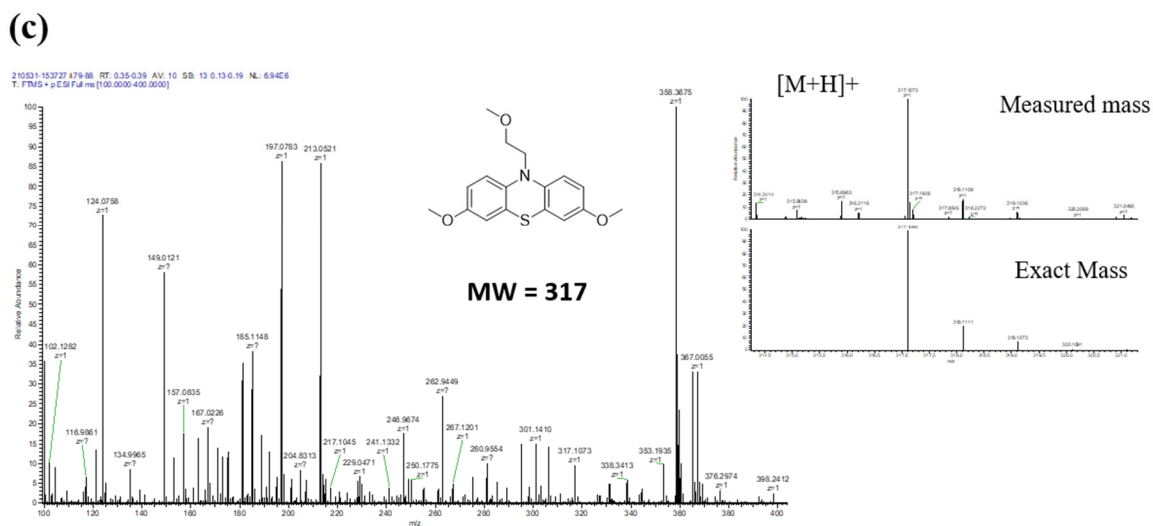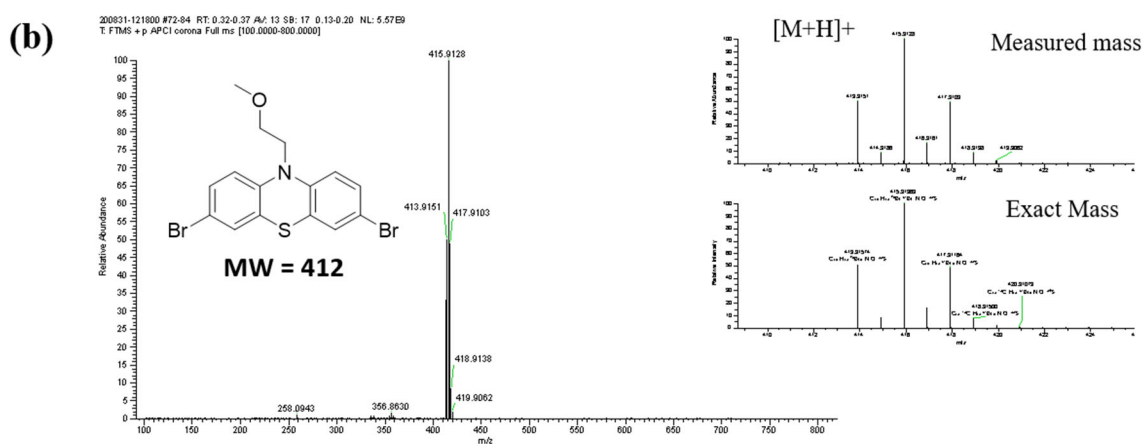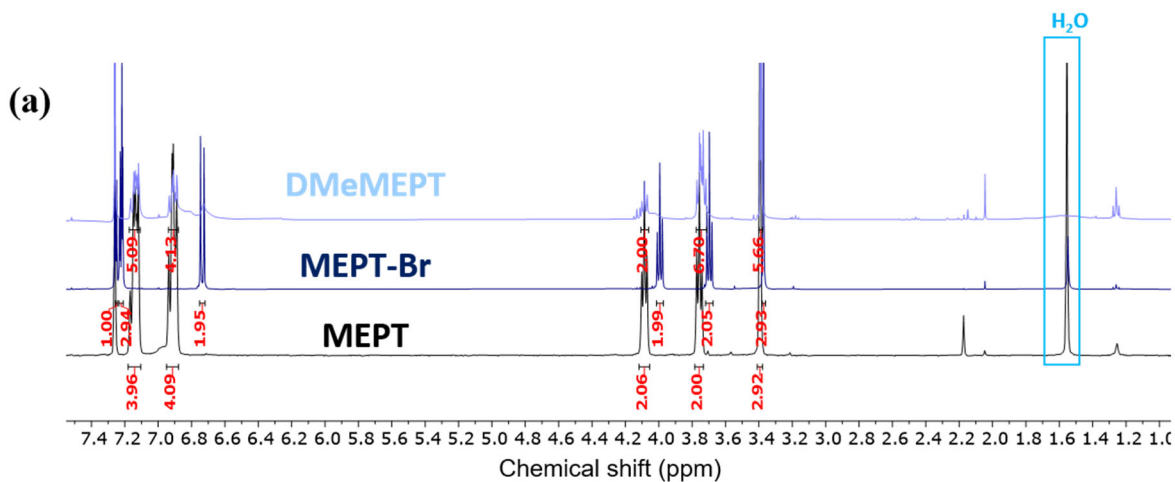
Figure A7.3. Characterization of DMeMEPT, (a) ^{1}H NMR, (b) ESI mass spec of MEPT-Br, (c) ESI mass spec of crude DMeMEPT.
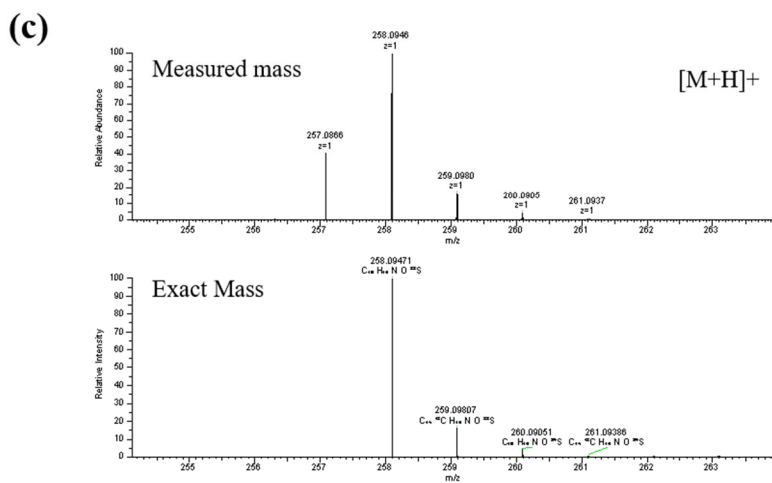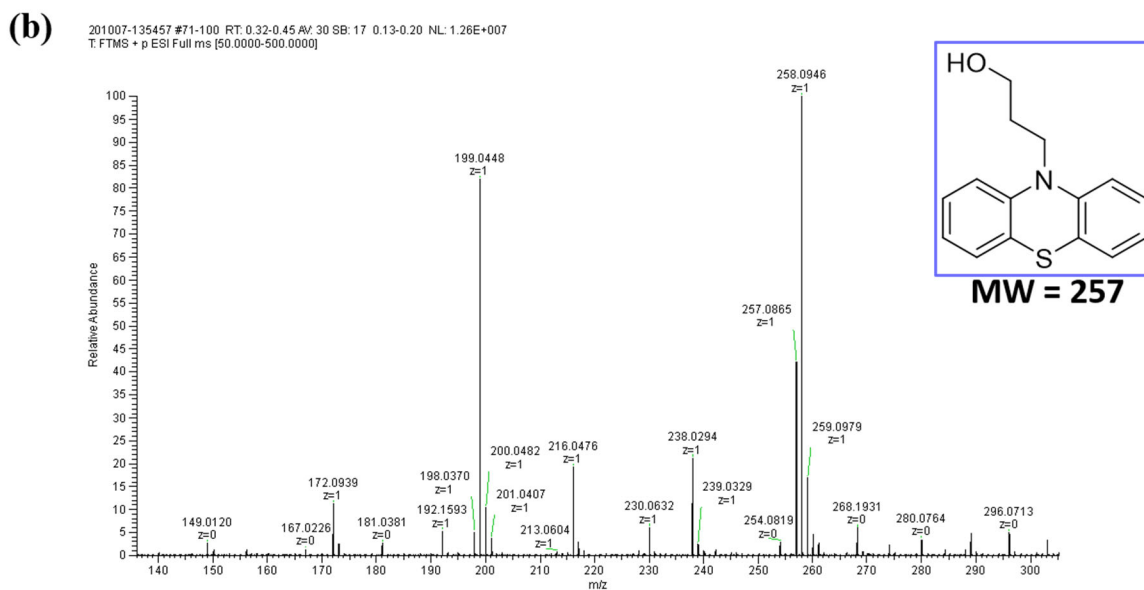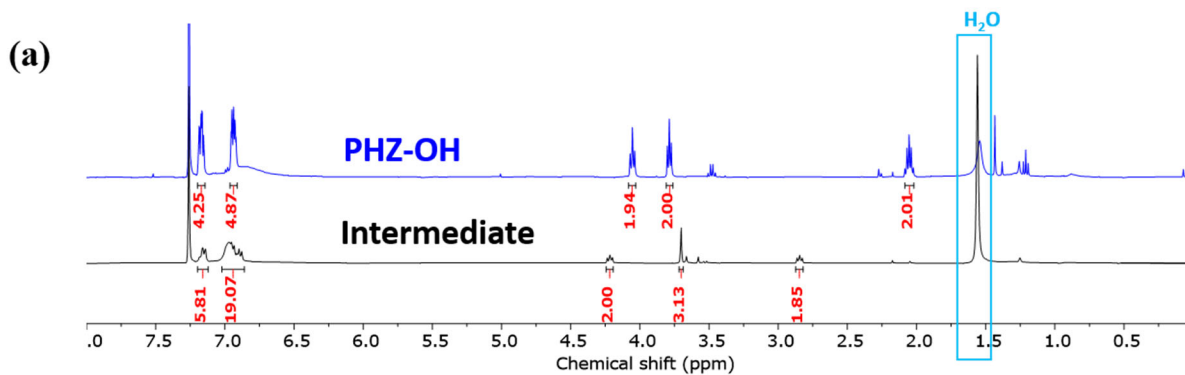
Figure A7.4. Characterization of PHZ-OH, (a) ^{1}H NMR, (b) ESI mass spec, (c) high resolution mass spec.
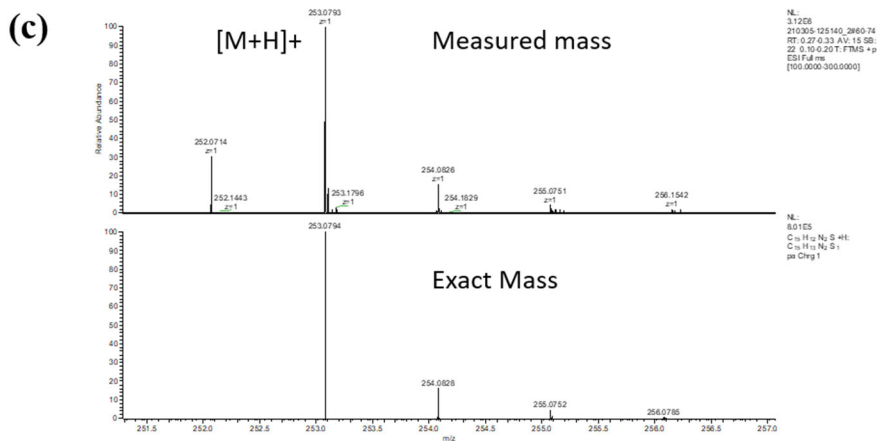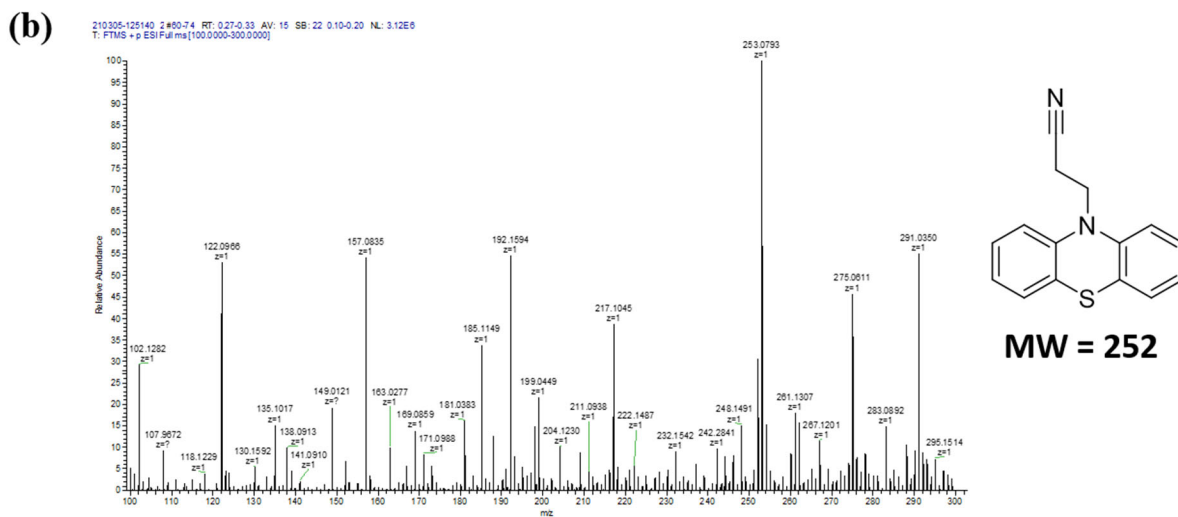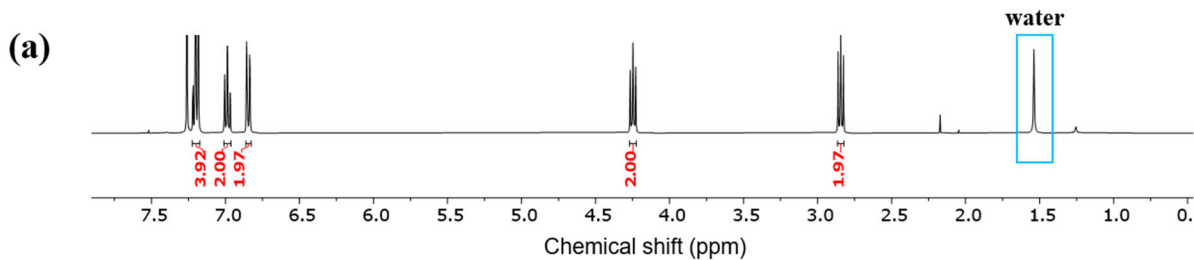
Figure A7.5. Characterization of PHZ-CN intermediate, (a) ^{1}H NMR, (b) ESI mass spec, (c) high resolution mass spec.
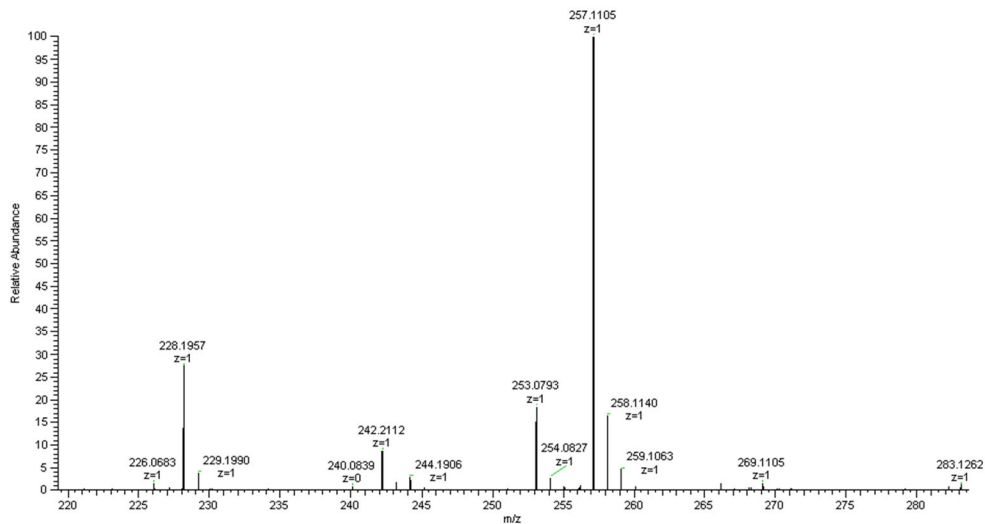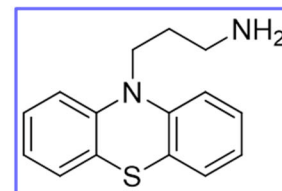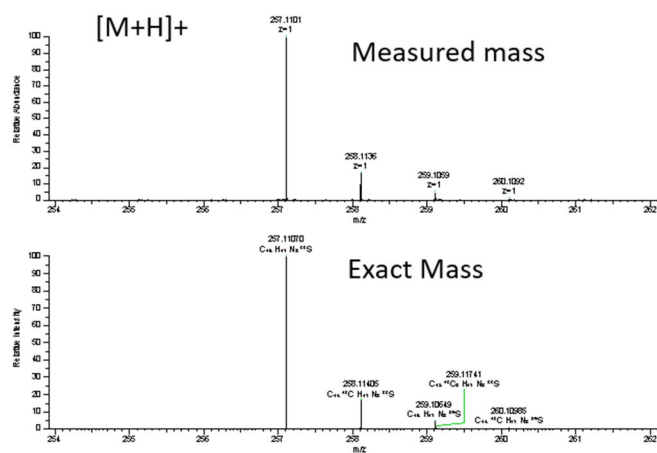
Figure A7.6. Characterization of PHZ-NH₂, (a) ESI mass spec, (b) high resolution mass spec.
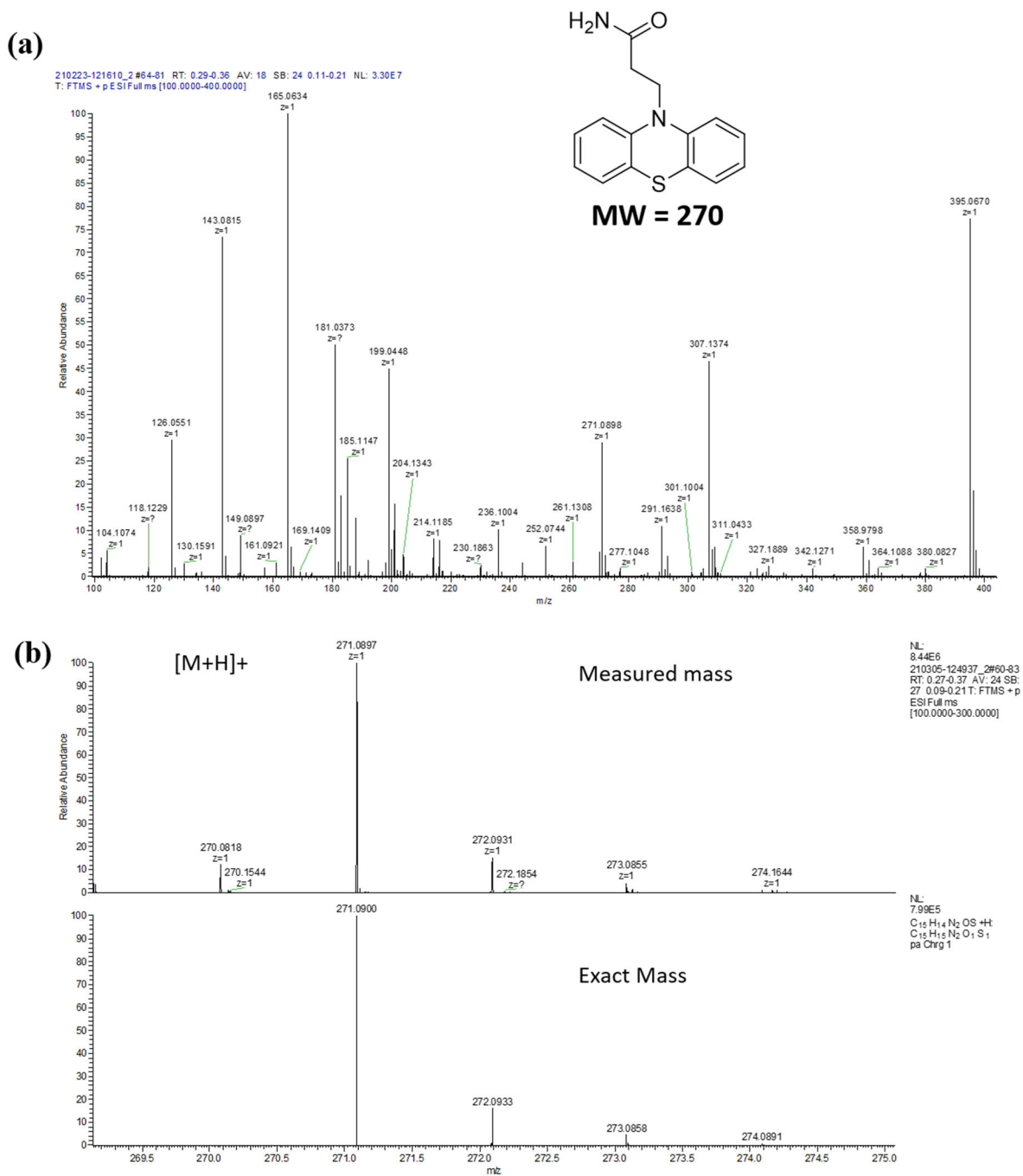
Figure A7.7. Characterization of PHZ-amide, (a) ESI mass spec, (b) high resolution mass spec.
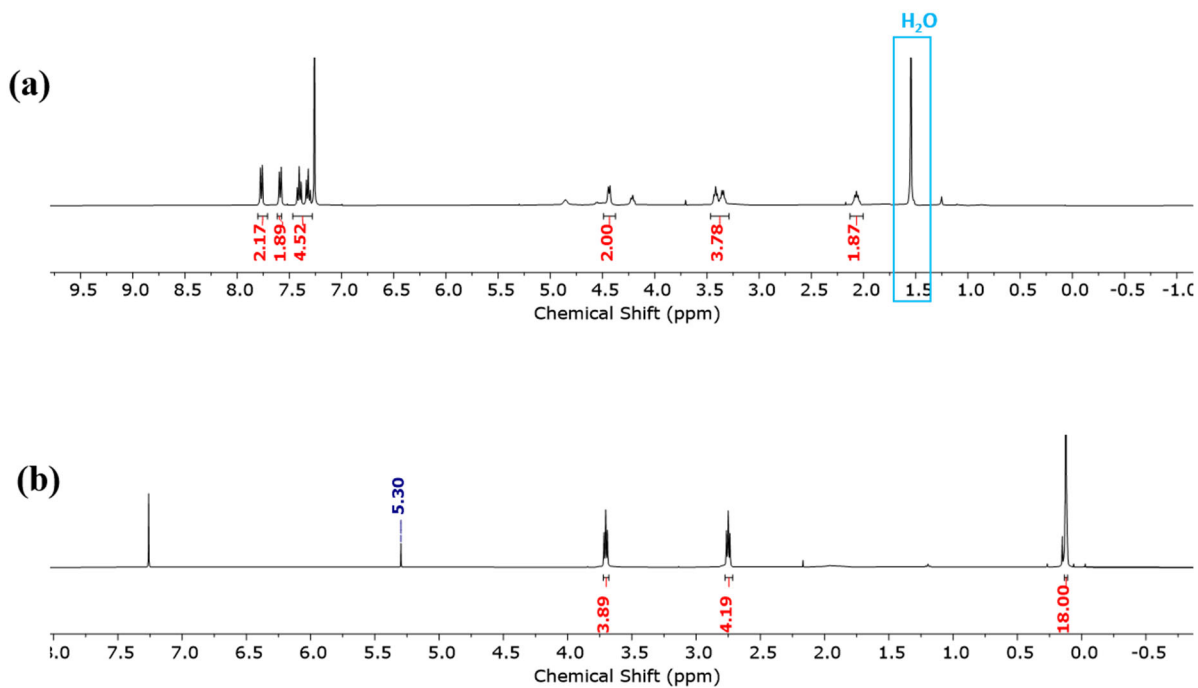
Figure A7.8. (a) ^{1}H NMR of Fmoc protected amine, (b) ^{1}H NMR of protected alcohol group for diethaneolamine.
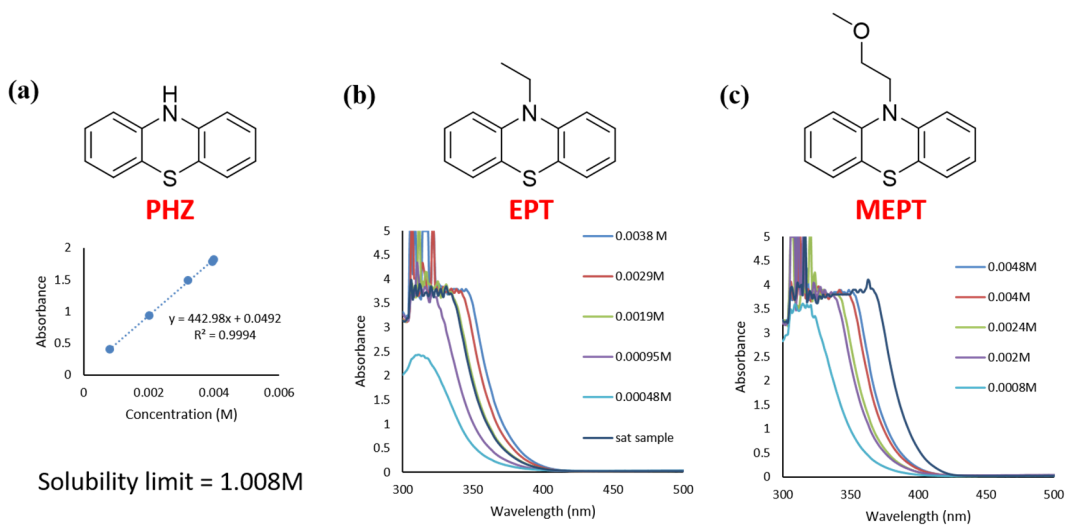
Figure A7.9. Solubility Studies (a) phenothiazine, (b) EPT, (c) MEPT.

7.8   References

(206) Paduszek, B.; Kalinowski, M. K. Redox Behaviour of Phenothiazine and Phenazine in Organic Solvents. Electrochim. Acta 1983, 28 (5), 639–642. https://doi.org/10.1016/0013-4686(83)85057-9.

(207) Puzanowska-Tarasiewicz, H.; Kuźmicka, L.; Karpińska, J.; Mielech-Łukasiewicz, K. Efficient Oxidizing Agents for Determination of 2,10-Disubstituted Phenothiazines. Anal. Sci. 2005, 21 (10), 1149–1153. https://doi.org/10.2116/analsci.21.1149.

(208) Kowalski, J. A.; Casselman, M. D.; Kaur, A. P.; Milshtein, J. D.; Elliott, C. F.; Modekrutti, S.; Attanayake, N. H.; Zhang, N.; Parkin, S. R.; Risko, C.; Brushett, F. R.; Odom, S. A. A Stable Two-Electron-Donating Phenothiazine for Application in Nonaqueous Redox Flow Batteries. J. Mater. Chem. A 2017, 5 (46), 24371–24379. https://doi.org/10.1039/c7ta05883g.

(209) Attanayake, N. H.; Kowalski, J. A.; Greco, K. V.; Casselman, M. D.; Milshtein, J. D.; Chapman, S. J.; Parkin, S. R.; Brushett, F. R.; Odom, S. A. Tailoring Two-Electron-Donating Phenothiazines to Enable High-Concentration Redox Electrolytes for Use in Nonaqueous Redox Flow Batteries. Chem. Mater. 2019, 31 (12), 4353–4363.

(226) Varga, B.; Csonka, Á.; Csonka, A.; Molnár, J.; Amaral, L.; Spengler, G. Possible Biological and Clinical Applications of Phenothiazines. Anticancer Res. 2017, 37 (11), 5983–5993. https://doi.org/10.21873/anticanres.12045.

(227) Al-Busaidi, I. J.; Haque, A.; Al Rasbi, N. K.; Khan, M. S. Phenothiazine-Based Derivatives for Optoelectronic Applications: A Review. Synth. Met. 2019, 257, 116189. https://doi.org/10.1016/j.synthmet.2019.116189.

(228)   Onoabedje, E. A.; Egu, S. A.; Ezeokonkwo, M. A.; Okoro, U. C. Highlights of Molecular Structures and Applications of Phenothiazine & Phenoxazine Polycycles. J. Mol. Struct. 2019, 1175, 956–962. https://doi.org/10.1016/j.molstruc.2018.08.064.

(229)   Šulcová, N.; Němec, I.; Waisser, K.; Kies, H. L. Study of the Electrochemical Oxidation of Phenothiazine Derivatives in Acetonitrile Medium: The Effect of the Structure on the Voltammetric Behavior. Microchem. J. 1980, 25 (4), 551–566. https://doi.org/10.1016/0026-265X(80)90222-2.

(230)   Milshtein, J. D.; Kaur, A. P.; Casselman, M. D.; Kowalski, J. A.; Modekrutti, S.; Zhang, P. L.; Harsha Attanayake, N.; Elliott, C. F.; Parkin, S. R.; Risko, C.; Brushett, F. R.; Odom, S. A. High Current Density, Long Duration Cycling of Soluble Organic Active Species for Non-Aqueous Redox Flow Batteries. Energy Environ. Sci. 2016, 9 (11), 3531–3543. https://doi.org/10.1039/c6ee02027e.

(231)   Pankratov, A. N.; Uchaeva, I. M.; Stepanov, A. N. Chemical and Electrochemical Oxidation of Phenothiazine. Can. J. Chem. 1993, 71, 674–677. https://doi.org/10.1021/jm00202a010.

(232)   Chen, B.; Mitchell, S.; Sinclair, N.; Wainright, J.; Pentzer, E.; Gurkan, B. Feasibility of TEMPO-Functionalized Imidazolium, Ammonium and Pyridinium Salts as Redox-Active Carriers in Ethaline Deep Eutectic Solvent for Energy Storage. Mol. Syst. Des. Eng. 2020, 5 (6), 1147–1157. https://doi.org/10.1039/d0me00038h.

(233)   Sheina, E. E.; Khersonsky, S. M.; Jones, E. G.; Mccullough, R. D. Highly Conductive, Regioregular Alkoxy-Functionalized Polythiophenes: A New Class of Stable, Low Band Gap Materials. Chem. Mater. 2005, 17 (13), 3317–3319. https://doi.org/10.1021/cm050083o.

(234)   Yu, J.; Zhao, B.; Nie, X.; Zhou, B.; Li, Y.; Hai, J.; Zhu, E.; Bian, L.; Wu, H.; Tang, W. Correlation of Structure and Photovoltaic Performance of Benzo[1,2-b:4,5-B′]Dithiophene Copolymers Alternating with Different Acceptors. New J. Chem. 2015, 39 (3), 2248–2255. https://doi.org/10.1039/c4nj02192d.

(235)   Ingoglia, B. T.; Buchwald, S. L. Oxidative Addition Complexes as Precatalysts for Cross-Coupling Reactions Requiring Extremely Bulky Biarylphosphine Ligands. Org. Lett. 2017, 19 (11), 2853–2856. https://doi.org/10.1021/acs.orglett.7b01082.

(236)   Cummins, D.; Boschloo, G.; Ryan, M.; Corr, D.; Rao, S. N.; Fitzmaurice, D. Ultrafast Electrochromic Windows Based on Redox-Chromophore Modified Nanostructured Semiconducting and Conduction Films. J. Phys. Chem. B 2000, 104, 11449–11459. https://doi.org/10.1021/jp001763b.

(237)   Gawande, M. B.; Branco, P. S. An Efficient and Expeditious Fmoc Protection of Amines and Amino Acids in Aqueous Media. Green Chem. 2011, 13 (12), 3355–3359. https://doi.org/10.1039/c1gc15868f.

(238)   He, C. X.; Meng, H.; Zhang, X.; Cui, H. Q.; Yin, D. L. Synthesis and Bio-Evaluation of Phenothiazine Derivatives as New Anti-Tuberculosis Agents. Chinese Chem. Lett. 2015, 26 (8), 951–954. https://doi.org/10.1016/j.cclet.2015.03.027.

(239)   Thiyagarajan, S.; Krishnakumar, V.; Gunanathan, C. KO t Bu-Catalyzed Michael Addition Reactions Under Mild and Solvent-Free Conditions. Chem. Asian J. 2020, 15, 518–523. https://doi.org/10.1002/asia.201901647.

(240)   Schafgen, B.; Khelwati, H.; Bechtel, D. F.; DeCuyper, A.; Schussler, A.; Neuba, A.; Pierik, A. J.; Ernst, S.; Muller, T. J. J.; Thiel, W. R. Phenothiazine Electrophores Immobilized on Periodic

Mesoporous Organosilicas by Ion Exchange. New J. Chem. 2019, 43, 16396–16410. https://doi.org/10.1039/c9nj04661e.

(241)   Reddy, N. N. K.; Rao, S. N.; Patil, R. D.; Adimurthy, S. Transition Metal-Free Hydration of Nitriles to Amides Mediated by NaOH. Adv. Mater. Sci. 2018, 3 (1), 1–7. https://doi.org/10.15761/AMS.1000137.

(242)   Ritu, S.; Pushkal, S.; D., S. S.; K., S. S. Synthesis and Biological Activity of 2-Oxo-Azetidine Derivatives of Phenothiazine. Org. Commun. 2011, 4 (2), 42–51. https://doi.org/10.1055/s-0033-1364001.

(243)   Chudzinski, M. G.; McClary, C. A.; Taylor, M. S. Anion Receptors Composed of Hydrogen- and Halogen-Bond Donor Groups: Modulating Selectivity with Combinations of Distinct Noncovalent Interactions. J. Am. Chem. Soc. 2011, 133 (27), 10559–10567. https://doi.org/10.1021/ja202096f.

(244)   Dekeukeleire, S.; D'Hooghe, M.; De Kimpe, N. Diastereoselective Synthesis of Bicyclic γ-Lactams via Ring Expansion of Monocyclic β-Lactams. J. Org. Chem. 2009, 74 (4), 1644–1649. https://doi.org/10.1021/jo802459j

Part II: The Incorporation of Redox Small Molecules into Deep Eutectic Solvents for the Development of New Electrolytes

Chapter 8

Summary and Future Directions of Incorporating Redox Active

Species into Deep Eutectic Solvents

8.1 Summary

The work presented in part two of this thesis explores the synthetic modification of redox active small molecules for their incorporation into deep eutectic solvents (DESs) to develop breakthrough electrolytes. DESs are great candidates as electrolytes for energy storage, due to their low vapor pressures and wide liquidous range, but for such use redox active species must be incorporated at high concentrations.[171] TEMPO was selected as the first redox active small molecule to study, due to the stable organic radical and synthetic tunability. The TEMPO derivatives synthesized were derived from a commercially available 4-hydroxy TEMPO (4HT) that has an alcohol in the 4 position. Three TEMPO salts were synthesized varying in cation identity, including imidazolium, ammonium, and pyridinium functionality (compounds **1**, **2**, and **3**, respectively). Each of these was incorporated into ethaline (1:2 choline chloride:ethylene glycol) and the physical properties of the solutions were examined (density, viscosity, and ionic conductivity).[232]

The electrochemical behavior of the solutions was also examined and compared to TEMPO and 4HT. Each derivative exhibited two, single-electron reactions that corresponded to an oxoammonium cation and aminoxyl anion. Compounds **1**, **2**, and 4HT were redox stable over 50 cycles whereas TEMPO and compound **3** exhibited reduced reduction currents upon cycling. Flow cell experiments were performed to further evaluate the stability of the 4HT/4HT$^+$ redox couple, which decreases overtime. It is hypothesized that the TEMPO unit oxidizes the primary alcohols present in the DES components which leads to these irreversible redox couples. Several additional TEMPO derivatives were synthesized, varying anion identity and di-functionality.

PHZ derivatives were also synthesized and chosen for the ability to tune their redox properties as well as solubility, and potential for two electron transfer reactions.[208,209] The selected derivatives examine substituents at the R_{10}, R_7, and R_3 positions, as well as incorporating H-bonding

functionality. EPT and MEPT were easily synthesized and produced on a large scale and MEPT was more soluble in ethaline than EPT. DMeMEPT and DMeEPT were selected to examine how the substituents impact electrochemical stability. A limitation of the current syntheses is the high purity of compounds required. Initial evaluation of the electrochemical properties was performed by collaborators at CWRU. Of the H-bonding PHZ derivatives synthesized (PHZ-OH and PHZ-NH$_2$), the later exhibited a very reversible redox couple and easily dissolved in ethaline. This inspires the synthesis of PHZ derivatives containing more nitrogen functionality (e.g., PHZ-amides), as well as PHZ derivatives containing pendant groups capable of a greater number of H-bonds.

8.2 Future Directions

8.2.1 Future of TEMPO Derivatives

The worked presented examined a variety of TEMPO derivatives, creating a large library of derivatives. There was the realization that the TEMPO structure maybe oxidizing the primary alcohols present in many DESs. Future work could explore DESs that do not contain primary alcohols, which could be tertiary alcohols or alternative functionality (Figure 8.1a). The TEMPO
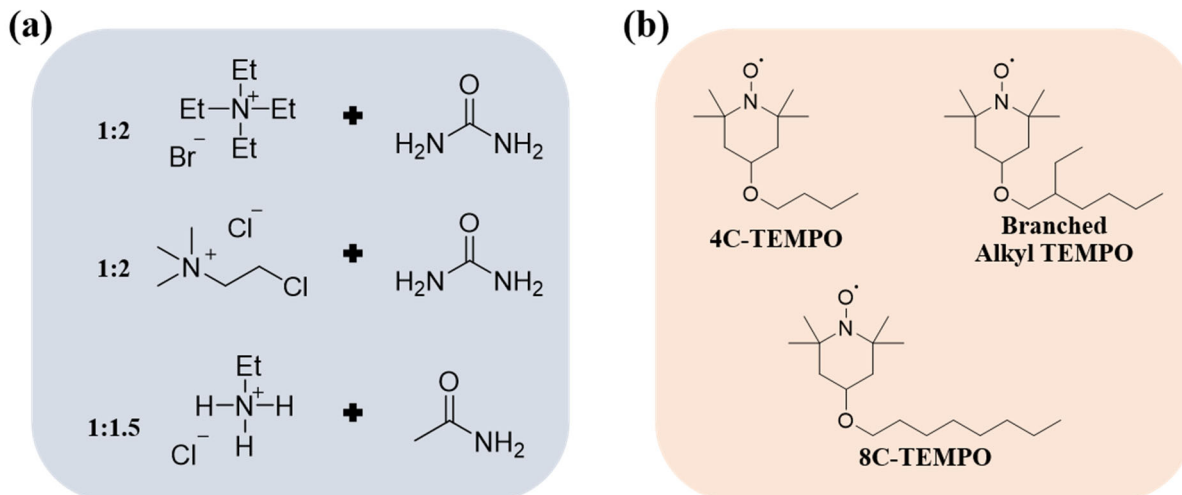
Figure 8.1. (a) Alcohol free DES and (b) alkyl-TEMPO derivatives.

derivatives could then be incorporated without the concern of irreversible side reactions. The TEMPO salts also have the potential to be the hydrogen bond acceptor (HBA) of a DES. In such a system, the redox active species would not be an additive, but rather a component of the DES. A downside to this, however, is the amount of material required to make a viable redox flow cell, this could become expensive and time consuming. Current work, involves electron paramagnetic resonance (EPR) spectroscopy and quantifying the radical of the TEMPO salts.

8.2.2 Future of Phenothiazine Derivatives

The work presented on the synthesis of PHZ derivatives is ongoing and current work is focused on the synthesis and purification of DMeMEPT and diethanolamine-PHZ (Figure 8.2a). Once these compounds are synthesized, purified, and fully characterized, the electrochemical behavior will be evaluated. If DMeMEPT does not exhibit two reversible redox couples, focus may shift to using PHZ as one component of an electrolyte. Specifically, combining methyl viologen and PHZ to form a mixed system in a DES (Figure 8.2b). The diethanolamine-PHZ was selected to synthesize for this reason and all of the PHZ derivatives can be examined in the mixed system. Ideally, the redox active species in the mixed system will perform similarly in a DES as a volatile and flammable solvent, such as acetonitrile. However, a major question to answer is the similarity and differences between the redox reactions in DES and more traditional electrolytes (aqueous, organic, and ionic liquids).
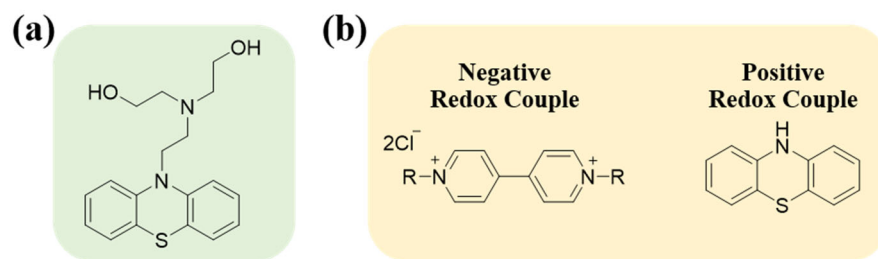
Figure 8.2. (a) diethanolamine-PHZ and (b) possible redox active mixed system.

8.2.3 New Redox Active Species

There are many different redox active species that exhibit various redox potentials and can be tailored for either a mixed system or used as a single compound exhibiting two redox couples (Figure 8.3).[196] Future work should focus on identifying potential redox active species that have high solubility and good electrochemical performance so that energy density can be increased. Screening commercially available parent compounds is a good starting point and if performance is acceptable then derivatives can be selected to synthesize. Identification of redox active compounds may also be aided by computational work. Compounds that maybe of interest include pthalimides, 1,4-dimethoxybenzenes (DBB), PTIO, and quinoxaline.
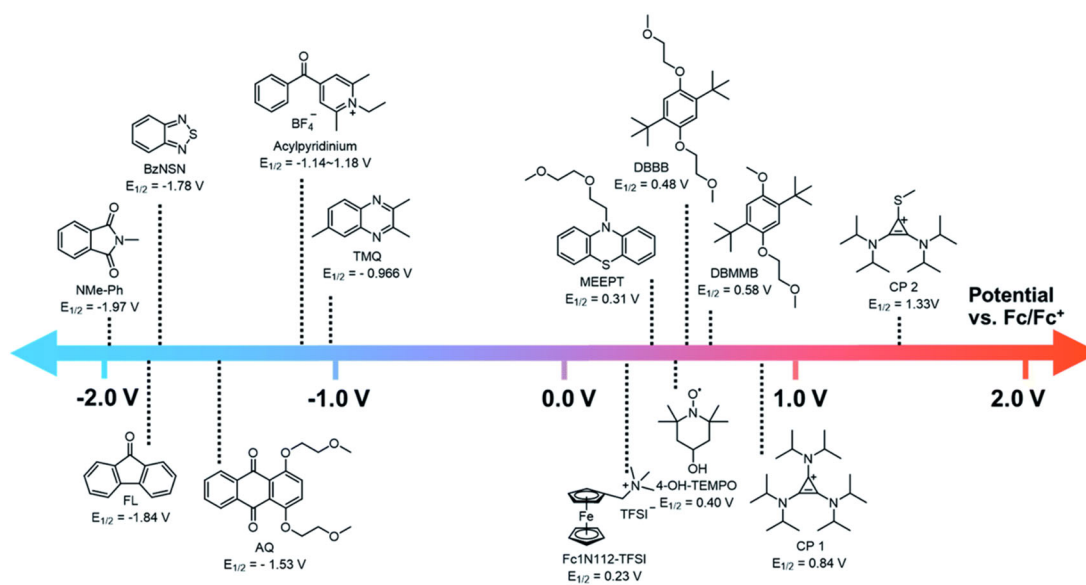
Figure 8.3. Redox potentials of common redox active species. (Reproduced from reference 196)

8.2.4 New Deep Eutectic Solvents

As a part of a Department of Energy, Energy Frontier Research Center (EFRC), the main DESs of focus have been ethaline, reline, and gylceline. Research has supported that phenol based DESs may be a good path for future work. Future work should examine a variety of DES with different

components and determine the viscosity and electrochemical window of the DES. When selecting a new DES, electrochemical window is of great importance so the electrolyte does not break down prior to the redox reaction occurring.

Current work within the EFRC focuses on understanding on a molecular level the interactions between the components of a DES and a redox active species. This includes NMR spectroscopic studies, molecular simulation, broadband dielectric spectroscopy, and AIMD simulations. On an experimental level future work involves examining tertiary alcohols as a HBD (Figure 8.5). These would form a DES that would not interact with the TEMPO derivatives, therefore not having an impact on electrochemical behavior of the TEMPO derivatives. Unfortunately, the desired tertiary alcohol is expensive commercially and difficult to synthesize, so alternatives are being examined that are commercially available. Additionally, the synthesized derivatives may be able to be used as a component in a DES as opposed to be an additive. This would remove the need to find a highly soluble derivative that is also electrochemically stable.

2,4-Dimethyl-2,4-pentanediol   Pinacol
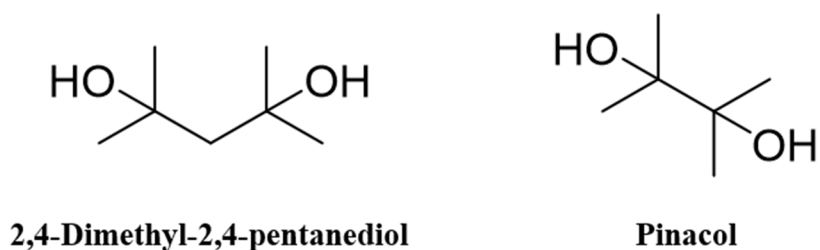
Figure 8.4. Tertiary alcohols that could be used as a hydrogen bond donor in a DES.

8.3   References

(171)   Wei, X.; Pan, W.; Duan, W.; Hollas, A.; Yang, Z.; Li, B.; Nie, Z.; Liu, J.; Reed, D.; Wang, W.; Sprenkle, V. Materials and Systems for Organic Redox Flow Batteries: Status and Challenges. ACS Energy Lett. 2017, 2 (9), 2187–2204. https://doi.org/10.1021/acsenergylett.7b00650.

(196) Li, M.; Rhodes, Z.; Cabrera-Pardo, J. R.; Minteer, S. D. Recent Advancements in Rational Design of Non-Aqueous Organic Redox Flow Batteries. Sustain. Energy Fuels 2020, 4 (9), 4370–4389. https://doi.org/10.1039/d0se00800a.

(208) Kowalski, J. A.; Casselman, M. D.; Kaur, A. P.; Milshtein, J. D.; Elliott, C. F.; Modekrutti, S.; Attanayake, N. H.; Zhang, N.; Parkin, S. R.; Risko, C.; Brushett, F. R.; Odom, S. A. A Stable Two-Electron-Donating Phenothiazine for Application in Nonaqueous Redox Flow Batteries. J. Mater. Chem. A 2017, 5 (46), 24371–24379. https://doi.org/10.1039/c7ta05883g.

(209) Attanayake, N. H.; Kowalski, J. A.; Greco, K. V.; Casselman, M. D.; Milshtein, J. D.; Chapman, S. J.; Parkin, S. R.; Brushett, F. R.; Odom, S. A. Tailoring Two-Electron-Donating Phenothiazines to Enable High-Concentration Redox Electrolytes for Use in Nonaqueous Redox Flow   Batteries.   Chem.   Mater.   2019,   31   (12),   4353–4363. https://doi.org/10.1021/acs.chemmater.8b04770.

(232) Chen, B.; Mitchell, S.; Sinclair, N.; Wainright, J.; Pentzer, E.; Gurkan, B. Feasibility of TEMPO-Functionalized Imidazolium, Ammonium and Pyridinium Salts as Redox-Active Carriers in Ethaline Deep Eutectic Solvent for Energy Storage. Mol. Syst. Des. Eng. 2020, 5 (6), 1147–1157. https://doi.org/10.1039/d0me00038h.

Bibliography

(1) Buss, B. L.; Miyake, G. M. Photoinduced Controlled Radical Polymerizations Performed in Flow: Methods, Products, and Opportunities. *Chem. Mater.* **2018**, *30* (12), 3931–3942. https://doi.org/10.1021/acs.chemmater.8b01359.

(2) Reis, M. H.; Leibfarth, F. A.; Pitet, L. M. Polymerizations in Continuous Flow: Recent Advances in the Synthesis of Diverse Polymeric Materials. *ACS Macro Lett.* **2020**, *9* (1), 123–133. https://doi.org/10.1021/acsmacrolett.9b00933.

(3) Holloway, J. O.; Wetzel, K. S.; Martens, S.; Du Prez, F. E.; Meier, M. A. R. Direct Comparison of Solution and Solid Phase Synthesis of Sequence-Defined Macromolecules. *Polym. Chem.* **2019**, *10* (28), 3859–3867. https://doi.org/10.1039/c9py00558g.

(4) Vrijsen, J. H.; Osiro Medeiros, C.; Gruber, J.; Junkers, T. Continuous Flow Synthesis of Core Cross-Linked Star Polymers: Via Photo-Induced Copper Mediated Polymerization. *Polym. Chem.* **2019**, *10* (13), 1591–1598. https://doi.org/10.1039/c9py00134d.

(5) Reis, M. H.; Davidson, C. L. G.; Leibfarth, F. A. Continuous-Flow Chemistry for the Determination of Comonomer Reactivity Ratios. *Polym. Chem.* **2018**, *9* (13), 1728–1734. https://doi.org/10.1039/c7py01938f.

(6) Radzinski, S. C.; Foster, J. C.; Scannelli, S. J.; Weaver, J. R.; Arrington, K. J.; Matson, J. B. Tapered Bottlebrush Polymers: Cone-Shaped Nanostructures by Sequential Addition of Macromonomers. *ACS Macro Lett.* **2017**, *6* (10), 1175–1179. https://doi.org/10.1021/acsmacrolett.7b00724.

(7) Lee, J.; Kalin, A. J.; Yuan, T.; Al-Hashimi, M.; Fang, L. Fully Conjugated Ladder Polymers. *Chem. Sci.* **2017**, *8* (4), 2503–2521. https://doi.org/10.1039/C7SC00154A.

(8) Kensy, V. K.; Tritt, R. L.; Haque, F. M.; Murphy, L. M.; Knorr, D. B.; Grayson, S. M.;

Boydston, A. J. Molecular Weight Control via Cross Metathesis in Photo-Redox Mediated Ring-Opening Metathesis Polymerization. *Angew. Chemie - Int. Ed.* **2020**, *59*, 2–8. https://doi.org/10.1002/anie.202000434.

(9)   Carmean, R. N.; Becker, T. E.; Sims, M. B.; Sumerlin, B. S. Ultra-High Molecular Weights via Aqueous Reversible-Deactivation Radical Polymerization. *Chem* **2017**, *2* (1), 93–101. https://doi.org/10.1016/j.chempr.2016.12.007.

(10)   Beyer, V. P.; Kim, J.; Remzi Becer, C. Synthetic Approaches for Multiblock Copolymers. *Polym. Chem.* **2020**, *11* (7), 1271–1291. https://doi.org/10.1039/c9py01571j.

(11)   Teo, Y. C.; Lai, H. W. H.; Xia, Y. Synthesis of Ladder Polymers: Developments, Challenges, and Opportunities. *Chem. - A Eur. J.* **2017**, *23* (57), 14101–14112. https://doi.org/10.1002/chem.201702219.

(12)   Shafranek, R. T.; Millik, S. C.; Smith, P. T.; Lee, C. U.; Boydston, A. J.; Nelson, A. Stimuli-Responsive Materials in Additive Manufacturing. *Prog. Polym. Sci.* **2019**, *93*, 36–67. https://doi.org/10.1016/j.progpolymsci.2019.03.002.

(13)   Wei, P.; Leng, H.; Chen, Q.; Advincula, R. C.; Pentzer, E. B. Reprocessable 3D-Printed Conductive Elastomeric Composite Foams for Strain and Gas Sensing. *ACS Appl. Polym. Mater.* **2019**, *1* (4), 885–892. https://doi.org/10.1021/acsapm.9b00118.

(14)   Ligon, S. C.; Liska, R.; Stampfl, J.; Gurr, M.; Mülhaupt, R. Polymers for 3D Printing and Customized Additive Manufacturing. *Chem. Rev.* **2017**, *117* (15), 10212–10290. https://doi.org/10.1021/acs.chemrev.7b00074.

(15)   Zaquen, N.; Yeow, J.; Junkers, T.; Boyer, C.; Zetterlund, P. B. Visible Light-Mediated Polymerization-Induced Self-Assembly Using Continuous Flow Reactors. *Macromolecules* **2018**, *51* (14), 5165–5172.

https://doi.org/10.1021/acs.macromol.8b00887.

(16)   Scott, P. J.; Kasprzak, C. R.; Feller, K. D.; Meenakshisundaram, V.; Williams, C. B.; Long, T. E. Light and Latex: Advances in the Photochemistry of Polymer Colloids. *Polym. Chem.* **2020**. https://doi.org/10.1039/d0py00349b.

(17)   Varlas, S.; Keogh, R.; Xie, Y.; Horswell, S. L.; Foster, J. C.; O'Reilly, R. K. Polymerization-Induced Polymersome Fusion. *J. Am. Chem. Soc.* **2019**, *141* (51), 20234–20248. https://doi.org/10.1021/jacs.9b10152.

(18)   Canning, S. L.; Smith, G. N.; Armes, S. P. A Critical Appraisal of RAFT-Mediated Polymerization-Induced Self-Assembly. *Macromolecules* **2016**, *49* (6), 1985–2001. https://doi.org/10.1021/acs.macromol.5b02602.

(19)   Arrington, K. J.; Haag, J. V.; French, E. V.; Murayama, M.; Edgar, K. J.; Matson, J. B. Toughening Cellulose: Compatibilizing Polybutadiene and Cellulose Triacetate Blends. *ACS Macro Lett.* **2019**, *8* (4), 447–453. https://doi.org/10.1021/acsmacrolett.9b00136.

(20)   Blasco, E.; Sims, M. B.; Goldmann, A. S.; Sumerlin, B. S.; Barner-Kowollik, C. 50th Anniversary Perspective: Polymer Functionalization. *Macromolecules* **2017**, *50* (14), 5215–5252. https://doi.org/10.1021/acs.macromol.7b00465.

(21)   Xu, J.; Eagan, J. M.; Kim, S. S.; Pan, S.; Lee, B.; Klimovica, K.; Jin, K.; Lin, T. W.; Howard, M. J.; Ellison, C. J.; Lapointe, A. M.; Coates, G. W.; Bates, F. S. Compatibilization of Isotactic Polypropylene (IPP) and High-Density Polyethylene (HDPE) with IPP-PE Multiblock Copolymers. *Macromolecules* **2018**, *51* (21), 8585–8596. https://doi.org/10.1021/acs.macromol.8b01907.

(22)   Xiang, T.; Wang, L. R.; Ma, L.; Han, Z. Y.; Wang, R.; Cheng, C.; Xia, Y.; Qin, H.; Zhao, C. S. From Commodity Polymers to Functional Polymers. *Sci. Rep.* **2015**, *4*, 4604.

https://doi.org/10.1038/srep04604.

(23)   Barkley, D. A.; Jiang, N.; Sen, M.; Endoh, M. K.; Rudick, J. G.; Koga, T.; Zhang, Y.; Gang, O.; Yuan, G.; Satija, S. K.; Kawaguchi, D.; Tanaka, K.; Karim, A. Chain Conformation near the Buried Interface in Nanoparticle-Stabilized Polymer Thin Films. *Macromolecules* **2017**, *50* (19), 7657–7665. https://doi.org/10.1021/acs.macromol.7b01187.

(24)   Chakma, P.; Konkolewicz, D. Dynamic Covalent Bonds in Polymeric Materials. *Angew. Chemie - Int. Ed.* **2019**, *58* (29), 9682–9695. https://doi.org/10.1002/anie.201813525.

(25)   He, C.; Shi, S.; Wang, D.; Helms, B. A.; Russell, T. P. Poly(Oxime-Ester) Vitrimers with Catalyst-Free Bond Exchange. *J. Am. Chem. Soc.* **2019**, *141* (35), 13753–13757. https://doi.org/10.1021/jacs.9b06668.

(26)   De Hoe, G. X.; Zumstein, M. T.; Tiegs, B. J.; Brutman, J. P.; McNeill, K.; Sander, M.; Coates, G. W.; Hillmyer, M. A. Sustainable Polyester Elastomers from Lactones: Synthesis, Properties, and Enzymatic Hydrolyzability. *J. Am. Chem. Soc.* **2018**, *140* (3), 963–973. https://doi.org/10.1021/jacs.7b10173.

(27)   Lundberg, D. J.; Lundberg, D. J.; Hillmyer, M. A.; Dauenhauer, P. J. Techno-Economic Analysis of a Chemical Process to Manufacture Methyl-ε-Caprolactone from Cresols. *ACS Sustain. Chem. Eng.* **2018**, *6* (11), 15316–15324. https://doi.org/10.1021/acssuschemeng.8b03774.

(28)   Li, L.; Chen, X.; Jin, K.; Torkelson, J. M. Vitrimers Designed Both to Strongly Suppress Creep and to Recover Original Cross-Link Density after Reprocessing: Quantitative Theory and Experiments. *Macromolecules* **2018**, *51* (15), 5537–5546. https://doi.org/10.1021/acs.macromol.8b00922.

(29)   El-Zaatari, B. M.; Ishibashi, J. S. A.; Kalow, J. A. Cross-Linker Control of Vitrimer Flow. *Polym. Chem.* **2020**. https://doi.org/10.1039/d0py00233j.

(30)   Lewis, S. E.; Wilhelmy, B. E.; Leibfarth, F. A. Upcycling Aromatic Polymers through C-H Fluoroalkylation. *Chem. Sci.* **2019**, *10* (25), 6270–6277. https://doi.org/10.1039/c9sc01425j.

(31)   Lewis, S. E.; Wilhelmy, B. E.; Leibfarth, F. A. Organocatalytic C–H Fluoroalkylation of Commodity Polymers. *Polym. Chem.* **2020**. https://doi.org/10.1039/c9py01884k.

(32)   Arslan, M.; Acik, G.; Tasdelen, M. A. The Emerging Applications of Click Chemistry Reactions in the Modification of Industrial Polymers. *Polym. Chem.* **2019**, *10* (28), 3806–3821. https://doi.org/10.1039/c9py00510b.

(33)   Short, G. N.; Nguyen, H. T. H.; Scheurle, P. I.; Miller, S. A. Aromatic Polyesters from Biosuccinic Acid. *Polym. Chem.* **2018**, *9* (30), 4113–4119. https://doi.org/10.1039/c8py00862k.

(34)   Gandini, A.; Lacerda, T. M.; Carvalho, A. J. F.; Trovatti, E. Progress of Polymers from Renewable Resources: Furans, Vegetable Oils, and Polysaccharides. *Chem. Rev.* **2016**, *116* (3), 1637–1669. https://doi.org/10.1021/acs.chemrev.5b00264.

(35)   Hatton, F. L. Recent Advances in RAFT Polymerization of Monomers Derived from Renewable Resources. *Polym. Chem.* **2020**, *11* (2), 220–229. https://doi.org/10.1039/c9py01128e.

(36)   Odian, G. *Principles of Polymerization*, 4th ed.; John Wiley & Sons, Inc.: Hoboken, New Jersey, 2004.

(37)   Rudin, A.; Choi, P. *The Elements of Polymer Science & Engineering*, 3rd ed.; Academic Press, 2012. https://doi.org/10.1016/B978-0-12-382178-2.00007-9.

(38)   *Handbook of Radical Polymerization*; Matyjaszewski, K., Davis, T. P., Eds.; John Wiley
        & Sons, Inc., 2002.

(39)   *Handbook of Ring-Opening Polymerization*; Dubois, P., Coulembier, O., Raquez, J., Eds.;
        Wiley-VCH Verlag GmbH & Co. KGaA, 2009.

(40)   Buchmeiser, M. R. Ring-Opening Metathesis Polymerization. In *Ring-Opening
        Polymerization*; Dubois, P., Coulembier, O., Raquez, J., Eds.; Wiley-VCH Verlag GmbH
        & Co. KGaA, 2009; pp 197–225.

(41)   Chen, Y.; Kakuchi, T. Organocatalyzed Group Transfer Polymerization. *Chem. Rec.* **2016**,
        16 (4), 2161–2183. https://doi.org/10.1002/tcr.201600034.

(42)   Stefan, M. C.; Javier, A. E.; Osaka, I.; McCullough, R. D. Grignard Metathesis Method
        (GRIM): Toward a Universal Method for the Synthesis of Conjugated Polymers.
        Macromolecules **2009**, *42* (1), 30–32. https://doi.org/10.1021/ma8020823.

(43)   Stefan, M. C.; Bhatt, M. P.; Sista, P.; Magurudeniya, H. D. Grignard Metathesis (GRIM)
        Polymerization for the Synthesis of Conjugated Block Copolymers Containing
        Regioregular Poly(3-Hexylthiophene). *Polym. Chem.* **2012**, *3* (7), 1693–1701.
        https://doi.org/10.1039/c1py00453k.

(44)   Ozaki, S. Recent Advances in Isocyanate Chemistry. *Chem. Rev.* **1972**, *72* (5), 457–496.
        https://doi.org/10.1021/cr60279a002.

(45)   Lyman, D. J. Polyurethanes. I. The Solution Polymerization of Diisocyanates with
        Ethylene Glycol. *J. Polym. Sci.* **1960**, *45* (145), 49–59.
        https://doi.org/10.1002/pol.1960.1204514505.

(46)   Shashoua, V. E. The Homopolymerization of Monoisocyanates. *J. Am. Chem. Soc.* **1959**,
        81 (12), 3156–3156.

(47) Sardon, H.; Pascual, A.; Mecerreyes, D.; Taton, D.; Cramail, H.; Hedrick, J. L. Synthesis of Polyurethanes Using Organocatalysis: A Perspective. *Macromolecules* **2015**, *48* (10), 3153–3165. https://doi.org/10.1021/acs.macromol.5b00384.

(48) Sharmin, E.; Zafar, F. *Polyurethane : An Introduction*; IntechOpen, 2012. https://doi.org/10.5772/51663.

(49) Shashoua, V. E.; Sweeny, W.; Tietz, R. F. The Homopolymerization of Monoisocyanates. *J. Am. Chem. Soc.* **1960**, *82* (4), 866–873.

(50) Okamoto, Y.; Nagamura, Y.; Hatada, K.; Khatri, C.; Green, M. M. An Unexpected Chiral Spiro Tetramer Offers Mechanistic Insight into an Improved Sodium Cyanide Initiated Polymerization of N-Hexyl Isocyanate in Toluene. *Macromolecules* **1992**, *25* (20), 5536–5538. https://doi.org/10.1021/ma00046a066.

(51) Lee, J. S.; Ryu, S. W. Anionic Living Polymerization of 3-(Triethoxysilyl)Propyl Isocyanate. *Macromolecules* **1999**, *32* (6), 2085–2087. https://doi.org/10.1021/ma9817065.

(52) Shin, Y. D.; Ahn, J. H.; Lee, J. S. Anionic Polymerization of Isocyanates with Optical Functionalities. *Polymer (Guildf).* **2001**, *42* (19), 7979–7985. https://doi.org/10.1016/S0032-3861(01)00324-X.

(53) Shin, Y. D.; Kim, S. Y.; Ahn, J. H.; Lee, J. S. Synthesis of Poly(n-Hexyl Isocyanate) by Controlled Anionic Polymerization in the Presence of NaBPh4. *Macromolecules* **2001**, *34* (8), 2408–2410. https://doi.org/10.1021/ma0019813.

(54) Chae, C.-G.; Seo, H.-B.; Bak, I.-G.; Lee, J.-S. Synthesis of Amphiphilic Helix−Coil−Helix Poly(3- (Glycerylthio)Propyl Isocyanate)-Block-Polystyrene-Block-Poly(3- (Glycerylthio)Propyl Isocyanate). *Macromolecules* **2018**, *51* (3), 697–704.

(55) Zorba, G.; Vazaios, A.; Pitsikalis, M.; Hadjichristidis, N. Anionic Polymerization of N-Hexyl Isocyanate with Monofuctional Initiators. Synthesis of Well-Defined Diblock Copolymers with Styrene and Isoprene. *J. Polym. Sci. Part A Polym. Chem.* **2005**, *43* (16), 3533–3542. https://doi.org/10.1002/pola.20831.

(56) Ahn, J. H.; Shin, Y. D.; Nath, G. Y.; Park, S. Y.; Rahman, M. S.; Samal, S.; Lee, J. S. Unprecedented Control over Polymerization of N-Hexyl Isocyanate Using an Anionic Initiator Having Synchronized Function of Chain-End Protection. *J. Am. Chem. Soc.* **2005**, *127* (12), 4132–4133. https://doi.org/10.1021/ja0427000.

(57) Min, J.; Shah, P. N.; Ahn, J. H.; Lee, J. S. Effects of Different Reactive Oxyanionic Initiators on the Anionic Polymerizaition of N-Hexyl Isocyanate. *Macromolecules* **2011**, *44* (9), 3211–3216. https://doi.org/10.1021/ma200414f.

(58) Min, J.; Yoo, H. S.; Shah, P. N.; Chae, C. G.; Lee, J. S. Enolate Anionic Initiator, Sodium Deoxybenzoin, for Leading Living Natures by Formation of Aggregators at the Growth Chain Ends. *J. Polym. Sci. Part A Polym. Chem.* **2013**, *51* (8), 1742–1748. https://doi.org/10.1002/pola.26550.

(59) Patten, T. E.; Novak, B. M. "Living" Titanium(IV) Catalyzed Coordination Polymerizations of Isocyanates. *J. Am. Chem. Soc.* **1991**, *113* (13), 5065–5066. https://doi.org/10.1021/ja00013a055.

(60) Patten, T. E.; Novak, B. M. Organotitanium(IV) Compounds as Catalysts for the Polymerization of Isocyanates: The Polymerization of Isocyanates with Functionalized Side Chains. *Macromolecules* **1993**, *26* (3), 436–439. https://doi.org/10.1021/ma00055a005.

(61) Patten, T. E.; Novak, B. M. Living Organotitanium(IV)-Catalyzed Polymerizations of

Isocyanates. *J. Am. Chem. Soc.* **1996**, *118* (8), 1906–1916. https://doi.org/10.1021/ja9534516.

(62)   Hoff, S. M.; Novak, B. M. Complex Architectures through Living Polymerizations. The Synthesis of "Once-Broken Worms" and Triblock Copolymers Using Bimetallic Initiators. *Macromolecules* **1993**, *26* (15), 4067–4069. https://doi.org/10.1021/ma00067a056.

(63)   Natta, G.; DiPietro, J.; Cambini, M. Crystalline Polymers of Phenyl- and n-Butylisocyanates. *Macromol. Chem. Phys.* **1962**, *56* (1), 200–207.

(64)   Goodman, M.; Chen, S. Optically Active Polyisocyanates. *Macromolecules* **1970**, *3* (4), 398–402. https://doi.org/10.1007/978-3-540-72816-0_15718.

(65)   Green, M. M.; Peterson, N. C.; Sato, T.; Teramoto, A.; Cook, R.; Lifson, S. A Helical Polymer with a Cooperative Response to Chiral Information. *Science (80-.).* **1995**, *268* (5219), 1860–1866. https://doi.org/10.1126/science.268.5219.1860.

(66)   Maeda, K.; Okamoto, Y. Synthesis and Conformation of Optically Active Poly(Phenyl Isocyanate)s Bearing an ((S)-(R-Methylbenzyl)Carbamoyl) Group. *Macromolecules* **1998**, *31* (4), 1046–1052. https://doi.org/10.1021/ma970948m.

(67)   Green, M. M.; Khatri, C. A.; Reidy, M. P.; Levon, K. Dilute-Solution Chiral Optical Changes Signal the Thermally Reversible Gelation of Poly(n-Hexyl Isocyanate) in Hydrocarbon Solvents. *Macromolecules* **1993**, *26* (17), 4723–4725. https://doi.org/10.1021/ma00069a050.

(68)   Maxein, G.; Mayer, S.; Zentel, R. Structure-Property Relations in Cholesteric Networks from Chiral Polyisocyanates. *Macromolecules* **1999**, *32* (18), 5747–5754. https://doi.org/10.1021/ma990326w.

(69)   Itou, T.; Teramoto, A. Isotropic-Liquid Crystal Phase Equilibrium in Solutions of

Semiflexible Polymers: Poly(Hexyl Isocyanate). *Macromolecules* **1988**, *21* (7), 2225–2230. https://doi.org/10.1021/ma00185a058.

(70)   Aharoni, S. M. Rigid Backbone Polymers. 2. Polyisocyanates and Their Liquid-Crystal Behavior. *Macromolecules* **1979**, *12* (1), 94–103. https://doi.org/10.1021/ma60067a021.

(71)   Taylor, D. R. The Chemistry of Allenes. *Chem. Rev.* **1967**, *67* (3), 317–359. https://doi.org/10.1021/cr60247a004.

(72)   Rivera-Fuentes, P.; Diederich, F. Allenes in Molecular Materials. *Angew. Chemie - Int. Ed.* **2012**, *51* (12), 2818–2828. https://doi.org/10.1002/anie.201108001.

(73)   Weinstein, B.; Fenselau, A. . Oligomers of Allene. Part II. Dimers and Trimers Formed in the Thermal Polymerisation of Liquid Allene. *J. Chem. Soc. C* **1967**, 368–372.

(74)   Weinstein, B.; Fenselau, A. H. Oligomers of Allene. III. Tetramers Formed in the Thermal Polymerization of Liquid Allene. *J. Org. Chem.* **1967**, *32* (7), 2278–2283. https://doi.org/10.1021/jo01282a041.

(75)   Dai, S. H.; Dolbier, W. R. Oligomerization and Co-Oligomerizations of Allene. *J. Org. Chem.* **1972**, *37* (7), 950–955. https://doi.org/10.1021/jo00972a007.

(76)   Takahashi, T.; Yokozawa, T.; Endo, T. Cationic Polymerization of Methoxyallene with Lewis Acids. *Die Makromol. Chemie* **1991**, *192* (5), 1207–1212. https://doi.org/10.1002/macp.1991.021920519.

(77)   Takahashi, T.; Yokozawa, T.; Endo, T. Cationic Polymerization of Gamma-Methyl- and Alpha-Methylphenylallene. *J. Polym. Sci. Part A Polym. Chem.* **1992**, *30*, 583–587.

(78)   Yokozawa, T.; Tanaka, M.; Endo, T. Radical Polymerization of Alkoxyallenes. *Chem. Lett.* **1987**, *16* (9), 1831–1834. https://doi.org/10.1246/cl.1987.1831.

(79)   Suzuki, M.; Takao, T.; Sakamoto, N.; Tomita, I.; Endo, T. Ni-Catalyzed Living

Coordination Polymerization of Allenes Having Si-Based Functional Groups. *Polymer Journal*. 1999, pp 1021–1024. https://doi.org/10.1295/polymj.31.1021.

(80)   Endo, T.; Takagi, K.; Tomita, I. Design and Synthesis of Polymerizable Cumulated Double Bond System. - Living Coordination Polymerization of Alkylallenes by Π-Allylnickel Catalyst-. *Tetrahedron* **1997**, *53* (45), 15187–15196. https://doi.org/10.1016/S0040-4020(97)00956-3.

(81)   Choi, J. C.; Osakada, K.; Yamaguchi, I.; Yamamoto, T. Polymerization of Arylallenes Catalyzed by Organo-Rhodium(I) and -Cobalt (I) Complexes to Give Structurally Regulated High-Mass Polymers. *Appl. Organomet. Chem.* **1997**, *11* (12), 957–961. https://doi.org/10.1002/(SICI)1099-0739(199712)11:12<957::AID-AOC654>3.0.CO;2-1.

(82)   Takagi, K.; Tomita, I.; Endo, T. A Novel Living Coordination Polymerization of Phenylallene Derivatives by π-Allylnickel Catalyst. *Macromolecules* **1997**, *30* (24), 7386–7390. https://doi.org/10.1021/ma9708959.

(83)   Lin, F.; Liu, Z.; Wang, T.; Cui, D. Highly 2,3-Selective Polymerization of Phenylallene and Its Derivatives with Rare-Earth Metal Catalysts: From Amorphous to Crystalline Products. *Angew. Chemie - Int. Ed.* **2017**, *56* (46), 14653–14657. https://doi.org/10.1002/anie.201707601.

(84)   Yamauchi, A.; Shirai, A.; Kawabe, K.; Iwamoto, T.; Wakiya, T.; Nishiyama, H.; Inagi, S.; Tomita, I. Well-Defined Polymer Microspheres Formed by Living Dispersion Polymerization: Precisely Functionalized Crosslinked Polymer Microspheres from Monomers Possessing Cumulated Double Bonds. *Asia Mater.* **2016**, *8*, 1–12. https://doi.org/10.1038/am.2016.123.

(85)   Sakai, K.; Nishiyama, H.; Inagi, S.; Tomita, I.; Hibi, Y.; Komura, M.; Nose, K.; Iyoda, T.

Synthesis of Well-defined Block Copolymer Composed of Flexible Amphiphilic Poly(Ethylene Glycol) and Hydrophobic Liquid Crystalline Segments by Living Coordination Polymerization of Allene Derivatives and Its Application to Thin Film with Perpendicularly. *J. Polym. Sci.* **2020**, No. January, 1–8. https://doi.org/10.1002/pol.20190165.

(86)   Havinga, R.; Schors, A.; Visser, J. W. Preparation and Properties of Polyallenes . II . Phase Transitions of Polyallene. *J. Macromol. Sci.* **1968**, *2* (1), 21–30. https://doi.org/10.1080/00222336808053344.

(87)   Huisgen, R.; Otto, P. The Mechanism of Dimerization of Dimethylketene. *J. Am. Chem. Soc.* **1968**, *90* (19), 5342–5343. https://doi.org/10.1021/ja01021a090.

(88)   Elam, E. U. Ketenes. XI. Preparation of β-Lactone Dimer by Dimerization of Dimethylketene in the Presence of Derivatives of Trivalent Phosphorus. *J. Org. Chem.* **1967**, *32* (1), 215–216. https://doi.org/10.1021/jo01277a053.

(89)   Hasek, R. H.; Clark, R. D.; Elam, E. U.; Martin, J. C. The Chemistry of Dimethylketene Dimer. IV. The Polyester and β-Lactone Dimer of Dimethylketene. *J. Org. Chem.* **1962**, *27* (1), 60–64. https://doi.org/10.1021/jo01048a015.

(90)   Staudinger, H. Ketene: Uber Additions Und Polymerisationreaktionen Des Dimethylketens. *Helvetica* **1925**, *8* (1), 306–332.

(91)   Natta, G.; Mazzanti, G.; Pregaglia, G.; Binaghi, M. Alternating Copolymers of Dimethylketene with Ketones. *J. Am. Chem. Soc.* **1960**, *82* (20), 5511–5512. https://doi.org/10.1021/ja01505a057.

(92)   Pregaglia, G. F.; Binaghi, M.; Cambini, M. Polydimethylketene with Carbon- Oxygen Backbone Stnicture. *Macromol. Chem. Phys.* **1963**, *67* (1), 10–30.

(93) Yamashita, Y.; Miura, S.; Nakamura, M. Ambient Nature of the Polydimethylketene Anion. *Die Makromol. Chemie* **1963**, *68* (1), 31–47. https://doi.org/10.1002/macp.1963.020680104.

(94) Natta, G.; Mazzanti, G.; Pregaglia, G. F.; Pozzi, G. Alternating Copolymers Having a Stereoregular Polyester Structure. *J. Polym. Sci.* **1962**, *58* (166), 1201–1210. https://doi.org/10.1002/pol.1962.1205816676.

(95) Tsunetsugu, T.; Arimoto, K.; Fueno, T.; Furukawa, J. Polymerization of Methylphenylketene and Its Copolymerization with Benzaldehyde. *Macromol. Chem. Phys.* **1968**, *112* (1), 210–219.

(96) Yamashita, S.; Nunomoto, Y. Polymerizability of Diphenylketene. *Kogyo Kagaku Zasshi* **1968**, *71* (12), 2067–2072.

(97) Dyer, E.; Sincich, E. Anionic Copolymerization of Isocyanates With Ketenes. *J. Polym. Sci. Polym. Chem. Ed.* **1973**, *11* (6), 1249–1260. https://doi.org/10.1002/pol.1973.170110612.

(98) Sudo, A.; Uchino, S.; Endo, T. Development of a Living Anionic Polymerization of Ethylphenylketene: A Novel Approach to Well-Defined Polyester Synthesis. *Macromolecules* **1999**, *32* (5), 1711–1713. https://doi.org/10.1021/ma981567r.

(99) Natta, G.; Mazzanti, G.; Pregaglia, G.; Binaghi, M.; Peraldo, M. Crystalline Polymers of Dimethylketene. *J. Am. Chem. Soc.* **1960**, *82* (17), 4742–4743. https://doi.org/10.1021/ja01502a073.

(100) Egret, H.; Couvercelle, J. P.; Belleney, J.; Bunel, C. Cationic Polymerization of Dimethyl Ketene. *Eur. Polym. J.* **2002**, *38* (10), 1953–1961. https://doi.org/10.1016/S0014-3057(02)00102-7.

(101) Nagai, D.; Sudo, A.; Endo, T. Stereocontrolled Anionic Alternating Copolymerization of Ethylphenylketene with Benzaldehyde by a Bisoxazoline Ligand. *J. Polym. Sci. Part A Polym. Chem.* **2004**, *42* (21), 5384–5388. https://doi.org/10.1002/pola.20310.

(102) Nagai, D.; Sudo, A.; Endo, T. Anionic Alternating Copolymerization of Ketene and Aldehyde: Control of Enantioselectivity by Bisoxazoline-Type Ligand for Synthesis of Optically Active Polyesters. *Macromolecules* **2006**, *39* (26), 8898–8900. https://doi.org/10.1021/ma0620971.

(103) Tidwell, T. T. *Ketenes II*, 2nd ed.; John Wiley & Sons, Inc.: Hoboken, New Jersey, 2006.

(104) Ruden, R. A. Trimethylsilylketene. Acylation and Olefination Reactions. *J. Org. Chem.* **1974**, *39* (24), 3607–3608. https://doi.org/10.1021/jo00938a041.

(105) Valentí, E.; Pericàs, M. A.; Serratosa, F. Convenient Synthesis of Silylketenes from 1-Tert-Butoxy-2-Silylethynes. *J. Org. Chem.* **1990**, *55* (1), 395–397. https://doi.org/10.1021/jo00288a081.

(106) Black, T. H.; Farrell, J. R.; Probst, D. A.; Zotz, M. C. A High Yielding, Reproducible Synthesis of Trimethylsilylketene. *Synth. Commun.* **2002**, *32* (13), 2083–2088. https://doi.org/10.1081/SCC-120004861.

(107) Pericàs, M. A.; Serratosa, F.; Valentí, E. An Efficient Synthesis of Tert-Alkoxyethynes. *Tetrahedron* **1987**, *43* (10), 2311–2316. https://doi.org/10.1016/S0040-4020(01)86815-0.

(108) Xiang, Y.; Burrill, D. J.; Bullard, K. K.; Albrecht, B. J.; Tragesser, L. E.; McCaffrey, J.; Lambrecht, D. S.; Pentzer, E. Polymerization of Silyl Ketenes Using Alkoxide Initiators: A Combined Computational and Experimental Study. *Polym. Chem.* **2017**, *8* (35), 5381–5387. https://doi.org/10.1039/C7PY00858A.

(109) Lutsenko, I. F.; Baukov, Y. I.; Kostyuk, A. S.; Savelyeva, N. I.; Krysina, V. K. Interaction

of Ketene with Silylated Amines or Amides. *J. Organomet. Chem.* **1969**, *17* (2), 241–262. https://doi.org/10.1016/S0022-328X(00)88613-1.

(110) Baigrie, L. M.; Seiklay, H. R.; Tidwell, T. T. Stereospecific Formation of Enolates from Reaction of Unsymmetrical Ketenes and Organolithium Reagents. *J. Am. Chem. Soc.* **1985**, *107* (19), 5391–5396. https://doi.org/10.1021/ja00305a012.

(111) Olah, G. A.; Wu, A.; Farooq, O. Intramolecular Dehydration of Dialkylacetic Acids and Trimethylsilylacetic Acid with Dicyclohexylcarbodiimide to the Corresponding Stable Ketenes. *Synthesis (Stuttg).* **1989**, 568.

(112) Sakurai, H.; Shirahata, A.; Sasaki, K.; Hosomi, A. A Convenient Synthesis of Iodotrimethylsilane and Its Use in the Preparation of Silylketenes. *Synthesis (Stuttg).* **1979**, 740.

(113) Pons, J.; Kocienski, P. A Synthesis of (-)-Tetrahydrolipstatin. *Tetrahedron Lett.* **1989**, *30* (14), 1833–1836.

(114) Brückmann, R.; Schneider, K.; Maas, G. Wolff Rearrangement of (1-Diazo-2-Oxoalkyl) Silanes. *Tetrahedron* **1989**, *45* (17), 5517–5530. https://doi.org/10.1016/S0040-4020(01)89498-9.

(115) Gerhard Maas; Brückmann, R. Preparation of 1-Aryl-2-Siloxyalkynes from Silylated Alpha-Diazo Carbonyl Compounds. *J. Org. Chem* **1985**, *50*, 2801–2802.

(116) Xiang, Y.; Rheingold, A. L.; Pentzer, E. B. Synthesis of Highly Functionalized 2-Pyranone from Silyl Ketene. *ACS Omega* **2018**, *3* (8), 9419–9423. https://doi.org/10.1021/acsomega.8b01531.

(117) Xiang, Y.; Mitchell, S.; Rheingold, A. L.; Lambrecht, D. S.; Pentzer, E. Oligomerization of Silyl Ketene: Favoring Chain Extension over Backbiting. *Macromolecules* **2019**, *52*

(16), 6126–6134. https://doi.org/10.1021/acs.macromol.9b00752.

(118) Brady, W. T.; Saidi, K. Trimethylsilylketene. Cycloadditions of Ketenes and Aldehydes. *J. Org. Chem* **1979**, *44* (5), 733–737.

(119) Yang, H. W.; Romo, D. Studies of the Asymmetric [2+2] Cycloaddition of Silylketenes and Aldehydes Employing Ti-TADDOL Catalysts. *Tetrahedron Lett.* **1998**, *39* (19), 2877–2880. https://doi.org/10.1016/S0040-4039(98)00422-5.

(120) Concepcion, A. B.; Maruoka, K.; Yamamoto, H. Organoaluminum-Promoted Cycloaddition of Trialkylsilylketene with Aldehydes: A New, Stereoselective Approach to Cis-2-Oxetanones and 2(Z)-Alkenoic Acids. *Tetrahedron* **1995**, *51* (14), 4011–4020. https://doi.org/10.1016/0040-4020(95)00142-U.

(121) Dymock, B. W.; Kocienski, P. J.; Pons, J. View Article Online / Journal Homepage / Table of Contents for This Issue 3-(Trimethylsilyl)Oxetan-2-Ones via Enantioselective [2+2] Cycloaddition of (Trimethylsily1)Ketene to Aldehydes Catalysed by Methylaluminoimidazolines. *Chem. Commun.* **1996**, No. 3, 1053–1054.

(122) Rossé, G.; Gerber, F.; Specklin, J. L.; Hubschwerlen, C. A Novel Synthesis of β-Sulfinyl- and β-Sulfonyl-Hydroxamic Acids via CsF-Mediated Ring Opening of Substituted β-Lactones. *Synlett* **2001**, No. 4, 538–540. https://doi.org/10.1055/s-2001-12311.

(123) Brady, W. T.; Cheng, T. C. Phenyl(Trimethylsilyl)Ketene. Some Ketene Reactions with Diazomethane. *J. Organomet. Chem.* **1977**, *137* (3), 287–292. https://doi.org/10.1016/S0022-328X(00)81435-7.

(124) Allen, A.; Tidwell, T. Trimethylsilylketene: Reactivity and Stabilization. *Tetrahedron Lett.* **1991**, *32* (7), 847–850.

(125) Green, I. X.; Tang, W.; Neurock, M.; Yates, J. T. Localized Partial Oxidation of Acetic

Acid at the Dual Perimeter Sites of the Au/TiO2 Catalyst-Formation of Gold

Ketenylidene. *J. Am. Chem. Soc.* **2012**, *134* (33), 13569–13572.

https://doi.org/10.1021/ja305911e.

(126) Hurd, C. D.; Blunck, F. H. The Pyrolysis of Esters. *J. Am. Chem. Soc.* **1938**, *60* (10),

2419–2425. https://doi.org/10.1021/ja01277a035.

(127) DeWitt, C. H. The Ketenic Decomposition Of Ketones. Ketene And Methyl Ketene. *J.

Am. Chem. Soc.* **1923**, *45* (12), 3095–3101. https://doi.org/10.1021/ja01665a042.

(128) Haller, I.; Srinivasan, R. Primary Processes in the Photochemistry of TetramethyI-1,3-

Cyclobutanedione. *J. Am. Chem. Soc.* **1965**, *87* (5), 1144–1145.

https://doi.org/10.1021/ja01083a044.

(129) Turro, N. J.; Leermakers, P. A.; Wilson, H. R.; Neckers, D. C.; Byers, G. W.; Vesley, G.

F. Photochemistry of 1,3-Cyclobutanediones. Decomposition Modes and Chemical

Intermediates. *J. Am. Chem. Soc.* **1965**, *87* (12), 2613–2619.

https://doi.org/10.1021/ja01090a017.

(130) Fisher, G. J.; MacLean, A. F.; Schnizer, A. W. Apparatus For The Preparation Of Ketene

By The Pyrolysis Of Acetic Anhydride. *J. Org. Chem.* **1953**, *18* (8), 1055–1057.

https://doi.org/10.1021/jo50014a021.

(131) Hertler, W. R.; Sogah, D. Y.; Webster, O. W.; Trost, B. M. Group-Transfer

Polymerization. 3. Lewis Acid Catalysis. *Macromolecules* **1984**, *17* (7), 1415–1417.

https://doi.org/10.1021/ma00137a021.

(132) Kojima, K.; Sawamoto, M.; Higashimura, T. Living Cationic Polymerization of Isobutyl

Vinyl Ether by Hydrogen Iodide/Lewis Acid Initiating Systems: Effects of Lewis Acid

Activators and Polymerization Kinetics. *Macromolecules* **1989**, *22* (4), 1552–1557.

https://doi.org/10.1021/ma00194a008.

(133) Corma, A.; García, H. Lewis Acids as Catalysts in Oxidation Reactions: From Homogeneous to Heterogeneous Systems. *Chem. Rev.* **2002**, *102* (10), 3837–3892. https://doi.org/10.1021/cr010333u.

(134) Román-Leshkov, Y.; Davis, M. E. Activation of Carbonyl-Containing Molecules with Solid Lewis Acids in Aqueous Media. *ACS Catal.* **2011**, *1* (11), 1566–1580. https://doi.org/10.1021/cs200411d.

(135) Ruden, R. A. Trimethylsilylketene. Acylation and Olefination Reactions. *J. Org. Chem.* **1974**, *39* (24), 3607–3608. https://doi.org/10.1021/jo00938a041.

(136) Kita, Y.; Sekihachi, J. I.; Hayashi, Y.; Da, Y. Z.; Yamamoto, M.; Akai, S. An Efficient Synthesis of A-Silylacetates Having Various Types of Functional Groups in the Molecules. *J. Org. Chem.* **1990**, *55* (3), 1108–1112. https://doi.org/10.1021/jo00290a058.

(137) Kita, Y.; Matsuda, S.; Kitagaki, S.; Tsuzuki, Y.; Akai, S. Chemistry of Silylketene: A One-Pot Synthesis of a-Silyl Ketones. *Synlett* **1991**, *6*, 401–402.

(138) Johnson, D. A.; Jennings, M. P. Tandem Copper-Catalyzed Conjugate Addition-Diastereoselective Protonation of (E)-α-Trialkylsilyl-β-Alkyl(Aryl)-α,β-Unsaturated Esters. *Org. Lett.* **2018**, *20* (19), 6099–6103. https://doi.org/10.1021/acs.orglett.8b02527.

(139) Fessenden, R. J.; Fessenden, J. S. A Convenient Synthesis of α-Silyl Esters. *J. Org. Chem.* **1967**, *32* (11), 3535–3537. https://doi.org/10.1021/jo01286a054.

(140) Larson, G. L.; Fuentes, L. M. α-Silylation of Lithium Ester Enolates. *J. Am. Chem. Soc.* **1981**, *103* (9), 2418–2419. https://doi.org/10.1021/ja00399a052.

(141) Van Staden, L. F.; Gravestock, D.; Ager, D. J. New Developments in the Peterson Olefination Reaction. *Chem. Soc. Rev.* **2002**, *31* (3), 195–200.

https://doi.org/10.1039/a908402i.

(142) Larson, G. L.; Hernandez, D.; de Lopez-Cepero, I. M.; Torres, L. E. Reaction of α-Silyl Esters with Grignard Reagents: A Synthesis of β-Keto Silanes and Ketones. Preparation of the Douglas Fir Tussock Moth Pheromone. *J. Org. Chem.* **1985**, *50* (25), 5260–5267. https://doi.org/10.1021/jo00225a053.

(143) Gennari, C.; Beretta, M. G.; Bernardi, A.; Moro, G.; Scolastico, C.; Todeschini, R. Lewis Acid Mediated Aldol Condensations Using Thioester Silyl Ketene Acetals. *Tetrahedron* **1986**, *42* (3), 893–909.

(144) Ireland, R.; Wipf, P.; Armstrong, J. Stereochemical Control in the Ester Enolate Claisen Rearrangement. 1. Stereoselectivity in Silyl Ketene Acetal Formation. *J. Org. Chem.* **1991**, *56* (2), 650–657. https://doi.org/10.1021/jo00002a030.

(145) Hattori, K.; Yamamoto, H. Highly Selective Generation and Application of (E)- and (Z)-Silyl Ketene Acetals from α-Hydroxy Esters. *J. Org. Chem.* **1993**, *58* (20), 5301–5303. https://doi.org/10.1021/jo00072a005.

(146) Rikkou-Kalourkoti, M.; Webster, O. W.; Patrickios, C. S. Group Transfer Polymerization. *Encycl. Polym. Sci. Technol.* **2013**, *6*, 527–543.

(147) Valentí, E.; Pericàs, M. A.; Serratosa, F. Convenient Synthesis of Silylketenes from 1-Tert-Butoxy-2-Silylethynes. *J. Org. Chem.* **1990**, *55* (1), 395–397. https://doi.org/10.1021/jo00288a081.

(148) Pericas, M. A.; Serratosa, F.; Valenti, E. An Efficient Synthesis of Tert-Alkoxyethynes. *Tetrahedron* **1987**, *43* (10), 2311–2316.

(149) Webster, O. W.; Hertler, W. R.; Sogah, D. Y.; Farnham, W. B.; RajanBabu, T. V. Group-Transfer Polymerization. 1. A New Concept for Addition Polymerization with

Organosilicon Initiators. *J. Am. Chem. Soc.* **1983**, *105* (17), 5706–5708.
https://doi.org/10.1021/ja00355a039.

(150) Sogah, D. Y.; Hertler, W. R.; Webster, O. W.; Cohen, G. M. Group Transfer
Polymerization. Polymerization of Acrylic Monomers. *Macromolecules* **1987**, *20* (7),
1473–1488. https://doi.org/10.1021/ma00173a006.

(151) Webster, O. W. Group Transfer Polymerization: Mechanism and Comparison with Other
Methods for Controlled Polymerization of Acrylic Monomers. *Adv. Polym. Sci.* **2004**, *167*,
1–34. https://doi.org/10.1007/b12303.

(152) Zhang, J.; Wang, M.; Wang, J.; Shi, Y.; Tao, J.; Wang, D. Group Transfer Polymerization
of Acrylonitrile in Bulk at Ambient Temperature. *Polym. Bull.* **2005**, *54* (3), 157–161.
https://doi.org/10.1007/s00289-005-0376-3.

(153) Kikuchi, S.; Chen, Y.; Kitano, K.; Sato, S. I.; Satoh, T.; Kakuchi, T. B(C6F5)3-Catalyzed
Group Transfer Polymerization of N,N-Disubstituted Acrylamide Using Hydrosilane:
Effect of Hydrosilane and Monomer Structures, Polymerization Mechanism, and
Synthesis of α-End-Functionalized Polyacrylamides. *Macromolecules* **2016**, *49* (8), 3049–
3060. https://doi.org/10.1021/acs.macromol.6b00190.

(154) Fuchise, K.; Chen, Y.; Satoh, T.; Kakuchi, T. Recent Progress in Organocatalytic Group
Transfer Polymerization. *Polym. Chem.* **2013**, *4* (16), 4278–4291.
https://doi.org/10.1039/c3py00278k.

(155) Raynaud, J.; Gnanou, Y.; Taton, D. Group Transfer Polymerization of (Meth)Acrylic
Monomers Catalyzed by N-Heterocyclic Carbenes and Synthesis of All Acrylic Block
Copolymers: Evidence for an Associative Mechanism. *Macromolecules* **2009**, *42* (16),
5996–6005. https://doi.org/10.1021/ma900679p.

(156) Scholten, M. D.; Hedrick, J. L.; Waymouth, R. M. Group Transfer Polymerization of Acrylates Catalyzed by N-Heterocyclic Carbenes. *Macromolecules* **2008**, *41* (20), 7399–7404. https://doi.org/10.1021/ma801281q.

(157) Muller, A. H. Group Transfer and Anionic Polymerization: A Critical Comparison. *Makromol. Chemie. Macromol. Symp.* **1990**, *32*, 87–104.

(158) Vlček, P.; Lochmann, L. Anionic Polymerization of (Meth)Acrylate Esters in the Presence of Stabilizers of Active Centres. *Prog. Polym. Sci.* **1999**, *24* (6), 793–873. https://doi.org/10.1016/S0079-6700(99)00017-9.

(159) Raynaud, J.; Liu, N.; Fèvre, M.; Gnanou, Y.; Taton, D. No Matter the Order of Monomer Addition for the Synthesis of Well-Defined Block Copolymers by Sequential Group Transfer Polymerization Using N-Heterocyclic Carbenes as Catalysts. *Polym. Chem.* **2011**, *2* (8), 1706–1712. https://doi.org/10.1039/c1py00077b.

(160) Imada, M.; Takenaka, Y.; Tsuge, T.; Abe, H. Kinetic Modeling Study of the Group-Transfer Polymerization of Alkyl Crotonates Using a Silicon Lewis Acid Catalyst. *Polym. Chem.* **2020**, *11* (37), 5981–5991. https://doi.org/10.1039/d0py00353k.

(161) Fuchise, K.; Tsuchida, S.; Takada, K.; Chen, Y.; Satoh, T.; Kakuchi, T. B(C6F5)3-Catalyzed Group Transfer Polymerization of n-Butyl Acrylate with Hydrosilane through in Situ Formation of Initiator by 1,4-Hydrosilylation of n -Butyl Acrylate. *ACS Macro Lett.* **2014**, *3* (10), 1015–1019. https://doi.org/10.1021/mz5004689.

(162) Mitchell, S. M.; Xiang, Y.; Matthews, R.; Amburgey, A. M.; Pentzer, E. B. Lewis Acid-Activated Reactions of Silyl Ketenes for the Preparation of α-Silyl Carbonyl Compounds. *J. Org. Chem.* **2019**, *84* (22), 14461–14468. https://doi.org/10.1021/acs.joc.9b01859.

(163) Seyferth, D. The Grignard Reagents. *Organometallics* **2009**, *28*, 1598–1605.

https://doi.org/10.1021/om900088z.

(164) Aoshima, S.; Kanaoka, S. A Renaissance in Living Cationic Polymerization. *Chem. Rev.* **2009**, *109* (11), 5245–5287. https://doi.org/10.1021/cr900225g.

(165) Hattori, K.; Yamamoto, H. Highly Selective Generation and Application of (E)- and (Z)-Silyl Ketene Acetals from α-Hydroxy Esters. *J. Org. Chem.* **1993**, *58* (20), 5301–5303. https://doi.org/10.1021/jo00072a005.

(166) Olabi, A. G.; Onumaegbu, C.; Wilberforce, T.; Ramadan, M.; Abdelkareem, M. A.; Al – Alami, A. H. Critical Review of Energy Storage Systems. *Energy* **2021**, *214*, 118987. https://doi.org/10.1016/j.energy.2020.118987.

(167) Guney, M. S.; Tepe, Y. Classification and Assessment of Energy Storage Systems. *Renew. Sustain. Energy Rev.* **2017**, *75* (October 2016), 1187–1197. https://doi.org/10.1016/j.rser.2016.11.102.

(168) MacHado, C. A.; Brown, G. O.; Yang, R.; Hopkins, T. E.; Pribyl, J. G.; Epps, T. H. Redox Flow Battery Membranes: Improving Battery Performance by Leveraging Structure-Property Relationships. *ACS Energy Lett.* **2021**, *6* (1), 158–176. https://doi.org/10.1021/acsenergylett.0c02205.

(169) Wang, H.; Sayed, S. Y.; Luber, E. J.; Olsen, B. C.; Shirurkar, S. M.; Venkatakrishnan, S.; Tefashe, U. M.; Farquhar, A. K.; Smotkin, E. S.; McCreery, R. L.; Buriak, J. M. Redox Flow Batteries: How to Determine Electrochemical Kinetic Parameters. *ACS Nano* **2020**, *14* (3), 2575–2584. https://doi.org/10.1021/acsnano.0c01281.

(170) Zhang, C.; Zhang, L.; Ding, Y.; Guo, X.; Yu, G. Eutectic Electrolytes for High-Energy-Density Redox Flow Batteries. *ACS Energy Lett.* **2018**, *3* (12), 2875–2883. https://doi.org/10.1021/acsenergylett.8b01899.

(171) Wei, X.; Pan, W.; Duan, W.; Hollas, A.; Yang, Z.; Li, B.; Nie, Z.; Liu, J.; Reed, D.; Wang, W.; Sprenkle, V. Materials and Systems for Organic Redox Flow Batteries: Status and Challenges. *ACS Energy Lett.* **2017**, *2* (9), 2187–2204. https://doi.org/10.1021/acsenergylett.7b00650.

(172) Li, L.; Kim, S.; Wang, W.; Vijayakumar, M.; Nie, Z.; Chen, B.; Zhang, J.; Xia, G.; Hu, J.; Graff, G.; Liu, J.; Yang, Z. A Stable Vanadium Redox-Flow Battery with High Energy Density for Large-Scale Energy Storage. *Adv. Energy Mater.* **2011**, *1* (3), 394–400. https://doi.org/10.1002/aenm.201100008.

(173) Luo, J.; Hu, B.; Hu, M.; Zhao, Y.; Liu, L. Status and Prospects of Organic Redox Flow Batteries toward Sustainable Energy Storage. *ACS Energy Lett.* **2019**, *4*, 2220–2240. https://doi.org/10.1021/acsenergylett.9b01332.

(174) Smith, E. L.; Abbott, A. P.; Ryder, K. S. Deep Eutectic Solvents (DESs) and Their Applications. *Chem. Rev.* **2014**, *114* (21), 11060–11082. https://doi.org/10.1021/cr300162p.

(175) Zhang, Q.; Vigier, K. D. O.; Royer, S.; Jerome, F. Deep Eutectic Solvents: Syntheses, Properties and Applications. *Chem. Soc. Rev.* **2012**, *41*, 7108–7146. https://doi.org/10.1039/c2cs35178a.

(176) Hayyan, M.; Ali, M.; Hayyan, A.; Al-saadi, M. A.; Alnashef, I. M.; Mirghani, M. E. S.; Kola, O. Are Deep Eutectic Solvents Benign or Toxic ? *Chemosphere* **2013**, *90* (7), 2193–2195. https://doi.org/10.1016/j.chemosphere.2012.11.004.

(177) Haerens, K.; Matthijs, E.; Chmielarz, A.; Bruggen, B. Van Der. The Use of Ionic Liquids Based on Choline Chloride for Metal Deposition : A Green Alternative ? *J. Environ. Manage.* **2009**, *90* (11), 3245–3252. https://doi.org/10.1016/j.jenvman.2009.04.013.

(178) Constantin, V.; Adya, A. K.; Popescu, A. M. Density, Transport Properties and Electrochemical Potential Windows for the 2-Hydroxy-N,N,N-Trimethylethanaminium Chlorides Based Ionic Liquids at Several Temperatures. *Fluid Phase Equilib.* **2015**, *395*, 58–66. https://doi.org/10.1016/j.fluid.2015.03.025.

(179) Yadav, A.; Kar, J. R.; Verma, M.; Naqvi, S.; Pandey, S. Densities of Aqueous Mixtures of (Choline Chloride + Ethylene Glycol) and (Choline Chloride + Malonic Acid) Deep Eutectic Solvents in Temperature Range 283.15–363.15 K. *Thermochim. Acta* **2015**, *600*, 95–101. https://doi.org/10.1016/j.tca.2014.11.028.

(180) Abbott, A. P.; Capper, G.; Davies, D. L.; Rasheed, R. K.; Tambyrajah, V. Novel Solvent Properties of Choline Chloride / Urea Mixtures. *Chem. Commun.* **2003**, 70–71.

(181) Sas, O. G.; Fidalgo, R.; Domínguez, I.; Macedo, E. A.; González, B. Physical Properties of the Pure Deep Eutectic Solvent, [ChCl]:[Lev] (1:2) DES, and Its Binary Mixtures with Alcohols. *J. Chem. Eng. Data* **2016**, *61* (12), 4191–4202. https://doi.org/10.1021/acs.jced.6b00563.

(182) Khalid, M.; Hayyan, M.; Abdulhakim, M.; Akib, S. Glycerol-Based Deep Eutectic Solvents: Physical Properties. *J. Mol. Liq.* **2016**, *215*, 98–103. https://doi.org/10.1016/j.molliq.2015.11.032.

(183) Ibrahim, R. K.; Hayyan, M.; Alsaadi, M. A.; Ibrahim, S.; Hayyan, A.; Hashim, M. A. Diethylene Glycol Based Deep Eutectic Solvents and Their Physical Properties. *Stud. Univ. Babes-Bolyai Chem.* **2017**, *62* (4), 433–450. https://doi.org/10.24193/subbchem.2017.4.37.

(184) Abbott, A. P.; Boothby, D.; Capper, G.; Davies, D. L.; Rasheed, R. K. Deep Eutectic Solvents Formed between Choline Chloride and Carboxylic Acids : Versatile Alternatives

to Ionic Liquids. *J. Am. Chem. Soc.* **2004**, *126* (9), 9142–9147.
https://doi.org/10.1021/ja048266j.

(185) Kareem, M. A.; Mjalli, F. S.; Hashim, M. A.; Alnashef, I. M. Phosphonium-Based Ionic
Liquids Analogues and Their Physical Properties. *J. Chem. Eng. Data* **2010**, *55*, 4632–
4637.

(186) Bahadori, L.; Chakrabarti, M. H.; Mjalli, F. S.; Alnashef, I. M.; Manan, N. S. A.; Hashim,
M. A. Physicochemical Properties of Ammonium-Based Deep Eutectic Solvents and Their
Electrochemical Evaluation Using Organometallic Reference Redox Systems.
Electrochim. Acta **2013**, *113*, 205–211. https://doi.org/10.1016/j.electacta.2013.09.102.

(187) Brett, C. M. A. Deep Eutectic Solvents and Applications in Electrochemical Sensing.
Curr. Opin. Electrochem. **2018**, *10*, 143–148.
https://doi.org/10.1016/j.coelec.2018.05.016.

(188) Chakrabarti, M.; Mjalli, F.; AlNashef, I.; Hashim, M. A.; Hussain, M. A.; Bahadori, L.;
Low, C. Prospects of Applying Ionic Liquids and Deep Eutectic Solvents for Renewable
Energy Storage by Means of Redox Flow Batteries. *Renew. Sustain. Energy Rev.* **2014**,
30, 254–270. https://doi.org/10.1016/j.rser.2013.10.004.

(189) Shen, X.; Sinclair, N.; Wainright, J.; Akolkar, R.; Savinell, R. F. Evaluating and
Developing a Reliable Reference Electrode for Choline Chloride Based Deep Eutectic
Solvents. *J. Electrochem. Soc.* **2020**, *167* (8), 086509. https://doi.org/10.1149/1945-
7111/ab913c.

(190) Gurkan, B.; Squire, H.; Pentzer, E. Metal-Free Deep Eutectic Solvents: Preparation,
Physical Properties, and Significance. *J. Phys. Chem. Lett.* **2019**, *10* (24), 7956–7964.
https://doi.org/10.1021/acs.jpclett.9b01980.

(191) Hansen, B. B.; Spittle, S.; Chen, B.; Poe, D.; Zhang, Y.; Klein, J. M.; Horton, A.; Adhikari, L.; Zelovich, T.; Doherty, B. W.; Gurkan, B.; Maginn, E. J.; Ragauskas, A.; Dadmun, M.; Zawodzinski, T. A.; Baker, G. A.; Tuckerman, M. E.; Savinell, R. F.; Sangoro, J. R. Deep Eutectic Solvents: A Review of Fundamentals and Applications. *Chem. Rev.* **2021**, *121* (3), 1232–1285. https://doi.org/10.1021/acs.chemrev.0c00385.

(192) Abbott, A. P.; Capper, G.; Davies, D. L.; Rasheed, R. K.; Tambyrajah, V. Quaternary Ammonium Zinc- or Tin-Containing Ionic Liquids: Water Insensitive, Recyclable Catalysts for Diels-Alder Reactions. *Green Chem.* **2002**, *4* (1), 24–26. https://doi.org/10.1039/b108431c.

(193) Singh, B.; Lobo, H.; Shankarling, G. Selective N-Alkylation of Aromatic Primary Amines Catalyzed by Bio-Catalyst or Deep Eutectic Solvent. *Catal. Letters* **2011**, *141* (1), 178–182. https://doi.org/10.1007/s10562-010-0479-9.

(194) Cong, G.; Lu, Y. C. Organic Eutectic Electrolytes for Future Flow Batteries. *Chem* **2018**, *4* (12), 2732–2734. https://doi.org/10.1016/j.chempr.2018.11.018.

(195) Lloyd, D.; Vainikka, T.; Kontturi, K. The Development of an All Copper Hybrid Redox Flow Battery Using Deep Eutectic Solvents. *Electrochim. Acta* **2013**, *100*, 18–23. https://doi.org/10.1016/j.electacta.2013.03.130.

(196) Li, M.; Rhodes, Z.; Cabrera-Pardo, J. R.; Minteer, S. D. Recent Advancements in Rational Design of Non-Aqueous Organic Redox Flow Batteries. *Sustain. Energy Fuels* **2020**, *4* (9), 4370–4389. https://doi.org/10.1039/d0se00800a.

(197) Nishide, H.; Iwasa, S.; Pu, Y. J.; Suga, T.; Nakahara, K.; Satoh, M. Organic Radical Battery: Nitroxide Polymers as a Cathode-Active Material. *Electrochim. Acta* **2004**, *50* (2-3 SPEC. ISS.), 827–831. https://doi.org/10.1016/j.electacta.2004.02.052.

(198) Winsberg, J.; Hagemann, T.; Janoschka, T.; Hager, M. D.; Schubert, U. S. Redox-Flow Batteries : From Metals to Organic Redox- Active Materials. *Angew. Chemie - Int. Ed.* **2017**, *56*, 686–711. https://doi.org/10.1002/anie.201604925.

(199) Liu, T.; Wei, X.; Nie, Z.; Sprenkle, V.; Wang, W. A Total Organic Aqueous Redox Flow Battery Employing a Low Cost and Sustainable Methyl Viologen Anolyte and 4-HO-TEMPO Catholyte. *Adv. Energy Mater.* **2016**, *6*. https://doi.org/10.1002/aenm.201501449.

(200) Chang, Z.; Henkensmeier, D.; Chen, R. Shifting Redox Potential of Nitroxyl Radical by Introducing an Imidazolium Substituent and Its Use in Aqueous Fl Ow Batteries. *J. Power Sources* **2019**, *418* (February), 11–16. https://doi.org/10.1016/j.jpowsour.2019.02.028.

(201) Winsberg, J.; Stolze, C.; Schwenke, A.; Muench, S.; Hager, M. D.; Schubert, U. S. Aqueous 2,2,6,6-Tetramethylpiperidine-N-Oxyl Catholytes for a High-Capacity and High Current Density Oxygen-Insensitive Hybrid-Flow Battery. *ACS Energy Lett.* **2017**, *2* (2), 411–416. https://doi.org/10.1021/acsenergylett.6b00655.

(202) Takechi, K.; Kato, Y.; Hase, Y. A Highly Concentrated Catholyte Based on a Solvate Ionic Liquid for Rechargeable Flow Batteries. *Adv. Mater.* **2015**, *27* (15), 2501–2506. https://doi.org/10.1002/adma.201405840.

(203) Li, Z.; Li, S.; Liu, S.; Huang, K.; Fang, D.; Wang, F.; Peng, S. Electrochemical Properties of an All-Organic Redox Flow Battery Using 2,2,6,6-Tetramethyl-1-Piperidinyloxy and N-Methylphthalimide. *Electrochem. Solid-State Lett.* **2011**, *14* (12), A171. https://doi.org/10.1149/2.012112esl.

(204) Park, S.; Shim, J.; Yang, J.; Shin, K.; Jin, C.; Suk, B.; Lee, Y.; Jeon, J. Electrochemistry Communications Electrochemical Properties of a Non-Aqueous Redox Battery with All-Organic Redox Couples. *Electrochem. commun.* **2015**, *59*, 68–71.

https://doi.org/10.1016/j.elecom.2015.07.013.

(205) Janoschka, T.; Martin, N.; Hager, M. D.; Schubert, U. S. An Aqueous Redox-Flow Battery with High Capacity and Power : The TEMPTMA / MV System. *Angew. Chemie - Int. Ed.* **2016**, *55*, 14427–14430. https://doi.org/10.1002/anie.201606472.

(206) Paduszek, B.; Kalinowski, M. K. Redox Behaviour of Phenothiazine and Phenazine in Organic Solvents. *Electrochim. Acta* **1983**, *28* (5), 639–642. https://doi.org/10.1016/0013-4686(83)85057-9.

(207) Puzanowska-Tarasiewicz, H.; Kuźmicka, L.; Karpińska, J.; Mielech-Łukasiewicz, K. Efficient Oxidizing Agents for Determination of 2,10-Disubstituted Phenothiazines. *Anal. Sci.* **2005**, *21* (10), 1149–1153. https://doi.org/10.2116/analsci.21.1149.

(208) Kowalski, J. A.; Casselman, M. D.; Kaur, A. P.; Milshtein, J. D.; Elliott, C. F.; Modekrutti, S.; Attanayake, N. H.; Zhang, N.; Parkin, S. R.; Risko, C.; Brushett, F. R.; Odom, S. A. A Stable Two-Electron-Donating Phenothiazine for Application in Nonaqueous Redox Flow Batteries. *J. Mater. Chem. A* **2017**, *5* (46), 24371–24379. https://doi.org/10.1039/c7ta05883g.

(209) Attanayake, N. H.; Kowalski, J. A.; Greco, K. V.; Casselman, M. D.; Milshtein, J. D.; Chapman, S. J.; Parkin, S. R.; Brushett, F. R.; Odom, S. A. Tailoring Two-Electron-Donating Phenothiazines to Enable High-Concentration Redox Electrolytes for Use in Nonaqueous Redox Flow Batteries. *Chem. Mater.* **2019**, *31* (12), 4353–4363. https://doi.org/10.1021/acs.chemmater.8b04770.

(210) Buhrmester, C.; Moshurchak, L.; Wang, R. L.; Dahn, J. R. Phenothiazine Molecules. *J. Electrochem. Soc.* **2006**, *153* (2), A288. https://doi.org/10.1149/1.2140615.

(211) Abbott, A. P.; Harris, R. C.; Ryder, K. S. Application of Hole Theory to Define Ionic

Liquids by Their Transport Properties. *J. Phys. Chem. B* **2007**, *111*, 4910–4913.

https://doi.org/10.1021/jp0671998.

(212) Abbott, A. P. Application of Hole Theory to the Viscosity of Ionic and Molecular Liquids. *ChemPhysChem* **2004**, *5* (8), 1242–1246. https://doi.org/10.1002/cphc.200400190.

(213) Cardellini, F.; Germani, R.; Cardinali, G.; Corte, L.; Roscini, L.; Spreti, N.; Tiecco, M. Room Temperature Deep Eutectic Solvents of (1S)-(+)-10-Camphorsulfonic Acid and Sulfobetaines: Hydrogen Bond-Based Mixtures with Low Ionicity and Structure-Dependent Toxicity. *RSC Adv.* **2015**, *5* (40), 31772–31786.

https://doi.org/10.1039/c5ra03932k.

(214) Reber, D.; Figi, R.; Kühnel, R. S.; Battaglia, C. Stability of Aqueous Electrolytes Based on LiFSI and NaFSI. *Electrochim. Acta* **2019**, *321*, 134644.

https://doi.org/10.1016/j.electacta.2019.134644.

(215) Manda, S.; Nakanishi, I.; Ohkubo, K.; Kawashima, T.; Matsumoto, K. I.; Ozawa, T.; Fukuzumi, S.; Ikota, N.; Anzai, K. Effect of Solvent Polarity on the One-Electron Oxidation of Cyclic Nitroxyl Radicals. *Chem. Lett.* **2007**, *36* (7), 914–915.

https://doi.org/10.1246/cl.2007.914.

(216) Park, S. K.; Shim, J.; Yang, J. H.; Shin, K. H.; Jin, C. S.; Lee, B. S.; Lee, Y. S.; Jeon, J. D. Electrochemical Properties of a Non-Aqueous Redox Battery with All-Organic Redox Couples. *Electrochem. commun.* **2015**, *59*, 68–71.

https://doi.org/10.1016/j.elecom.2015.07.013.

(217) Stoyanovsky, A. D.; Stoyanovsky, D. A. 1-Oxo-2,2,6,6-Tetramethylpiperidinium Bromide Converts α -H N,N- Dialkylhydroxylamines to Nitrones via a Two-Electron Oxidation Mechanism. *Sci. Rep.* **2018**, *8* (May), 15323. https://doi.org/10.1038/s41598-018-33639-

w.

(218) Lucio, A. J.; Shaw, S. K. Pyridine and Pyridinium Electrochemistry on Polycrystalline Gold Electrodes and Implications for CO2 Reduction. *J. Phys. Chem. C* **2015**, *119* (22), 12523–12530. https://doi.org/10.1021/acs.jpcc.5b03355.

(219) Escalante-García, I. L.; Wainright, J. S.; Thompson, L. T.; Savinell, R. F. Performance of a Non-Aqueous Vanadium Acetylacetonate Prototype Redox Flow Battery: Examination of Separators and Capacity Decay. *J. Electrochem. Soc.* **2015**, *162* (3), A363–A372. https://doi.org/10.1149/2.0471503jes.

(220) Hoyt, N. C.; Hawthorne, K. L.; Savinell, R. F.; Wainright, J. S. Plating Utilization of Carbon Felt in a Hybrid Flow Battery. *J. Electrochem. Soc.* **2016**, *163* (1), A5041–A5048. https://doi.org/10.1149/2.0061601jes.

(221) Angelin, M.; Hermansson, M.; Dong, H.; Ramstrom, O. Direct, Mild, and Selective Synthesis of Unprotected Dialdo-Glycosides. *European J. Org. Chem.* **2006**, No. 19, 4323–4326. https://doi.org/10.1002/ejoc.200600288.

(222) Wu, X.-E.; Ma, L.; Ding, M.; Gao, L. TEMPO-Derived Task-Specific Ionic Liquids for Oxidation of Alcohols. *Synlett* **2005**, *4*, 607–610. https://doi.org/10.1055/s-2005-862396.

(223) Miao, C.; Wang, J.; Yu, B.; Cheng, W.; Sun, J.; Chanfreau, S.; He, L.-N.; Zhang, S.-J. Synthesis of Bimagnetic Ionic Liquid and Application for Selective Aerobic Oxidation of Aromatic Alcohols under Mild Conditions. *Chem. Commun.* **2011**, *47*, 2697–2699. https://doi.org/10.1039/c0cc04644b.

(224) Shen, D.; Steinberg, K.; Akolkar, R. Avoiding Pitfalls in the Determination of Reliable Electrochemical Kinetics Parameters for the $Cu^{2+} \rightarrow Cu^{1+}$ Reduction Reaction in Deep Eutectic Solvents. *J. Electrochem. Soc.* **2018**, *165* (14), E808–E815.

https://doi.org/10.1149/2.1011814jes.

(225) Selverston, S.; Nagelli, E.; Wainright, J. S.; Savinell, R. F. All-Iron Hybrid Flow Batteries with In-Tank Rebalancing. *J. Electrochem. Soc.* **2019**, *166* (10), A1725–A1731. https://doi.org/10.1149/2.0281910jes.

(226) Varga, B.; Csonka, Á.; Csonka, A.; Molnár, J.; Amaral, L.; Spengler, G. Possible Biological and Clinical Applications of Phenothiazines. *Anticancer Res.* **2017**, *37* (11), 5983–5993. https://doi.org/10.21873/anticanres.12045.

(227) Al-Busaidi, I. J.; Haque, A.; Al Rasbi, N. K.; Khan, M. S. Phenothiazine-Based Derivatives for Optoelectronic Applications: A Review. *Synth. Met.* **2019**, *257*, 116189. https://doi.org/10.1016/j.synthmet.2019.116189.

(228) Onoabedje, E. A.; Egu, S. A.; Ezeokonkwo, M. A.; Okoro, U. C. Highlights of Molecular Structures and Applications of Phenothiazine & Phenoxazine Polycycles. *J. Mol. Struct.* **2019**, *1175*, 956–962. https://doi.org/10.1016/j.molstruc.2018.08.064.

(229) Šulcová, N.; Němec, I.; Waisser, K.; Kies, H. L. Study of the Electrochemical Oxidation of Phenothiazine Derivatives in Acetonitrile Medium: The Effect of the Structure on the Voltammetric Behavior. *Microchem. J.* **1980**, *25* (4), 551–566. https://doi.org/10.1016/0026-265X(80)90222-2.

(230) Milshtein, J. D.; Kaur, A. P.; Casselman, M. D.; Kowalski, J. A.; Modekrutti, S.; Zhang, P. L.; Harsha Attanayake, N.; Elliott, C. F.; Parkin, S. R.; Risko, C.; Brushett, F. R.; Odom, S. A. High Current Density, Long Duration Cycling of Soluble Organic Active Species for Non-Aqueous Redox Flow Batteries. *Energy Environ. Sci.* **2016**, *9* (11), 3531–3543. https://doi.org/10.1039/c6ee02027e.

(231) Pankratov, A. N.; Uchaeva, I. M.; Stepanov, A. N. Chemical and Electrochemical

Oxidation of Phenothiazine. *Can. J. Chem.* **1993**, *71*, 674–677.
https://doi.org/10.1021/jm00202a010.

(232) Chen, B.; Mitchell, S.; Sinclair, N.; Wainright, J.; Pentzer, E.; Gurkan, B. Feasibility of
TEMPO-Functionalized Imidazolium, Ammonium and Pyridinium Salts as Redox-Active
Carriers in Ethaline Deep Eutectic Solvent for Energy Storage. *Mol. Syst. Des. Eng.* **2020**,
5 (6), 1147–1157. https://doi.org/10.1039/d0me00038h.

(233) Sheina, E. E.; Khersonsky, S. M.; Jones, E. G.; Mccullough, R. D. Highly Conductive,
Regioregular Alkoxy-Functionalized Polythiophenes: A New Class of Stable, Low Band
Gap Materials. *Chem. Mater.* **2005**, *17* (13), 3317–3319.
https://doi.org/10.1021/cm050083o.

(234) Yu, J.; Zhao, B.; Nie, X.; Zhou, B.; Li, Y.; Hai, J.; Zhu, E.; Bian, L.; Wu, H.; Tang, W.
Correlation of Structure and Photovoltaic Performance of Benzo[1,2-b:4,5-B′]Dithiophene
Copolymers Alternating with Different Acceptors. *New J. Chem.* **2015**, *39* (3), 2248–
2255. https://doi.org/10.1039/c4nj02192d.

(235) Ingoglia, B. T.; Buchwald, S. L. Oxidative Addition Complexes as Precatalysts for Cross-
Coupling Reactions Requiring Extremely Bulky Biarylphosphine Ligands. *Org. Lett.*
2017, *19* (11), 2853–2856. https://doi.org/10.1021/acs.orglett.7b01082.

(236) Cummins, D.; Boschloo, G.; Ryan, M.; Corr, D.; Rao, S. N.; Fitzmaurice, D. Ultrafast
Electrochromic Windows Based on Redox-Chromophore Modified Nanostructured
Semiconducting and Conduction Films. *J. Phys. Chem. B* **2000**, *104*, 11449–11459.
https://doi.org/10.1021/jp001763b.

(237) Gawande, M. B.; Branco, P. S. An Efficient and Expeditious Fmoc Protection of Amines
and Amino Acids in Aqueous Media. *Green Chem.* **2011**, *13* (12), 3355–3359.

https://doi.org/10.1039/c1gc15868f.

(238) He, C. X.; Meng, H.; Zhang, X.; Cui, H. Q.; Yin, D. L. Synthesis and Bio-Evaluation of Phenothiazine Derivatives as New Anti-Tuberculosis Agents. *Chinese Chem. Lett.* **2015**, *26* (8), 951–954. https://doi.org/10.1016/j.cclet.2015.03.027.

(239) Thiyagarajan, S.; Krishnakumar, V.; Gunanathan, C. KO t Bu-Catalyzed Michael Addition Reactions Under Mild and Solvent-Free Conditions. *Chem. Asian J.* **2020**, *15*, 518–523. https://doi.org/10.1002/asia.201901647.

(240) Schafgen, B.; Khelwati, H.; Bechtel, D. F.; DeCuyper, A.; Schussler, A.; Neuba, A.; Pierik, A. J.; Ernst, S.; Muller, T. J. J.; Thiel, W. R. Phenothiazine Electrophores Immobilized on Periodic Mesoporous Organosilicas by Ion Exchange. *New J. Chem.* **2019**, *43*, 16396–16410. https://doi.org/10.1039/c9nj04661e.

(241) Reddy, N. N. K.; Rao, S. N.; Patil, R. D.; Adimurthy, S. Transition Metal-Free Hydration of Nitriles to Amides Mediated by NaOH. *Adv. Mater. Sci.* **2018**, *3* (1), 1–7. https://doi.org/10.15761/AMS.1000137.

(242) Ritu, S.; Pushkal, S.; D., S. S.; K., S. S. Synthesis and Biological Activity of 2-Oxo-Azetidine Derivatives of Phenothiazine. *Org. Commun.* **2011**, *4* (2), 42–51. https://doi.org/10.1055/s-0033-1364001.

(243) Chudzinski, M. G.; McClary, C. A.; Taylor, M. S. Anion Receptors Composed of Hydrogen- and Halogen-Bond Donor Groups: Modulating Selectivity with Combinations of Distinct Noncovalent Interactions. *J. Am. Chem. Soc.* **2011**, *133* (27), 10559–10567. https://doi.org/10.1021/ja202096f.

(244) Dekeukeleire, S.; D'Hooghe, M.; De Kimpe, N. Diastereoselective Synthesis of Bicyclic γ-Lactams via Ring Expansion of Monocyclic β-Lactams. *J. Org. Chem.* **2009**, *74* (4),

1644–1649. https://doi.org/10.1021/jo802459j.